Exploring the role of the lipid phosphatase SHIP2 in systemic metabolism and vascular biology

_____

Dr Peysh Acyuta Patel

**Submitted in accordance with the requirements for
the degree of Doctor of Philosophy**

The University of Leeds
School of Medicine

June 2018

Intellectual Property and Publication Statements

The candidate confirms that the work submitted is his own, except where work which has formed part of jointly authored publications has been included. Details of this publication are as follows:

Watt, N.T., Gage, M.C., Patel P.A., et al., *Endothelial SHIP2 Suppresses Nox2 NADPH Oxidase-Dependent Vascular Oxidative Stress, Endothelial Dysfunction, and Systemic Insulin Resistance.* Diabetes, 2017. **66**(11): p. 2808-2821.

The contribution of the candidate and the other authors to this work has been explicitly indicated in the thesis below. The candidate confirms that appropriate credit has been given within the thesis where reference has been made to the work of others.

Acknowledgements

thank my clinical colleagues who have offered excellent company (and distraction) to preserve my sanity. Lastly, I ought to acknowledge the contribution of Dr Suhanya Nagendran who is my wife and lifelong companion. She has little understanding (or interest!) in the work I've conducted during my PhD, but nonetheless, has provided unremitting support and valued the importance of allowing me to accomplish personal career goals and fulfil potential.

Although I am now returning back to clinical training, I look back at my experience with great fondness. It was a privilege to secure the opportunity to pursue this fellowship and I wish the faculty all the best for the future.

Abstract

Metabolic dysregulation in the form of insulin-resistant type 2 diabetes mellitus leads to premature death and disability, primarily as a consequence of vascular dysfunction. This relates to accelerated atherosclerosis, diminished vascular repair and dysfunctional angiogenesis. A number of complementary systems exist to regulate insulin sensitivity, and maladaptive activation of these may contribute to pathophysiology. SHIP2 is a lipid phosphatase which catalyses the conversion of phosphatidylinositol (3,4,5)-triphosphate (PI(3,4,5)P$_3$) to phosphatidylinositol (3,4)-biphosphate PI(3,4)P$_2$ in insulin responsive tissues. It therefore suppresses activation of signalling cascades downstream of phosphoinositide-3-kinase (PI3K), consistent with a negative role of SHIP2 in insulin signalling. However, the effects of SHIP2 manipulation on metabolic and vascular function have not been clearly elucidated.

We hypothesised that SHIP2 inhibition would have favourable effects on insulin-mediated glucose lowering, vascular repair and angiogenesis. Studies were primarily performed on mice with germline endothelium-specific (ECSHIP2$^{\Delta/+}$), or whole body inducible (SHIP2i$^{\Delta/+}$) SHIP2 catalytic domain haploinsufficiency, using a Cre-*lox* approach. A complementary model was explored in human umbilical vein endothelial cells (HUVECs) using shRNA-mediated knockdown or pharmacological inhibition of SHIP2.

ECSHIP2$^{\Delta/+}$ mice exhibited impaired vascular formation in the developing postnatal retinas, associated with increased endothelial PI3K/AKT signalling and Nox2-mediated vascular oxidative stress. Alterations in these signalling intermediates and superoxide

generation were recapitulated in HUVECs. This was associated with defects in endothelial cell migration and polarisation, although no differences in proliferative capacity were observed. SHIP2i$^{\Delta/+}$ mice had enhanced whole body glucose disposal and insulin sensitivity. They exhibited skeletal muscle hypervascularity in the context of hindlimb ischaemia, which was manifest as increased vessel thickness without alterations in vessel abundance. No differences in re-endothelialisation after denuding arterial injury were apparent in this model.

In conclusion, SHIP2 activity appears critical in preservation of metabolic and vascular homeostasis during health and disease. Elements of this role may relate to suppression of oxidative stress that arises from unrestrained PI3K-Nox2 signalling. Further exploration to extend our mechanistic understanding is required, but the findings of this project suggest that caution is warranted before SHIP2 inhibition can be considered as a viable therapeutic strategy in clinical contexts.

Table of Contents

List of Figures

List of Tables

Abbreviations

AAS	Antibiotic-antimycotic solution
ACAT1	Acyl:cholesterol acyltransferase 1
ACE	Angiotensin-converting-enzyme
Ach	Acetylcholine
AGE	Advanced glycation end products
AMPK	AMP-activated protein kinase
Ang	Angiopoietin
APC	Allophycocyanin
APOE4	Apolipoprotein E4
ATP-CL	Adenosine triphosphate-citrate lyase
AUC	Area under curve
BCA	Bicinchoninic acid
BH_4	Tetrahydrobiopeterin
Bim	BCL2-like 11
BSA	Bovine serum albumin
$CaCl_2$	Calcium chloride
cAMP	Cyclic adenosine monophosphate
CAP	c-Cbl associated protein
cGMP	3',5'-cyclic guanosine monophosphate
CHF	Chronic heart failure
CHO	Chinese hamster ovary
CMV	Cytomegalovirus

CoA	Coenzyme A
Cryo-ET	Electron cryotomography
$CuSO_4$	Copper sulphate
DHE	Dihydroethidium
DM	Diabetes mellitus
DMEM	Dulbecco's modified eagle's medium
DMSO	Dimethylsulfoxide
DNA	Deoxyribonucleic acid
dNTP	Deoxynucleotide triphosphate
DPP-4	Dipeptidyl peptidase-4
ECGS	Endothelial cell growth supplement
ECM	Extracellular matrix
EDRF	Endothelium dependent relaxing factor
EDTA	Ethylenediaminetetraacetic acid
EDU	5-ethynyl-2'-deoxyuridine
EGF	Epidermal growth factor
EGM	Endothelial growth medium
ELISA	Enzyme-linked immunosorbent assay
EPC	Endothelial progenitor cells
ESMIRO	Endothelium-specific mutant IR overexpression
ER	Endoplasmic reticulum
ET	Endothelin
FACS	Fluorescence-activated cell sorting
FAK	Focal adhesion kinase

FasL	Fas-ligand
FBS	Foetal bovine serum
FGF	Fibroblast growth factor
FFA	Free fatty acids
FITC	Fluorescein isothiocyanate
FRET	Fluorescence resonance energy transfer
FSC	Forward scatter
GEF	Guanine nucleotide exchange factor
GFP	Green fluorescent protein
GLP	Glucagon-like peptide
GLUT	Glucose transporter protein
GPCR	G-protein-coupled receptors
Grb	Growth-factor-receptor-bound protein
GSK3	Glycogen synthase kinase 3
GTP	Guanosine triphosphate
GTN	Glyceryl trinitrate
GTT	Glucose tolerance testing
GWAS	Genome-wide association studies
HCl	Hydrochloric acid
HCS	High content screening
HDL	High-density lipoprotein
HEPES	4-(2-hydroxyethyl)-1-piperazineethanesulfonic acid
HIF	Hypoxia-inducible factor

HMG-CoA	3-hydroxyl-3-methyl-glutaryl-coenzyme A
HPLC	High performance liquid chromatography
HRP	Horseradish peroxidase
HUVEC	Human umbilical vein endothelial cell
H_2O	Water
H_2O_2	Hydrogen peroxide
ICAM	Intercellular adhesion molecule
IGF	Insulin-like growth factor
IKKβ	Inhibitor of nuclear factor kappa-B kinase subunit beta
INPPL1	Inositol polyphosphate phosphatase like 1
IL	Interleukin
IMPK	Inositol phosphate multikinase
IP	Intraperitoneal
IPP	Inositol phosphatidyl phosphatase
IRKO	Insulin receptor knockout
IRS	Insulin-receptor substrate
ITT	Insulin tolerance testing
IVC	Inferior vena cava
JNK	c-Jun N-terminal kinases
LDL	Low-density lipoprotein
LIMK	Lim kinases
L-NMMA	NG-monomethyl-L-arginine
LSCM	Laser scanning confocal microscopy
MAPK	Mitogen-activated protein kinase

MES SDS	2-(N-morpholino)ethanesulfonic acid/sodium dodecyl sulphate
$MgCl_2$	Magnesium chloride
$MnCl_2$	Manganese chloride
MI	Myocardial infarction
MLC	Myosin light chain
MMP's	Matrix metalloproteinases
MOI	Multiplicity of infection
mRNA	Messenger RNA
mTOR	Mammalian target of rapamycin
NADPH	Nicotinamide adenine dinucleotide phosphate
NaCl	Sodium chloride
NaOH	Sodium hydroxide
Nox	NADPH oxidase
NF-κB	Nuclear factor kappa-light-chain-enhancer of activated B cells
NO	Nitric oxide
NOS	Nitric oxide synthase
OCT	Optimal cutting temperature
$ONOO^-$	Peroxynitrite
O_2	Oxygen
O_2^-	Superoxide
O_3	Ozone
PACT	PKR activating protein
PAK	p21-activated kinase

PBS	Phosphate buffered saline
PCI	Percutaneous coronary intervention
PCR	Polymerase chain reaction
PDGF	Platelet derived growth factor
PDK	Phosphoinositide-dependent kinase
PFA	Paraformaldehyde
PH	Pleckstrin homology
PHLPP	PH-domain leucine-rich-repeat protein phosphatase
PI3K	Phosphoinositide-3-kinase
PI4P	Phosphatidylinositol 4-phoshate
PIP3	Phosphatidylinositol 3,4,5-triphosphate
PIPP	Proline-rich inositol polyphosphate 5-phosphatase
POD	Peroxidase
PKC	Protein kinase C
PPAR	Peroxisome proliferator-activated receptor
PP2A	Phosphatase-2A
PTB	Phosphotyrosine-binding
PTEN	Phosphate and tensin homolog
PtdIns(3,4)P2	Phosphatidylinositol 3,4-bisphosphate
PtdIns(4,5)P2	Phosphatidylinositol 4,5-bisphosphate
PtdIns4P	Phosphatidylinositol 4-phosphate
PTP	Protein tyrosine phosphatase
PVD	Peripheral vascular disease
PVDF	Polyvinylidene fluoride

RAAS	Renin-angiotensin-aldosterone system
RBL2	Retinoblastoma-like 2
RCT	Randomised controlled trial
RICTOR	Rapamycin-insensitive companion on mTOR
RIPA	Radio-immunoprecipitation assay
RISC	RNA-induced silencing complex
RLP	Remnant-like particle
ROCK	Rho-stimulated kinase
ROS	Reactive oxygen species
RTK	Receptor tyrosine kinase
SCAR	Suppressor of cAMP receptor
SCC	Squamous cell carcinoma
SEM	Standard error of mean
SHIP2	Shc homology 2-containing inositol 5' phosphatase 2
shRNA	Short hairpin RNA
siRNA	Small interfering RNA
SH2	Src-homology-2
SKIP	Skeletal muscle and kidney enriched inositol phosphatase
SMI	Small molecule inhibitor
SNP	Sodium nitroprusside
SNP	Single nucleotide polymorphism
SNS	Sympathetic nervous system
SOCS	Suppressor of cytokine signalling

SOD	Superoxide dismutase
SOS	Son-of-sevenless
SRA	Scavenger receptor class A
SSC	Side scatter
TAE	Tris-acetate-EDTA
TAPP	Tandem pleckstrin homology domain containing protein
Taq	*Thermophilus aquaticus*
TMB	Tetramethylbenzidine
TNF	Tumour necrosis factor
TRBP	Tat-RNA-binding protein
UK	United Kingdom
UIM	Ubiquitin interacting motif
UTR	Untranslated region
UV	Ultraviolet
VASP	Vasodilator-stimulated phoshoprotein
VCAM	Vascular cell adhesion molecule
VEGF	Vascular endothelial growth factor
VENIRKO	Vascular endothelium insulin receptor knockout
VLDL	Very low-density lipoprotein
VSMC	Vascular smooth muscle cell
vWF	von Willebrand factor
WASP	Wiskott-Aldrich-syndrome protein
WAT	White adipose tissue
WHO	World Health Organisation

Chapter 1 – Introduction

_____

1.1 Diabetes mellitus and cardiovascular disease

1.1.1 Overview

Nutrient delivery has to be coordinated with energy storage and cell growth in normal physiology. This coupling enables regulation of a plethora of cell processes, including glucose, lipid and protein metabolism [1]. Multiple systems are implicated in these homeostatic processes, of which the insulin and insulin-like growth factor 1 (IGF-1) signalling cascades are pivotal. However, in the context of environmental stresses posed by chronic, caloric excess, metabolic dysregulation can ensue. This may manifest as insulin resistance with secondary glucose intolerance, defined clinically as pre-diabetes and type II diabetes mellitus (DM) [2]. These conditions are associated with significant morbidity and mortality, relating primarily to microvascular dysfunction and accelerated atherogenesis in the macrovasculature.

1.1.2 Epidemiology

As a consequence of an ageing population and increased prevalence of truncal obesity, type 2 DM has become a major global public health burden. World Health Organisation (WHO) estimates indicate that 550 million people are likely to suffer from the disorder by 2030, a projected increase of 50% compared to contemporary data [3]. Over 25% of patients presenting to hospital with acute myocardial infarction (MI) have comorbid DM [4], and indeed, this proportion is substantially higher when those with evidence of impaired glycaemic control (pre-diabetes) are included [5]. It is also strongly associated with chronic heart failure (CHF), with several studies quoting prevalence in excess of 25% [6, 7].

1.1.3 Cardiovascular morbidity and mortality

The burden of disease imposed by DM relates primarily to increased cardiovascular sequelae. The Framingham study was a landmark study in highlighting this association, and was based on 20 years of surveillance data with a reported 2-3 fold enhanced risk [8]. Macrovascular disease constitutes the predominant burden, with ischaemic heart disease, CHF, cerebrovascular events and peripheral vascular disease (PVD) all strongly implicated [9]. Patients with DM appear to develop these sequelae 15 years earlier than the general population [10]. Those with pre-diabetes are also at increased cardiovascular risk (see Figure 1-1) [11].

Improving therapeutic strategies in the contemporary era have played a significant role in reducing morbidity associated with cardiovascular disorders [12]. However, despite these interventions, it appears that the presence of DM continues to confer a prognostic disadvantage. This extends beyond morbidity into mortality risk. In the context of acute MI, for instance, patients with DM have an adjusted risk of all-cause death which is nearly 50% higher [13]. This adverse prognosis has also been shown in the context of CHF, of both ischaemic and non-ischaemic aetiologies [14].
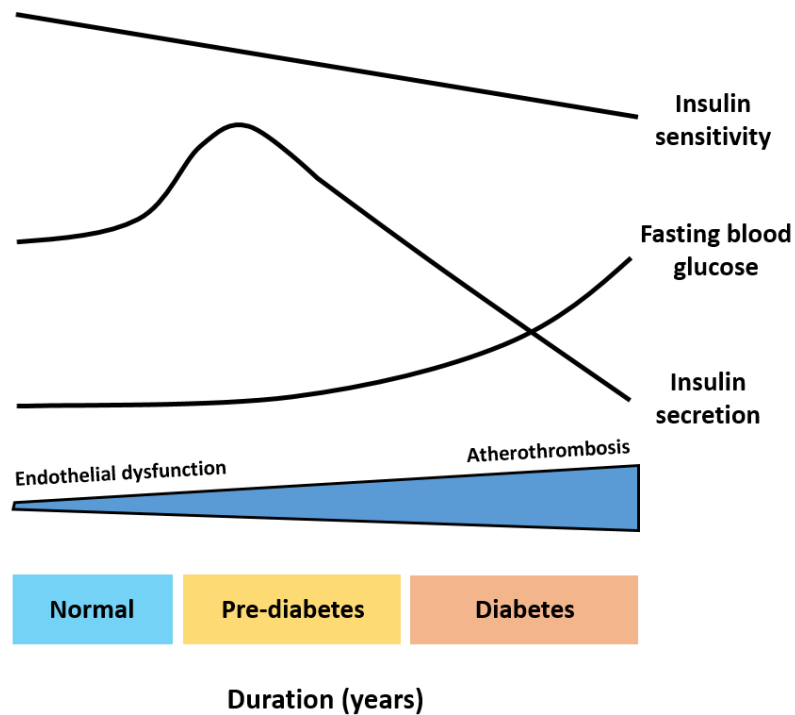
Figure 1-1 – **Evolution of diabetes and its association with vascular dysfunction.**
Adapted from Wheatcroft *et al.* Diabet Med 2003; 20(4):255-68 [15].

Insulin sensitivity is reduced as type II DM develops. Initial, compensatory hyperinsulinaemia results in glucose homeostasis until manifestation of frank DM. There is a progressively increased risk of atherogenesis throughout this period.

1.1.4   Atherothrombosis

The macrovascular risk associated with DM primarily relates to accelerated atherosclerosis in large and medium-sized arteries [16]. For many decades, it was considered that atherosclerosis was principally a pathophysiological process of lipid accumulation within the arterial wall [17]. However, despite aggressive strategies to improve lipid profile via lifestyle measures and pharmacotherapy, it is evident from epidemiological studies that cardiovascular disease continues to be associated with significant morbidity and mortality. Hence, it is now generally accepted that

atherogenesis is a multi-faceted disease process and can be perhaps best described as an 'inflammatory' disorder involving vessel walls [18].

1.1.4.1　Endothelial dysfunction

The pathology of atherosclerotic lesions in patients with DM is in many regards indistinguishable from those without DM, although lesions are generally more advanced and diffusely distributed [19]. A unifying concept to explain initiation of atherogenesis is that of 'endothelial dysfunction' [20]. It refers to a subtle alteration in endothelial phenotype (discussed later) that precedes structural changes in the arterial wall. This unfavourable shift is accelerated by systemic components of whole body insulin resistance syndrome, such as hyperglycaemia, dyslipidaemia and hypertension, and triggers a complex disturbance of endothelial biology that permits progression of the atherogenic cascade [21]. An overview is provided in Figure 1-2.

1.1.4.2　Fatty streak and foam cells

Atherosclerosis is a chronic disease and typically take decades to manifest clinically. However, the earliest discernible lesion is the so-called 'fatty streak' which is often present in young adults [22]. Cholesterol levels, and particularly low-density lipoprotein (LDL) cholesterol, are deemed as major contributors to susceptibility. However, it is worthy of note that patients with DM do not classically have raised LDL levels, but rather an abnormal dyslipidaemic profile consisting of small, dense LDL in combination with low high-density lipoprotein (HDL) and elevated triglycerides [23]. Other features such as endothelial permeability and biosynthesis of the basement membrane and extracellular matrix (ECM) components are also implicated [24].

The fatty streak occurs as a response to receptor-mediated endocytosis of LDL, and other apoB-containing lipoproteins, across the endothelium with trapping in the arterial intima [25]. Once sequestered, lipids contained in LDL are modified, for example by fusion, enzymatic cleavage, incorporation into immune complexes and oxidation, mediated by cells of the vessel wall [26]. The pro-inflammatory effects of oxidised LDL result in recruitment of monocytes to the intima, and terminal differentiation of these into macrophages. Oxidised LDL can then be internalised by macrophages via scavenger receptor class A (SRA)-I, SRA-II, CD36, LOX-1 and CXCL16 [27]. These lipoproteins are targeted to the lysosome, where their cholesteryl esters are hydrolysed to unesterified cholesterol. This free cholesterol is delivered to the endoplasmic reticulum (ER), where acyl-coenzyme A:cholesterol acyltransferase 1 (ACAT1) mediates predominant conversion back to esterified forms where it is stored as cytoplasmic lipid droplets [28]. A progressive accumulation of these droplets results in the formation of 'foam cells', named so because of the morphological appearance of soap bubbles. These foam cells characterise lesion progression from early to intermediate stage, and in combination with T lymphocytes, are the pathological hallmark of lipid streaks.

1.1.4.3   VSMC remodelling and necrotic core

Foam cells directly and indirectly mediate the release of chemokines and cytokines, such as interleukin-1 (IL-1) and tumour necrosis factor (TNF)-α, and promote endothelial cell expression of adhesions receptors including integrins and selectins [29]. These mediators can orchestrate mobilisation, adhesion, transmigration and proliferation of monocyte-derived macrophages and T cells, resulting in perpetuation

of the inflammatory process. Supplementary release of growth factors such as platelet derived growth factor (PDGF), fibroblast growth factor (FGF) and tissue factor results in stimulation of vascular smooth muscle cells (VSMCs) which mediate vascular remodelling [30]. Under normal physiological states, VSMCs in the media produce the main components of the ECM found in the intimal layer, such as collagen and elastin, in addition to enzymes required for the delicate equilibrium between ECM synthesis and degradation [21]. In the context of atherogenesis, however, a transition into a proliferative and synthetic phenotype occurs. Indeed, the migration of VSMC into the vascular intima defines intimal thickening, provides the major source of ECM in the plaque and contributes to the formation of a fibrous cap [31].

Sequential deactivation and apoptosis of foam cells within the lesion results in the formation of a necrotic core [32], which is essential in the development of a rupture-prone plaque. This region is also impregnated with oxidised lipids and tissue factors, making it highly thrombogenic when exposed to circulating blood [33]. The lipid-rich core is overlaid by a fibrous cap, with its constituents primarily derived from VSMCs and their synthesis of ECM components, namely collagen and proteoglycans. There is also involvement of macrophage-derived foam cells, albeit to lesser proportions [34].

1.1.4.4 Plaque rupture and acute thrombus

Such advanced lesions often remain stable for years, and can remain entirely asymptomatic if non-occlusive. However, activated T cells may stimulate production of matrix metalloproteinases (MMP's), collagenases, elastases and stromelysin, by macrophages within the lesions [35]. Apoptosis of VSMCs can have adjunct

destabilising effects by reducing quantities of collagen-synthesising cells within the plaque [36]. Degradation of the fibrous cap can result in exposure of the underlying necrotic core and surrounding extracellular components, such as collagen and von Willebrand factor (vWF) to circulating blood, resulting in acute plaque rupture and activation of endogenous haemostatic cascades. Although these processes are crucial in physiological haemostasis, their activation in the context of acute plaque rupture generates thrombus within the already narrowed vascular lumen [37]. If this causes sufficient impairment of blood flow, ischaemic injury occurs downstream and is typified by clinical presentations such as acute MI.

Studies suggest that propensity for acute rupture depends upon plaque constituents and vulnerability, rather than extent of stenosis [38]. Factors that enhance vulnerability to rupture are associated with presence of DM, and include thinned fibrous cap, increased macrophage infiltration, increased size of necrotic core and reduced abundance of VSMCs [39]. The extent of plaque vascularisation has also been implicated in instability [40]. In the early phases of atherogenesis, plaque neovascularisation may have anti-apoptotic effects, whilst facilitating lesion growth [40]. In more advanced lesions, however, release of cytokines secondary to local inflammation can result in dysregulated neointimal proliferation of microvessels which are leaky, fragile, of poor quality and hence susceptible to rupture [41]. Studies in humans have reported higher proportions of neovessel formation in the most advanced atherosclerotic plaques, with increased abundance in those with DM [42]. Expression of proteolytic enzymes, such as MMP's, is also increased by hyperglycaemia, and increases propensity for fibrous cap rupture [43].

Platelets initiate plaque thrombosis upon detection of ECM and necrotic core constituents, and their aggregation is augmented in the setting of insulin resistance by reduced NO bioavailability, altered calcium regulation, oxidative stress and increased circulating vWF. Notably, atheromatous plaques in those with DM have been shown to exhibit increased intracoronary thrombus compared to controls [44]. Normoglycaemic patients with insulin resistance, and those with type II DM, have altered circulating components of the coagulation and fibrinolytic pathways, with increased levels of plasminogen activator inhibitor (PAI)-1 particularly implicated [45]. PAI-1 binds to tissue plasminogen activator (tPA) to inhibit its conversion of plasminogen to plasmin, an enzyme that is essential to degrade fibrin clots. Indeed, PAI-1 levels are lowered in patients with DM by weight reduction and pharmacotherapies, such as metformin and thiazolidinediones [46]. Hyperglycaemia can also directly cause post-translational modification of coagulation proteins, such as fibrinogen. This results in a fibrin clot which is denser, with thinner fibres, and is more resistant to plasmin-mediated lysis [47].
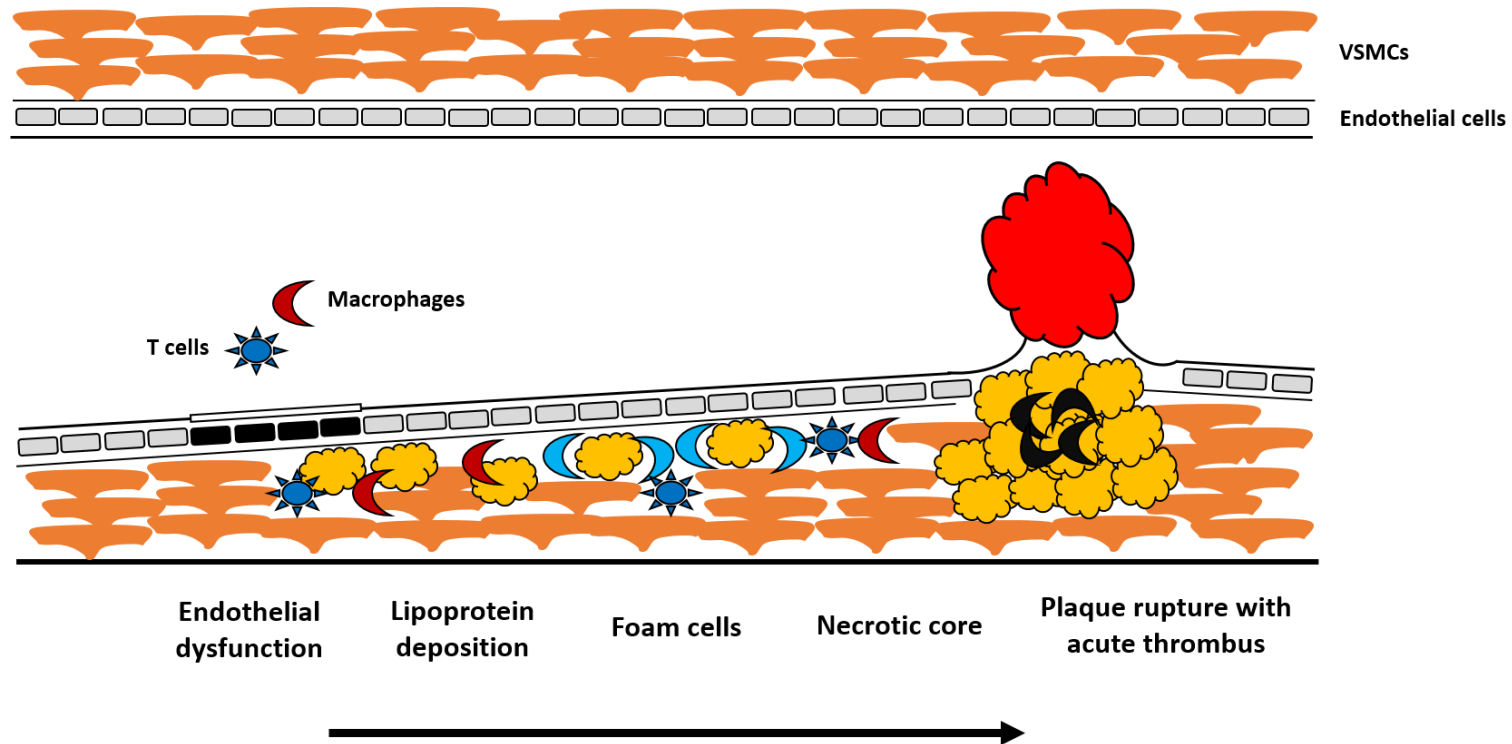
Figure 1-2 – Pathogenesis of atherothrombosis.

Initiation occurs via endothelial dysfunction. This is associated with subsequent oxidative stress, leucocyte recruitment and lipoprotein deposition. Formation of foam cells characterise lesion progression, with sequential apoptosis resulting in a necrotic core. Rupture of its fibrous cap precipitates endogenous haemostatic cascades and acute thrombus formation, typified by clinical presentations such as AMI.

1.2 Vascular endothelium

1.2.1 Overview

The vascular endothelium is a monolayer compromised of approximately 10^{14} cells [48]. It divides the vessel lumen from surrounding cells and thus provides a direct mechanical interface between blood and tissue [49]. However, beyond its role as a structural barrier, it expresses insulin receptors and is therefore metabolically active with a critical role in physiological regulation. Its functions include transport of nutrients and solutes across the endothelium, and release of a plethora of vasoprotective components such as nitric oxide (NO) [21]. The endothelium is also a key mediator of endogenous responses to tissue and vascular injury, as part of processes broadly defined as 'vascular regeneration' (or angiogenesis) and 'vascular repair', respectively.

1.2.2 Nitric oxide (NO)

1.2.2.1 Historical perspective

NO was first discovered as a clear, colourless gas by Joseph Priestley in 1772 [50]. It was subsequently established as an atmospheric pollutant, but the concept that it plays a fundamental role in vascular homeostasis was not apparent until two centuries later. The first experiments showed that the presence of endothelial cells was essential for acetylcholine (Ach)-mediated relaxation in aortas isolated from rabbits [51]. This process was influenced by an endogenous mediator termed endothelium derived relaxing factor (EDRF), which was subsequently identified to be NO [52].

1.2.2.2 Synthesis via NOS

NO can be synthesised by one of three isoforms of nitric oxide synthase (NOS): endothelial (eNOS), neuronal (nNOS) and macrophage/inducible (iNOS). These are encoded by genes on chromosomes 7, 12 and 17, respectively [53]. For all three, NO synthesis depends upon binding of the enzyme to the calcium-regulatory protein calmodulin. However, iNOS is fundamentally different from the other two isoforms in that activity is independent of intracellular calcium concentration [54]. Of the three, iNOS is not constitutively present and expression is induced only in specific contexts such as inflammation or infection. It is the constitutively expressed eNOS that is implicated in the production of NO within the vascular endothelium, and an overview is provided in Figure 1-3.

The amino acid L-arginine is the main eNOS substrate for NO biosynthesis, but several co-factors are also required, including nicotinamide adenine dinucleotide phosphate (NADPH), flavin mononucleotide, flavin adenine nucleotide, tetrahydrobiopeterin (BH_4), calmodulin and a haem group. It occurs in a two-step process. The first stage involves electron transfer from NADPH to the haem group, which hydroxylates L-arginine to form the intermediate N-hydroxyl L-arginine [55]. This is then oxidised to form NO, with the formation of L-citrulline as a by-product. Once synthesised, NO diffuses across the cell membrane of endothelial cells and enters VSMCs where activation of guanylate cyclase occurs. This catalyses the reaction of guanosine triphosphate (GTP) to 3',5'-cyclic guanosine monophosphate (cGMP) and

pyrophosphate [56]. cGMP is an important secondary messenger which determines many of the biological targets implicated in vascular function.
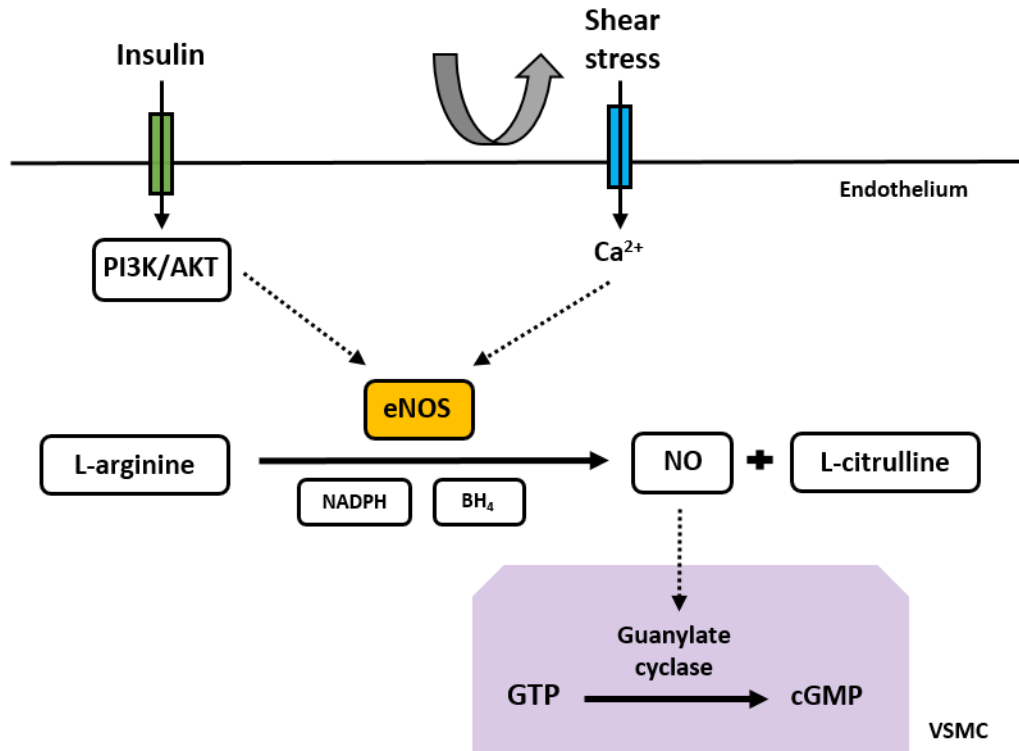
Figure 1-3 – NO synthesis within the vasculature.

eNOS synthesis via insulin signalling results in formation of NO, with L-arginine as the primary substrate. This activates guanylate cyclase and catalyses cGMP production in VSMCs.

1.2.2.3   Metabolism

In plasma, NO is oxidised to nitrite which is stable for a period of several hours. However, in whole blood, the nitrite is rapidly degraded into nitrate [57]. Basal blood concentrations of nitrate, therefore, appear to be of a magnitude 100 fold greater at around 15-60µM [58]. In humans, this excess nitrate is excreted predominantly in the urine. NO also appears to be rapidly oxidised to higher oxides of nitrogen, such as peroxynitrite ($ONOO^-$), which is implicated in a broad range of pathophysiological

37

effects relating to inflammation, diabetes and cardiovascular disease [59]. Other interactions of NO exist with haem-containing proteins, such as myoglobin and deoxyribonucleic acid (DNA), in addition to thiols which is deemed to be an important step in oxidant modification of protein cysteine residues [60].

1.2.2.4   Physiological effects

NO has a broad range of physiological effects, owing in large part to the fact that eNOS expression and activation can be regulated by multiple stimuli, including insulin, shear stress and vascular endothelial growth factor (VEGF) [50]. Promotion of enzymatic activity occurs predominantly via phosphorylation at the serine 1177 residue [48], but other post-translational modifications include palmitoylation, most commonly associated with the covalent addition of fatty acids such as palmitic acid to cysteine, nitrosylation and O-GlcNAcylation [61].

There is continuous, basal synthesis of NO to maintain vasodilatory tone in vessels, with most of its effects exerted on the arterial system rather than in veins. Consistent with this, treatment with specific NOS inhibitors produces a hypertensive response in rats [62]. Pharmacological agents such as glyceryl trinitrate (GTN) and sodium nitroprusside (SNP) have functional effects after conversion into NO, via cGMP-dependent mechanisms as described [63]. Indeed, the beneficial effects of angiotensin-converting-enzyme (ACE) inhibitors may be related to amplification of the actions of bradykinin, which potentiates NO release through calcium-dependent signalling pathways [64].

NO is also implicated in retarding the progression of atherogenesis. It has inhibitory effects on platelet adhesion and aggregation, which is again dependent on cGMP [65]. However, there is a synergistic association with prostacyclin release from the endothelium, which operates through enhanced bioavailability of cyclic adenosine monophosphate (cAMP) to impede aggregation. Platelets may themselves synthesise NO which provides a regulatory negative feedback loop. It is also implicated in attenuation of local inflammatory responses, by limiting leukocyte-endothelial cell interactions through downregulation of surface glycoproteins. This includes CD11 and CD18 on leukocytes, and intercellular adhesion molecule-1 (ICAM-1) and vascular cell adhesion molecule-1 (VCAM-1) on endothelial cells [66]. NO has additional suppressive effects on the mitogenesis and proliferation of fibroblasts and VSMCs [67]. This appears to be through cGMP-independent mechanisms. Hence, NO appears to participate heavily in the provision of an overall anti-atherogenic and anti-thrombotic environment within the vasculature to preserve normal physiology. Consistent with this perception, polymorphisms of the eNOS gene (Glu298 $\rightarrow$ Asp) have been associated with detrimental changes in brachial flow-mediated vessel dilatation and carotid intima-media thickness, two markers of early atherosclerosis [68]. This increased susceptibility is supported by results from a meta-analysis of case-control studies though significant inter-study heterogeneity was noted [69].

1.2.3   Endogenous protective mechanisms

1.2.3.1   Nomenclature

'Vascular repair' denotes re-endothelialisation of existing conduit vessels, and refers primarily to the response to injury in the context of atherogenesis or revascularisation with stenting procedures [70]. Though contexts are highly heterogeneous, vascular repair relies broadly upon generation and recruitment of bone marrow-derived cells, particularly leukocytes, and proliferation and migration of endothelial cells adjacent to the site of insult to restore a seamless endothelial monolayer [71]. Notably, whilst bone marrow-derived cells may promote this process via paracrine mechanisms, they do not directly contribute to the neo-endothelium [72] [73].

'Vascular regeneration' is a diverse, context-dependent process which encompasses de novo vessel formation and vascular network expansion in response to physiological and pathological insults. Various sub-definitions exist. 'Vasculogenesis' refers to de novo vessel development in utero and arises from heterogeneous mesenchymal progenitor cells [74]. Subsequent maturation and remodelling of neovessels into larger, functional conduits by exerted shear stress is referred to as 'arteriogenesis', with luminal enlargement and recruitment of mural cells [75]. In the adult, vessels are quiescent once formed. However, endothelial cells retain the ability to send and respond to pro-angiogenic stimuli, such as VEGF. Activation results in a complex cascade of cell processes involving guided sprouting, proliferation, anastomosis and regression to create a complex hierarchical plexus.

'Angiogenesis' specifically defines sprouting of neovessels from existing vasculature [76]. In pathological contexts, i.e. tissue injury, the two primary triggers are chronic tissue ischaemia and inflammation, though there is a reciprocal and co-existent relationship between these two mediators [77]. In physiological states, it can be

subcategorised as developmental when occurring during the embryonic/foetal period and postnatal, with mechanisms somewhat distinct from pathological angiogenesis. Lastly, 'collateral growth' refers to the expansive remodelling of pre-existing collateral vessels, in response to local arterial or arteriolar occlusion, to salvage the region of ischaemia.

1.2.3.2   Endothelial progenitor cells (EPCs)

The recruitment of endothelial progenitor cells (EPCs) into the circulation has been proposed as a potential mechanism of endogenous vascular repair and regeneration [78]. However, there is considerable debate regarding the existence, definition and function of such cells, both in the context of physiology and pathology. Multiple stimuli have been identified to mobilise putative EPCs into the circulation of humans, including pro-inflammatory cytokines, chemokines, VEGF and physical activity [79]. Regulatory mechanisms remain poorly understood, though experimental studies have indicated that EPC mobilisation in response to VEGF or exercise is critically reliant on NO bioavailability [80] [81]. Furthermore, exercise-induced EPC mobilisation into the circulation is impaired in men of South Asian ethnicity, who demonstrate endothelial dysfunction and increased preponderance of atherosclerosis [82].

Culture-derived EPCs are characterised based on expression of the haematopoietic surface marker CD34 [83]. It is likely that population subsets exist, and indeed some early outgrowth cells are now recognised to be monocytic in origin but expressing a subset of non-specific 'endothelial' surface markers [84]. The relevance of these cells *in vivo r*emains unclear. However, it is putatively speculated that 'early-outgrowth'

EPCs (also known as myeloid angiogenic cells) do not demonstrate significant proliferative capability and do not appear to directly integrate into vascular structures. Instead, they may provide paracrine stimulation of resident cells to orchestrate repair and also offer a pro-angiogenic milieu to promote vascular regeneration [85]. In contrast, 'late-outgrowth' EPCs (also known as outgrowth endothelial cells) very closely mimic endothelial cell function and gene expression. These cells are highly proliferative, with a progenitor hierarchy and can directly form new vessels. As highlighted, however, evidence from *in vivo* murine studies has shown that bone marrow-derived cells do not incorporate directly into the endothelial monolayer after injury, but may promote repair via paracrine mechanisms [73].

1.2.3.3   Cell motility

Cell motility has an essential role in the biology of organisms. It occurs as a response to gradients of chemokines ('chemotaxis'), extracellular matrix density ('haptotaxis'), electric fields ('electrotaxis') or substrate rigidity ('durotaxis') [86]. In prokaryotes, this process is important in the sourcing of nutrients depending on the temporal characteristics of chemoattractant signals [87]. In eukaryotes, however, these mechanisms are intrinsic to survival and have therefore been optimised through evolutionary development [88]. As a consequence, there appears to be broad generalisation in the harnessing of temporal and spatial information across a spectrum of cell types, including amoebae, neurones, leucocytes and endothelial cells. Cell motility in these contexts are crucial for various cell processes implicated in physiology and pathophysiology [89]. This includes embryogenesis, the immune

response of neutrophils to sites of active infection and the pathogenic process of tumour cell invasion and metastatic spread. Crucially, it is critical to the endogenous protective responses during vascular repair and regeneration. An exploratory discussion of underlying stages and mechanisms is now provided.

1.2.3.3.1   Stages of cell migration

An overview of the stages implicated in cell migration is provided in Figure 1-4. The first step in cell motility is determination of the direction of motion. It is apparent that even during random migration, cells have an inherent ability to control directional persistence, i.e. the duration during which migration is sustained in a specific direction [90]. However, cells also are able to respond to external chemotactic cues such as VEGF ('directional sensing'), which results in spatial asymmetry via a polarised morphology that provides distinction between cell front and rear [91].

A consequence of polarisation is the protrusion of cytoplasm as a sheet-like structure at the leading edge of the cell. This region is defined as the 'lamellipodium' [92]. Depending on cell type, this can vary in breadth from approximately 1-5µm. It is devoid of organelles but instead exhibits concentrated actin filaments (and associated proteins) of inherent polarity, which can be coordinated and cross-linked into a lattice-like meshwork by filamin to enhance cell rigidity as it extends. Filaments can also be grouped into cylindrical bundles. If these are contained within the lamellipodial region, they are referred to as 'microspikes'. If these precursors protrude beyond the cell edge as finger-like protrusions, conventional nomenclature defines them as 'filopodia' [93]. Filopodia in particular are regarded as sensors for

chemotactic stimuli to detect and transmit changes, and can support residual, slow migration in the absence of lamellipodia [94]. It is clear, however, that extension of lamellipodia and filopodia is coupled with the engagement of protein complexes to drive local actin polymerisation [95]. In particular, the balance between actin branching and elongation influences persistence, and speed, of lamellipodial protrusions. For instance, persistent branching results in a stiffer, actin network that generates more persistent but slower protrusion [96]. Moreover, integration of positive and negative feedback loops enables oscillatory behaviour of the lamellipodium, i.e. sequential protrusion and retraction, which contributes to the fine-tuning of cell steering during chemotaxis [97].

Once cell directionality is established, the next stage involves cell adhesion via interaction between integrin receptors and ECM, with the cell front appearing to be a preferential locus [98]. These adhesion sites initially appear as small aggregates, which expand in size and intensity ('focal adhesions') to provide anchorage for cell migration. In addition to the protrusive force and anchorage, a separate contractile force is necessary for cell migration [99]. This is an active myosin II-dependent process that results in contraction of actin filaments, including those linked to integrin receptors and hence bound to ECM ligands [100]. Of note, the local substratum also exerts an adhesive traction in an opposing direction. This balance must also incorporate the asymmetry in traction between cell front and rear, enabling forward attachments to remain whilst those at the rear are released [101]. Exact mechanisms are not fully appreciated, but may relate to cytoskeletal tension and key signalling intermediates such as Rho A (discussed later). Lastly, concentration of myosin II filaments at the back

of the cell enables tail retraction and disassembling of adhesions to complete the cycle

[102]. These myosin filaments also appear to extend to the sides of the cells and

appear to suppress the formation of lateral filopodia which may otherwise evoke the

tendency for deviations in movement [103].
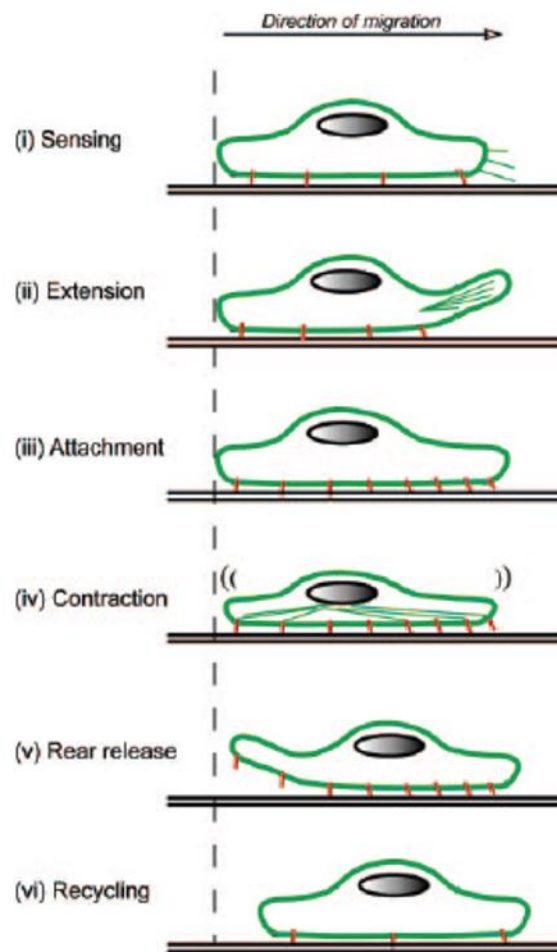
Figure 1-4 – Stages of cell migration.
Lamalice *et al*. Circ Res 2007; 100(6):782-94 [104].

Filopodia act as chemotactic sensors and establish cell directionality with protruding
lamellipodia. Focal adhesions provide anchorage to the ECM with filament-mediated
contraction. Tail retraction and disassembling of adhesions complete the cycle.

1.2.3.3.2   Key signalling proteins

It is evident that spatial orchestration of signalling proteins is critical in mediating the dynamics of cell motility. In multiple cell types, it has been shown that there is local accumulation of proteins expressing plekstrin homology (PH) domains, which bind membrane phosphoinositides, notably phosphatidylinositol (3,4,5)-triphosphate (PIP3), at the leading edge of cells [105]. This in turn can activate guanine nucleotide exchange factors (GEFs) such as Vav [106] and SOS [107], which are implicated in spatial activation of the Rho family of guanosine triphosphate (GTP)ases. This family of proteins, which includes the Rac subfamily and Cdc42, provide critical regulation of all cellular processes involved in the cytoskeletal remodelling and dynamics that results in motility [108]. Rho GTPases switch between an inactive GDP-bound state, which is sequestered and cytosolic, and an active GTP-bound conformation which can be targeted to cell surfaces by post-translational modifications [109].

Activated Cdc42 interacts specifically with Wiskott-Aldrich-syndrome protein (WASP), and its family member N-WASP [110]. It then mediates activation of the Arp2/3 complex which directly promotes branching of actin filaments [111]. Two other proteins known to bind and activate Arp2/3 are cortactin and Abp1, and have been putatively suggested as actin network stabilisers [112]. Other implicated proteins include α-actinin and filamin. Indeed, filamin is able to associate with signalling proteins such as Rho GTPases through its C-terminal domain, and may therefore additionally provide a docking site for signal interactions in close vicinity [113]. Arp2/3 activation also occurs indirectly through Rac. This is mediated via a member of the

WASP family, suppressor of cAMP receptor (Scar)/WAVE, which itself is activated by adapter protein Irsp53 in response to Rac [114].

More recently, a direct interaction between Irsp53 and Cdc42 has been determined, occurring through a partial Cdc42/Rac interactive binding (CRIB) motif [115]. This can bind the Ena/vasodilator-stimulated phoshoprotein (VASP)-family protein Mena and initiate filopodia formation, hence providing an Arp2/3-independent mechanism. Both Cdc42 and Rac can activate the serine/threonine p21-activated kinase (PAK) family, by disrupting its autoinhibitory conformation [116]. These engage in multiple downstream effects. Notably, expression and activation of myosin light chain (MLC) is enhanced which is deemed vital for cell adhesion and anchorage [117]. In addition, phosphorylation of Lim kinases (LIMK) can inhibit the depolymerising activity of cofilin and hence regulate turnover in the lamellipodium [118]. Production of serine/threonine Rho-stimulated kinases (ROCK) via phosphoinositide-3-kinase (PI3K) signalling can have potentiating effects via MLC and LIMK phosphorylation [119]. ROCK also plays a role in the assembling of focal adhesions, by activating focal adhesion kinase (FAK). This is additionally activated by integrin receptor/ECM interactions, and functions as an adapter protein to recruit proteins such as talin, paxillin and p130^{Cas} which allow anchorage of actin filaments [120].

Directional cell migration also involves reorientation of the Golgi towards the leading edge, with GOLPH3 implicated as a potential effector of phosphatidylinositol 4-phosphate (PtdIns(4)P) that bridges the organelle with the actin cytoskeleton to enable effective trafficking [121]. Consistent with this notion, GOLPH3 overexpression has been reported to augment cell migration [122]. Beyond the crucial roles of the

signalling proteins highlighted above, it is apparent that nitric oxide (NO) is a strong regulator. There is early upregulation of NO in endothelial cells activated by VEGF [123], and specific inhibition of NO abrogates its chemotactic effects [124]. Moreover, in bovine lung endothelial cells, administration of NO appears to augment migratory capacity in response to VEGF exposure [125].

1.2.3.4   Vasculogenesis

The cardiovascular system constitutes the first functional organ in the embryo, with *de novo* vessel formation arising from mesenchymal precursors, defined as angioblasts [126]. These assemble as vascular cords prior to differentiation into endothelial cells. One important distinction between vessels is that of arteries and veins, which is determined by pathways specifying identity. In particular, the Notch pathway is upregulated in arteries and suppressed in veins, even prior to the onset of flow [127]. In zebrafish, Sonic Hedgehog upregulates VEGF which in turn elevates Notch components [128]. Transcriptional factors such as FOXC1 and FOXC2 also drive arterial specification by interacting with Notch and VEGF signalling. It was initially postulated that the venous fate occurred by default, but it is now apparent that active regression of Notch signalling is required by the nuclear receptor COUP-TFII [129]. Crucially, the process of arterial-venous differentiation has distinct phenotypic plasticity, as evidenced by endothelial cell differentiation in the developing embryo, neonatal retina and the adult heart [130].

1.2.3.5 Angiogenesis

ECM proteins form a layer around endothelial cells defined as the basement membrane [131]. Its composition must be altered with proteolytic breakdown to initiate cell migration and onset of vessel sprouting. This is mediated by activation of proteinases, such as MMP's, plasminogen activators and tryptases, and angiopoietin-2 (Ang-2)-stimulated detachment of mural cells [132]. These processes also liberate matrix-bound VEGF and activate pro-angiogenic chemokines such as IL-1β. A critical balance is important for effective sprouting, as excessive ECM degradation may result in a lack of matrix support for branch development [133].

Subsequent endothelial cell specification into tip and stalk cells occurs, mediated predominantly by the Notch pathway. In utero blockade of Notch increases tip cell formation, indicating that this phenotype is the default response to pro-angiogenic signals such as VEGF [134]. Endothelial cells at the angiogenic front use tip cells and their emerging filopodia to migrate along the VEGF gradient, with expression of guidance receptors such as ROBO4, UNC5B, PLEXIN-D1 and semaphorins to probe the environment [76]. These are followed by a column of stalk cells which, in comparison with tip cells, have lower abundance of filopodia but much greater proliferative capacity and can form a vascular lumen [135]. Notch signalling is deemed critical for stalk cell specification. Dynamic shuffling of tip-stalk cell position occurs at the angiogenic front with regular exchange, dependent upon Notch/Dll4 signalling in response to VEGF [136]. Moreover, tip and stalk cells ought not to be considered as defined cell fates because dynamic transition between the phenotypes is required to enable sequential cycles of elongation and branching [137].

Lumen formation occurs through different mechanisms [138]. There appears to be coalescence of intracellular vacuoles which associates with those in adjacent cells in a process termed 'cell hollowing'. However, contemporary studies also implicate direct alterations of cell morphology, driven by VEGF and ROCK, that rearrange the actin cytoskeleton and adherens junctions to create a vascular lumen ('cord hollowing'). Direct interactions between adherens junctions on adjacent tip cells ('fusion') expands the network, promoted by macrophage activity though not a pre-requisite [139]. Lumen extension results in the initiation of blood flow, which remodels connections. In zebrafish, shear stress results in upregulation of miR-126 to modulate PI3K and mitogen-activated protein kinase (MAPK) signalling [140]. This stage reflects the formation of a primitive vascular labyrinth, akin to P5 in a mouse retina.

It is evident that insulin-dependent PI3K/AKT signalling contributes towards VEGF expression. This may be partially mediated by upregulation of hypoxia-inducible factor (HIF)-1α suggestive of overlapping expression profiles in response to both insulin and hypoxia [141]. Diabetic mice appear to have inhibited HIF-1α activity and VEGF production in response to soft tissue ischaemia [142]. Nanoparticle-mediated delivery of the insulin sensitizer pioglitazone augments VEGF-mediated neovascularisation in a murine model of hindlimb ischaemia [143]. Significantly, however, insulin-resistant disorders in humans are broadly associated with elevated basal VEGF concentrations, potentially suggestive of 'VEGF resistance' [144]. This may reflect downstream signalling defects or inadequate resolution of underlying hypoxic drive due to poor neovessel quality.

1.2.3.6   Arteriogenesis

Subsequent remodelling of the vascular plexus results in a complex, hierarchical network of arteries, veins and capillaries and maturation from nascent into durable vessels. This roughly correlates with P18 of a mouse retina. The Eph-Ephrin system is critical in establishing demarcation, with EphrinB2 as a marker for arterial endothelial cells and VSMCs, and EphB4 for veins [145]. Indeed, EphrinB2 expression also extends into capillaries midway between terminal arterioles and post-capillary venules. The system also contributes to the formation of arteriovenous anastomoses by arresting cell migration at the interface.

Stability is conferred by deposition of ECM components into the basement membrane, and recruitment of mural cells. Pericytes confer direct cell-cell contact with endothelial cells in capillaries and immature vessels, whilst VSMCs envelop arteries and veins [146]. TGF-β signalling enables mural cell differentiation, migration and proliferation [147]. Indeed, mice with TGF-β knockdown demonstrate impaired vascular morphogenesis resulting from defects in mural cell development. Signalling via the PDGF-β pathway also plays a role by recruiting mesenchymal progenitors. Embryonic deficiency in PDGF-β results in bleeding, vessel fragility and enlargement [148]. Components derived from mural cells, such as angiopoietin-1 (Ang-1), can additionally activate the endothelial receptor Tie-2, which promotes endothelial quiescence and maturation of intercellular junctions [149]. FGF signalling mediates adhesion of adherens junctions to preserve vascular integrity [150]. Notch signalling also has regulatory effects, with Notch3 gene mutations in humans causing VSMC

degeneration and the clinical disorder termed cerebral autosomal dominant arteriopathy with subcortical infarcts and leukoencephalopathy (CADASIL) [151].

Once maturation has adequately progressed, oxygen and nutrient delivery reduces VEGF expression and a transition towards a quiescent phenotype. Endothelial cells also adopt a survival phenotype to preserve integrity of the vessel lining. Intracrine VEGF activity is particularly implicated through influences on the PI3K/AKT pathway. Endothelium-specific deficiency of VEGF in mice results in bleeding, vascular rupture and microinfarcts [152]. Established blood flow and its accompanying shear stress can have direct anti-apoptotic effects. This involves KLF2-mediated upregulation of eNOS and the anti-coagulant thrombomodulin, which preserves vessel dilatation and clot disintegration [153]. Flow may equally determine conditional regression of neovessels in the context of non-perfusion, as a physiological mechanism of perfusion-demand matching. Disruption of interactions between endothelial cells and pericytes also heightens propensity for regression [154].

1.2.3.7   Collateral growth

Distal capillaries enable local flow to individual cells whilst proximal arterioles determine bulk perfusion of large tissue regions. In the context of arterial or arteriolar occlusion with accompanying ischaemia, pre-existent collaterals can mature and expand into an extensive network via angiogenesis and arteriogenesis ('collateral growth') to improve perfusion to the depleted region. Hypoxia is the principal stimulus, through HIFs which upregulate pro-angiogenic genes such as VEGF [155]. The process involves shear stress-mediated activation of endothelial cells and

recruitment of leukocyte subsets, such as monocytes, that produce proteinases to facilitate VSMC migration and proliferation. Consistent with this, pro-inflammatory cytokines such as TNF-α have been shown to positively modulate arteriogenesis [156] whilst depletion of monocytes was functionally associated with impaired growth [157].

1.3 Insulin signalling in health

1.3.1 Overview

The insulin/insulin like growth factor (IGF-1) system is crucial for nutrient homeostasis, particularly coordination of systemic glucose metabolism. In addition to tissues directly involved in metabolism, such as skeletal muscle, liver and adipose tissue, insulin receptors are also expressed in vascular tissue, cardiac myocytes, leukocytes and human bone marrow-derived stem cells. Insulin therefore has diverse effects on metabolism and cardiovascular homeostasis. Insulin signalling is initiated by intrinsic receptor tyrosine kinase (RTK) activity of the ligand-bound insulin receptor, and orchestrates a complex, highly integrated cascade of downstream signalling events, particularly via the PI3K/AKT and Grb2/MAPK pathways.

1.3.2 Historical perspective

The first postulation that a substance released by the pancreas might be involved in metabolic homeostasis was in 1889, by German scientists Minkowski and von Mering. This was based on laboratory studies in dogs where total pancreatic resections resulted in onset of severe DM [158]. In 1921, insulin was isolated in purified form by

Banting, a surgeon from Toronto, Canada [159]. They administered saline preparations of pancreas to dogs via intravenous injection and noted a discernible lowering of blood glucose. In the subsequent year, experiments were extended to human subjects with marked findings. Banting was a subsequent recipient of the Nobel Prize in 1923 for his work.

1.3.3   Synthesis, release and regulation

The gene encoding insulin is located on the short arm of chromosome 11, and is synthesised in the pancreatic β-cells of the islets of Langerhans as its precursor, proinsulin [160]. Vesicles transport pro-insulin to the Golgi apparatus of these cells, where the abundance of calcium and zinc enables formation of soluble, pro-insulin hexamers [161]. Cytoplasmic enzymes subsequently convert pro-insulin into insulin and C-peptide. These insoluble products are secreted into the circulation by exocytosis. As with other hormones, secretion can be manipulated by changes in synthesis due to transcriptional, translation and post-translational modifications in the Golgi apparatus. Chronic alterations in insulin release may occur through changes in β-cell mass and differentiation [162].

Glucose is the principle stimulus for insulin release. However, other nutrient secretagogues including amino acids and fatty acids are also implicated. Hormones such as glucagon and glucagon-like peptide-1 (GLP-1) can act as mediators, in addition to regulation from neural stimuli via cholinergic and adrenergic pathways [163]. In normal health, insulin secretion is typically biphasic. The initial rapid phase relates to release of insulin stored in secretory granules, whilst the second phase represents

both stored and newly synthesised insulin [164]. It is evident that complex, pleiotropic processes form regulatory feedback loops which preserve homeostasis in normal physiology [165].

1.3.4 Physiological effects

1.3.4.1 Metabolism

Insulin is the primary hormone which regulates macronutrient balance and coordinates this with cellular energy metabolism [166]. Insulin is critical for the non-constitutive membrane transit of glucose, which is mediated via ATP-independent glucose transporter (GLUT) proteins. There are five subtypes, which enables heterogeneity in response of cell types according to function [167]. GLUT4 is the transporter implicated for responses to insulin in dependent metabolic tissues such as the liver, skeletal muscle and adipose tissue, and is transported to cell membranes as a result of insulin-stimulated PI3K/AKT signalling. In the fed state, it has overall anabolic effects in muscle. This occurs through promotion of glycogen and lipid synthesis, whilst suppressing hepatic gluconeogenesis and lipolysis. Uptake into adipose tissue constitutes approximately 10% of the total mediated by insulin stimulation [168]. In comparison, uptake into hepatocytes is not insulin-dependent, yet it determines 30% of whole-body glucose availability in tissues.

1.3.4.2 Haemodynamics

Beyond classical metabolic tissues, the insulin receptor is also expressed in vascular tissue (endothelium and VSMC), cardiac myocytes, monocytes, granulocytes and

human bone marrow-derived stem cells [169]. This can result in diverse effects on the cardiovascular system.

Signalling in the endothelium can produce an array of vascular responses which, in healthy conditions, help to augment tissue perfusion during periods of glucose disposal. Vasodilatory effects are mediated by insulin-dependent release of NO [170], through heterogeneous mechanisms occurring in distinct stages. Within a few minutes, dilatation of terminal arterioles enhances capillary recruitment but without concomitant alterations in total blood flow [171]. Subsequent increases in total blood flow are mediated by dilatation of larger resistance vessels, and is maximal at 2 hours. This has been demonstrated in skeletal muscle in humans at both physiological (100-500pM) [172] and supraphysiological [173] insulin concentrations.

In addition to vasodilatory effects, insulin also induces opposing vasoconstriction. This is governed principally by sympathetic activation, presumed α-adrenergic, and has been demonstrated in rats [174] and humans [175]. The synthesis and release of endothelin-1 (ET-1) from the endothelium is also implicated, via MAPK signalling. In VENIRKO mice with endothelium-specific deletion of the insulin receptor, expression of eNOS and ET-1 is reduced and steady state blood pressure appears lower on both low- and high-salt diets [176]. Results from assessment of plasma ET-1 levels in humans appear ambiguous, but as a paracrine factor, the local concentrations may be more functionally relevant. In support of this proposition, insulin-mediated vasodilation is amplified in the context of ET-1 receptor blockade in humans [177].

These opposing forces result in negligible, overall effects on systemic blood pressure in the context of health [178]. Insulin is also known to have effects on nephrons, by promoting sodium retention in the distal convoluted tubules. This has been observed in healthy individuals [179] and in patients with DM [180]. However, these effects are small and there is resultant, secondary natriuresis consequent to enhanced renal perfusion [181]. Hence, it is unlikely that the renal action of insulin plays a substantial role in modulation of blood pressure.

It is more firmly apparent, however, that a critical regulation appears to exist between vasoconstrictor and vasodilator actions as a result of insulin signalling. Indeed, a transition in this balance may be important in promoting endothelial dysfunction associated with systemic insulin resistance.

1.3.4.3   Coupling of metabolic and haemodynamic physiology

Insulin appears to be crucial in effective coupling of metabolic and haemodynamic physiology. Endothelial signalling mediates capillary recruitment and increased total blood flow, as described above. This enhanced perfusion facilitates the delivery and disposal of substrates, namely insulin and glucose, to metabolic tissues. In humans, there appears to be a dose-dependent response between insulin, glucose mobilisation and skeletal muscle blood flow [182]. This appears to be mediated by NO, as trends are abrogated in the context of NG-monomethyl-L-arginine (NMMA), a competitive eNOS inhibitor [183]. There is also increasing evidence that myocardial blood flow is enhanced in response to insulin. In healthy subjects, it has been shown that there are

regional variations in perfusion that are associated with the extent of glucose uptake [184].

1.3.5 Insulin signalling cascade

1.3.5.1 Insulin receptor

The gene encoding the insulin receptor is located on the short arm of chromosome 19 [163]. The protein structure is a hetrotetramer consisting of two extracellular α and two transmembrane β glycoprotein subunits linked by disulphide bonds [185]. It constitutes a subfamily of RTK, which also includes the highly homologous IGF-1 receptor [186]. Hybrid complexes involving the insulin receptor and IGF-1 receptor also exist.

An overview of insulin signalling cascades is provided in Figure 1-5. Binding of its substrate, insulin, to the α subunit of the receptor results in a conformational change of the β subunit and allows binding of ATP (adenosine triphosphate) [185]. This facilitates autophosphorylation, conferring tyrosine kinase activity. In view of its potential for profound and diverse metabolic sequelae, stringent regulation of the activity of the insulin receptor is required. This is achieved, in part, by the existence of two splice isoforms, either with or without exon 11 [187]. These have differential expression patterns in tissues and differing affinities for insulin and IGF-1 [188]. Control of activity is also achieved by negative regulators. One such class are tyrosine phosphatases, particularly protein tyrosine phosphatase 1B (PTP1B). *In vivo* models with PTP1B knockout demonstrate enhanced insulin signalling [189]. Other proteins, such as suppressor of cytokine signalling-1 (SOCS-1) and growth-factor-receptor-

bound protein 10 (Grb10), regulate function by modifying intrinsic kinase activity or binding to downstream targets [190]. Additionally, downregulation via ligand-mediated receptor internalisation is a feature of the majority of insulin-resistant states, including DM [191].

1.3.5.2   Insulin-receptor substrates (IRS)

In contrast to many other RTKs, insulin and IGF1 receptors directly recruit specialised adaptor proteins. These become tyrosine phosphorylated in response to receptor activation, but also allow diverse negative regulatory mechanisms to occur [192]. These are collectively termed insulin receptor substrates (IRS), and there are six identified isoforms, IRS1-6 [193]. Out of these, IRS1 and IRS2 are the most ubiquitously expressed [194, 195]. Their localisation in proximity to the insulin receptor is determined by the PH and phosphotyrosine-binding (PTB) domains at the N terminus. The central and C terminus regions of IRS contain multiple tyrosine phosphorylation sites which, once activated, bind to 'docking' proteins containing Src-homology-2 (SH2) domains. In broad terms, proteins bearing SH2 domains can be subdivided into two classes: SH2 enzymes such as PI3K, and SH2 adaptor proteins such as growth factor receptor-bound protein 2 (Grb2). In the case of the latter, there is no intrinsic activity but instead, signal transmission is by direct protein-protein interactions [196]. The two most important mediators are PI3K and Grb2, so downstream signalling cascades for both shall now be discussed.

1.3.5.3   PI3K/AKT pathway

PI3Ks can be classified according to sequence homology and substrate affinity into three broad classes, I-III [197]. Relatively little is known about classes II and III, though the latter is implicated in the regulation of vesicle trafficking [198]. Class I PI3Ks have been more extensively studied. Class I can be subdivided into IA, which are activated by RTK, and IB which instead are modulated by G-protein-coupled receptors (GPCR). Both are involved in the regulation of cell polarity and motility through effects on cytoskeletal dynamics via activation of the Rho family of GTPases (see Section 1.2.3.3.2) [89]. Class IA PI3K are most strongly implicated in downstream insulin signalling. The protein is a heterodimer, and composed of a p85 regulatory unit (85 kDa), stoichiometrically in excess, which provides basal allosteric inhibition of a p110 catalytic unit (110 kDa). The regulatory component is flanked by two SH2 domains, which can bind to phosphorylated residues on adapter proteins such as IRS [199]. This binding results in conformational changes that reverse basal inhibition. It also recruits the complex to the plasma membrane where it is in close proximity to its substrate, phosphatidylinositol 4,5-bisphosphate (PtdIns(4,5)P2), which becomes phosphorylated on the 3' position of the inositol ring into phosphatidylinositol (3,4,5)-triphosphate (PIP3) [200]. This is a lipid secondary messenger that is able to activate multiple downstream cascades by binding to proteins that manifest specific PH domains [201].

Two PH-bearing proteins of particular relevance are phosphoinositide-dependent kinase (PDK) 1/2 and AKT, also termed protein kinase B (PKB). AKT is a serine/threonine kinase that mediates the predominant metabolic effects of insulin, and is hence deemed as a critical regulatory node in signalling [193]. Three isoforms

exist in mammals, AKT1-3, each encoded by a different gene. AKT2 is specifically enriched in insulin-sensitive tissue and is the isoform most strongly implicated in metabolic pathology [202]. Specificity of action for the different isoforms is dependent upon temporal and spatial segregation in addition to downstream targets. Recruitment to the cell membrane by PIP3 enables phosphorylation of AKT by PDK 1/2 at the threonine 308 residue. However, a second phosphorylation at the serine 473 residue of AKT is required for full activation, and this appears to be mediated by a complex of mTOR and rapamycin-insensitive companion of mTOR (RICTOR) through poorly defined mechanisms [203]. Direct, negative regulators of AKT include the enzymes phosphatase-2A (PP2A) and PH-domain leucine-rich-repeat protein phosphatase (PHLPP) [204].

Activated AKT has multiple downstream targets which allows regulation of an array of cellular functions. In metabolic tissues, it results in phosphorylation and inhibition of the Rab-GTPase-activating protein, AS160 [205]. This precipitates alterations in actin dynamics required for the translocation of cytosolic glucose transporter protein 4 (GLUT4)-containing vesicles to the plasma membrane, which directly facilitates glucose uptake into cells [206]. GLUT1 transporters are also implicated in glucose metabolism, but in contrast, they are not located intracellularly. Hence, they are not translocated in response to insulin, and are instead involved in basal glucose uptake [207]. AKT also promotes glycogenesis through inhibition of glycogen synthase kinase 3 (GSK3) [208] and synthesis of fatty acids through activatory effects on ATP citrate lyase (ATP-CL) [209]. Enhanced protein synthesis occurs through mobilisation of the

stoichiometric mTOR-RICTOR complex and resultant phosphorylation of eukaryotic translation initiation factor 4E-binding protein (4E-BP1) [210].

In addition to metabolic regulation, activated AKT has a critical role in vascular homeostasis. In endothelial cells, it causes direct phosphorylation of eNOS at its serine 1177 residue, enhancing calcium-induced activation and production of NO [211]. This is an independent pathway from eNOS activation mediated by calcium signalling in response to shear stress and other modulators such as acetylcholine, serotonin and bradykinin [212], although a certain degree of pathway convergence exists [213]. AKT is also imperative in promotion of cell survival and cell cycle progression. Cell cycle transition is achieved by inhibition of the forkhead family of transcription factors (FOXO), retinoblasma-like 2 (RBL2) and p27Kip1 [214]. Its pro-survival effects occurs through inhibition of FOXO-mediated transcription of proteins such as BCL2-like 11 (Bim) and Fas-ligand (FasL), which are pro-apoptotic [215].

1.3.5.4   Grb2/MAPK pathway

Whilst the PI3K pathway broadly relate to metabolic and vascular function, the Grb2/MAPK pathway predominantly mediates insulin's mitogenic effects [185]. Grb2 binds to phosphorylated IRS or Shc, which are both activated in response to insulin binding to its receptor. Bound Grb2 enables recruitment of the guanine nucleotide-exchange factor son-of-sevenless (SOS) followed by downstream activation of the GTPase Ras and subsequently Raf. A cascade of signalling events results in the phosphorylation of the dual specificity kinases MEK (and ERK) 1/2 (MAPK) on threonine and tyrosine residues. Activated ERK can phosphorylate a range of cellular

targets, which includes the transcription factor ELK1 and p90 ribosomal protein S6 kinase (p90RSK), both implicated in gene expression, cellular differentiation and mitogenesis [216]. Moreover, there is promotion of the expression of adhesion markers on endothelial cells which enables leucocyte recruitment. Signalling potentiates the release of ET-1 which has potent vasoconstrictor and potentially pro-atherogenic effects [217]. ET-1 can also directly increase IRS-1 phosphorylation leading to impaired PI3K signalling in VSMCs [218], and has been found to impair GLUT4 translocation in adipocytes [219]. ERK is also involved in negative regulatory feedback loops by direct, inhibitory phosphorylation of IRS1 on serine residues [220].
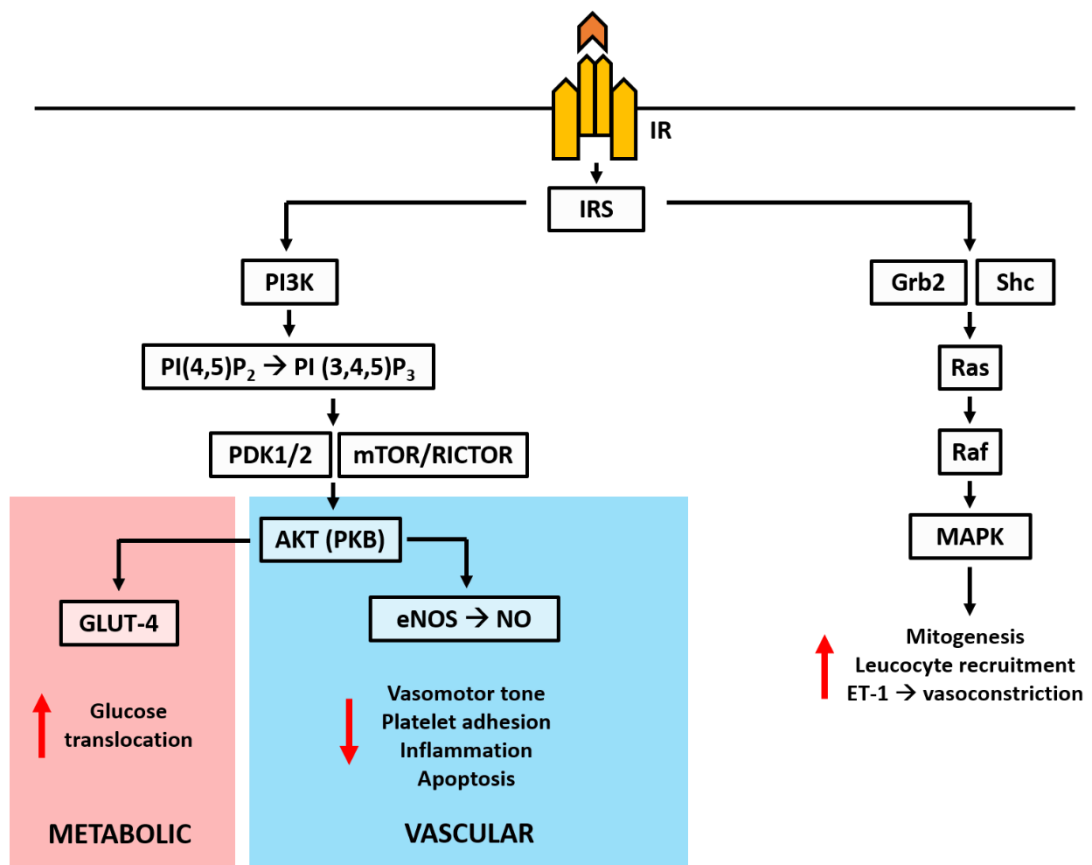
Figure 1-5 – Insulin signalling cascades.

Activatory autophosphorylation of the insulin receptor in response to ligand binding recruits IRS. Subsequent activation of the PI3K/AKT pathway enables tissue-specific effects on glucose translocation and NO synthesis, whilst Grb2/MAPK pathway activation has broad mitogenic effects.

1.3.5.5 Complexity of the signalling network

The pathways described above provide a linear description of the signalling cascades involved in insulin responses. However, the process involves considerable intricacy and complexity, due in substantial part to a multitude of inter-related pathways with positive and negative feedback communication [221]. As mentioned, the insulin receptor itself has two isoforms with functional heterogeneity. There are at least six IRS proteins, which all have the capacity to interact with a plethora of targets, including eight forms of the PI3K regulatory subunit and three known subclasses of the catalytic unit. Activation of AKT as a consequence of PIP3 production can itself result in one of three potential isoforms, with divergent functions. Further critical regulation of this expansive network is achieved through extensive cross-talk between pathways and intracellular localisation of signalling targets.

1.4 Insulin signalling in disease

1.4.1 Overview

Insulin resistance is a critical pathophysiological determinant of the metabolic and vascular dysregulation implicated across the spectrum of dysglycaemia. Systemic components are encompassed by the 'metabolic syndrome', a clustering of factors such as hyperglycaemia, dyslipidaemia, inflammation and oxidative stress that are

associated with obesity. The presence of insulin receptors in many non-metabolic cells, such as vascular endothelium and leukocytes, suggests that cellular insulin resistance may directly contribute to the progression of diabetic vascular disease independent of systemic metabolic perturbations. Moreover, these systemic and cellular changes caused by insulin resistance may interfere with endogenous vascular repair and regeneration (see Figure 1-6).
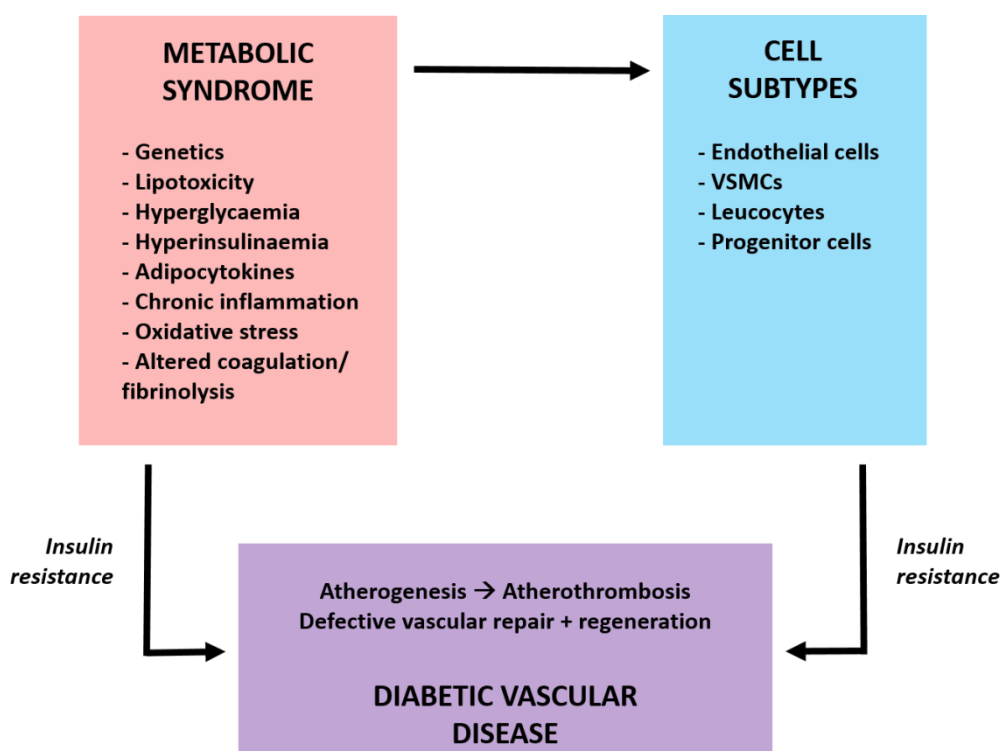
Figure 1-6 – **Interplay between systemic components and cell subtypes in diabetic vascular disease.**

There are multiple systemic components depicted in the metabolic syndrome. In combination with cellular insulin resistance, these are implicated in progression of atherogenesis as well as contributing towards defective endogenous repair and regeneration.

1.4.2 Genetic predisposition

Insulin resistance can be broadly defined as a loss of the normal temporo-spatial signalling cascades activated by the binding of insulin to its receptor. At a molecular level, direct mutations of the insulin receptor are not commonly implicated in insulin resistance within populations [222]. Resistance can occur secondary to IRS-1 polymorphisms with increased serine phosphorylation [223]. This causes direct inhibition of tyrosine phosphorylation, and a subsequent suppression of downstream PI3K-mediated signalling. In humans, rare mutations within the YMXM motif of the IRS-1 gene are associated with insulin resistance [224]. In mice, homozygous deletion results in a mild, resistant phenotype [225]. Polymorphisms of the regulatory p85 subunit appears to affect glucose homeostasis, though an association with DM has not yet been established [226]. Nonetheless, polygenic influences are likely to be important considering the significant heritable component of insulin resistance and DM [227].

1.4.3 Systemic insulin resistance

1.4.3.1 The metabolic syndrome

Perhaps the most significant contributors to systemic insulin resistance are environmental influences. The 'metabolic syndrome' describes the aggregation of factors, promoted by obesity, and insulin resistance [228]. They characterise the broader metabolic and vascular dysregulation that develops in the natural history of DM, including pre-diabetes, and collectively have pro-atherosclerotic effects. Whilst various diagnostic criteria exist, these generally describe the co-existence of central obesity, dysglycaemia, dyslipidaemia and hypertension, although broader descriptions

also include factors such as inflammation, oxidative stress and pro-thrombotic

tendency (see Figure 1-7). Although the incremental value of the syndrome beyond its

constituent parts has been questioned, it serves as an important reminder that insulin

resistance is a unifying driver of pro-atherogenic phenomena.
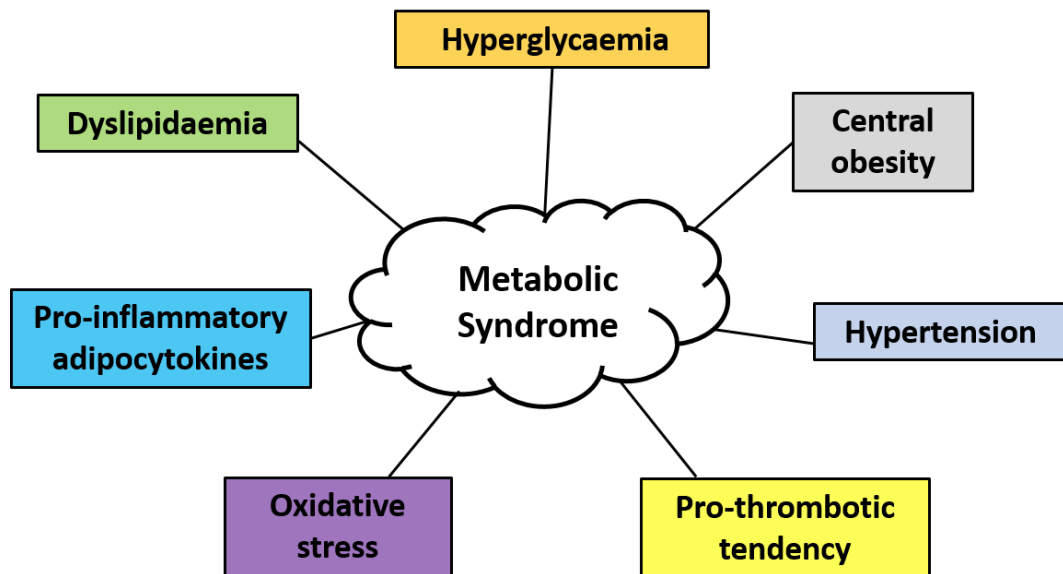
Figure 1-7 – **Components of the metabolic syndrome**.
Adapted from Cubbon *et al*. Curr Vasc Pharmacol 2012; 10(3):271-84 [229].

There is a clustering of risk factors that are promoted by obesity and characterise the broader
metabolic and vascular dysregulation implicated in the natural history of DM.

1.4.3.2   Hyperglycaemia

In the context of insulin resistance, the earliest change that develops in the

myocardium in animal models is impaired glucose uptake [230]. This relates to

reductions in GLUT4 protein expression and translocation, and interestingly precedes

detectable defects in PI3K signalling. This has also been corroborated in skeletal

muscle biopsies from people with DM [231]. Hyperglycaemia itself, however, can potentiate insulin resistance. It can result in the formation of advanced glycation end products (AGE) [232]. This can cause serine phosphorylation of docking proteins such as IRS-1 and IRS-2, with inhibiting downstream signalling as described above. By binding of AGE to specific receptors termed RAGEs, there is also Nox2-mediated promotion of vascular oxidative stress (see Section 1.4.3.5) [233]. Reactive oxygen species (ROS) create a pro-inflammatory milieu, through activation of transcription factor nuclear factor kappa-light-chain-enhancer of activated B cells (NF-κB). Shunting of excess intracellular glucose through the hexosamine biosynthesis pathway results in modification of proteins, such as AKT, via O-linked N-acetylglucosamine (O-GlcNAcylation). This is associated with increased vascular calcification in the context of DM [234]. Hyperglycaemia also activates protein kinase C (PKC) which augments monocyte recruitment, foam cell formation and promotes switching to a synthetic VSMC phenotype which enables cell migration and proliferation [235]. Consistent with this observation, atherosclerosis-prone mice with genetic deletion of PKC display reduced atherosclerosis [236].

A significant elevation of AGE has been found in patients with type II DM compared to healthy and type I DM patients [237]. Moreover, their abundance appears to be increased in patients with DM and coronary disease compared to those without coronary disease [238]. Glycated haemoglobin (HbA1c) levels appear to correlate with AGE, and pharmacotherapy with agents that lower blood glucose and AGE is associated with reductions in microvascular sequelae such as nephropathy and

retinopathy. However, no similar associations have yet been observed in the context of macrovascular disease [239].

1.4.3.3   Dyslipidaemia

As alluded to previously, the dyslipidaemic profile precipitated by obesity and characteristic of the metabolic syndrome comprises elevated triglycerides, low HDL and small, dense LDL [23]. Triglycerides are the source of excess free fatty acids (FFA) which can result in lipotoxicity through various mechanisms. In skeletal muscle, they appear to induce mitochrondrial dysfunction, resulting in reduced FFA oxidation and mitochondrial superoxide generation [240]. The subsequent increase in levels of intracellular metabolites, including fatty acyl coenzyme A (CoA) and diacylglycerol, promotes novel PKC and inhibitory phosphorylation of IRS-1 leading to insulin resistance. Concurrently, mitochondrial dysfunction further promotes an oxidative environment through activation of nicotinamide adenine dinucleotide phosphate (NADPH) oxidases (see Section 1.4.3.5.2) [241]. Furthermore, this is associated with dysregulated adipocytokine production, and activation of pro-inflammatory cascades that are directly implicated in insulin resistance (see below) [242]. Lastly, ceramide is a derivative of saturated FFAs. Increased levels have been found in skeletal muscle of human subjects with obesity [243], and it appears to directly inhibit AKT signalling and GLUT4-mediated glucose translocation in response to insulin stimulation [244]. It has also been shown to contribute to oxidised LDL-induced calcification of human VSMCs, a feature of advanced atherosclerosis [245].

1.4.3.4   Pro-inflammatory adipocytokines

Chronic inflammation is an important driver of atherosclerosis [246]. As discussed, it is intrinsically coupled with the lipotoxicity and glucotoxicity of the metabolic syndrome and aggravated by oxidative stress (see Section 1.4.3.5). Dysfunctional visceral adipose depots are a particularly important contributor of systemic inflammation, due to altered adipocytokine (or adipokine) secretion profiles. Adipokines are a diverse group of cytokines derived from adipose tissue, and include interleukin (IL)-1β, IL-6, tumour necrosis factor (TNF)-α, adiponectin, leptin and visfatin, amongst many others [247]. Their impact extends beyond adipose tissue biology and wider metabolic homeostasis, with direct effects on vascular function also being apparent.

TNF-α activates various serine kinases, including c-Jun N-terminal kinases (JNK) and inhibitor of nuclear factor kappa-B kinase subunit beta (IKKβ), which results in inhibitory phosphorylation of IRS-1 and IRS-2 [248]. The expression of SOCS-3 is also enhanced, which antagonises the interactions between insulin receptor and IRS and facilitates proteasomal degradation of the latter [249]. Consistent with the role of chronic inflammation in insulin resistance, elevated levels of the inflammatory marker C-reactive protein (CRP), whose expression is promoted by TNF-α, has been identified as a potential risk factor in diabetogenesis [250].

Adiponectin is generally less abundant in insulin-resistant states. It is broadly considered as an anti-inflammatory cytokine, and appears to suppress atherosclerotic burden in apolipoprotein E-deficient mice [251]. Levels also appear to be inversely predictive of coronary plaque calcification and fibrous cap vulnerability [252] [253]. Leptin circulates at greater concentrations in those with insulin resistance and is an

independent predictor of acute cardiovascular events and early in-stent re-stenosis

[254]. Visfatin has similarly been suggested as an indicator of plaque burden, and

correlates with markers of myocardial necrosis in the context of ST-elevation

myocardial infarction (STEMI) [255].

1.4.3.5   Oxidative stress

Oxidative stress plays an instrumental role in amplifying the downstream effects that

occur through constellation of the above stressors, with modulatory roles in the

context of lipotoxicity, hyperglycaemia and pro-inflammatory adipocytokines. In view

of this, it is worthwhile exploring the concept of oxidative stress in further detail.

1.4.3.5.1   ROS metabolism

'Oxidative stress' refers to a disrupted spatio-temoral balance between production of

oxidants, in particular ROS, and their scavenging by anti-oxidant defences [256]. This

results in detrimental modification of lipids, proteins and nucleic acids. ROS

encompasses highly reactive derivatives of oxygen (O_2). They can be loosely

categorised into free radicals, such as superoxide (O_2^-) and peroxynitrite ($ONOO^-$), and

non-radicals such as hydrogen peroxide (H_2O_2) and ozone (O_3) [257]. An overview of

ROS synthesis and metabolism is depicted in Figure 1-8. Formation may occur through

dysfunctional mitochondrial respiration and uncoupled eNOS activity, arising from

depleted cofactors or direct enzymatic modification. Moreover, membrane-bound

enzymes such as NADPH oxidases (NOX) are particularly implicated within the

vasculature (explored below). The breakdown of O_2^- depends upon the activity of

superoxide dismutase (SOD), which results in the formation of H_2O_2 [257]. H_2O_2 is further degraded into water (H_2O) and O_2 by the actions of catalase and glutathione peroxidase.
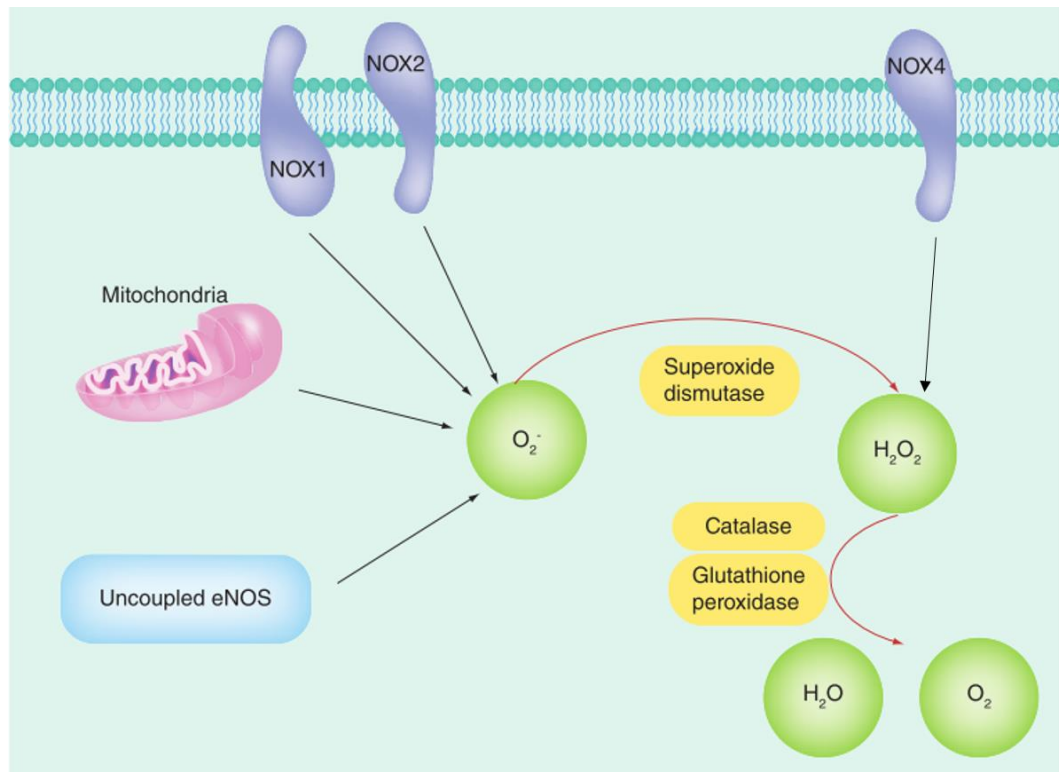
Figure 1-8 – **ROS synthesis and metabolism**.
Adapted from Ali *et al*. Diabetes Management 2015; 5(3):203-13 [258].

Formation of superoxide occurs via membrane-bound NOX enzymes, mitochondrial activity and uncoupled eNOS. The action of SOD results in breakdown of superoxide into hydrogen peroxide, which undergoes further degradation.

1.4.3.5.2   NADPH oxidases

There are currently five known homologues of the NOX enzyme (NOX1-5) [259]. Nox2 is the most strongly expressed isoform in the vasculature [260], and primarily

produces O_2^-. It was first isolated from phagocytes where it was shown to produce a 'respiratory burst' of ROS to enable the anti-microbial response [261]. Its activity is dependent upon a catalytic subunit (gp91phox), whose function is also reliant on binding of various cytosolic components such as p40phox, p47phox and Rac [262]. Nox1 has structural homology with Nox2 and also results in O_2^- production. It is present in the vascular wall but most strongly expressed in colonic epithelium [263]. In contrast, the primary product of Nox4 activity is H_2O_2 and it appears to be constitutively active [262]. Although Nox5 has demonstrable expression in human vasculature, it does not appear to be present in rodents [264].

1.4.3.5.3   Redox signalling

All NOX isoforms produce ROS by transferring electrons from NADPH to molecular oxygen, a phenomenon termed 'electron transfer' [265]. O_2^- and H_2O_2 are relatively mild oxidants in comparison with other ROS, and this enables relative selectivity in the reversible modification of proteins. As with other intracellular signalling intermediates, specificity is also enabled by spatial orchestration through discrete compartmentalisation of NOX enzymes. The primary targets for redox regulation are kinases, including receptor tyrosine kinases such as the insulin receptor in addition to AKT and MAPK [266] [267]. Indirect regulation may also occur through inhibitory oxidation of protein tyrosine phosphatases (PTP), which usually reverse kinase activity [268]. Beyond kinases, proteinases such as MMP's have also shown redox sensitivity and are implicated in progression of atherogenesis [265].

1.4.3.5.4   Linkage with the insulin resistance syndrome

Genetic and pharmacological manipulation of ROS-producing enzymes has shown oxidative stress to play a causal role in multiple forms of insulin resistance [269]. It can increase expression of pro-inflammatory cytokines, such as TNF-α and IL-6, which inhibit transcription of intermediates such as IRS-1 and GLUT-4 to attenuate downstream signalling [270]. Additionally, it results in activation of a specific subtype of MAPK, termed 'stress-activated protein kinases' (SAPK) [269]. Examples include IκB kinase (IKK) and c-Jun-N-terminal kinase (JNK), which suppress MAPK phosphatases and also interfere with PI3K/AKT signalling to potentiate resistance.

Mechanistic data has also been derived from *in vivo* manipulation of vascular insulin signalling. Mice with endothelium-targeted over-expression of a dominant-negative mutant human insulin receptor (ESMIRO), or with global haploinsufficiency of the insulin receptor (IRKO), have enhanced vascular superoxide production. This could be suppressed with a pharmacological Nox-2 inhibitor, and was associated with improved endothelium-mediated vasorelaxation [271]. Consistent with this notion, diabetic blood vessels in hamsters demonstrate improved endothelium-dependent relaxation when treated with superoxide dismutase (SOD), an anti-oxidant [272]. However, conflicting data has arisen from studying mice with endothelium-specific overexpression of the human insulin receptor (hIRECO), a model of increased endothelial insulin signalling, which also exhibited reduced NO bioavailability and superoxide-mediated oxidative stress [273].

It is clear that regulation of ROS abundance preserves a physiological balance in health. At the correct concentrations, they are fundamental to cellular homeostasis by

driving appropriate differentiation, mitogenesis and migration in cells and acting

primarily as a reversible signalling mechanism [274]. Hence, the benefits of

suppressing ROS production are disparate depending on the context, i.e. physiology or

pathology. This notion is best supported by the 'redox window' hypothesis, as shown

in Figure 1-9 [275]. In the context of health, excess reduction of ROS levels beyond a

hypothetical cut-off is deleterious to function. However, in the context of underlying

pathophysiology such as DM where the oxidative state is enhanced, suppression of

ROS provides benefit by shifting levels into an optimal window. This nuanced response

is likely to involve complex temporo-spatial orchestration of multiple signalling

radicals. Indeed, this may provide a plausible explanation for the disappointing results

from clinical trials that have sought to improve cardiovascular outcomes with broad-

spectrum anti-oxidants [276, 277], in addition to intensive insulin regimens [278].
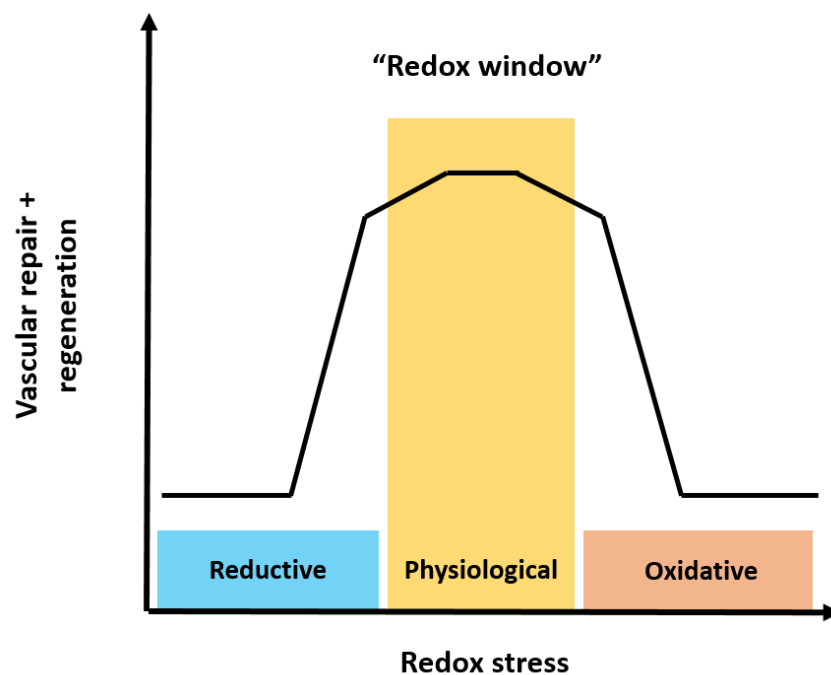
Figure 1-9 – **'Redox window' hypothesis**.

Adapted from Yun *et al*. Antioxid Redox Signal 2009; 11(8):1961-74 [275].

A hypothetical "redox window" exists in which vascular repair and regeneration is permitted and amplified. However, a shift to either an overly oxidative or reductive environment can be disruptive depending on clinical context.

1.4.4 Cell-specific insulin resistance

1.4.4.1 Vascular endothelial cells

1.4.4.1.1 Reduced NO bioavailability

Earlier sections have explored the sequence of pathological events implicated in progression of atherogenesis. However, the earliest alterations in endothelial cell phenotype occur before manifestation of structural abnormalities. One of the most important features is a subtle but crucial reduction in NO bioavailability in the insulin-responsive endothelium. As described, NO has many anti-atherogenic and anti-thrombotic properties required to preserve normal physiology. In the context of health, there is continuous, basal vascular synthesis of NO which is essential for vascular function, by promoting vasodilation, inhibiting platelet aggregation, suppressing inflammation and limiting leukocyte adhesion molecule expression. It is therefore apparent that this reduced bioavailability plays a pivotal role in coupling insulin resistance with vascular dysfunction. Indeed, eNOS knockout mice are hypertensive, insulin resistant and develop accelerated atherosclerosis [279] [280].

Other facets of relevance are the existence of parallel signalling pathways in metabolic and vascular tissues, and the presence of shared stressors mediating dysfunction [281]. The phenomenon of 'pathway-specific insulin resistance' is also noteworthy, in

addition to the compounding effects of compensatory hyperinsulinaemia. These concepts are now explored in greater detail.

1.4.4.1.2 Shared signalling cascades

As outlined during discussion of the insulin signalling cascade, there exists parallel pathways in metabolic and vascular tissue using PI3K/AKT signalling to achieve distinct tissue-specific effects. In metabolic tissues such as skeletal muscle, downstream effectors result in glucose uptake into cells, whilst in vascular endothelium, activation of eNOS results in NO production. Subsequently, defects in the signalling cascade upstream of AKT activation result in co-existence of metabolic and endothelial dysfunction. Consistent with this notion, a homozygous mouse model with targeted disruption of the IRS-1 gene displayed metabolic insulin resistance and impaired endothelium-dependent vasorelaxation [282]. Furthermore, a genetic polymorphism of the IRS-1 gene, which is implicated in metabolic insulin resistance, is associated with reduced NO production in human umbilical vein endothelial cells (HUVECs) [283].

1.4.4.1.3 Common stressors

It is also apparent that there are shared stressors implicated in insulin resistance and vascular dysfunction (see Figure 1-10). In the context of ROS, increased superoxide degrades NO and forms the oxidant peroxynitrite [284]. This impairs NO bioavailability and perpetuates oxidative stress. Activation of pro-inflammatory signalling cascades play a critical role in modulation and propagation of the atherogenic response. This occurs, in part, through inhibition of eNOS expression and phosphorylation in

response to insulin [285]. Further, it has been shown that hyperglycaemia has direct pro-apoptotic effects on endothelial cells and can promote leucocyte recruitment through upregulation of cell surface adhesion markers such as ICAM and VCAM [286]. AGE formation is additionally implicated in structural modifications of ECM proteins, such as collagen and laminin, which contributes to interactions between different cell types and progression of the atherosclerotic plaque [287]. The inflammatory marker CRP has also been shown to suppress eNOS expression [288] and enhance surface leukocyte adhesion molecule expression [289], thus contributing to pathogenesis in metabolic and vascular disease.
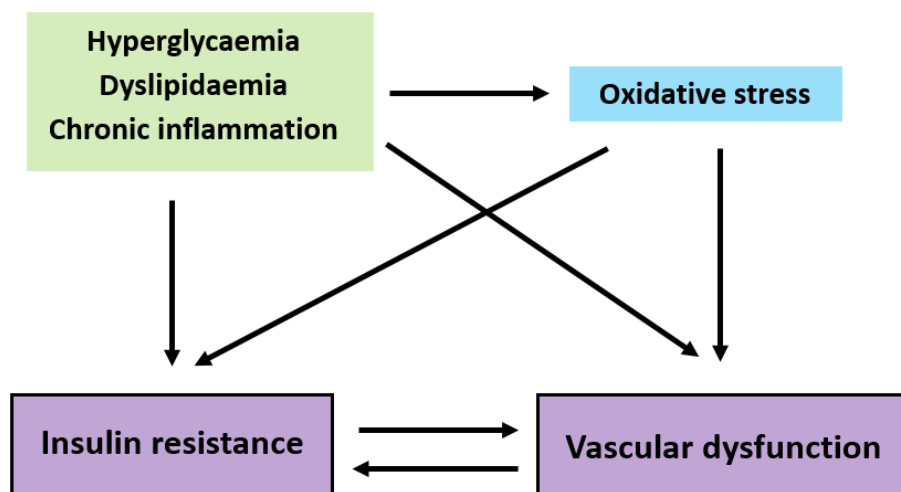
Figure 1-10 – **Shared stressors contributing to insulin resistance and vascular dysfunction.**

Adapted from Kim *et al*. Circulation 2006; 113:1888-1904 [281].

Glucotoxicity, lipotoxicity and chronic inflammation underpin reciprocal relationships that contribute to the linkage between metabolic and vascular disorders.

1.4.4.1.4   Pathway-specific insulin resistance

The concept of 'pathway-specific insulin resistance' is of particular relevance in appreciating the intricate cross-talk between different tissues in the context of DM (see Figure 1-11). A key feature of the signalling perturbations that underpin insulin resistance is that aside from reduced PI3K/AKT pathway signalling, other branches such as that of the mitogenic Grb2/MAPK pathway are unaffected [290]. This concept becomes increasingly relevant because during the initial phase of metabolic resistance, there is compensatory hyperinsulinaemia to preserve glucose homeostasis [291]. This adaptive response can, however, result in overdrive signalling through the Grb2/MAPK pathway [292]. Hence, there will be a hyperglycaemic state with reduced NO bioavailability but with augmented pro-atherogenic sequelae via increased endothelial cell leukocyte adhesion molecule expression and vasoconstriction mediated by ET-1 release. This has been corroborated in human subjects with DM, who have elevated baseline levels of ET-1 [293] and improved endothelial function when treated with a pharmacological antagonist [294].

Insulin also plays a vital role in regulation of sympathetic nervous system (SNS) activity by acting on the arcuate nucleus of the hypothalamus [295]. In the context of obesity, there is SNS hyperactivity arising from chronic hyperinsulinaemia. This promotes vasoconstriction and can secondarily activate the renin-angiotensin-aldosterone system (RAAS), resulting in systemic hypertension [296]. This is an independent risk factor for development of atherosclerosis.
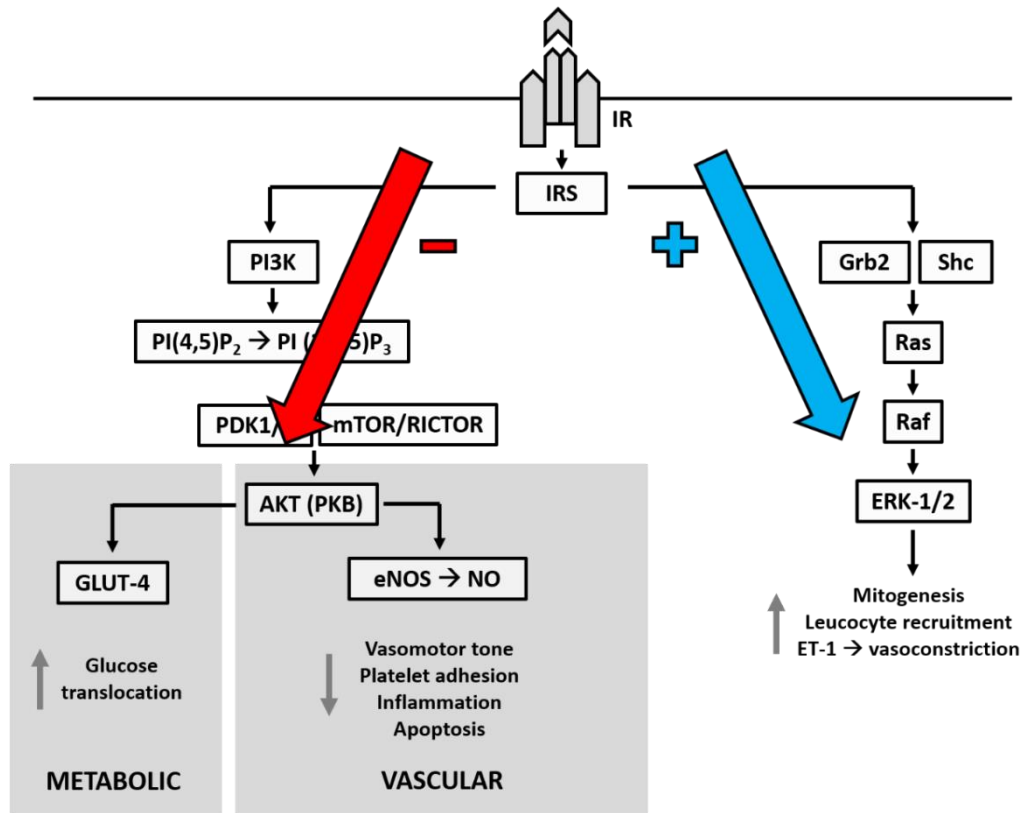
Figure 1-11 – Pathway-specific insulin resistance.

Reduced PI3K/AKT signalling in the context of insulin resistance is accompanied by unopposed Grb2/MAPK pathways. This can be exaggerated by compensatory hyperinsulinaemia that occurs in the initial stages.

1.4.4.1.5   Murine models of insulin resistance

Mice with diet-induced obesity exhibit vascular insulin resistance associated with reduced expression of the insulin receptor [297]. However, this insulin-resistant phenotype is complex, due to the presence of multiple contributory factors such as hyperglycaemia, dyslipidaemia and obesity that co-exist and provide confounding effects. It is therefore challenging to dissect the mechanistic contribution of insulin resistance *per se* to vascular disease in the context of DM, and to distinguish between

causation and association. Consequently, our laboratory has performed considerable work using *in vivo* murine models of isolated insulin resistance.

Mice with homozygous knockdown of the insulin receptor are non-viable, developing profound hyperglycaemia and early neonatal mortality [298]. However, mice with whole body haploinsufficiency for the insulin receptor (IRKO) demonstrated a mild perturbation of insulin signalling (approximately 30%), and provided a useful non-obese, non-diabetic model for further studies on vascular function [299]. IRKO mice have been studied extensively by our laboratory. They have been shown to maintain normoglycaemia through compensatory hyperinsulinaemia, but this is associated with extensive vascular dysregulation with reduced NO bioavailability, oxidative stress, impaired endothelium-dependent vasorelaxation and raised blood pressure.

A complementary model with endothelium-specific mutant dominant negative insulin receptor overexpression (ESMIRO) has been subsequently generated, under control of the *Tie*-2 promoter. The mutant receptor incorporates the substitution of alanine with threonine at the 1134 position in the tyrosine kinase domain, and although ligand binding is preserved, no downstream signalling occurs [300]. These mice had comparable glucoregulation to control littermates, but endothelium-specific insulin resistance was still sufficient to reduce NO bioavailability, cause vascular oxidative stress and impair endothelial function [301]. When crossed with atherosclerosis-prone Apolipoprotein E (ApoE) knockout mice, they develop accelerated atherosclerosis. This appeared independent of systemic metabolic perturbations, but was associated with superoxide-dependent oxidative stress [302]. In ApoE knockout mice, deletion of

endothelial insulin receptors has also been shown to induce expression of the leukocyte adhesion molecule VCAM-1 and increase atherosclerotic lesion area [303].

The emerging theme from the work performed using IRKO and ESMIRO models is that there may be a rationale for early intervention in insulin resistance, where glucoregulation is preserved but vascular phenotypic abnormalities have already manifest. However, as highlighted previously, murine models of increased endothelial insulin signalling also paradoxically exhibit enhanced superoxide abundance and oxidative stress-induced endothelial dysfunction. This highlights the complexity in interplay between metabolic and vascular function, and the narrow ideal range of vascular insulin signalling.

1.4.4.2   Macrophages

There is also some evidence that myeloid-specific insulin resistance can accelerate atherogenesis. Macrophages from obese mice have reduced insulin receptor expression, alongside increased expression of surface receptors such as scavenger receptor A (SRA) and CD36 [304]. These are implicated in the internalisation and cytoplasmic storage of oxidised LDL. Using murine bone marrow transplantation studies, it has been shown that macrophage insulin receptor deficiency increases endoplasmic reticulum (ER) stress-induced apoptosis and necrotic core formation in advanced atherosclerotic lesions [305]. However, conflicting data also exists, indicating that myeloid lineage-specific insulin resistance can protect atherosclerosis-prone mice from the development and progression of atherosclerotic lesions [306].

This may relate to insulin receptor-deficient macrophages having impaired capacity to produce pro-inflammatory cytokines, such as IL-1β and IL-6.

1.4.5   Defects in vascular repair and regeneration

As highlighted, vascular repair and regeneration are of crucial relevance in the response to vessel and tissue injury. However, these processes themselves may be retarded in patients with DM. Although the benefits of percutaneous coronary intervention (PCI) for functionally significant angiographic lesions are undisputed, numerous clinical studies have convincingly shown that patients with DM have higher rates of re-stenosis and late vessel occlusion after intervention [307, 308]. Collateral vessel formation also appears to be poorer in comparison with patients without DM [309].

1.4.5.1   Systemic insulin resistance

Systemic components of the metabolic syndrome are causally linked with vascular complications of insulin resistance, as already discussed. It is therefore reasonable to conceive that these same stressors may be linked with abnormalities in vascular reparative and regenerative strategies. Though relative contributions are difficult to dissect, studies have elucidated potential mechanisms.

Hyperglycaemia appears to have detrimental effects on vascular repair. This may relate to EPC downregulation, either via reduction in their NO production [310] or through excessive activation of the Grb2/MAPK cascade [311]. In a chicken chorioallantoic membrane model, hyperglycaemia impaired angiogenesis through

induction of apoptosis in endothelial cells and pericytes, and suppression of endothelial cell proliferation. This occurred without altered expression of VEGF [312]. *In vitro* injection of remnant-like particles (RLPs) derived from hypertriglyceridaemic patients appears to accelerate EPC senescence and functional capacity by increasing oxidative stress [313]. Elevated FFAs, namely palmitic and linoleic acids, appear to downregulate PI3K signalling and result in suppressed proliferation of EPCs [314]. Reduced HDL cholesterol is a core component of the dyslipidaemic profile associated with the metabolic syndrome. *In vivo* studies in mice have shown that HDL stimulates endothelial cell migration in a NO-independent manner, via activation of Rac GTPase, and augments carotid artery re-endothelialisation after perivascular electric injury [315]. In human subjects with low HDL, EPC abundance and migratory potential was reduced [316]. Though not strictly part of the diagnostic criteria for metabolic syndrome, DM is also associated with elevated levels of oxidised LDL cholesterol. In HUVECs, this appears to induce endothelial cell apoptosis through enhancement of caspase 3 activity via excess ROS production [317]. Furthermore, it appears to severely impair monocyte chemotaxis in response to VEGF in human patients and this may be implicated in suppressing regenerative potential [318].

Adipocytokines also appear to influence vascular reparative capacity. Chronic exposure of both TNF-α and CRP has negative effects on EPC abundance and function, explained in part by reduction in eNOS expression [319]. However, the inflammatory response has been determined to be a crucial mediator of angiogenesis and atherogenesis, corroborated by similarities in transcriptional responses to VEGF and IL-1 within the endothelium [320]. Hence, magnitude and temporo-spatial

characteristics are likely to be critical in determining overall outcome. Adiponectin levels are reduced in states of insulin resistance, and has been associated with EPC senescence through enhanced Grb2/MAPK signalling [321], and with diminished angiogenesis *in vitro* and *in vivo* [322]. Lastly, leptin levels are raised in the context of insulin resistance. Its effects on EPC function are more ambiguous, enhancing at physiological concentrations but inhibiting when levels are higher [323].

A converging theme from the above discussion relates to an unifying role for oxidative stress, which is associated with glucotoxicity, lipotoxicity and states of chronic inflammation. As established, however, ROS also confers important roles in cell physiology that are critical for function and this extends to reparative strategies. For instance, generation of superoxide by Nox2 is vital for EPC mobilisation and proliferation in the context of carotid artery re-endothelialisation *in vivo* [324]. The pro-angiogenic effects of VEGF also appear to be promoted in part by Nox2 mediated superoxide production [325]. This is consistent with the perceived hypothesis of a 'redox window' discussed earlier, where maintenance of ROS within a critical zone is essential for normal physiology but with the caveat that excess production can cause pathology.

1.4.5.2   Cellular insulin resistance

The effects of insulin resistance on repair and regeneration at a cellular level has not been extensively explored. Initial studies were performed using murine models that were genetically diabetic (*db/db*) and were compared with heterozygous controls. EPC abundance, migration and adhesion to site of vessel injury was impaired, concurrent

with reduced re-endothelialisation [326]. Although providing useful insights, the model was unable to account for confounding effects of hyperglycaemia.

To address this, our laboratory studied the effects of insulin resistance *per se* on EPC biology using the IRKO mouse model. IRKO mice are hypertensive but with broadly preserved metabolic sensitivity to insulin. Notably, they demonstrated marked impairment in re-endothelialisation of the femoral artery after denuding wire injury [327]. This was associated with reduced abundance of EPCs in peripheral blood but preserved levels in bone marrow and spleen, suggesting a mobilisation defect. Importantly, infusion of wild-type littermate bone marrow-derived c-Kit expressing progenitors could rescue vascular repair in IRKO mice. Outgrowth endothelial cells derived from South Asian men, who are insulin-resistant and have increased risk of cardiovascular sequelae, also exhibit impaired vascular reparative capacity due to suppression of AKT signalling [328].

As alluded to, the reduction in NO bioavailability associated with insulin resistance is also strongly implicated in hindering the reparative response. There is convincing evidence to indicate that NO is vital in initiating the angiogenic response that occurs secondary to hypoxia and inflammation [329]. eNOS expression appears reduced in diabetic EPCs, and associated with impaired migration and adhesion capacity [326]. Reduced endothelial NO bioavailability in the context of insulin resistant states may be pertinent in promoting cell senescence and impairing migration in response to chemotactic stimuli, factors likely to be relevant in promoting conduit repair [330]. Indeed, NO has more potent inhibitory effects on neointimal hyperplasia after arterial injury in rats with metabolic syndrome and frank DM, in comparison with

normoglycaemic controls [331]. VENIRKO mice with endothelium-specific deletion of the insulin receptor have impaired retinal neovascularisation in response to hypoxia, which is associated with reduced expression of vascular mediators such as VEGF and eNOS [332]. Genetic knockdown of AKT1, which results in reduced downstream eNOS activation, has been shown *in vivo* to impede VEGF-induced angiogenesis concurrent with reductions in EPC mobilisation [333].

As highlighted, pathway-specific insulin resistance and compensatory hyperinsulinaemia results in overdrive signalling in the Grb2/MAPK pathways. Its consequences are more debatable, with separate studies demonstrating stimulatory [334] and inhibitory effects on angiogenesis [217].

1.5 Shc homology 2-containing inositol 5' phosphatase 2

1.5.1 Overview

A range of complementary systems exist to suppress excess insulin signalling during periods of cellular stress. Shc homology 2-containing inositol 5' phosphatase 2 (SHIP2) is a 5' phosphatase that tightly regulates membrane PIP3 abundance and therefore downstream signalling. In addition to its catalytic activity, it also acts as a docking site for a large number of proteins implicated in insulin signalling and cytoskeletal dynamics. PtdIns(3,4)P2 is the product of SHIP2 activity, and accumulating evidence indicates that it is not inert but instead exerts influence over a variety of cellular processes. *In vitro* and *in vivo* studies have broadly demonstrated SHIP2 to be a negative regulator of insulin signalling, which is quiescent in basal states but rapidly activated in response to growth factors that include insulin and IGF-1. Studies to

delineate the role of SHIP2 in vascular function are rather sparse, though some mechanistic insights have emerged from contemporary research.

1.5.2   Inositol polyphosphate 5-phosphatases

The family of inositol polyphosphate 5-phosphatases is comprised of ten mammalian isoenzymes and four derived from the yeast *Saccharomyces cerevisiae* [335]. Each 5-phosphatase has a conserved catalytic domain, consisting of 300 amino acids, which removes the phosphate from the 5-position of the inositol ring on phosphoinositides. The first family member identified was 5-phosphatase-I, which is involved in the regulation of intracellular calcium signalling [336]. Skeletal muscle and kidney enriched inositol phosphatase (SKIP) has not been extensively characterised but appears to have selective expression in the heart, kidneys and skeletal muscle [337]. Proline-rich inositol polyphosphate 5-phosphatase (PIPP) also shows differential expression that is higher in brain, heart, kidneys, lungs and gastrointestinal tract [338]. The activities of synaptojanin 1 and 2 are PI3K-independent, and they are thought to play a particular role in synaptic vesicular trafficking which is relevant in the process of phagocytosis [339].

In broad terms, the 5-phosphatase family modify membrane concentrations of phosphoinositides to regulate a plethora of cellular functions including insulin signalling, cell survival and proliferation, vesicular trafficking, endocytosis and cytoskeletal remodelling [340]. This will be explored in greater detail in the context of SHIP2.

5-phosphatases	
SHIP1	5-phosphatase-II/Inpp5b
SHIP2	OCRL1
SKIP	Synaptojanin1
PIPP	Synaptojanin2
5-phosphatase-1	72-5ptase/Type IV/Inpp5e

Table 1-1 – **Family of mammalian 5-phosphatases.**

1.5.3   Expression and structure of SHIP proteins

The Shc homology 2-containing inositol 5' phosphatase (SHIP) proteins were first observed in blood cells where their activation occurred via tyrosine phosphorylation in response to growth factors [341]. Both SHIP1 and 2 are the products of distinct genes. The expression of SHIP1 is restricted to cells of haematopoietic and spermatogenic origin [342], whilst the isoenzyme SHIP2 is more widely distributed. It is encoded by the inositol polyphosphate phosphatase like 1 (INPPL1) gene on chromosome 11 [343]. It is ubiquitous in mice, and highly expressed in human heart, skeletal muscle, brain, placenta and pancreas [344]. SHIP2 was originally cloned as a product named 51C, which potentially complemented the gene defect observed in Fanconi anaemia [345]. Subsequent work with myeloid cells renamed the product to SHIP2 [344]. It is observed as a 139kDa protein consisting of 1258 amino acids, and exhibits approximately 38% homology with SHIP1 [346]. Both contain specific, identifiable motifs which are critical in exerting their actions (see Figure 1-12).
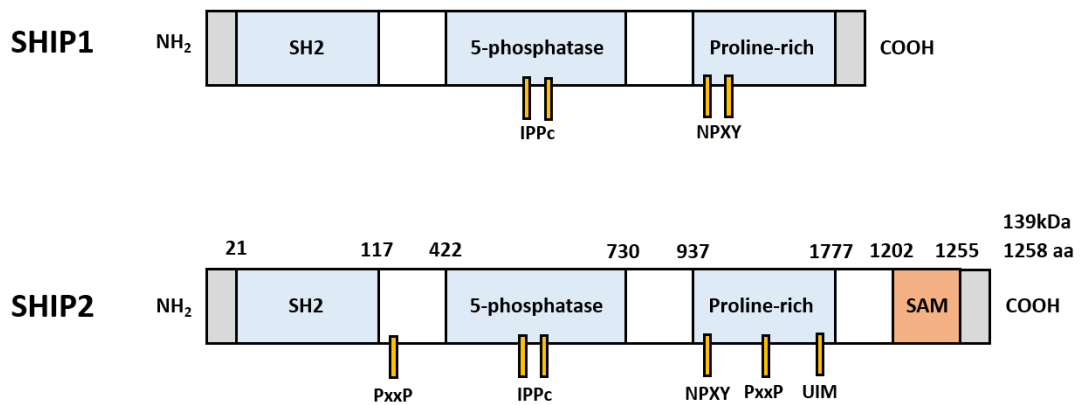
Figure 1-12 – Structural homology of SHIP1 and SHIP2 proteins.

Adapted from Suwa *et al*. Expert Opin Ther Targets 2010; 14(7):727-37 [347].

SHIP2 is composed of 1258 amino acids, with SH2, 5-phosphatase and proline-rich regions that are structurally analogous to SHIP1. However, there is an additional SAM at the C-terminal end.

The SH2 domain at the N-terminus is vital in mediating the interactions of SHIP2 with a number of other activated intracellular signalling proteins, such as Shc, Gab, p130[Cas], the FcγRIIB receptor in B cells and the hepatocyte growth factor receptor c-Met. The central portion incorporates the inositol phosphatidyl phosphatase (IPP) region, with an undefined ~ 300 amino acid segment separating the two.

At the C-terminal end, there is a distinct proline-rich region of ~ 350 amino acids which differs most significantly with the structure of SHIP1. It provides a single NPXY motif, which undergoes activation through reversible tyrosine phosphorylation at residues 986 and 1125 [348]. This has been shown to occur in response to a range of growth factors, including EGF, PDGF, IGF-1 and insulin [349]. Once activated, the motif has the potential to bind a range of proteins bearing a PTB domain, including Shc, talin, filamin, vinexin, c-Cbl and c-Cbl associated protein (CAP). The complex formation

of SHIP2 with c-Cbl and CAP has been implicated in mediating multi-ubiquitination of

epidermal growth factor receptor (EGFR) and subsequent endocytosis [350]. The

remainder of this region has numerous PxxP motifs, possibly eight, which can bind to

proteins bearing SH3 domains such as the protein kinase Abl. Lastly, a ubiquitin

interacting motif (UIM) has also been reported in the SHIP2 protein, which appears to

enable ubiquitin-binding capacity [351].

In comparison with SHIP1, there is an additional sterile alpha motif (SAM) of ~ 50

amino acids at the C-terminus of SHIP2. This motif is widespread in many proteins,

and is implicated putatively in protein-protein interactions [352]. Hence, through its

various domains, SHIP2 is able to interact with a wide spectrum of protein partners

including receptors, adaptors, kinases, phosphatases and cytoskeletal proteins (see

Figure 1-13). A broad inference from this understanding is that SHIP2 is likely to have

effector function via scaffolding properties and through its enzymatic capacity. A

discussion of the latter is now provided.
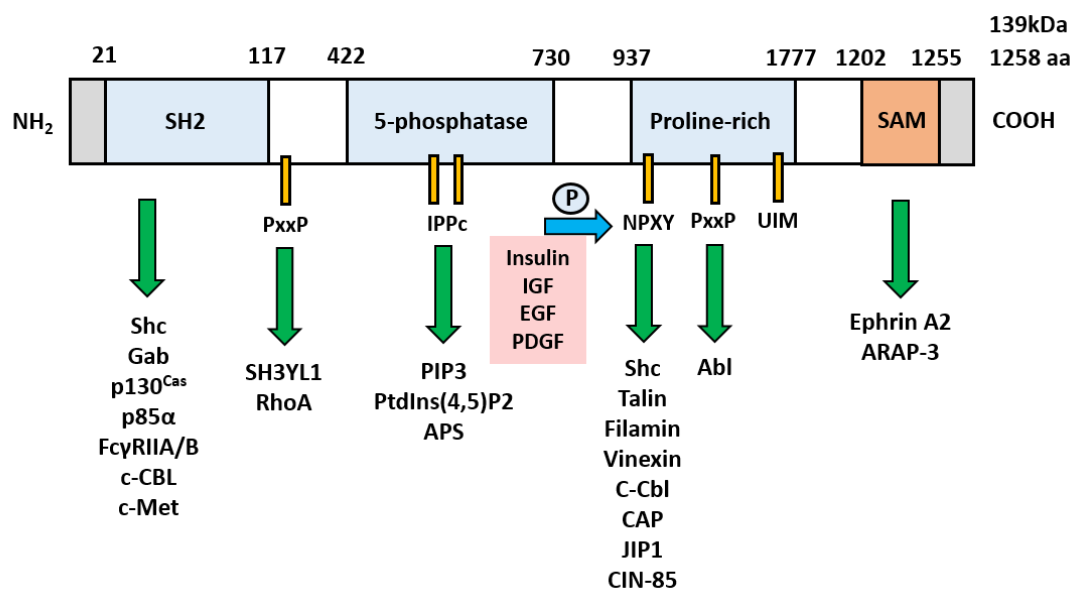
Figure 1-13 – SHIP2 effector proteins.

SHIP2 is able to interact with a wide range of protein partners including receptors, adaptors, kinases, phosphatases and cytoskeletal proteins.

1.5.4   Enzymatic activity of SHIP2

The central, enzymatic domain of SHIP2 is closely conserved between murine and human forms, and folds in a similar manner to that of the endonuclease family of DNA-modifying enzymes [353]. It has approximately 65% amino acid homology with SHIP1 [344]. Its activity as a 5-phosphatase primarily removes the phosphate group from the 5' position of PIP3 to produce phosphatidylinositol 3,4-bisphosphate (PtdIns(3,4)P2) [354]. In other words, it acts as a negative regulator in the insulin signalling cascade (see Figure 1-14). The 3' position of the inositol phospholipid must be phosphorylated before this process can occur, implying that SHIP2 acts sequentially with PI3K [341]. PIP3 is the primary substrate. However, it can also dephosphorylate PtdIns(4,5)P2 to produce phosphatidylinositol 4-phoshate (PI4P) [355], though this has been observed in fewer models.

Enzymatic activity is not mediated by SHIP2 tyrosine phosphorylation or direct interaction with adapter proteins in isolation. Instead, cellular localisation is deemed to be a key determinant of effector function [356]. In serum-starved conditions, SHIP2 is localised to peri-nuclear regions and likely associates to nuclear proteins such as lamin A/C [357]. It could also potentially control nuclear PtdIns(3,4)P2. However, translocation to the cell membrane appears to occur in response to stimulation, i.e. at the site of PIP3 production [358]. This will be explored in a subsequent section.

The interplay between tyrosine phosphorylation of SHIP2 and phosphatase activity has not been fully elucidated. However, a recent study has demonstrated enhancement of phosphorylation in response to EGF stimulation, which subsequently augmented its phosphatase activity [359]. Indeed, it was also implied that the SH2 domain of SHIP2, in conjunction with the C-terminus, may confer inhibitory effects to suppress activity under basal conditions, which can be overcome via activatory phosphorylation.

Aside from SHIP2, PIP3 degradation is also mediated through the separate actions of the tumour suppressor, phosphate and tensin homolog (PTEN). This acts as a 3-phosphatase and hydrolyses the 3-position phosphate from PIP3 to form PtdIns(4,5)P2 [360]. *In vitro* studies have also shown that PTEN hydrolyses the 3-position phosphate from PtdIns(3,4)P2 to produce phosphatidylinositol 4-phosphate (PtdIns4P), but this does not appear to be replicable *in vivo* [361]. Despite SHIP2 and PTEN metabolising the same target, i.e. PIP3, modulation has differing effects as a consequence of cell localisation, cell-specific factors and variations in reaction products resulting in disparate secondary messenger effects. Cellular levels of PIP3 are generally maintained at low levels due to basal inhibitory effects of PTEN, but a rapid increase occurs upon PI3K activation in response to insulin and growth factors.

A discussion of *in vitro* and *in vivo* studies that have explored the role of SHIP2 in insulin signalling is now provided.
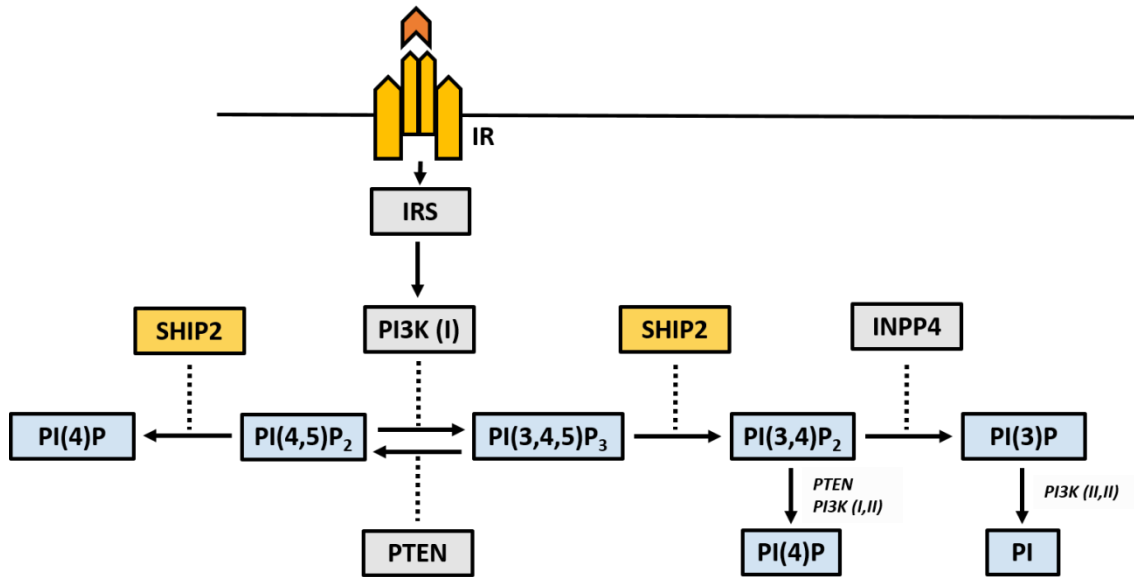
Figure 1-14 – **Key pathways in phosphoinositide metabolism.**

SHIP2 acts as a negative regulator of insulin signalling, mediated via 5-phosphatase activity on PIP3. PTEN is also able to metabolise the same target, with effects dependent upon cell localisation and secondary messenger effects.

1.5.5 SHIP2 and insulin signalling

1.5.5.1 *In vitro* studies

Consistent with the role of SHIP2 as a negative regulator of insulin signalling, over-expression has been demonstrated to inhibit insulin-mediated PI3K signalling and AKT activation in various cell types, including 3T3-L1 adipocytes [362], B lymphocytes [363] and Chinese Hamster Ovary (CHO) cells [364]. However, conflicting results have been suggested using RNA interference of SHIP2 in adipocytes, where no modulatory effects on insulin signalling were detectable [365]. SHIP2 has also been shown to form complexes with CAP in the vicinity of the insulin receptor, with CAP directly implicated in the process of transmembrane glucose transport [366]. Additionally, in response to insulin, SHIP2 appears to form a functionally significant complex with the actin-binding

protein, filamin [367]. This interaction may enable spatial localisation of SHIP2 to submembranous PIP3, allowing regulation through its phosphatase activity. In VSMCs, SHIP2 has additionally been shown to play a negative regulatory role in MAPK pathway activation in response to PDGF and IGF-1, by competing with Grb2 for Shc phosphorylation at its Tyr (317) residue [368]. In the context of SHIP2 inhibition, there is amelioration of high glucose-induced lipogenesis and VLDL production by HepG2 hepatocytes which was contributed by regulation of ROS production [369]. This suggests its role as an important regulator of hepatic *de novo* lipogenesis and lipoprotein secretion in insulin-resistant states.

Most recently, studies have been performed in the context of a small molecule inhibitor (SMI), obtained via high-throughput screening based on mass spectrometry [370]. These function by competing with SHIP2 for target substrates at the catalytic site. Treatment with AS1949490 (IC_{50} for SHIP2 = 0.62μM) augmented insulin-mediated AKT phosphorylation and glucose uptake in L6 myotubes. It appeared to be a potent and selective inhibitor, with no exerted effects on other intracellular phosphatases such as SHIP1, PTEN and synaptojanin. Other SMI have also been reported in the literature with comparable inhibitory activity to AS1949490 [371], but their selectivity and effects, both *in vitro* and *in vivo*, have not been investigated to any extent.

1.5.5.2 *In vivo* studies

Most *in vivo* studies assessing the role of SHIP2 on insulin signalling have been performed using murine disease models. The basal expression of SHIP2 protein has

been found to be elevated in the skeletal muscle and adipose tissue of diabetic *db/db* mice [372]. In transgenic mice over-expressing SHIP2 under the control of a modified chicken β-actin promoter with cytomegalovirus immediate-early (CMV-IE) enhancer, insulin-stimulated AKT activation was reduced in various tissues including skeletal muscle, adipose tissue and liver [373]. Expression of UCP1 in adipocytes was also reduced, implying reduced browning.

Homozygous deletion of exons 19-29 of the SHIP2 gene to produce a truncated protein induced early cyanosis and lethargy in the first 24 hours of life. This was associated with significant hypoglycaemia and rapid mortality. Littermates with heterozygous deletion were viable littermates. However, they demonstrated enhanced insulin sensitivity and glycogen synthesis in skeletal muscle, associated with reduced serum insulin concentrations [374]. However, there was controversy surrounding the gene modification of these mice, as it later became apparent that the strategy had inadvertently resulted in accompanying partial deletion of the *Phox2a* gene, which would result in non-functionality. *Phox2a* is a homeo-domain containing transcription factor that is implicated in neuronal development and differentiation [375]. The exact consequences of *Phox2a* loss-of-function are not fully comprehended but it is reasonable to speculate that the severe hypoglycaemic phenotype observed could be the result of truncated SHIP2, *Phox2*a or a combination of both.

A later strategy circumvented this limitation by producing mice with targeted deletion of exons 1-18 of the SHIP2 gene, commencing at the translation-initiating ATG codon [376]. This segment discretely encodes the SH2 and 5-phosphatase catalytic domains. Homozygous deletion resulted in complete absence of messenger RNA (mRNA) and

protein. It was surprisingly non-lethal, although mice demonstrated characteristic abnormalities in facial development. AKT activation was enhanced though this was not associated with detectable abnormalities in glucose and insulin tolerance. Knockout mice fed with a high-fat diet appeared to be resistant to weight gain and had higher uncoupling protein 03 (UCP3) mRNA levels in skeletal muscle, a correlate of basal metabolic rate. However, they too did not become insulin resistant.

Most recently, a third mouse model has been generated in which the SHIP2 protein is expressed but has germline catalytic inactivity [377]. This was achieved by inserting DNA recognition sites (*lox*P) in the introns surrounding exons 18 and 19 of the INPPL1 gene to enable specific, Cre-mediated recombination. These form the basis of one of the murine models utilised in this project, and will therefore be elaborated upon in a subsequent section. The formation of a mutant mouse line with systemic SHIP2 catalytic domain haploinsufficiency resulted in significant, multi-organ developmental defects. Perturbations in lipid metabolism and insulin secretion were observed, but glucose tolerance and insulin-induced AKT phosphorylation were not affected. However, these developmental confounders made it difficult to dissect the relative role of altered SHIP2 activity *per se* to systemic insulin sensitivity.

1.5.5.3   Human studies

INPPL1 polymorphisms have been implicated in human disease states. A 16 base pair deletion in the 3'-untranslated region occurred more frequently amongst patients with DM, compared to healthy controls, in Caucasian populations from the United Kingdom (UK) and Belgium [378]. Polymorphisms have also been associated with

metabolic syndromes, including DM, in British and French cohorts [379]. In a Japanese population, several gene polymorphisms located in the 5-phosphatase domain of SHIP2 appeared more commonly in controls than in patients with DM [380]. In the context of CHO cells expressing human insulin receptor (CHO-IR), expression of these SHIP2 mutants appeared to afford protection against insulin resistance by enhancing PIP3 levels and AKT phosphorylation. Additionally, in a study of British patients with DM, a significant association with SHIP2 single nucleotide polymorphisms (SNPs) was found [379]. Most recently, a study in a Japanese cohort has found SNPs in the promoter and 5'-untranslated region (UTR) segments of the SHIP2 gene to be strongly associated with impaired fasting glycaemia [381].

1.5.5.4   PtdIns(3,4)P2 and effector proteins

Importantly, the negative regulatory role of SHIP2 in the insulin signalling cascade extends beyond the effects mediated through reductions in PIP3. As described, SHIP2 activity also results in enhanced formation of PtdIns(3,4)P2. It is found mostly at the plasma membrane but also in early endocytic vesicles [382]. It is not functionally redundant, but instead is thought to be relevant in exerting critical secondary messenger effects, such as lamellipodial dynamics implicated in cell migration, endocytosis and insulin signalling [90].

PtdIns(3,4)P2 has been shown to bind directly to lamellipodin, and this enables recruitment of the Ena/VASP complex to mediate assembly of actin filaments. This has been shown convincingly in the process of neuronal migration [383]. The influence on insulin signalling is underscored by evidence of binding to the C-terminal PH domains

of tandem pleckstrin homology domain containing protein-1 (TAPP1) and TAPP2 adapters [384]. Studies using knock-in mice expressing mutant TAPP1/2 that are incapable of binding PtdIns(3,4)P2 have shown enhanced AKT activation and whole body insulin sensitivity.

Collectively, these observations provide support for the suggestion that PtdIns(3,4)P2, a product of SHIP2 activity, may itself act as a negative regulator of insulin signalling pathways. Regulation is also likely to be achieved through feedback loops which may potentially downregulate the components of the PI3K network. Indeed, in the catalytically inactive murine model described above, the observed phenotype was postulated not to depend upon an overstimulated PI3K/AKT pathway but instead on reductions in SHIP2-produced PtdIns(3,4)P2 and its derivative, PtdIns(3)P [377]. The data remains somewhat conflicting, however, as PtdIns(3,4)P2 has also been shown to directly interact with PH domain of AKT and exert activatory effects [385].

PtdIns(3,4)P2 interactors	
Lamellipodin	DAPP1
TAPP1/2	Irgm-1
AKT	PLC γ1
PDK1	βARK1
P47(phox)	Grp1
SWAP70	ARKO
ARAP-1	PH30
Pleckstrin-2	Evectin-2

Table 1-2 – Identified PtdIns(3,4)P2 interactors.

1.5.6 SHIP2 in atherogenesis

As outlined above in the description of stages involved in atherogenesis, VSMCs mediate vascular remodelling and plaque stabilisation. Indeed, their apoptosis has been implicated in the process of fibrous cap rupture [36]. In studies of rat VSMCs, SHIP2 inhibited AKT phosphorylation in response to PDGF and IGF-1 in a phosphatase-dependent manner as predicted [368]. Interestingly, SHIP2 overexpression also had a negative influence on the mitogenic and anti-apoptotic Grb2/MAPK pathway. This occurred via SHIP2 competing with Grb2 to bind to Shc, i.e. a phosphatase-independent mechanism. Chronic treatment of VSMCs with insulin appeared to reduce SHIP2 expression. Overall, it can be surmised that SHIP2 may regulate PDGF and IGF-1 signalling in VSMCs by both phosphatase-dependent and -independent mechanisms. It may therefore be a modulator of the atherogenic process.

A more recent study has proposed a novel regulatory role for SHIP2 in atherosclerosis. Polymorphisms of the ApoE4 allele are established as risk factors for DM, Alzheimer's disease and cardiovascular disease [386]. This are thought to be through modulatory effects on lipoproteins, such as reductions in circulating HDL cholesterol. In endothelial cells, it has been shown that ApoE4-very low-density lipoproteins (VLDLs) suppress PIP3-mediated AKT signalling and inhibit the anti-apoptotic pathways activated by HDL [387]. Interestingly, this appears to occur by recruitment of SHIP2 and not through PTEN.

1.5.7   SHIP2 in oncogenesis

The predominant work assessing the role of SHIP2 on the processes of cell migration and proliferation has been in the field of oncogenesis, though primarily in the context of non-endothelial cells.

SHIP2 protein expression has been shown to be elevated in several malignant breast cancer lines compared to non-transformed cells [388]. These cells had higher migratory and proliferative capacity, which can be profoundly pro-oncogenic and augment metastastic spread. SHIP2 may act as a scaffolding protein to mediate interactions with proteins involved in cell adhesion and spread, such as talin and p130^{Cas} [348]. Effects on cell proliferation may be via regulation of EGF receptor signalling which is known to mediate multiple cellular events. Both vinexin and C-Cbl are focal adhesion proteins which can bind to SHIP2 but also regulate the ubiquitination of EGF receptor [389].

However, there also exists conflicting data which supports SHIP2 having anti-oncogenic effects. In glioblastoma tumour cells, SHIP2 overexpression resulted in potent cell cycle arrest [390]. A similar effect has also been observed in cells derived from squamous cell carcinoma (SCC) [391]. Additionally, SHIP2 expression has not been shown to affect cell growth or apoptotic potential in a multiple myeloma cell line [392]. Overall, it is credible to postulate that SHIP2 is likely to exert differing effects in different contexts depending on cell type and milieu. The complexity is likely to be further compounded by potentially distinct effects of PtdIns(4,5)P2, which is also a target of SHIP2. Indeed, a recent study implicated the interaction of PtdIns(4,5)P2 with

myosin 1c in forming focal adhesions to regulate cell migration of glioblastoma cells [393].

1.5.8 SHIP2 in lymphangiogenesis

The effects of SHIP2 on endothelial function *per se* has been documented in the context of *in vitro* lymphangiogenesis studies, prompted by familial defects of lymphatic function associated with SHIP2 mutations [394]. In human lymphatic endothelial cells with SHIP2 knockdown, with small interfering RNA (siRNA) or inhibition with SMI, there was reduced migration, proliferation and adherence to ECM proteins [394]. This was observed in basal conditions and following stimulation with growth factors. The increase in Grb2/MAPK signalling was more significant than that of PI3K/AKT, and it was therefore speculated whether sustained signalling may be paradoxically detrimental to cell survival through activation of caspases [395].

1.5.9 SHIP2 and cell motility

Further studies have attempted to provide a mechanistic insight into interactions between SHIP2 and its binding partners which may mediate the observed effects on cell motility. It has already been conveyed that PIP3 accumulation occurs at the leading edge of migrating cells, where polymerisation of actin filaments, filamin-mediated cross-linking into networks and lamellipodium formation occurs. In COS-7 cells, LL5β appears to be recruited to this submembranous region by PIP3, enabled by its PH domain [396]. This in turn mediates binding of filamin which has affinity for SHIP2 and can facilitate its translocation from the cytosol to the cell membrane in

response to EGF stimulation. Consistent with this, the expression of SHIP2 in filamin-deficient cells is exclusively cytosolic [367]. This machinery complex involving LL5β, SHIP2 and filamin with precise regulation of PIP3 levels may assist in driving the cell to mobilise precisely and dynamically to external signals.

The notion of spatial orchestration is consistent with that seen in other cell types. For instance, in human astrocytoma cells, SHIP2 appeared to localise to the cell periphery in response to serum and could be detected at the leading edge of polarised cells [357]. Additionally, in HeLa cells, SHIP2 has been demonstrated to associate with p130[Cas] at sites of focal adhesions [397]. Of further note, in glioma cells, SHIP2 has been shown to associate with active Rho GTPases via PxxP motifs in the SH2 domain [398], which has already been defined as a key effector of front-rear cell polarity and migration.

1.6 Treatment strategies

1.6.1 Overview

Current recommendations to manage patients with type II DM rely upon lifestyle modifications and pharmacotherapies to improve glycaemic control (see Figure 1-15). However, although improvements have occurred in prevention of microvascular sequelae, such as nephropathy and retinopathy, improvements in macrovascular outcomes have been much less marked. Contemporary research is using murine models to explore a broad portfolio of novel molecular targets, and it is hoped that

these may be exploited in the future to modulate the macrovascular complications associated with DM.

1.6.2   Lifestyle modifications

A conceptual understanding of the metabolic syndrome has provided clear rationale for recommended lifestyle modifications, including regulation of diet, weight and physical exercise [399]. This has been associated with reductions in insulin resistance [400] and concurrent improvements in endothelial function [401]. Restriction of calorific intake appears to improve NO-mediated vasodilatation in obese and hypertensive cohorts [402]. Furthermore, a two month regimen of regulated dietary intake correlates with increased adiponectin levels and reductions in insulin resistance in patients with and without DM [403]. However, intensive lifestyle intervention achieving sustained moderate weight loss has surprisingly been shown not to reduce cardiovascular morbidity and mortality in adults with type II DM [404].

1.6.3   Pharmacotherapies

In view of shared signalling cascades, common stressors and coupling of metabolic and haemodynamic physiology, pharmacotherapies that target insulin resistance or endothelial dysfunction may have concurrent beneficial effects.

Conventional therapies for hypertension, such as ACE inhibitors, have adjunct benefits on vascular profile by suppressing angiotensin II levels which lowers blood pressure and enhances endothelial function [405]. They have also been shown to augment adiponectin levels and improve insulin sensitivity without altering body weight [406].

Statins operate as 3-hydroxyl-3-methyl-glutaryl-coenzyme A (HMG-CoA) reductase inhibitors and reduce endogenous cholesterol synthesis [407]. They have similarly been shown to reduce inflammation, ET-1 levels and improve endothelial dysfunction in patients with DM [408].

Metformin is in the biguanide class and is a first-line treatment of hyperglycaemia. It enhances insulin sensitivity and decreases hepatic gluconeogenesis [409]. Therapy has also been shown to enhance endothelial NO production by increasing AMP-activated protein kinase (AMPK)-mediated phosphorylation of eNOS [410]. It also reduces circulating ET-1 levels in the context of insulin resistance [411]. Treatment with PPAR-α agonists such as fenofibrate reduce inflammatory markers and concomitantly enhance insulin sensitivity in patients with hypertriglyceridaemia [412].

Thiazolidinediones, such as rosiglitazone and pioglitazone, are peroxisome proliferator-activated receptor (PPAR)-γ ligands that primarily enhance insulin sensitivity in adipose tissue [413]. They also appear to improve endothelium-dependent vasomotor function in response to insulin [414]. In addition, they demonstrate anti-atherogenic properties by inhibiting VSMC proliferation and lipid accumulation in macrophages [415]. However, preliminary analyses showed rosiglitazone to be associated with a paradoxical rise in MI and cardiovascular mortality [416], necessitating temporary withdrawal from the market until more robust studies suggested a neutral association [417].

Glucagon-like peptide (GLP)-1 is released into the circulation in response to feeding and augments insulin secretion in a glucose-dependent manner. Analogues such as

exenatide and liraglutide are incretin mimetics in clinical use, with some evidence suggesting beneficial effects on cardiovascular outcomes in those with type 2 DM when added to standard care [418]. However, therapy with dipeptidyl peptidase-4 (DPP-4) inhibitors such as sitagliptin, which prevent GLP-1 breakdown, does not demonstrate superiority over placebo with regards to cardiovascular outcomes [419].

Empagliflozin is a recent addition to the portfolio of oral hypoglycaemics, and operates as a sodium-glucose co-transporter-2 (SGLT2) inhibitor to increase glucose excretion in the urine [420]. A randomised controlled trial (RCT) has shown that adjunct therapy with empagliflozin reduced cardiovascular mortality [421], which may relate to wider metabolic effects beyond reduction of serum glucose levels alone [422].
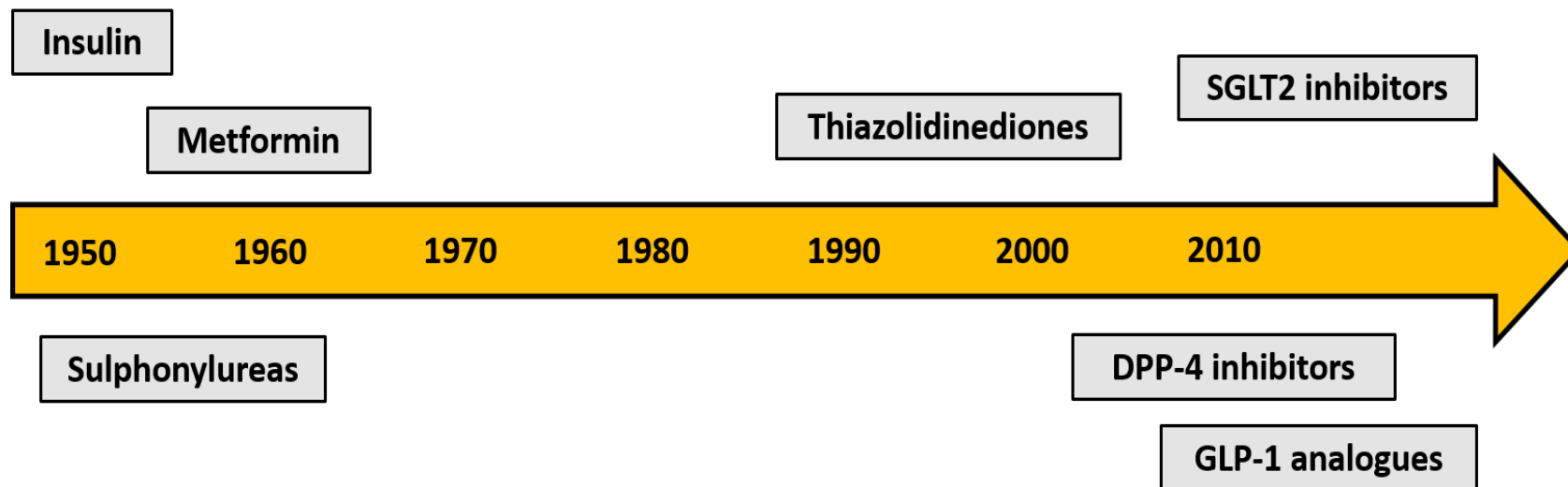
Figure 1-15 – Pharmacotherapies for insulin resistance.

Evolution of pharmacological therapies that may have concurrent benefits on insulin resistance and endothelial dysfunction. Broad classes include biguianides, sulphonylureas and thiazolidinediones, in addition to novel agents such as DPP-4 inhibitors, GLP-1 analogies and SGLT2 inhibitors.

1.6.4 Contemporary research

Despite established evidence-based treatment strategies, DM continues to be associated with persistently adverse cardiovascular outcomes. Some contemporary research has therefore shifted focus to the promotion of vascular renewal. This goal remains speculative, however, and there have been inevitable challenges in translating effects from pre-clinical models to the complex abnormalities occurring in people with DM.

Murine studies support the potential for acute insulin treatment in augmenting angiogenesis [423] and vascular repair after injury [424]. Gene-based delivery of therapies such as Ang1 [425] and HIF-1α have shown some promising findings by normalising immature vasculature in diabetic *db/db* mice [426]. VEGF gene therapy with concurrent administration of a Notch inhibitor (DAPT) appears to enhance neovascularisation and perfusion recovery in diabetic mice in the setting of hindlimb ischaemia [427]. However, the interference of Notch signalling concurrently leads to poor neovessel quality with leaky, fragile vasculature [428]. Our own laboratory has shown that EPCs derived from South Asian men, who are insulin resistant and at increased risk of cardiovascular sequelae, exhibit impaired vascular repair and angiogenesis which can be rescued with expression of constitutively active AKT1 [328].

In addition to SHIP2, PTEN is an established negative regulator of insulin signalling. However, it is also clearly defined as a tumour suppressor and consistent with this, mice deficient in PTEN have a strong propensity for development of malignancy [429]. Hence, SHIP2 lends itself more convincingly as a potential therapeutic target that may

have translational capacity. Modulation of SHIP2 has already been explored in murine models, as described. Heterozygous deletion has shown enhanced insulin sensitivity, and knockout mice fed a high-fat diet appeared resistance to weight gain and also did not become insulin resistant. It can therefore be reasonably postulated that rescuing diminished PI3K/AKT signalling via SHIP2 inhibition may be beneficial in promoting vascular endothelial function and repair along with improving metabolic control. As outlined earlier, mice with SHIP2 catalytic inactivity have been generated but whole-body haploinsufficiency resulted in impaired growth and developmental defects that impeded clarity [377]. In order to circumvent this limitation, our laboratory has created mice with germline endothelium-specific SHIP2 catalytic domain haploinsufficiency (ECSHIP2$^{\Delta/+}$). Moreover, we have created mice with whole-body inducible SHIP2 catalytic domain haploinsufficiency (SHIP2i$^{\Delta/+}$) to assess the potential benefits of transient SHIP2 inhibition. This may define the value of pursuing pharmacological inhibitors for therapeutic purposes. *In vivo* data generated from these two models forms the basis of this PhD thesis.

Chapter 2 – Aims & Hypotheses

_____

The broad aim of this project was to assess the effects of SHIP2 modulation on metabolic and vascular function.

To address these goals, *in vivo* studies were performed on 10 month aged mice with germline endothelium-specific SHIP2 catalytic domain haploinsufficiency (ECSHIP2$^{\Delta/+}$), and on younger mice (2-3 months) with whole body inducible SHIP2 catalytic domain haploinsufficiency (SHIP2i$^{\Delta/+}$). Studies were extended *in vitro* through use of HUVECs after SHIP2 silencing using lentiviral shRNA transduction or pharmacological inhibition. This exploration highlighted the relevance of observations to human pathophysiology, and potential benefits of clinical translation.

Specifically, the effects of SHIP2 manipulation were explored in the following ways:

1. Vascular formation (developmental angiogenesis in retinas)

2. Vascular regeneration (using model of hindlimb ischaemia)

3. Vascular repair (after injury to femoral artery)

4. Studies of downstream endothelial cell signalling

5. Studies of endothelial cell biology (including migration, proliferation, morphology and polarisation)

6. Metabolic profiling

The primary hypothesis for this project is that SHIP2 inhibition has favourable effects on insulin-mediated glucose lowering, vascular repair and regeneration.

Chapter 3 – Materials

_____

3.1 Animal husbandry

Chow feed	B&K Universal Ltd
SHIP2$^{(18\text{-}19lox/+)}$ mice	Stephane Schurmans
CreER$^{+/0}$ mice	Jax strain 004453
*Tie*2-Cre$^{+/0}$ mice	Jax Labs Bar Harbor
CO_2 chamber	Vet Tech Solutions
Isoflurane	Abbott Logistics BV
Dry ice	BOC
Liquid nitrogen	Statebourne Cryogenics
27G needle	BD Microlance
Pierse Fixation forceps	Fine Science Tools

3.2 Genotyping

1.5mL microcentrifuge tubes	Eppendorf
Sodium hydroxide	Thermo Fisher Scientfic
Ethylenediaminetetraacetic acid (EDTA)	Sigma-Aldrich
Tris-HCl	Thermo Fisher Scientfic
TaqMan Master mix	Bioline
Forward and reverse primers	Invitrogen
Distilled water	BD Biosciences
Laminar flow hood	LabCaire
PCR reaction tubes	Thermo Fisher Scientific
PTC-200 thermal cycler	MJ Research

Agarose gel	Bioline
Ethidium bromide	Sigma-Aldrich
Fume cupboard	Mach-Aire Criterion
Gel tray	Invitrogen
100 base pair ladder	Thermo Fisher Scientific
Chemi XT4 illuminator	Syngene
Gene Sys V1.4.0.0	Syngene

3.3 Pulmonary endothelial cell (PEC) isolation

MV2 basal media	PromoCell
Foetal bovine serum (FBS)	Biosera
Endothelial cell growth supplement (ECGS)	PromoCell
Antibiotic-antimycotic solution (AAS)	Invitrogen
Bovine skin gelatin powder	Sigma-Aldrich
Siliconized glass bottle	Sigma-Aldrich
Bovine serum albumin (BSA) solution	Sigma-Aldrich
Phosphate buffered saline (PBS)	Sigma-Aldrich
Bonn scissor	Fine Science Tools
15mL Falcon	Sarstedt
Dulbecco's Modified Eagle's Medium (DMEM)	Life Technologies
Laminar flow hood	Envair Bio2+
Type II collagenase (#11097113001)	Roche
Water bath	Grant

5cm petri dish	Thermo Fisher Scientific
Size 22 scalpel blade	Swann-Morton
5mL stripette	Corning
MACSMix rotator	Miltenyi Biotec
Incubator	Sanyo
10mL syringe	BD Biosciences
50mL Falcon	Sarstedt
14G orange cannula	BD Biosciences
70μm cell sieve	Greiner Bio-One
Centrifuge	Eppendorf
CD146 antibody-coated magnetic beads	Miltenyi Biotec
Magnetic particle concentrator	BD Biosciences
MiniMACS column	Miltenyi Biotec
6-well plate	Corning

3.4 SHIP2 activity assay

5' phosphatase fluorescence polarisation activity assay (K-1400)	Echelon
Reaction buffer (cat# K-S2RB)	Echelon
POLARstar Omega platereader	BMG Labtech

3.5 Vascular formation in retinas

Dumont micro-blunted tip forcep	Fine Science Tools
Tissue well plate	Transnetyx

24-well plate	Falcon
Paraformaldehyde (PFA)	Thermo Fisher Scientific
KL1500 LCD dissection microscope	Meyer Instruments
Triton X-100	Sigma-Aldrich
Sodium deoxycholate	Sigma-Aldrich
Bovine serum albumin (BSA) powder	Sigma-Aldrich
Sodium azide	Sigma-Aldrich
Calcium chloride	Sigma-Aldrich
Magnesium chloride	Sigma-Aldrich
Manganese chloride	Sigma-Aldrich
Microtitre plate shaker	Stuart
Isolectin B4 pre-conjugated to Alexa Fluor 488	Life Technologies
Vannas spring scissors	Fine Science Tools
Poly-L-lysine coated glass slide	Sigma-Aldrich
22 x 22mm coverslip	VWR
Prolong Gold	Invitrogen
LSM880 confocal microscope	Zeiss
Image J software (v1.46r)	National Institutes of Health

3.6 HUVEC culture and manipulation

Pooled human umbilical vein endothelial cells (HUVECs)	Promo-Cell
M199 basal media	Sigma-Aldrich
HEPES solution	Thermo Fisher Scientific

Sodium pyruvate	Sigma-Aldrich
Heparin	Wockhardt
Endothelial cell growth supplement (ECGS)	Sigma-Aldrich
10cm petri dishes	Corning
Trypsin-EDTA	Sigma-Aldrich
Haemocytometer	Hawksley
Trypan blue	Sigma-Aldrich
SHIP2-targeting short hairpin RNA (shRNA) lentivirus (SHCLNV-NM001567)	Sigma-Aldrich
GFP-targeting short hairpin RNA (shRNA) lentivirus (SHC002H) Sigma-Aldrich	Sigma-Aldrich
AS1938909	Merck
AS1949490	Cambridge Bioscience
Dimethylsulfoxide	Sigma-Aldrich
Gp91ds-tat	Genscript
Gp91ds-tat scrambled peptide	Genscript
Wortmannin (ab120148)	Abcam
LY294002 (ab120243)	Abcam

3.7 Endothelial cell functional assays

3.7.1 Scratch wound

ImageLock 96-well plate	Essen Biosciences
IncuCyte woundmaker 96-pin device	Essen Biosciences
CKX-41 light microscope	Olympus
Cell F software (v3.4)	Olympus

3.7.2 Boyden chamber

Vascular endothelial growth factor (VEGF)	BD Biosciences
8µM polycarbonate inserts	Falcon
Ethanol	Thermo Fisher Scientific
Cotton bud	Johnson+Johnson
Haematoxylin	Sigma-Aldrich
Eosin	Sigma-Aldrich

3.7.3 5-ethynyl-2'-deoxyuridine (EdU) incorporation

Click-iT EdU Alexa Fluor 647 imaging kit	Life Technologies
Fluorescence-activated cell sorting (FACS) tubes	Fisher
BD-LSR Fortessa flow cytometer	BD Biosciences
FACSDiva (v6.2)	BD Biosciences

3.7.4 Bead sprouting

EGM-2 basal media	Lonza
Bulletkit	Lonza
Cytodex-3 beads	Amersham
T25 cell culture flask	Corning
Fibrinogen	Sigma-Aldrich
Aprotinin	Sigma-Aldrich
Thrombin	Sigma-Aldrich

3.8 Immunofluorescence

3.8.1 Lamellipodial staining

35mm imaging dish	Ibidi
Phalloidin pre-conjugated to Alexa Fluor 647 (A22287)	Life Technologies

3.8.2 GM130 staining

24-well imaging plate	Ibidi
Goat serum	Sigma-Aldrich
Mouse anti-GM130 antibody pre-conjugated to to Alexa Fluor 488 (#560257)	BD Pharmingen
Hoescht 33342 (#561908)	BD Sciences

3.8.3 SHIP2 staining

Rabbit anti-SHIP2 primary antibody (ab166916)	Abcam
Goat anti-rabbit secondary antibody pre-conjugated to Alexa Fluor 647 (#A-21245)	Invitrogen
Ulex Europaeus pre-conjugated with fluorescein isothiocyanate (FITC) (#553929)	BD Sciences

3.9 Dihydroethidium (DHE) assay

96-well plate	Thermo Scientific
Dihydroethidium	Life Technologies
Krebs-HEPES buffer	Sigma-Aldrich
Flex Station 3 microplate reader	Sunnyvale
SoftMax pro (v5.4.5)	Molecular Devices

3.10 Western blotting

Cell extraction buffer	Sigma-Aldrich
Protease inhibitor	Santa Cruz Biotechnology
Phosphatase inhibitor	Santa Cruz Biotechnology
1.8cm blade cell scraper	Corning
-40°C freezer	Sanyo
6mm cone ball	Retsch
Tissue lyser	Qiagen
Bicinchoninic acid (BCA) assay kit	Thermo Fisher Scientific
DMX TC microplate reader	Dynex Technologies
Revelation software (v4.21)	Dynex Technologies
Sample buffer	Invitrogen
Reducing buffer	Invitrogen
Heating block	Fisher-Scientific
Bis-Tris polyacrylamide gel	Bio-Rad
Marker	Bio-Rad
Criterion cell tank	Bio-Rad
2-(N-morpholino)ethanesulfonic acid/sodium dodecyl sulphate (MES SDS)	Invitrogen
Polyvinylidene fluoride (PVDF) membrane	Merck Millipore
Metal stirrer	Stur Lab
Methanol	Fisher Scientific
Magnetic rotary plate	Heidolph
Tris-buffered saline with Tween (TBST)	Sigma-Aldrich

Primary antibodies (see Table 4-5)	Cell Signalling
Secondary antibodies (see Table 4-5)	Dako
Cling film	Viking Direct
Immobilon western chemiluminescent horseradish peroxidase (HRP) substrate	Merck Millipore
Camera scanner (Image Station 2000R)	Kodak
Restore PLUS stripping buffer	Thermo Scientific
GeneTools (v1.6.1)	Syngene

3.11 Tamoxifen induction

Tamoxifen (#T5648)	Sigma-Aldrich
Corn oil	Sigma-Aldrich

3.12 Metabolic profiling

3.12.1 Gross body weights

Electronic scales	Kern

3.12.2 Glucose tolerance testing (GTT)

Glucose	Sigma-Aldrich
Glucometer	Aviva
Accu-Chek testing strips	Aviva

3.12.3 Insulin tolerance testing (ITT)

Actrapid insulin	Novo Nordisk

3.12.4 Plasma insulin measurement (ELISA)

1mL syringe	Terumo
-80°C freezer	Panasonic
Ultra-sensitive mouse insulin ELISA kit	Crystal Chem

3.13 Angiogenesis after hindlimb ischaemia

Electric razor	Contura
Veet cream	Reckitt Benckiser
Oxygen	BOC Medical
Microporous surgical tape	Jax First AId
Buprenorphine	Alsatoe Animal Health
Povidone-iodine solution	Sigma-Aldrich
Vicryl suture	Ethicon
Optimal cutting temperature (OCT) compound	CellPath
2-methylbutane (isopentane)	VWR Chemicals
Long forceps	Agar Scientific
20mm cork plates	Fisher Scientific
CM1900 cryostat	Leica
Stainless steel S35 microtome blade	Feather
Superfrost Plus slides	Thermo Fisher Scientific
PAP pen	Kisker Biotech MKP-1
22 x 22mm coverslip	VWR

3.14 Vascular repair after denuding injury

OPMI 1-FC dissecting microscope	Zeiss
Iris scissors	World Precision Instruments
Lignol (1% lignocaine and adrenaline)	Arnolds
0.014 inch angioplasty guide wire	Abbott Vascular
Irripod (sterile sodium chloride (NaCl))	Unither
Evans blue solution	Acros Organics
Dissecting Stereo microscope	Olympus
QiCam digital camera	Olympus
ImagePro Plus 7.2	Media Cybernetics

Chapter 4 – Methods

_____

4.1 Animal husbandry

4.1.1 General housing

All murine work was performed in accordance with accepted standards of care as per the Experimental Animals (Scientific Procedures) Act 1998, and with UK Home Office approval (project licence 40/3523 and P144DD0D6, personal licence IB8837F68). Mice were housed in a designated facility at University of Leeds. Environment was maintained at a fixed temperature and humidity, and with the use of a 12 hour light/dark cycle. Unless deliberately specified, mice were fed with a standard chow diet and provided with unrestricted access to water. All littermates were maintained with parents until 3 weeks of age, at which point they were weaned and ear notches obtained for genotyping. Littermates were grouped into cages containing a maximum of 5 mice. Every effort was made to utilise mice promptly for experimental purposes, once sufficiently mature to tolerate procedural testing.

4.1.2 Breeding

All mice were bred onto a C57 black 6 (C57BL/6J) background for at least 10 successive generations. This was performed in a conventional animal facility using general housing conditions as described above. Initially, Cre-recombinase specific *lox*P sites were inserted into introns surrounding exons 18 and 19 of the INPPL1 gene in a heterozygous fashion (SHIP2$^{(18-19lox/+)}$) [377].

For production of germline ECSHIP2$^{\Delta/+}$ mice, female SHIP2$^{(18-19lox/+)}$ mice were crossed with male *Tie*2-Cre$^{+/0}$ mice. The Cre/lox system is particularly useful for lineage-specific genetic manipulation in murine models. Cre is a bacteriophage P1-derived

recombinase that excises DNA flanked by two correctly orientated *lox*P recognition sites [430]. Promoter and enhancer regions of the mouse *Tie*2 gene were used to drive Cre transgene expression specifically in endothelial cells [431]. Tie2 is an angiopoietin receptor, which remains expressed throughout development and adulthood and is detectable in the endothelial cells of virtually all quiescent and angiogenic mature adult tissues [432]. To produce the separate SHIP2i$^{\Delta/+}$ colony, female SHIP2$^{(18-19lox/+)}$ mice were crossed with male mice that expressed a mutated fusion protein of Cre recombinase and the human oestrogen receptor (CreERT2$^{+/0}$) in all cell lineages. Expression of this fusion protein is driven by a CAG promoter (**C**ytomegalovirus (CMV) early enhancer element, chicken β-**A**ctin gene and splice acceptor of the rabbit β-**G**lobin gene) to enable tamoxifen-inducible global SHIP2 haploinsufficiency [433]. The protocol used for tamoxifen induction is outlined in Section 4.11.

Breeding cages consisted of one male and two female mice. As anticipated, progeny of various genotypes were born, the identities of which were confirmed using DNA from ear notches. Females were occasionally used to establish new breeding trios, but it was only males that were used for experimental purposes. This was to negate confounding effects pertaining to cyclical variations in reproductive hormones. Comparative controls ("WT") were always littermates that expressed Cre recombinase but lacked SHIP2 *lox*P sites (SHIP2$^{+/+}$), and hence did not undergo SHIP2 catalytic domain deletion.
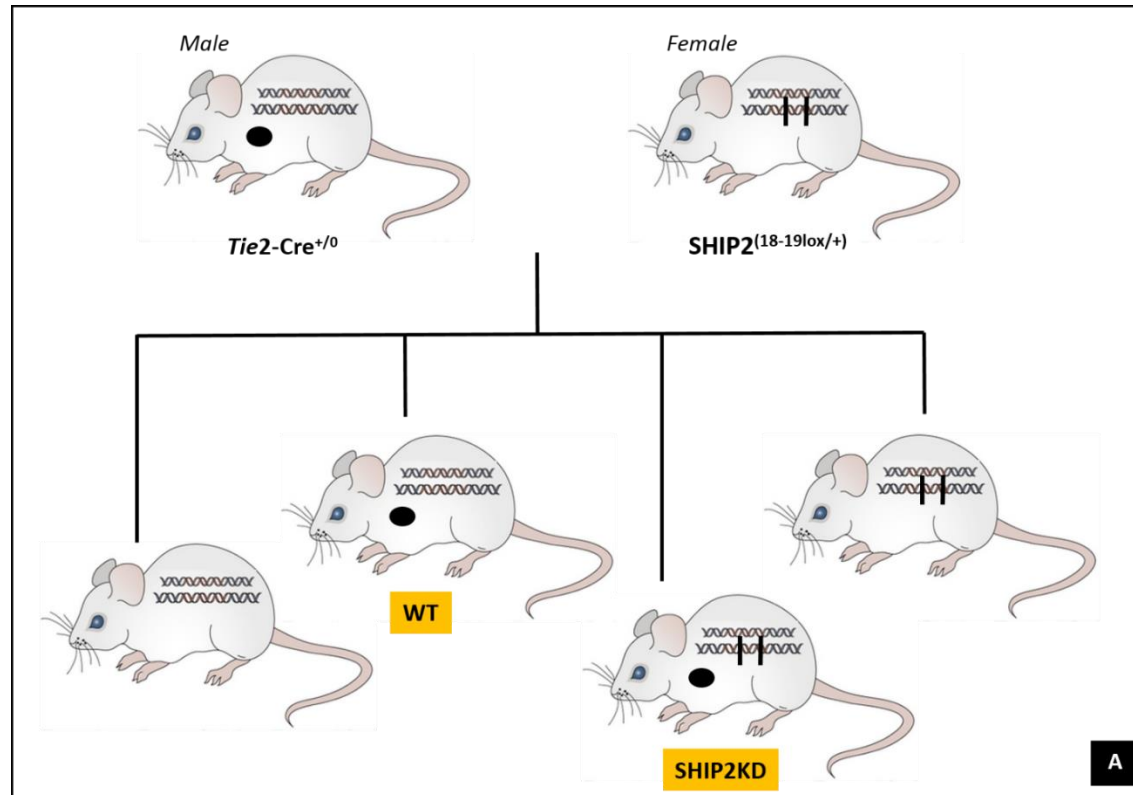
Figure 4-1 – Breeding of ECSHIP2$^{\Delta/+}$ colony. "WT" represents controls mice. "SHIP2KD" represents mice with endothelium-specific germline SHIP2 catalytic domain haploinsufficiency.
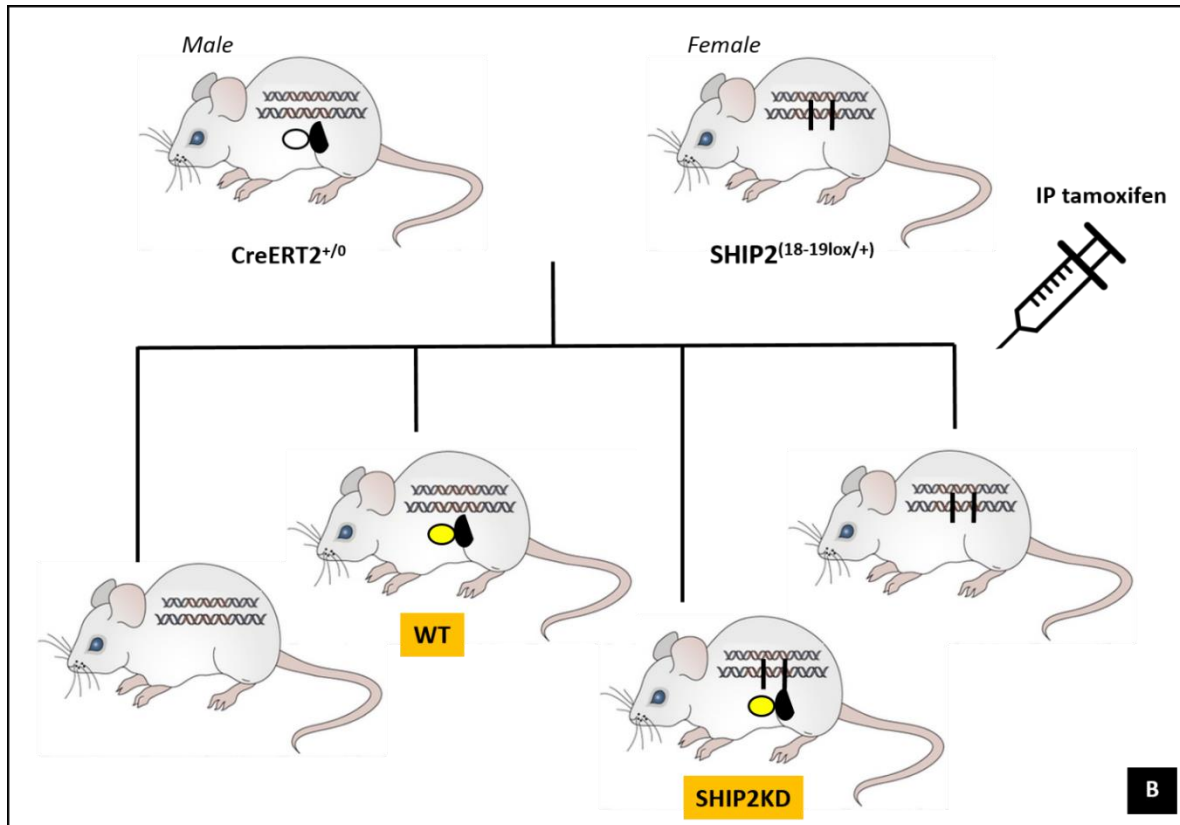
Figure 4-2 – Breeding of SHIP2i$^{\Delta/+}$ colony. "WT" represents controls mice. "SHIP2KD" represents mice with inducible whole-body SHIP2 catalytic domain haploinsufficiency.

4.1.3   Euthanasia

Sacrifice of mice was performed using Home Office approved techniques at all times. This predominantly involved use of a chamber allowing exposure to rising concentrations of carbon dioxide (CO_2) within a 12 minute cycle. Death was subsequently confirmed by a secondary means such as cervical dislocation. When blood sampling or organ harvesting was required, euthanasia was performed using terminal anaesthetic with isoflurane inhalation. Exsanguination via intra-cardiac puncture using a 27G needle was performed rapidly to derive whole blood, and organs were then harvested prior to transfer in ice or liquid nitrogen for immediate processing or storage. Sacrifice of pups prior to retinal harvesting was achieved by cervical dislocation using Pierse Fixation forceps followed by prompt decapitation.

4.2   Genotyping

4.2.1   DNA extraction

Tissue samples were derived from ear notching, for the purpose of identification, at the time of weaning (3 weeks of age). Samples were kept in 0.5mL microcentrifuge tubes in a freezer at -20°C until required. At the time of genotyping, heat blocks were set to 95°C. 100μL of 25mM sodium hydroxide (NaOH) mixed with 0.2mM ethylenediaminetetraacetic acid (EDTA) was added to each tissue sample before placing in the heat block for a duration of 10 minutes. This enabled disruption of cell walls and the hydrogen bonds between DNA bases, converting double strands to single strands. Once extracted, 100μL of 40mM Tris-HCl (hydrochloric acid with a tris

base) was introduced for 10 minutes to decrease alkalinity of the mixture and allow hydrogen bonds to be re-established. All samples were subsequently vortexed.

4.2.2 Polymerase chain reaction (PCR)

Most of the reagents used for DNA PCR were stored in a -20°C freezer. Components included a pre-ordered 'TaqMan Master mix' stock solution, distilled water and specific primers (see Table 4-1). The 'Master mix' solution contained deoxynucleotide triphosphate (dNTP), thermostable *Thermophilus aquaticus* (Taq)-derived DNA polymerase, magnesium chloride ($MgCl_2$) as a bivalent cation and a buffer solution to maintain an optimal chemical environment for enzymatic activity. Stocks of the forward and reverse primers were sourced commercially, and working solutions made by reconstitution in TE buffer (10mM Tris and 1mM EDTA) with a 1:10 dilution in distilled water. These short fragments were complementary to the 3' ends of the sense and anti-sense strands of the respective DNA target (i.e. Cre or floxed SHIP2), with the following primer sequences:

Cre – forward	5' – GCA TTA CCG GTC GAT GCA ACG AGT GAT GAG – 3'
Cre – reverse	5' – GAG TGA ACG AAC CTG GTC GAA ATC AGT GCG – 3'
SHIP2 – forward	5' – GCT TAG ACA TGG ATA TCC AG – 3'
SHIP2 – reverse	5' – CAG TTG GCT TCT GCT TGT GC – 3'

Table 4-1 – Cre and SHIP2 primers for DNA sequencing. These were used on tissue derived from both ECSHIP2$^{\Delta/+}$ and SHIP2i$^{\Delta/+}$ mice.

Samples were prepared in a laminar flow hood to reduce the risk of contamination. Individual reagents were kept on ice prior to use, and added in the volumes listed below (Table 4-2), to produce a final working solution of 24µL in individually labelled PCR tubes. These samples were vortexed prior to addition of 1µL of DNA using a designated Gilson pipette. Both negative and positive controls were also prepared, with tissue derived from mice that had been previously genotyped. A final vortex was performed to ensure adequate mixing. PTC thermal cyclers with pre-specified programmes were utilised to enable DNA amplification. This incorporated stages of initialisation, denaturation, annealing, elongation and a final hold (detailed in Table 4-3). All products were subsequently refrigerated at 4°C until use for gel electrophoresis.

Reagent	Volume (µL)
'Master mix'	10.0
Forward primer	0.5
Reverse primer	0.5
Distilled water	13.0
DNA	1.0
Total	**25**

Table 4-2 – Constituents of stock solution for genotyping.

Cre			SHIP2		
95°C	1 min		95°C	3 minutes	
95°C	15 secs	⎱ 35 cycles	94°C	30 secs	⎱ 35 cycles
51°C	30 secs		59°C	30 secs	
72°C	1 min		72°C	1 min	
72°C	6 minutes		72°C	5 minutes	
4°C	Hold		4°C	Hold	

Table 4-3 – Cre and SHIP2 DNA amplification cycles.

4.2.3 Agarose gel electrophoresis

This was performed using 1.5% agarose gel, which was made by mixing 1.8g of agarose using a spatula into 120mL of Tris-acetate-EDTA (TAE) buffer in a conical flask. This was heated in a microwave at 800W in two stages (60 secs and 30 secs) before addition of 3µL of ethidium bromide in a fume cupboard, which intercalates into DNA and fluoresces under ultraviolet (UV) light to allow visualisation. The agarose gel was subsequently poured into a gel tray and allowed to set for 30 minutes. The gel contained a plastic comb to form wells into which reaction samples could be loaded. The agarose gel was maintained in a tank containing 600mL of TAE buffer, derived from a 50X stock solution containing 242g Tris, 100mL of 0.5mM EDTA and 57mL of acetic acid diluted up to 1L using distilled water. 5µL of a 100 base pair ladder was loaded for reference purposes, with adjacent wells containing 20µL of each of the individual PCR products. Agarose gel is composed of unbranched chains of uncharged

carbohydrates without cross-links, resulting in a gel with large pores. Application of an electric current at 110 V for 60 minutes enabled movement of negatively charged DNA from cathode to anode through these pores, with distance travelled being inversely related to molecular size. Imaging of produced bands was conducted in a Chemi XT4 illuminator using Gene Sys software, with a single band at 408 base pairs for the Cre transgene and two bands at 411 and 500 base pairs for the SHIP2 transgene.

4.3   Pulmonary endothelial cell (PEC) isolation

4.3.1   Preparation of reagents

Pulmonary endothelial cell (PEC) isolation was achieved using a modified technique derived from Sobczak *et al* [434]. Certain reagents were prepared in advance. 500mL basal endothelial medium MV2 was supplemented with 50mL batch-tested foetal bovine serum (FBS), 27.1mL endothelial cell growth supplement (ECGS) and 10mL antibiotic-antimycotic solution (AAS). This stock solution was divided into individual 50mL aliquots and maintained in sterile conditions for up to 1 month. A stock solution of 2% gelatin was also prepared, derived from 2g of bovine skin gelatin powder mixed in 100mL of distilled water. This was placed in a siliconized glass bottle and autoclaved prior to use. Lastly, 666µL of 7.5% bovine serum albumin (BSA) was added to 50mL phosphate buffered saline (PBS) to produce 0.1% PBS/BSA stock solution.

4.3.2   Lung harvest and single cell suspension

ECSHIP2$^{\Delta/+}$ mice were euthanised in a CO_2 chamber, followed by a midline sternotomy incision using Bonn scissors and careful dissection of lung tissue to avoid excess

connective tissue or thrombi. This was placed in 15mL Falcon tubes containing 10mL of sterile Dulbecco's Modified Eagle's Medium (DMEM) and transferred on ice to a laminar flow hood in the tissue culture laboratory. Here, lungs were transferred to separate Falcons, containing 10mL of 1mg/mL type II collagenase mixed in DMEM, that were pre-warmed to 37°C in a water bath. Lung tissue derived from single mice was transferred onto a 5cm diameter petri dish and 500µL of type II collagenase solution added to aid enzymatic digestion. Specimens were minced thoroughly with two size 22 scalpel blades until a homogenous paste was formed and bubbles visualised. This was aspirated using a 5mL stripette into its original Falcon tubes before incubation on a MacsMix rotator in an incubator at 37°C for 45 minutes. Once the incubation period was complete, solutions were transferred to fresh 50 mL Falcons. A 10mL syringe was attached to the end of a 14G orange cannula, and the solution agitated 20 times gently to avoid bubble formation.

4.3.3   Magnetic bead coating and cell isolation

This single cell suspension was passed through 70µm cell sieves into separate 50mL Falcon tubes and neutralised with 5mL of MV2. The filtrate was centrifuged at 400g for 5 minutes before gentle aspiration of the supernatant. Cells were re-suspended in 200µL PBS/BSA mixed with 20µL anti-CD146 antibody-coated magnetic beads and transferred to 1.5mL microcentrifuge tubes. CD146 is expressed in endothelial cells in vascular tissue throughout the body, and is involved in cell adhesion and cohesion of the endothelial monolayer at intercellular junctions [435]. Samples were spun on the MACSMix rotator for 20 minutes in a cold room, before addition of 1mL PBS/BSA and

centrifugation at 4000 revolutions per minute (rpm) for 5 minutes. During this phase, a magnetic particle concentrator was assembled in the hood and loaded with MiniMACS columns which had been primed with 500µL PBS/BSA. Each sample was applied to an individual column and once fully drained and washed through three times with 500µL PBS/BSA, 1mL of fresh PBS/BSA was added and a plunger used to mechanically expel the CD146+ cells into fresh 15mL Falcon tubes. After centrifugation at 400g for 2 minutes, this process was repeated three times over to wash debris from the selected cells. The final samples were re-suspended in 2mL of MV2 media and added to individual wells of a 6 well plate that had been pre-coated with 2% gelatin. A full media change was performed after 24 hours, followed by a half media change every 48 hours until confluence was reached. PECs were utilised for the SHIP2 activity and dihydroethidium (DHE) assays, and to assess protein expression of SHIP2 in the ECSHIP2$^{\Delta/+}$ colony.

4.4 SHIP2 activity assay

This was performed using both PECs and HUVECs. The purchased kit operates as a 5' phosphatase fluorescence polarization activity assay using the following components: 10µg PI(3,4,5)P$_3$ substrate, 0.6µg PI(3,4)P$_2$ standard, 10µg vials of PI(3,4)P$_2$ detector, 10µM probe, PBS tablet and a 384-well assay plate with acetate sealer. First, reagents were prepared. The PBS tablet was dissolved in 200mL distilled water and was used as the PBS buffer solution. A 40µM stock solution of PI(3,4,5)P$_3$ substrate was produced by reconstituting 10µg in 255µL distilled water. A standard buffer containing 2µM of PIP3 substrate was made by diluting the 40µM stock solution 20-fold in a reaction

buffer (purchased separately). The PI(3,4)P$_2$ standard was produced by reconstituting 0.6µg in 350µL distilled water for a 2µM stock solution. 1mL PBS was added to 10µg of PI(3,4)P$_2$ detector to produce a 10µg/mL working solution. The 10µM probe stock was diluted 200-fold for a working solution of 50nM.

At commencement, 45µL of each sample was mixed with 45µL of 4µM PI(3,4,5)P$_3$ substrate, a 10-fold dilution of the original 40µM stock, and incubated at 37°C for 1 hour. The reaction was then terminated by heating to 95°C for 3 minutes. Samples were allowed to cool and centrifuged at 5,000 rpm for 2 minutes. Five serial two-fold dilutions of the 2µM PI(3,4)P$_2$ standard in standard buffer were made (i.e. 1.0µM, 0.5µM, 0.25µM, 0.125µM and 0.0625µM). A 0µM control containing just standard buffer was also used. 40µL of these diluents were added to wells of the plate in duplicate, succeeded by addition of each sample as duplicates in separate wells. Subsequently, 40µL PI(3,4)P$_2$ detector and 20µL probe was added to all wells.

The plate was covered in foil to protect from light, and transferred to a POLARstar Omega platereader. This enabled fluorescence polarisation detection with use of appropriate filters (550nm excitation, 580nm emission). Values were expected to decrease as probe binding to the PI(3,4)P$_2$ detector was displaced by PI(3,4)P$_2$ produced from SHIP2 enzymatic activity. Kinetic readings were obtained every 10 minutes for a duration of 90 minutes. A PI(3,4)P$_2$ standard curve was plotted using a non-linear regression curve fit. Polarisation values obtained from the enzymatic reactions were then used to interpolate PI(3,4)P$_2$ values from the standard curve, enabling quantification of PIP3 substrate conversion.

4.5 Vascular formation in retinas

4.5.1 Ocular harvesting

Dissection and staining of retinas was performed on littermates derived from the ECSHIP2$^{\Delta/+}$ colony. These were harvested at 5 days of age to assess primitive vascular labyrinth formation during post-natal developmental angiogenesis, using an established and well-reported protocol [436]. Pups were first separated from their parents and weighed. Euthanasia was performed by cervical dislocation using Dumont micro-blunted tip forceps followed by decapitation, with the tail tip collected in individual wells of a tissue plate for genotyping purposes.

A longitudinal incision was made on the upper and lower surfaces of the head with fine scissors. The head was turned to one side, to allow the subcutaneous tissue to be gently peeled forward. This extended beyond the nasal bridge to allow exposure of both orbits. Traction was placed on the large pedicle close to the orbit to enable removal of as much adherent tissue as possible from the eyeball. Subsequently, blunt curved forceps were placed in the inferior border of the orbit to allow the eyeball to be lifted out on its optic nerve pedicle. Both eyeballs were placed in individual wells of a 24-well plate containing 1mL of 4% paraformaldehyde (PFA) in PBS and uniquely labelled for subsequent identification purposes. Samples were stored at room temperature for 2 hours to enable a 'strong fix'. After a wash in 1mL of PBS, they were maintained in 2mL of fresh PBS at 4°C until time of dissection.

4.5.2 Retinal dissection

This was performed using a KL1500 LCD dissection microscope. First, eyeballs were carefully transferred into a petri dish filled with PBS to prevent drying. A needle was used to pierce the cornea, which enabled advancement of a scissor blade into the anterior chamber to remove all but a small rim of cornea. The cornea was carefully pulled apart, which advanced the tear into the sclera and choroid and facilitated gradual detachment from the iris. Using this technique, layers were removed to expose the retina. The lens was extracted with a forceps and a small volume of PBS added into the posterior chamber. This enhanced visualisation of hyaloid vessels, which could be circumferentially fractured from the posterior chamber by pulling gently at the ciliary shelf and removed in bulk from the region of the optic nerve. Great care was taken at this stage to avoid damage to the retinal surface itself. The retinas were subsequently returned to their original wells and maintained in PBS to enable staining.

4.5.3 Isolectin B4 staining

Permeabilisation and blocking buffer was made using the following constituents: 50mL PBS (pH 6.8), 0.5% Triton X-100, 0.01% sodium deoxycholate, 1% BSA, 0.02% sodium azide and 1M each of calcium chloride ($CaCl_2$), magnesium chloride ($MgCl_2$) and manganese chloride ($MnCl_2$). 2mL of this buffer was added to each well and retinas left overnight at 4°C on a microtitre plate shaker at 250 rpm. They were subsequently rinsed for 10 minutes in 2mL of PBLEC solution, which was made using 49.5mL of PBS (pH 6.8), 1% Triton and 1M each of $CaCl_2$, $MgCl_2$ and $MnCl_2$. *Griffonia simplicifolia* (Bandeiraea) isolectin B4 pre-conjugated to Alexa Fluor 488 was added at

a 1:100 dilution, dissolved in PBLEC solution. This specifically binds terminal α-galactosyl residues expressed by various cells including, but not limited to, endothelial cells [437].

Overnight labelling was performed at 4°C, covered in foil to protect from light. This was followed by three washes with 0.2% Triton mixed in PBS, each for 20 minutes at room temperature. After the completion of staining, liquid was carefully aspirated from wells using a 1mL pipette. The orbit was partially cut using spring scissors at 12, 3, 6 and 9 o'clock positions, which enabled the retina to remain intact but capable of flat mounting. This was achieved on a poly-L-lysine coated glass slide and after placement of a 22 x 22mm coverslip preloaded with Prolong Gold, specimens were sealed with nail varnish. Samples were covered in foil prior to imaging using a LSM880 confocal microscope. This final step was performed by Dr Richard Cubbon to allow blinded imaging.

4.5.4   Analyses of vasculature

Analyses were performed with Image J software using reported methodology [436]. Individual sections of retina were imaged at 10X magnification to assess the primitive plexus at P5. Radial outgrowth was defined as the distance from the centre of the optic disc to the peripheral vasculature (in μm). For quantification of vascular area and branch points, a subjective region of interest was first established to differentiate frontal from central regions within each quadrant based on vascular density and extent of remodelling. 'Vascular area' was subsequently quantified as the proportional area of isolectin B4 staining within the total region of interest (i.e. frontal or central).

Magnified $0.04mm^2$ (200 x 200μm) regions of interest, set back 200μm from the vascular front between arteries and veins, were used for quantification of 'branching points'. These were deemed to be at junctions of capillary segments. Tip cells were quantified per mm of 'vascular front', defined as the line connecting the bases of the sprouting endothelial cells. There are no specific criteria available for defining tip cells, as there is no data available on endothelial markers that selectively label sprouting tip cells [436]. Filopodia were quantified per 100μm of 'angiogenic front', and this was defined as the line navigating to the tip of the sprouts. Images were collected at a 40X objective. The average of multiple regions (≥ 4) per pair of retinas for each mouse was used for all statistical analyses.
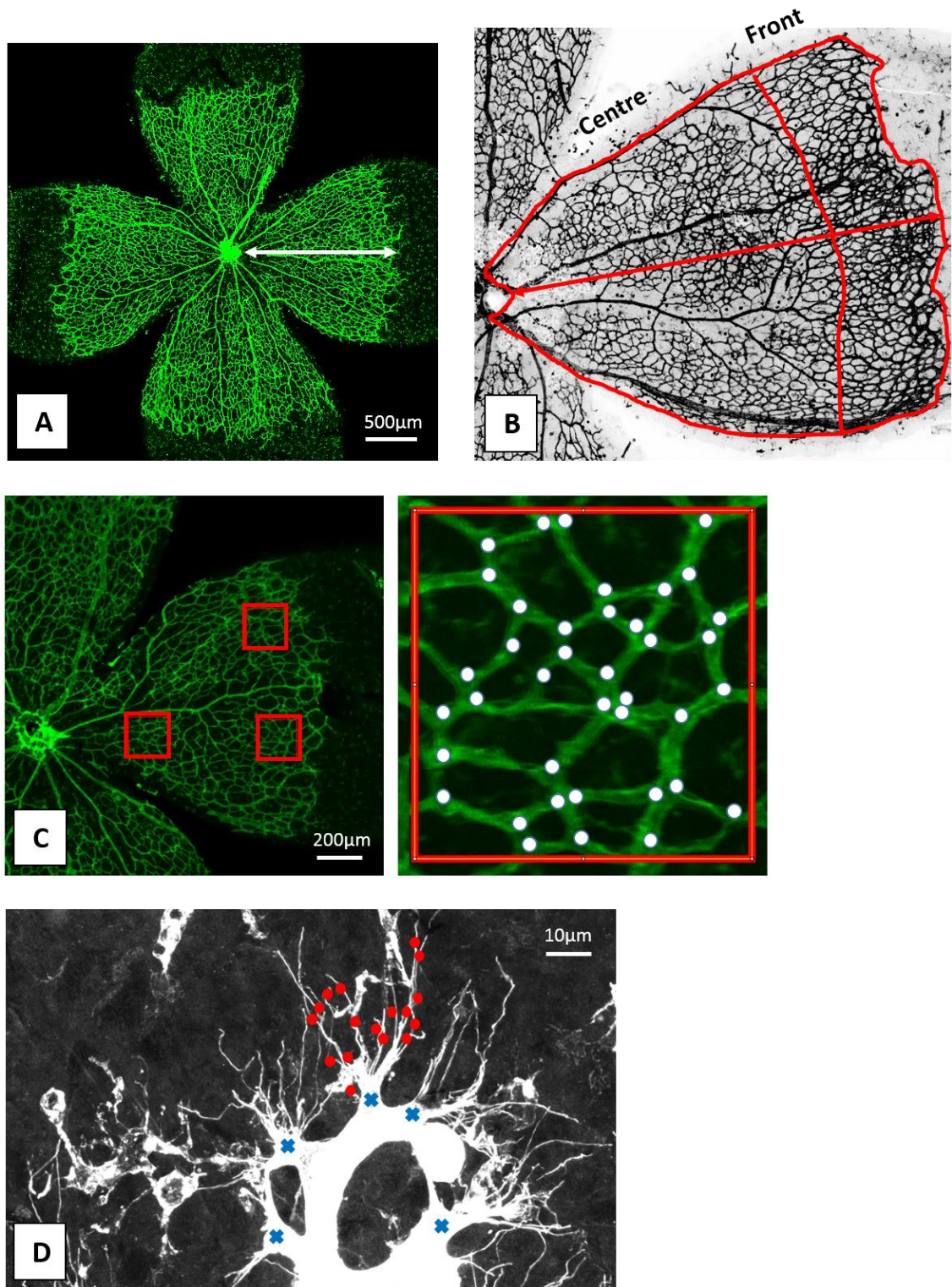
Figure 4-3 – Mounted retinas were stained with isolectin B4 (*green*) and analysed for the following parameters: radial outgrowth **(Panel A)**, frontal and central vascular area **(Panel B)**, number of branch points as depicted by *white circle* **(Panel C)** and abundance of tip cells (*blue cross*) and filopodia (*red circle*) **(Panel D)**.

4.6 HUVEC culture and manipulation

4.6.1 Cell culture

Human umbilical vein endothelial cells (HUVECs), as the name suggests, line single umbilical cord veins. In foetal development, this carries oxygenated blood from the placenta into the growing foetus and thus provides an useful analogue for adult human macrovascular endothelial cells. HUVECs are relatively cost-effective and isolation from umbilical cords is reasonably simple. They proliferate rapidly in defined tissue culture conditions and are therefore of particular use when performing functional *in vitro* assays.

Healthy pooled donor samples were obtained commercially and maintained as aliquots in liquid nitrogen. At time of use, P2 aliquots were removed from storage and transferred in ice. After prompt defrosting of the 1mL sample in a water bath at 37°C, it was added to 9mL of M199 media. This had been pre-prepared and contained 380mL of M199 basal media, 100mL of FBS, 10mL of 1M HEPES buffer, 5mL of AAS, 10mL of sodium pyruvate, 2500 IU of heparin and 2.5mL of ECGS. After thorough vortexing, cells were divided equally into three 10cm petri dishes which had been pre-coated with 0.1% gelatin. 6.67mL of M199 media was added to produce a total solution of 10mL in each dish. They were incubated at 37°C, with a full media change every 48 hours. Subsequently, either shRNA lentiviral transduction (see Section 4.6.3) or small molecule inhibition (SMI) (see Section 4.6.4) was performed prior to use in functional assays.

4.6.2   Cell counting

For all the functional assays conducted with HUVECs, it was necessary to count absolute numbers of cells so that the correct amounts were used in individual experiments. To achieve this, one of the three 10cm petri dishes was washed twice in warmed, sterile PBS to remove media and debris. Specific volumes of 0.25% trypsin-EDTA were added depending on the size of well (3mL for a 10cm petri dish, 1mL for a 6-well plate), and incubated at 37°C for 2 minutes. Visualisation under light microscopy confirmed adequate detachment of cells, which were then neutralised by the addition of M199 media (5mL in the petri dish, 2mL in the 6-well plate). Samples were thoroughly mixed with a 10mL stripette prior to transfer into a 10mL Falcon tube for centrifugation at 400g for 5 minutes. The supernatant was carefully discarded and the resultant pellet reconstituted in 1mL of M199 media. This was vortexed prior to mixing of 20μL with an equivalent volume of trypan blue solution. This diazo dye traverses the cell membrane of dead cells (i.e. necrotic or apoptotic), conferring a blue colour to distinguish them from live cells which remain white. The mixture was injected carefully into a haemocytometer and by visualising the number of white cells, an extrapolated value could be used to quantify number of live HUVECs in 1mL. This enabled calculations to vary seeding densities depending on the assay performed.

4.6.3   SHIP2 lentiviral transduction

All work that included lentiviral transduction was conducted in a designated viral laboratory ('Category 2') with appropriate precautions taken at every step. Once cells had been seeded for 3 days, a commercially-obtained short hairpin RNA (shRNA)

lentivirus was used to transduce SHIP2-targeting shRNA or control green fluorescent

protein (GFP)-targeting shRNA. This modality was preferred to small interfering RNA

(siRNA), which requires higher dosage, has a higher likelihood of 'off target' effects

and allows only transient knockdown [438]. The shRNA is an artificial RNA molecule

with a tight hairpin turn. Once it has integrated into the host genome through its

expression vector, i.e. lentivirus, there is nuclear transcription mediated by

promoters. The resulting pre-shRNA is exported out of the nucleus and processed into

a RNA-induced silencing complex (RISC). The antisense strand directs RISC to mRNA

that has a complementary sequence. There is subsequent cleavage or regression of

translation of the mRNA, in this case SHIP2, resulting in targeted gene silencing.
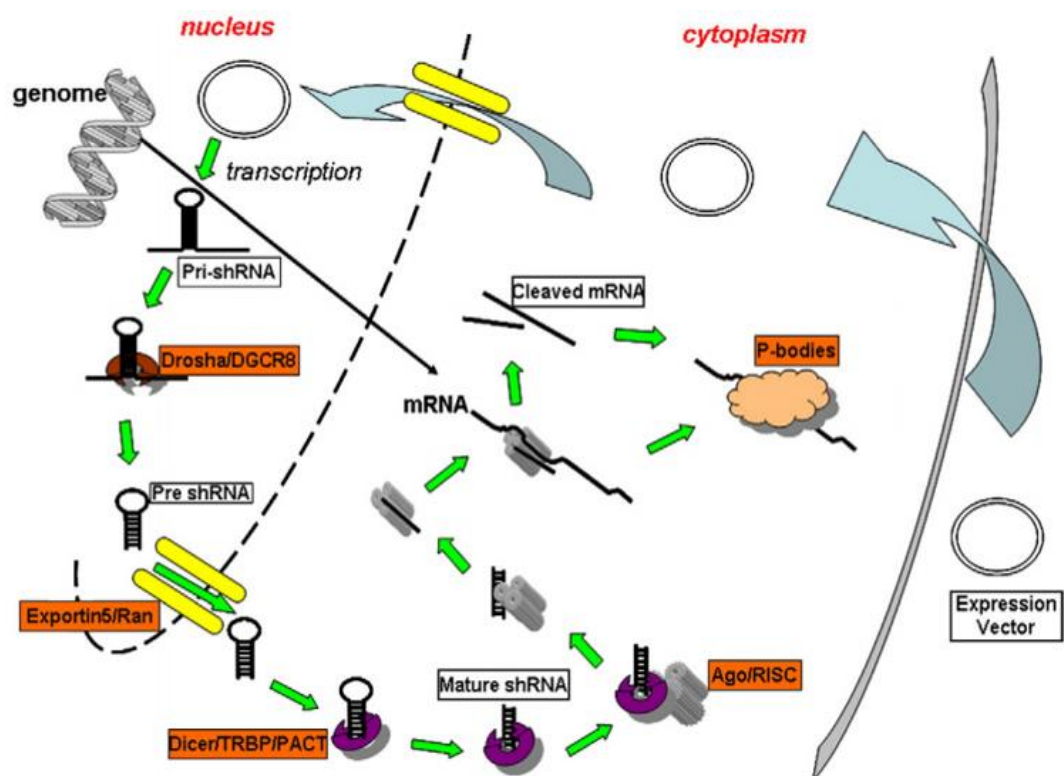
Figure 4-4 – Schematic of shRNA-mediated lentiviral transduction. TRBP = Tat-RNA
binding protein; PACT = PKR activating protein; RISC = RNA-interfering silencing

complex. Rao *et al*. Adv Drug Deliv Rev 2009; 61(9):746-59 [438].

Prior laboratory experience of shRNA lentiviruses enabled clarification that addition of 10μL of shRNA to 300,000 cells results in 10 multiplicity of infection (MOI), i.e. 10 vector particles per cell. This was used to calculate respective volumes of SHIP2 shRNA and control lentivirus that needed to be added to generate 5, 10 and 20 MOI, respectively. This was introduced directly into the petri dishes seeded with HUVECs using a sterile 200μL pipette, with gentle mixing for 45 seconds to ensure spatial distribution. After 24 hours, a full media change was performed and a further 3 days were allowed to elapse before splitting of cells for their respective assays. This was to ensure that translational effects of knockdown were discernible.
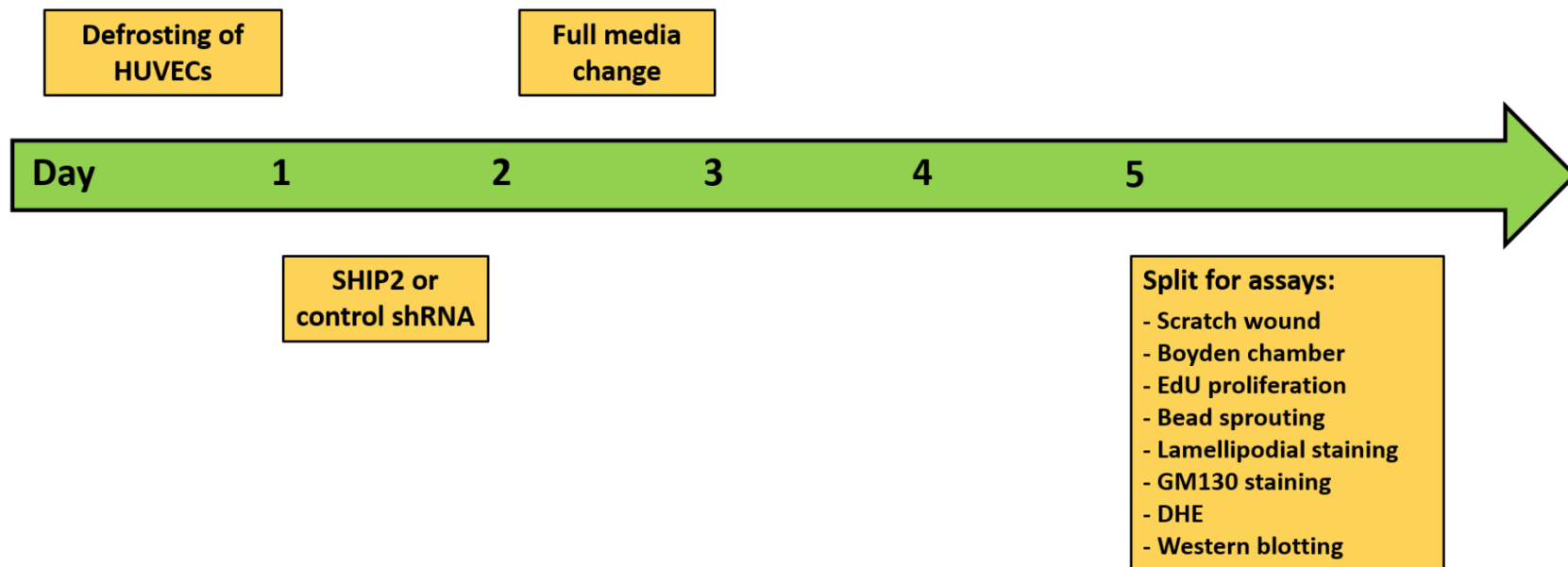
Figure 4-5 – Timeline for HUVEC culture, lentiviral transduction and splitting for assays. HUVEC = human umbilical vein endothelial cells; shRNA = short hairpin RNA; EdU = 5-ethynyl-2'-deoxyuridine; DHE = dihydroethidium.

4.6.4   SHIP2 small molecule inhibition (SMI)

This was performed on plated HUVECs without lentiviral manipulation. Firstly, dose response was assessed in the context of a mechanical scratch assay. Cells were split and seeded at 50,000 cells/well, with a minimum of 4 replicates, and grown to confluence. They were serum depleted using 1% FBS-containing M199 media for a duration of 4 hours. A mechanical wound was made with the tip of a 1000μL pipette to generate longitudinal scratches, washed in 100μL PBS and replaced with 300μL of 2% FBS-containing M199 media, mixed with differing concentrations (0-20μM) of commercially available SHIP2 SMI for 18 hours duration. Two different types were used, AS1949490 and AS1938909, pre-dissolved in dimethylsulfoxide (DMSO) to generate a stock solution of 5mM. Control cells were exposed to an equivalent volume of DMSO without SMI. 10μM corresponds to maximum inhibition of SHIP2 in activity assays [370, 439] and was therefore used for statistical analysis and further functional assays.

Exposure to the inhibitor was for the duration of the assay, i.e. 18 hours for scratch wound, 4 hours for 5-ethynyl-2'-deoxyuridine (EdU) proliferation, 6 hours for bead sprouting and 30 mins for GM130 staining.

4.6.5   Nox2 and PI3K peptide inhibition

In the case of the DHE assay to measure superoxide abundance in PECs and HUVECs (see Section 4.9), the influence of Nox2 was determined by addition of gp91ds-tat. This is a chimeric peptide that inhibits p47(phox) association with gp91(phox) and has

appropriate selectivity for Nox2 [440]. Initially, 29mg was dissolved in a 1mL solution composed of 100mL distilled water, 0.9g sodium chloride and 57.5μL acetic acid, to produce a 10mM stock. This was diluted in M199 media to produce a working solution of 50μM. An equivalent scrambled peptide reconstituted in a comparable fashion was used as a control. These were added to the 10cm petri dishes on day 3 after lentiviral transduction, with exposure for 24 hours in total.

To assess the effects of PI3K signalling on oxidative stress, two potent and selective PI3K inhibitors were utilised: Wortmannin (IC_{50} of ~ 3nM) and LY294002 (IC_{50} of 0.5μM). Both were dissolved in DMSO as 10mM stocks and diluted to working solutions of 50nM and 5μM, respectively. The equivalent volume of DMSO was used as controls. Incubation was for 30 minutes and immediately preceded the DHE assay for PECs and HUVECs.

4.7 Endothelial cell functional assays

4.7.1 Scratch wound

This was performed on HUVECs in a 0.1% gelatin-coated 96-well plate. Cells were initially seeded at 50,000 per well in quadruplicate, and allowed to grow to full confluence in 100μL M199 media for 24 hours. Once this had been achieved, cells were serum deprived by washing in PBS and adding 1% FBS-containing M199 media for a duration of 4 hours. A mechanical Woundmaker 96-pin device was used to generate homogenous, longitudinal cell-free scratch wounds in the centre of each well. Visualisation using a CKX-41 light microscope was conducted to ensure adequate wounding, with the procedure repeated if required. Cells were subsequently washed

with 100μL of PBS to remove floating cells and debris, and replaced with 300μL of 2% FBS-containing M199 media.

Imaging was performed on each of the wells individually to obtain baseline images (t0). Two images per scratch at 40X magnification were obtained using the light microscope and Olympus Cell F software (v3.4). All samples were incubated at 37°C for 18 hours, followed by repeat imaging (t18). Image J software was utilised to quantify wound area at each time point. Subtraction of t18 from t0 enabled calculation as a proportion of t0 to quantify % wound closure.
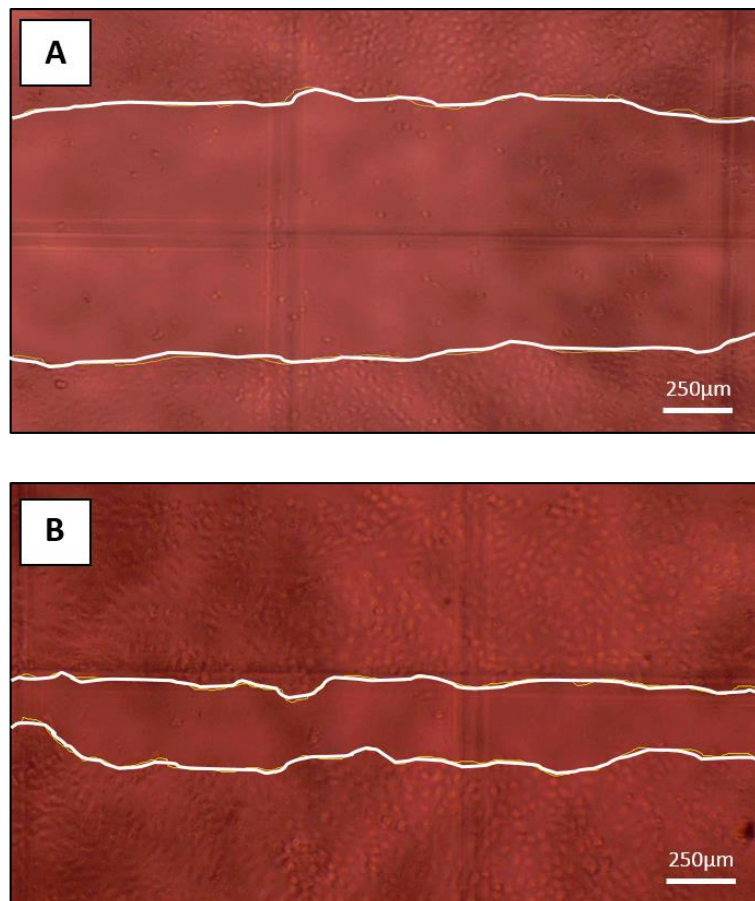
Figure 4-6 – Representative image of scratch wound at T0 **(Panel A)** and T18 **(Panel B)**.

4.7.2 Boyden chamber

HUVECs were defrosted, plated and exposed to shRNA as outlined previously.

50ng/mL VEGF was pre-prepared by adding 3mL basal media to 7.5μL 100μg/mL

human VEGF. A non-coated 24-well plate was used, with addition of either 750μL

basal media and VEGF (as experimental) or 750μL basal media and DMSO (as control).

A sterile polycarbonate insert with 8μm pores was carefully placed into each well

using sterile forceps. Cells were split and counted, and 50,000 HUVECs suspended in

500μL basal media were added to each insert. The plate was gently rotated to ensure

that inserts were adequately bathed in basal media. The bottom of the plate was

assessed to confirm absence of air bubbles.

Cells were incubated at 37°C for 6 hours, following which inserts were transferred

using forceps into separate wells and fully submerged in 750μL of 70% ethanol. Each

insert was subsequently rinsed briefly in a clean beaker of water before placement in

separate wells containing 750μL of distilled water. 300μL was additionally added to

each insert. These were then removed and a cotton bud used to thoroughly clear the

inner surface and remove non-migrating cells. Inserts were re-rinsed in fresh water.

Cells were sequentially stained with haematoxylin and eosin by placing for 30 seconds

in wells containing 750μL of one then the other, with a wash in between, before

rinsing and imaging.

This was performed using the CKX-41 light microscope at 20X magnification, with data

storage using Olympus Cell F software. Five images were obtained per well, with

specific avoidance of peripheries where cells clump due to incomplete wiping of the

upper membrane. Cells were identified based on staining for both nucleus and

cytoplasm. Abundance was determined using Image J software, and data expressed as net migration by subtracting mean number of visualised cells in the control wells from those containing VEGF.
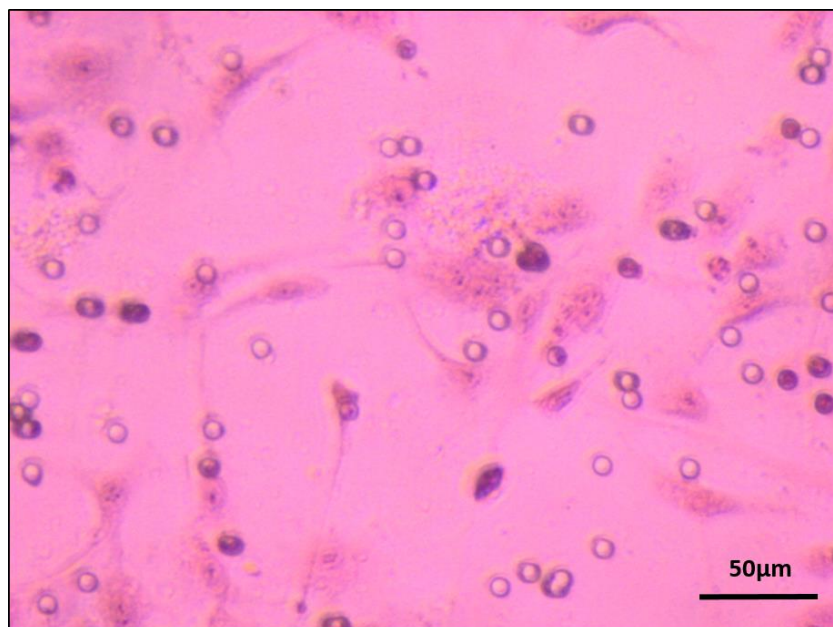
Figure 4-7 – Representative image from Boyden chamber assay with visualisation of circular pores and migrant HUVECs.

4.7.3 5-ethynyl-2'-deoxyuridine (EdU) incorporation

4.7.3.1 Click-iT kit

This assay was performed with manipulated HUVECs (shRNA or SMI) on 0.1% gelatin-coated 6-well plates. Cells were initially seeded at 100,000 cells/well in 1mL M199 media, with 3-4 replicates, and incubated for 48 hours which ensured ~ 80% confluence (based on prior optimisation experiments in our laboratory). Reagents were obtained commercially from a Click-iT EdU Alexa Fluor 647 flow cytometry kit. This was composed of 10mg EdU, Alexa Fluor 647 azide, 4.25mL of DMSO, 5mL

fixative, saponin-based permeabilisation and wash reagent, EdU buffer additive and 500μL of 100mM copper sulphate ($CuSO_4$).

Measurement of DNA synthesis provides a marker of active proliferation. EdU is a nucleoside analogue of thymidine and is incorporated into DNA during synthesis. Detection is based on a copper-catalysed covalent reaction between azide (Alexa Fluor 647) and alkyne (EdU). Unlike older assays, there is no denaturation step and therefore, integrity of double-stranded DNA is not compromised to improve reproducibility. Moreover, EdU assays utilise biologically unique moieties which produce low background noise and high detection sensitivities. DMSO is a solvent used to facilitate the entry of organic molecules into cells.

Prior to commencement, working solutions for some of these reagents were prepared. 4mL of DMSO was added to EdU to produce a 10mM stock solution which was stored at -20°C. Similarly, 130μL of DMSO was added to Alexa Fluor 647 azide and again stored in the freezer until use. A 10x stock solution of the EdU reaction buffer additive for freezer storage was made through addition of 2mL of deionised water. Lastly, the saponin-based permeabilisation and wash reagent was diluted 1:10 in 1% PBS/BSA and this was stored with the remainder of the reagents in a fridge set at 4°C. All experimentation from this point onwards was performed in a low light environment.

Initially, 10μM EdU was added and mixed in each well with incubation at 37°C for a period of 4 hours. Media was aspirated and cells washed twice in PBS to remove debris. Subsequently, 1mL trypsin was added with incubation for 2 minutes to harvest

cells. After direct visualisation under CKX-41 light microscopy to confirm cell detachment, the solution was neutralised with 2mL M199 media and centrifuged at 400g for 1 minute to discard the supernatant from the cell pellet. There was a further wash step with 3mL of 1% PBS/BSA with repeat centrifuging to enhance purity of isolated samples.

100µL of the PFA-based fixative was added and mixed for 15 minutes at room temperature. After a further wash and centrifuge, the pellet was re-suspended for 15 minutes in 100µL of saponin-based permeabilisation and wash reagent which contained 0.5% Triton X-100 (sodium azide in BSA). During this incubation period, the Click-iT reaction cocktail was produced, as outlined in Table 4-4. A working solution of EdU reaction buffer additive was generated by diluting the original 10x stock using a 1:10 ratio in deionised water. 500µL of this reaction mix was added to each sample with a further incubation for 30 minutes. On completion, there was one last wash with 3mL of saponin reagent and after a final centrifuge, samples were re-suspended in 500µL of saponin reagent prior to transfer in ice for analysis by flow cytometry

Reagents	Number of reactions		
	2	5	10
PBS	875µL	2.19mL	4.38mL
Copper sulphate	20µL	50µL	100µL
Alexa Fluor 647 azide	5µL	12.5µL	25µL
Reaction buffer additive	100µL	250µL	500µL
Total	**1mL**	**2.5mL**	**5mL**

Table 4-4 – Components of Click-iT reaction cocktail. PBS = phosphate buffered saline.

4.7.3.2   Flow cytometry

This was performed using a BD-LSR Fortessa flow cytometer, with analysis using FACSDiva software to quantify the proportion of proliferating cells in each sample (i.e. those that had incorporated EdU). All samples were thoroughly mixed prior to loading into fluorescence-activated cell sorting (FACS) tubes. The flow cytometer is able to generate a column of fluid, which is converted into single cell droplets via hydrodynamic focusing. A laser beam is used to excite cells with specific fluorochrome labelling with quantification of emitted light from each cell. Alexa Fluor 647 was utilised as it has photostability, a high Stokes shift (excitation 634nm, emission 660nm) and distinct profile for ease of identification. Prior to formal analysis, a plot of side scatter area (SSC-A) versus forward scatter area (FSC-A) was visualised to identify the homogenous cell population of interest, and to exclude the remainder which are likely to constitute dead cells (low FSC, low SSC) and clumped cells (non-proportional FSC-A [area] and FSC-H [height]). The first 10,000 cells in the sample mixture were used for analysis purposes. Gating criteria were used to differentiate proliferating cells from background fluorescence.
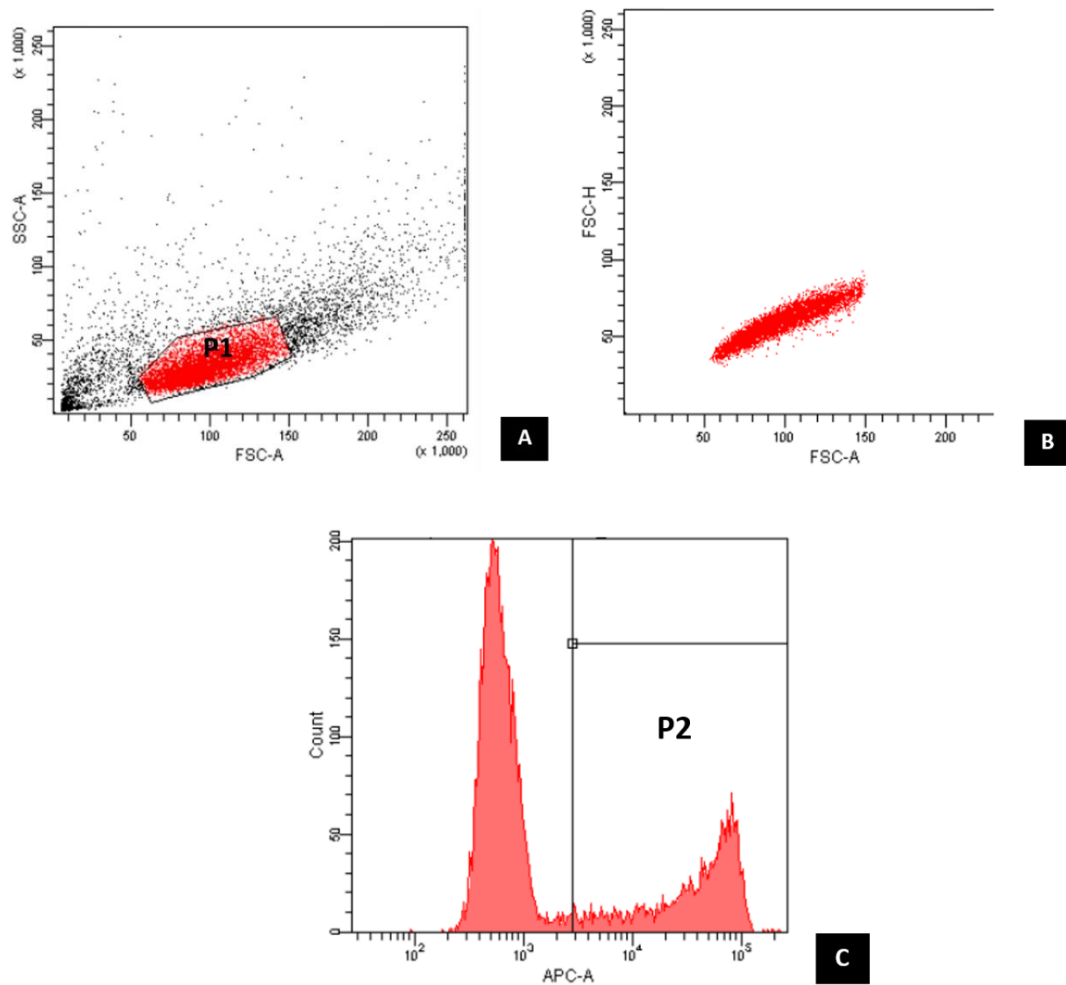
Figure 4-8 – Flow cytometer analysis. Homogenous HUVEC population of interest identified, depicted by gating as *P1* **(Panel A)**. Linearity of distribution established based upon area and height to ensure elimination of clumped cells **(Panel B)**. Cell count histogram used to establish proliferating cells (*P2*) which could be quantified as proportion of total **(Panel C)**. FSC = forward scatter; SSC = side scatter; APC = allophycocyanin.

4.7.4   Bead sprouting

4.7.4.1   Coating with HUVECs

To allow greater control of media composition, EGM-2 basal media was used rather than M199. This was mixed with additional supplements (BulletKit): 10mL FBS, 0.2mL

hydrocortisone, 2mL human FGF, 0.5mL VEGF, 0.5mL IGF-1, 0.5mL ascorbic acid, 0.5mL human EGF, 0.5mL GA-1000 and 0.5mL heparin. Cells were trypsinised and quantified using the haemocytometer. 10 wells of a 24-well plate were used per condition, with 100,000 cells per well. The desired number was reconstituted in 1.5mL EGM-2 media for later use.

Commercially-obtained cytodex-3 polystyrene beads were utilised. These were sourced as 0.5g dry aliquots which were reconstituted in a Falcon tube with 50mL PBS and mixed on a rocker at room temperature for 3 hours. Following this, the beads were allowed to settle for 15 minutes. The supernatant was discarded and the beads washed in 50mL of fresh PBS. They were then re-suspended in 25mL PBS to produce a 20mg/mL working solution containing 60,000 beads/mL. This was placed in a siliconized glass bottle and autoclaved prior to storage at 4°C.

At time of use, cytodex-3 beads were agitated and the desired volume pipetted carefully into a 1.5mL microcentrifuge tube. For use of 20 wells (10 per condition), this equated to 84µL with approximately 400 cells/bead. They were allowed to settle for 5 minutes, with the supernatant subsequently discarded. Beads were re-suspended in 1mL EGM-2 media, and left to settle for 5 minutes prior to aspiration. The aliquoted cell suspension was added to the beads and the resultant solution carefully pipetted into an autoclaved FACS tube. It was placed in an incubator at 37°C for 4 hours, with gentle mechanical agitation of the base every 20 minutes. Once complete, the solution was carefully transferred into a T25 cell culture flask. Further EGM-2 media was added to a resultant total of 6mL and kept overnight in the incubator.

4.7.4.2　Embedding in fibrin gel

First, 2mg/mL fibrinogen was made by reconstitution in distilled PBS and maintenance in a water bath at 37°C for 5 minutes. A 0.2μm filter was used to sterilise the solution. 6mL of fibrinogen solution was used for 10 wells, corresponding to approximately 500μL per well after accounting for loss during filter sterilisation. 4U/mL aprotinin was produced by reconstituting 10mg in 10mL distilled water and passing through a sterilisation filter. 0.15U/mL was added to the fibrinogen solution and set aside. The T25 flask was gently tapped to dislodge the coated beads, which were gently aspirated into a 15mL Falcon tube using a stripette. The flask was washed twice with 3mL EGM-2 media to enable transfer of any residual beads. Beads were allowed to settle for 5 minutes, with the media subsequently aspirated and re-suspended in 1mL EGM-2 media. 3 subsequent washes with 1mL media was performed.

At this point, wells were prepared by adding 12.5μL of 50U/mL thrombin to the centre of each well. After the final wash, coated beads were re-suspended gently in the fibrinogen/aprotinin solution and transferred to a 15mL Falcon tube. The solution was gently pipetted to ensure adequate mixing, followed by addition of 500μL to each well directly onto the pre-deposited thrombin. The suspension was spread evenly with a cautious approach to avoid introducing air bubbles. The thrombin converts fibrinogen into fibrin, which produces a solidified matrix which the beads are embedded in. To facilitate this, the plate was left undisturbed for 5 minutes followed by cautious transfer to an incubator for 15 minutes. 1mL of EGM-2 media was then added to each well in a dropwise fashion and kept overnight to allow sprout formation.

4.7.4.3   Imaging of sprouts

After a period of 24 hours, imaging was performed using a Olympus CKX-41 light microscope, with storage of data using Olympus Cell F software. 10 individual beads were imaged per condition. Analysis was conducted using Image J software, with calculations of mean number of sprouts per bead and sprout length. Divergent sprouts were considered as separate if the length distal to their branch point was > 50% of the total sprout length.
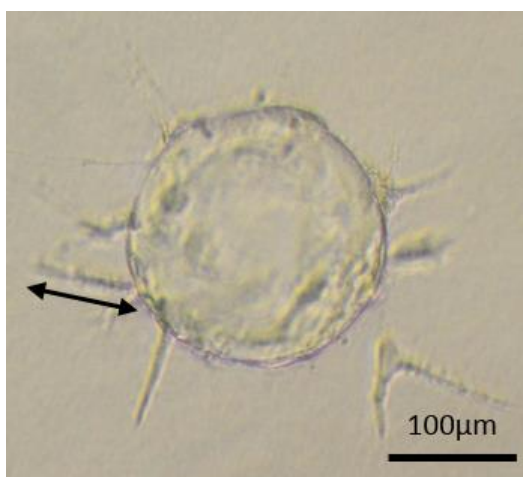
Figure 4-9 – Representative image of cytodex-3 bead with cell sprouting. Measurement of sprout length depicted *(black arrow)*.

4.8 Immunofluorescence

4.8.1   Lamellipodial staining

Cells were defrosted and plated, before being exposed to control or SHIP2 shRNA lentivirus (as described in Section 4.6.3). Cells were subsequently split onto pre-coated 35mm imaging dishes at a density of 15,000 per dish, and maintained in 1% FBS-containing M199 media overnight to quiesce cells. 50ng/mL human VEGF, or PBS

vehicle control, was added to each sample for 30 minutes, followed by fixation with

PFA. Permeabilisation was performed with 0.25% Triton X-100 in PBS for 30 minutes,

followed by 3 wash steps in PBS. Lamellipodial staining was achieved by the addition

of phalloidin at a 1:50 dilution, mixed in 1% PBS/BSA, that had been commercially

purchased in a pre-conjugated form bound to Alexa Fluor 647. Phalloidin binds

filamentous actin at the interface between subunits and prevents filament

depolymerisation [441]. Samples were kept overnight at 4°C covered in foil, followed

by further washes and maintenance in fresh PBS until imaging of single cells with

LSM880 confocal microscopy. This step was performed by Dr Richard Cubbon. Analysis

was conducted using Image J software, with assessment of cell parameters including

total area and perimeter, lamellipodial area and perimeter, and a crude assessment of

lamellipodial distribution based on arbitrary quadrants (with Q1 designated as the one

with the greatest proportion of lamellipodia and Q4 with the least). This was

performed in a fashion broadly consistent with published techniques [442].
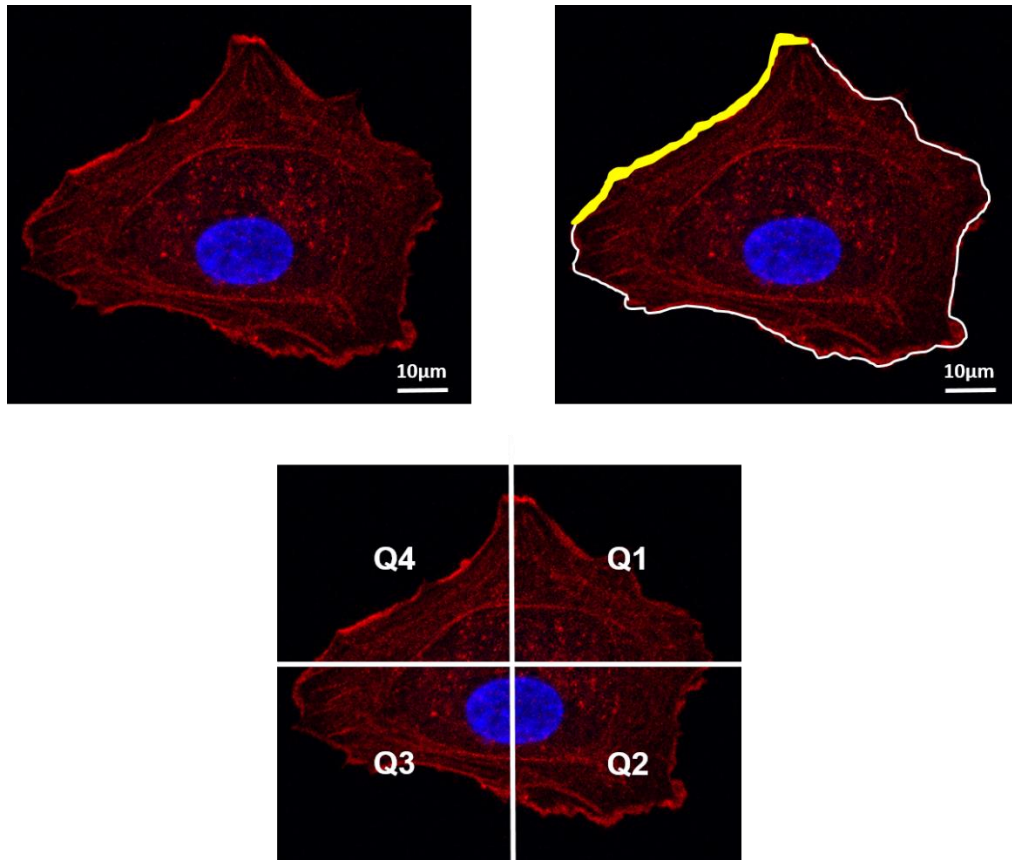
Figure 4-10 – Representative image of single HUVEC stained with phalloidin (*red*). Whole perimeter of cell depicted (*white*) with concentrated region of phalloidin representing lamellipodia (example shown in *yellow*). Cell was split into quadrants (*Q1-Q4*) to quantify lamellipodial distribution.

4.8.2   GM130 staining

HUVECs were plated in triplicate in imaging 24-well plates for 24 hours to achieve confluence. On the day of assessment, serum starvation was performed in 1% FBS-containing M199 media for 4 hours, proceeded by a mechanical scratch using the tip of a 1000µL pipette. After incubation for 30 minutes, cells were fixed in 4% PFA at 37°C for 10 minutes and stored in PBS. At time of staining, initial permeabilisation was performed in 0.25% Triton-X100 in PBS with the addition of 5% goat serum. This was

conducted at 4°C for 1 hour. Cells were subsequently incubated with mouse anti-GM130 antibody pre-conjugated to Alexa Fluor 488 at 5 µg/mL (1:200 dilution) and left overnight wrapped in foil on a microtitre plate shaker in the cold room. GM130 is homologous to the Golgi autoantigen golgin-95 and operates as a structural element of the Golgi apparatus, in addition to providing attachment sites for membranes and other proteins. Notably, the monoclonal anti-GM130 antibody interacts regardless of phosphorylation status.

After three 5 min washes in PBS, phalloidin pre-conjugated to Alexa Fluor 647 was added at a 1:50 dilution in 1% PBS/BSA and kept for 24 hours on the shaker. After three subsequent washes, Hoescht 33342 was used for nuclear staining at a 1:2000 dilution in PBS, added for 15 minutes at room temperature. After one last set of washes in PBS, the samples were stored in PBS at 4°C until time of confocal imaging. This final step was performed by Dr Richard Cubbon.

Each cell on stored images was analysed using Image J software. Specifically, the angulation of the Golgi apparatus relative to the nucleus was determined to establish overall direction of cell polarity, with a horizontal direction towards the scratch being considered as 0°C. This was repeated for each individual cell, both in images obtained at the site of scratch and also in remote areas that were fully confluent. Cells were determined to be forward facing (i.e. towards the site of scratch) if polarity was between -45 and +45° to a line perpendicular to the scratch.
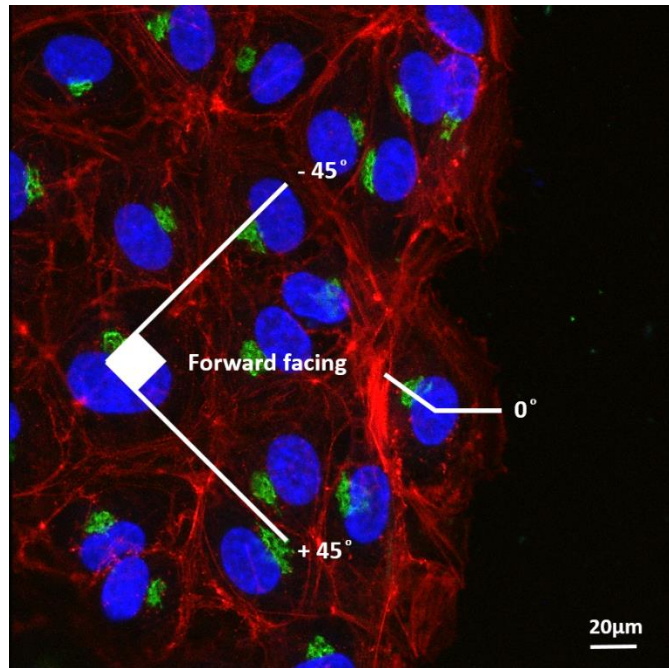
Figure 4-11 – Confluent HUVECs adjacent to site of mechanical scratch, with staining of filamentous actin (*red*), Golgi apparatus (*green*) and nuclei (*blue*). The relative position of the Golgi apparatus to the nucleus was used to establish cell directionality, and this was repeated for individual cells to quantify proportion that were forward facing.

4.8.3   SHIP2 staining

HUVECs were defrosted and plated as described, but without exposure to lentivirus or SMI. Once culture dishes were 80% confluent, cells were trypsinised and counted. 100,000 cells were plated onto pre-coated 35mm imaging dishes, with repeated pipetting performed prior to extraction to avoid clumping. Cells were subsequently serum starved in 1% FBS-containing M199 media for 4 hours. A longitudinal scratch was subsequently made mechanically using the tip of a 1000µL pipette, followed by incubation at 37°C in 2% FBS-containing M199 media for either 30 mins or 1 hour. Cells were then washed three times in non-sterile PBS prior to fixation by mixing with

500µL of pre-warmed 4% PFA for 10 minutes at 37°C. Samples were stored in a fridge at 4°C until time of staining. At this point, cells were permeabilised in 0.25% Triton-X100 (made using 125µL Triton, 50mL PBS, 0.5g BSA and 250µL goat serum to block non-specific binding) and left at 4°C for 1 hour. Three washes in 1mL 0.1% PBS/BSA were conducted to remove debris and enhance image quality, with 5 minute durations between each.

Rabbit anti-SHIP2 primary antibody (ab166916) was added at 1:100 dilution in the permeabilisation/blocking buffer. This was left overnight at 4°C prior to 3 washes in PBS adhering to the regimen above. Subsequently, goat anti-rabbit secondary antibody pre-conjugated to Alexa Fluor 647 was introduced as the secondary antibody, at a 1:200 dilution in the permeabilisation/blocking buffer, prior to incubation at room temperature for 1 hour whilst covered in foil. After 3 further washes in PBS, fluorescein isothiocyanate (FITC)-conjugated Ulex Europaeus was added at 10µg/mL (1:100 dilution), mixed in PBS, and incubated for 1 hour at room temperature to label the cell membrane. This is a glycoprotein known to interact with -L fucosyl residues in oligosaccharides on the membranes of human endothelial cells in addition to red blood cells (erythrocytes) and a variety of human and animal epithelial cells [443]. After three further washes, Hoescht 33342 at 1:2000 dilution mixed in PBS was added for 15 minutes at room temperature.

After a final set of washes, samples were maintained in 2mL of fresh PBS to prevent drying of cells and left in a light-protective environment until time of confocal imaging using 80X magnification. This was performed by Dr Richard Cubbon no later than two weeks after staining to avoid issues relating to degradation in image quality. In the

case of negative controls, the above protocol was adhered to with precision but no primary antibody was included.

4.9 Dihydroethidium (DHE) assay

For this assay, cells were seeded onto a clear 96-well plate at a concentration of 50,000 PECs or 30,000 HUVECs per well. No pre-coating with gelatin was performed based on prior optimisation experiments. 100μL of respective media (i.e. MV2 or M199) was added and cells incubated for 24 hours at 37°C to enable confluence to be reached. 4 unlabelled/control and 4 labelled wells were required for each sample, 2 of each receiving gp91ds-tat (or scrambled peptide), or one of the PI3K inhibitors in a separate experiment. All conditions also had 2 replicates, making use of 16 wells in total per experiment.

The assay required use of DHE to quantify superoxide abundance. In its presence, DHE is oxidised into 2-hydroxy-ethidium. This integrates into cellular DNA and stains the nucleus red, which enables indirect superoxide quantification. DHE was purchased as a 5mM stock dissolved in DMSO, and diluted 1:200 in sterile Krebs-HEPES buffer to produce a working solution of 25μM. This buffer contained various constituents as outlined: sodium chloride (99mM), potassium chloride (5mM), dipotassium phosphate (1mM), sodium bicarbonate (25mM), magnesium sulphate (1mM), calcium chloride dehydrate (3mM), HEPES-sodium salt (20mM) and glucose (6mM).

All wells were washed with 100μL of PBS. 'Unlabelled' control wells were replaced with 100μL of Krebs-HEPES buffer, and 'labelled' wells with 100μL of diluted DHE.

M199 media could not be utilised as a suitable vehicle because it generated autofluorescence in preliminary experiments due to the phenol red. After gentle mixing, the plate was incubated at 37°C for 20 minutes. This was followed by two washes in PBS, and replacement with 100μL of fresh Krebs-HEPES buffer. Transfer for analysis was in tin foil to protect from light.

A Flex Station 3 microplate reader was used with processing in SoftMax Pro to enable quantification of fluorescence. This was performed at excitation of 500nm and emission of 600nm to capture 2-hydroxy-ethidium fluorescence. A run time of 3 minutes was conducted for each well, with readings at 10 second intervals. Prior studies have confirmed that the fluorescent signal does not decay over this time period. A mean of all readings allowed calculation of an average value for each well, and 'unlabelled' values were subtracted from 'labelled' to obtain net fluorescence.

4.10 Western blotting

4.10.1 Preparation of lysates

PECs were derived from 10 month old ECSHIP2$^{\Delta/+}$ mice to validate SHIP2 knockdown and measure basal Nox2 protein expression. These cells were initially grown to confluence in individual wells of a 6-well plate. At time of lysate preparation, they were washed in 2mL of PBS to remove excess media followed by two washes in ice-cold PBS (containing calcium and magnesium), each for a duration for 5 minutes, to arrest cellular processes. 100μL of cell extraction buffer was added, made from 50mM stock, with the addition of 10μL each of 1% protease and phosphatase inhibitor cocktail. The cells were mechanically detached in the wells using 1.8cm blade cell

scrapers. Samples were immediately transferred to 0.5mL microcentrifuge tubes and stored at -40°C until time of Western blotting.

A similar approach was used for HUVECs, which had been transduced with appropriate shRNA viruses (see Section 4.6.3). These lysates derived from confluent wells were used to assess extent of SHIP2 knockdown at differing lentiviral MOI, basal Nox2 protein expression and downstream signalling intermediates such as total and phosphorylated AKT, eNOS and ERK. Lastly, organs were harvested from SHIP2i$^{\Delta/+}$ mice to confirm adequate knockdown of the SHIP2 catalytic domain. This was conducted once metabolic testing had been completed, and immediately subsequent to Sch1 using the CO_2 chamber as described. White adipose tissue (WAT) and tissue from liver, aorta and skeletal muscle (quadriceps) was harvested, prior to transfer into 1.5mL microcentrifuge tubes and storage at -40°C until time of requirement.

4.10.2 Protein quantification

PEC and HUVEC lysates were removed from storage and allowed to defrost on ice for 30 minutes. In the case of tissue samples, they were kept in ice until thawed. Once achieved, 30mg was isolated and mixed with 400µL of cell extraction buffer mixed with both protease and phosphatase inhibitors. A 6mm cone ball was added to each sample and homogenised using a tissue lyser for 15 seconds at a frequency of 30/second. This was repeated twice. The lysate was pipette transferred into fresh 1.5mL microcentrifuge tubes and vortexed, prior to storage on ice for 30 minutes with a brief, intermediate vortex at 15 minutes. Centrifugation was performed at 13,000

rpm for 45 minutes at 4°C, with 100µL of the remaining supernatant transferred to fresh tubes.

Protein quantification was achieved using a bicinchoninic acid (BCA) assay kit in a 96-well plate format. Firstly, 8µL of each of the supernatant was mixed with 56µL of RIPA buffer (i.e. 1:8 ratio) and briefly vortexed. These were pipetted in duplicates as 25µL aliquots into individual wells. Nine standards of BSA at known concentrations were also loaded, again in duplicate. The assay kit relied on two reagents for colorimetric analysis: Reagent A (sodium carbonate, bicinchoninic acid and sodium tartrate in 0.1M sodium hydroxide) and Reagent B (4% cupric sulphate). These were mixed in a 50:1 ratio and 200µL individually added to each well. The plate was covered with a lid and incubated at 37°C for 30 minutes. A Dynex MRX TC microplate reader with Revelation software was used for analytic purposes, at a wavelength of 562nm. Use of BSA standards enabled construction of a standard curve, which was appraised for linearity by quantification of the correlation coefficient (r^2) and accepted when > 0.99. Protein concentrations were derived from use of this curve, with values only accepted when the coefficient of variation between duplicate samples was < 10%.

4.10.3 SDS-polyacrylamide gel electrophoresis

The calculated concentration (in µg/mL) was used to establish sample volumes equating to 30µg protein (cell samples) and 50µg protein (tissue samples), accounting for the 1:8 dilution during protein quantification. This was mixed with loading buffer (1:4 dilution) and reducing agent (1:10 dilution), and topped up with cell extraction buffer, if needed, to a total volume of 30µL. After a short spin, samples were placed in

a heating block set at 95°C for 5 minutes, prior to loading onto a 4-12% Bis-Tris polyacrylamide gel. 3.5μL of a marker was loaded for reference purposes. The gel was placed in a Criterion Cell tank. 500mL of running buffer was produced in a conical flask by mixing 25mL of 2-(N-morpholino)ethanesulfonic acid/sodium dodecyl sulphate (MES SDS) with 475mL of deionised water, and subsequently poured gently into the tank. Electrophoresis was conducted at 180V for 1.5 hours. The gels were visually checked every 30 minutes to ensure that samples were running correctly.

4.10.4 Membrane transfer

Once complete, the gel was briefly washed in deionised water. The iBlot system was used to transfer proteins onto a polyvinylidene fluoride (PVDF) membrane. First, transfer buffer was made from a 10X stock solution composed of 6.06g tris, 29g glycine, 400mL methanol and 1600mL distilled water. A transfer tank was set up with a metal stirrer. The transfer membrane was activated with sequential spraying of methanol and transfer buffer, with direct visualisation of air bubbles used for confirmatory purposes. The membrane was soaked in transfer buffer, as were the sponges and filter paper. The pack was assembled within the cassette so that the gel and membrane were flanked on each side by filter paper, which were themselves encompassed by sponges. A plastic roller was used to remove any air bubbles that may ordinarily prevent adequate transfer. The cassette was placed in the transfer tank and transfer buffer added, before application of an electric current at 100V for 45 minutes.

4.10.5 Immunostaining for signalling components

After transfer, the membrane was carefully removed from the cassette and allowed to dry on tissue paper. It was then washed in a blocking solution containing 5% BSA in 0.1% Tween for 5 minutes, before being cut at appropriate regions to enable simultaneous staining for multiple signalling components of varying molecular weights. Membranes were then incubated at room temperature on a shaker in 15mL of Tween/BSA for 1 hour to prevent non-specific antibody binding.

After discarding the solution, the relevant primary antibodies were prepared in Tween/BSA at the appropriate dilution (see Table 4-5). β-actin was used as a control. Incubation was overnight at 4°C. After washing the membrane three times in 0.1% TBST, each for 5 minutes, appropriate horseradish peroxidase (HRP)-conjugated secondary antibodies were prepared. This was applied to the membrane for 1 hour at room temperature, prior to three subsequent washes in Tween of 15 minutes duration. The membrane was transferred onto cling film and carefully flattened. Visualisation of protein bands was achieved via enhanced chemiluminescence, through addition of 1mL of Immobilon Western Chemiluminescent HRP Substrate containing 500μL peroxide solution and 500μL enhancer solution. Imaging was performed using a camera scanner (Image Station 2000R) with densitometric analysis using Syngene GeneTools software.

4.10.6 Stripping membrane

Assessment of phosphorylated protein levels was generally performed first. However, further analysis of total protein levels could be performed using the original

membrane by application of a Western blot Restore PLUS stripping buffer.

Membranes were washed in TBST to remove excess substrate solution, and

subsequently incubated in 10mL of stripping buffer at room temperature for 10

minutes with gentle agitation. After three 5 min washes in TBST, 5% TBST-BSA was

applied for 1 hour as a blocking solution prior to re-use with new primary and

secondary antibodies.

Primary antibody	Host	Dilution	Molecular weight (kDa)	Manufacturer
B-actin	Mouse	1:3000	43	Cell Signalling #4970
Mouse SHIP2	Rabbit	1:1000	160	Gift from Stephane Schurmans, University of Liege
Human SHIP2	Rabbit	1:1000	139	Abcam ab166916
Nox2	Mouse	1:1000	65	Abcam ab129068
Total AKT	Mouse	1:1000	60	Cell Signalling #4685
pAKT (T308)	Rabbit	1:1000	60	Cell Signalling #4060
Total eNOS	Mouse	1:1000	140	BD Biosciences #610296
peNOS (S1177)	Rabbit	1:1000	140	BD Biosciences #612393
Total ERK	Mouse	1:1000	42	Cell Signalling #9102
pERK (Y202/204)	Rabbit	1:1000	42	Cell Signalling #9101

Secondary antibody	Dilution	Manufacturer
Polyclonal goat anti-mouse IgG	1:20000	Dako #P0161
Polyclonal goat anti-rabbit IgG	1:20000	Dako #P0217

Table 4-5 – Primary and secondary antibodies used for Western blotting.

4.11   Tamoxifen induction

The utilisation of Cre to mediate recombination between its *lox*P target sites has transformed genomic manipulation of mice [444]. Its inducible nature enables temporally controlled modulation of the genome. Generation of the SHIP2i$^{\Delta/+}$ colony involved ubiquitous expression of a mutated fusion protein of Cre and the human oestrogen receptor (Cre-ERT2$^{+/0}$) [433]. As mentioned, this protein was driven by a CAG promoter-enhancer which was insensitive to endogenous oestrogens. Instead, rapid and efficient Cre-mediated recombination could be induced by administration of tamoxifen [433].

In view of its hazardous nature and potential teratogenic effects, protected handling of tamoxifen was conducted in a fume cupboard at all times. Samples were initially produced at a concentration of 10 mg/mL, dissolved in corn oil, and maintained as 1mL aliquots. They were thoroughly vortexed prior to incubation at 37°C overnight to enable proper dissolution of crystals, and kept as 1mL aliquots at 4°C until use. In view of its degradation by bright light, vials were wrapped in aluminium foil. Injections were performed in a designated facility with strict adherence to local regulations, including use of gown and skin protection using a double-gloved technique when handling.

Mice were selected for experimentation based on genotype confirmed via polymerase chain reaction (PCR). Additionally, they were required to be of a weight > 24 grams to tolerate the procedure, with a typical age of 9 weeks. Once identified, they were separated into a distinct cage and transferred to the facility a day prior so that they were accustomed to surroundings. Tamoxifen was injected intraperitoneally (IP) at a concentration of 40 mg/kg for five consecutive days. Cre-positive control mice were exposed to an identical regimen, but their absence of *lox*P sites prevented targeted recombination. After the final injection, mice were maintained in their usual environment and monitored on a daily basis for a week. They were subsequently transferred to fresh cages in preparation for further testing.

4.12   Metabolic profiling

4.12.1 Gross body weights

All metabolic profiling was performed on SHIP2i$^{\Delta/+}$ mice. They were weighed using electronic scales on a weekly basis from 1 to 3 months of age. This included baseline weights at commencement of tamoxifen induction to ensure that dosing was appropriate and tolerable. Measurements were also undertaken at the end of the 5 day course to ensure that the induction regime had not compromised growth. If multiple readings were taken within a particular week, the mean value was used for statistical purposes.

4.12.2 Glucose tolerance testing (GTT)

This was performed after overnight fasting, with transfer into new cages conducted to prohibit consumption of chow fragments on cage floors. Access to water was maintained throughout. On the day of testing, which occurred at 8am, 20% glucose was made by filtering 2g of glucose into 10mL of sterile PBS and vortexing thoroughly to ensure adequate dissolution. This was transferred to the animal facility in ice.

To calculate required volumes, a baseline weight was obtained for each mouse in grams, and this value was multiplied by a factor of 4 to produce a volume (in µL) equating approximately to 1mg/g. Capillary blood sampling was performed by obtaining blood droplets from a superficial tail incision, performed using a sterile size 22 scalpel. Mice were consciously restrained in a plastic box with protective padding and a small hatch to adequately expose the tail. Readings were processed using a glucometer and Accu-Chek testing strips.

At commencement, a baseline blood glucose reading provided a fasting glucose value (in mM). Subsequent IP injection of glucose at the desired volume was conducted, with restraining of mice by a scruffing technique. This was followed by repeat glucose readings at 30 minutes, 60 minutes, 90 minutes and 120 minutes. Sampling was invariably achieved using the original tail incision with gentle massaging, but if this proved troublesome, a further incision proximal to the initial site was performed. Gentle mopping of dried blood ensured that fresh samples were being tested at each individual time point. Between readings, mice were relocated to their original cages and maintained in a quiet environment so that distress was minimised. Throughout this period, access to water was maintained but they remained fasted until termination of the experiment. In the unlikely instances where mice displayed

evidence of symptomatic hypoglycaemia, such as somnolence or seizures, blood testing was immediately performed and if this was < 2mM, a repeat injection of IP glucose was administered and mice excluded from further testing. At the end of the experiment, tail tips were assessed to ensure adequate haemostasis and mice transferred to fresh cages with free access to chow.

4.12.3 Insulin tolerance testing (ITT)

ITT was performed one week after GTT to ensure normalisation of metabolic and haemodynamic physiology, and to allow adequate healing of tissue within the tail tip. The protocol was comparable to GTT, but mice were fasted from 8am for 2 hours only. Human recombinant insulin solution was produced by mixing 20μL of 100 IU/mL Actrapid in 10mL of sterile PBS. The sample was vortexed before transfer in ice. Baseline weights were utilised once more to calculate injecting volumes, which was a 3.75 multiplication of body weight in grams. This derived an administration dose of 0.75 IU/kg. Once again, a fasting glucose measurement was obtained prior to IP administration of insulin. This was followed by subsequent readings at stages of 30 minutes, 60 minutes, 90 minutes and 120 minutes. Glucose solution was kept readily available at all times, and mice were observed stringently in case of significant hypoglycaemia. Similar animal husbandry to GTT was observed at the end of experimentation. Euthanasia was then performed using Home Office approved scheduling as outlined previously.

4.12.4 Plasma insulin measurement (ELISA)

This was derived from SHIP2i$^{\Delta/+}$ mice that had undergone tamoxifen induction but no prior metabolic testing. Mice were fasted overnight prior to intra-cardiac puncture under isoflurane anaesthesia, with a 27G needle attached to a 1mL syringe that was pre-filled with 100μL of 1000 IU/mL sterile liquid heparin. This enabled collection of 800-900μL whole blood into 1.5mL microcentrifuge tubes, of which a drop was applied onto a Accu-Chek testing strip and processed using a glucometer to derive a corresponding blood glucose reading in mM. The remainder of the samples were transferred on ice and centrifuged at 6000 rpm for 5 minutes to isolate plasma from cell debris. Samples were stored at -80°C until time of use.

An ultra-sensitive mouse insulin ELISA kit was used for quantification of plasma insulin, with 'low-range' assay conditions (defined as 0.1-6.4 ng/mL). All reagents were brought to room temperature prior to use. The lyophilized mouse insulin standard was reconstituted in 100μL distilled water to produce a stock solution containing 25.6ng/mL of mouse insulin, which was then serially diluted. 5μL of each standard was dispensed in duplicate into wells of a microplate which was pre-coated with guinea pig anti-insulin antibody and loaded with 95μL of sample diluent. This enabled a standard curve to be constructed, and the remaining wells were filled in duplicate with 5μL of each sample. The microplate was incubated for two hours at 4°C, before aspiration of well contents and five washes with 300μL wash buffer to remove unbound material. Once complete, 100μL of horse radish peroxidase (POD)-conjugated anti-insulin antibody solution was dispensed and incubated for 30 minutes at room temperature. Wells were subsequently washed seven times to remove excess POD-conjugate, prior to addition of 100μL of 3,3',5,5'-tetramethylbenzidine (TMB) enzyme substrate.

Samples were covered in foil to protect against light and incubated for 40 minutes at room temperature. The reaction was terminated with 100µL of enzyme reaction stop solution, and absorbance was measured for individual wells within 30 minutes using a 96-well DMX TC microplate reader.

Analysis was performed using Revelation software with colorimetric analysis at 450nm wavelength. A linear fit for the insulin standard curve was constructed by plotting the mean absorbance for each standard (y axis) against the corresponding standard insulin concentration (x axis). This was accepted if the correlation coefficient (r^2) exceeded 0.99. It was utilised to derive mean plasma insulin concentrations for each set of duplicates, with exclusion of individual readings if co-efficient of variation was > 10%.
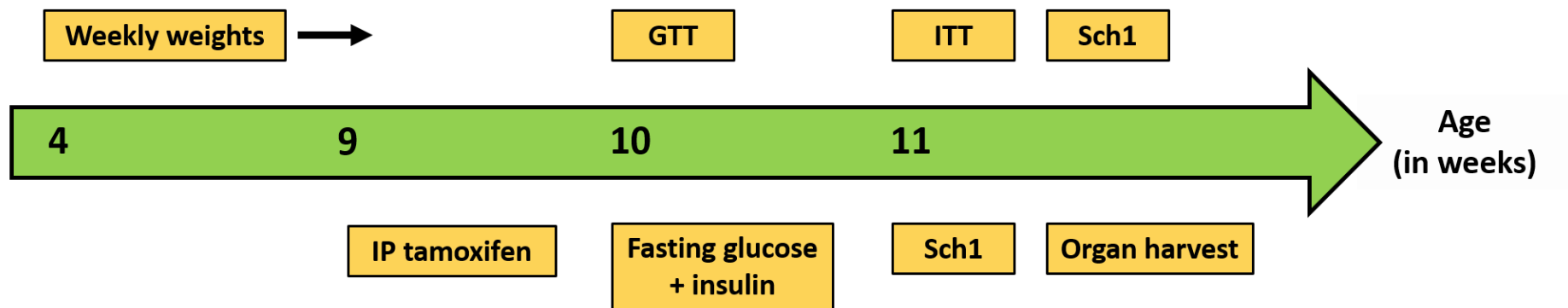
Figure 4-12 – Timeline for whole body metabolic profiling. IP = intraperitoneal; GTT = glucose tolerance testing; ITT = insulin tolerance testing.

4.12.5 Homeostasis model assessment (HOMA)

Readings derived from fasting glucose and insulin measurements were applied to a homeostatic model (HOMA-IR) to enable a crude quantification of systemic insulin resistance. The accuracy and precision of this estimate has been corroborated with use of euglycaemic clamps (r = 0.88), albeit only in humans and reliant on the hypothesis that basal glucose and insulin interactions are primarily determined by a simple feedback [445].

The following formula was applied:

$$\text{HOMA-IR} = \frac{\text{Glucose (mmol/L)} \times \text{Insulin (U/L)}}{22.5}$$

4.13   Angiogenesis after hindlimb ischaemia

In vivo assessment of the angiogenic phase of vascular regeneration after hindlimb ischaemia was performed in the SHIP2i$^{\Delta/+}$ colony. Mice were 11 weeks of age to enhance likelihood of tolerating the procedure. Initially, at 9 weeks, a 5 day course of IP tamoxifen was administered as outlined previously. After the final dose, mice were observed for a period of 1 week. At this stage, surgery was performed in designated operating theatres using inhalation of isoflurane anaesthetic. This procedural work was performed by Dr Nadira Yuldasheva, and is consistent with techniques published in the wider literature [446].

4.13.1 Induction of anaesthesia

24-48 hours pre-procedure, mice were shaved bilaterally from the lower abdominal wall to hindlimbs using an electric razor followed by topical application of Veet cream to remove residual fur. Mice were placed in an induction chamber and exposed to 5% isoflurane with concurrent administration of oxygen at 2L/min. Isoflurane was chosen due to its volatile properties allowing rapid induction and recovery. Adequate anaesthesia was confirmed by loss of muscle tone and absence of purposeful movements, in conjunction with changes in depth and frequency of respiration and a lack of response to averse stimuli such as tail pinch. Mice were transferred to the operating table, which had been pre-warmed to 38°C, and connected to a nose cone, which emitted 2% isoflurane that had been diverted away from the induction chamber via a valve. They were secured in a supine position using microporous surgical tape and injected with additional analgesia using IP buprenorphine at 0.25mg/kg. Depending on feedback from the mouse's behaviour, the concentration of isoflurane could be adjusted to maintain equilibrium.
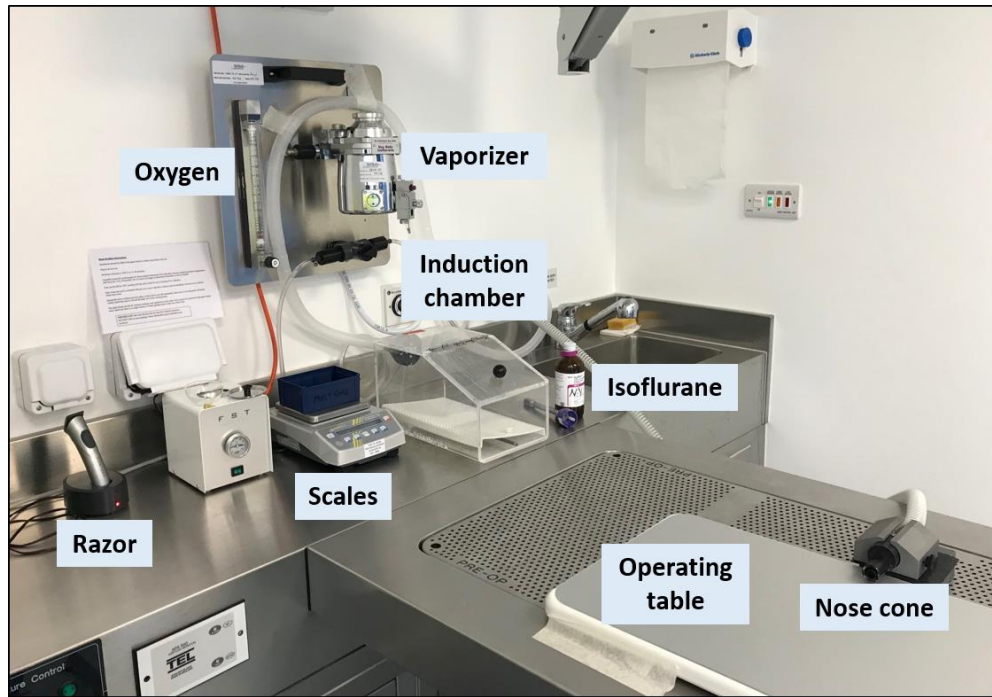
Figure 4-13 – Apparatus for general anaesthesia.

4.13.2 Femoral artery excision

Once adequately anaesthetised and secured onto the operating table, the area of

interest was disinfected with 0.75% povidone-iodine solution. An incision in the mid-

thigh was made through the skin layers to enable exposure of the left femoral artery.

Vicryl sutures were applied proximally at the level of the inguinal ligament and distally

at the bifurcation of the saphenous and popliteal vessels. This enabled ligation of the

femoral artery, which could subsequently be excised as a whole intervening segment.

This is a standard procedure performed in our facility, and laser Doppler imaging has

shown that it reduces distal limb perfusion to < 10% of the contralateral limb. The

wound was closed in layers using a continuous 6.0 Vicryl suture. The right limb was

used for control purposes and did not undergo any procedure. After discontinuation

of isoflurane and commencement of oxygen, 0.25mg/kg of IP buprenorphine was

administered for post-operative analgesia. This was followed by a period of monitored recovery, with the provision of a soaked diet for 24 hours prior to transfer into their usual cages.

4.13.3 OCT embedding of muscle specimens

This was performed on mice 1 week after hindlimb ischaemia. Sch1 was performed using isoflurane anaesthesia and intracardiac puncture and blood aspiration. 1mL of PBS was slowly injected via a cardiac puncture prior to slow administration of 1mL 4% PFA. After 5 minutes, gastrocnemius muscle was carefully harvested from both limbs (ischaemic and non-ischaemic). Spleen was also harvested for the first experiment as a positive control. Tissue was immediately placed into ice cold 4% PFA for 2 hours, after which it was washed and maintained in PBS.

Embedding was performed with optimal cutting temperature (OCT) compound. First, 2-methylbutane (isopentane) was poured into a glass beaker and placed into a plastic beaker containing liquid nitrogen using long forceps. The correct temperature for use was established by observing the formation of crystals. 20mm cork plates were used to mount the muscle specimens. Each was labelled before making a platform of OCT compound in the centre and lowering into the isopentane. Once frozen, the specimen was placed on top and layered in a circumferential fashion with OCT compound. This was continued until the sample was fully covered. Once complete, specimens were lightly covered in foil and kept on dry ice prior to storage at -80°C.

4.13.4 Cryosectioning

This was performed on a CM1900 cryostat. At commencement, the temperature of the apparatus was reduced to -20°C. A stainless steel S35 microtome blade was carefully placed in its holder. The embedded tissue specimen was subsequently mounted onto a metal platform and locked onto its respective holder. The cryotome was adjusted to obtain thicker 50µM sections initially. Once the central region of tissue was reached, sections were reduced to 10µM thickness. A fine paintbrush was utilised to gently manoeuvre sliced sections underneath the anti-roll glass sheet. From here, they were directly loaded onto Superfrost Plus slides by heating the area of attachment with the fingertip. This was repeated to obtain roughly 5-6 sections per slide. A separate slide was utilised for control non-ischaemic limb tissue. All samples were maintained at -80°C until time of staining.

4.13.5 Isolectin B4 staining

At the time of staining, slides were first allowed to dry at room temperature for 30 minutes. A PAP pen was used to draw a thin water-repellent region around the mounted tissue specimens on each individual slide, and then allowed to dry completely. A small gap was left between the margins and the tissue sections to ensure that there was sufficient space to accommodate 200µL of liquid, which was used for all wash and incubation steps in the protocol.

After addition of 200µL PBS for rehydration, specimens were permeabilised in 0.25% Triton-X100 with 5% goat serum for one hour at 4°C. After three 5 minute washes in PBS, isolectin B4 pre-conjugated to Alexa Fluor 488 was added at 1:100 dilution and

left overnight at 4°C. Once this was washed three times in PBS, Hoescht 33342 diluted 1:2000 in PBS was applied for 15 minutes at room temperature. After a final set of washes, the slides were mounted with individual 22 x 64mm coverslips using Prolong Gold and sealed with nail varnish in preparation for confocal imaging. This final step was performed by Dr Richard Cubbon.

4.13.6 Quantification of vascularity

Analyses were performed using Image J software, with acquisition at 20X magnification. Total vascular area was quantified as the proportional area of isolectin B4 staining within a 400μm x 400μm region of interest. Horizontal lines were drawn across the width of the image, and used to quantify the number of vessels with the average of four readings used for statistical analyses. The threshold of each image was subsequently altered to black and white (black = non-endothelial, white = endothelial) and transformed using the 'distance map' binary function. For each individual pixel within the image, this illustrates the number of pixels required to reach a black pixel and this was quantified using the frequency histogram function. This was used to derive a proxy of vessel wall thickness by presenting the distance to non-vascular pixels from every vascular pixel. The average of multiple images (≥ 3) per genotype were used for all quantification purposes.
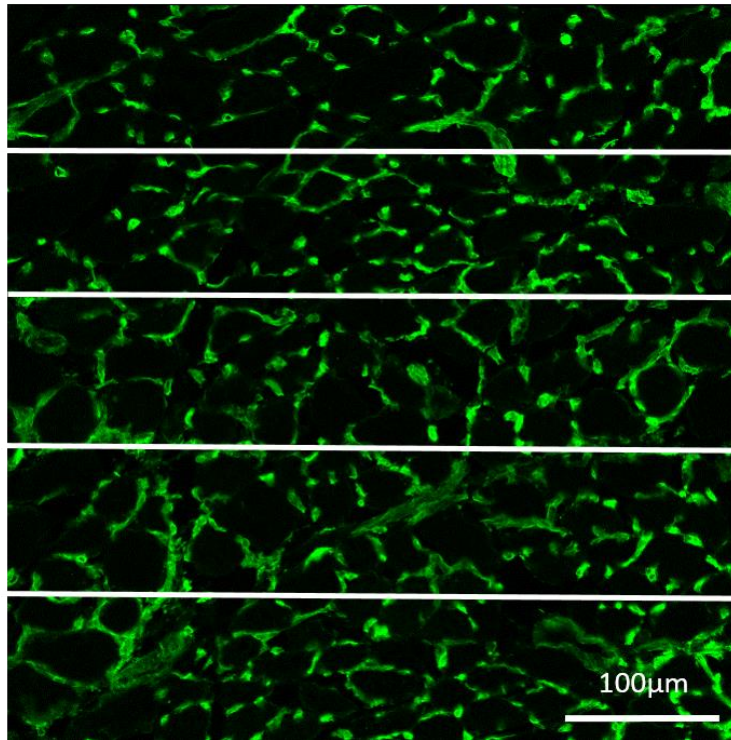
Figure 4-14 – Representative image of skeletal muscle (20X magnification) stained for endothelium with isolectin B4. Four horizontal lines (*white*) were drawn at equal distances across the image width and used to quantify vessel number.

4.14 Vascular repair after denuding injury

In vivo assessment of endothelial repair was performed after vascular injury, using methodology comparable to other protocols in published literature [447] [448]. Mice in the SHIP2i$^{\Delta/+}$ colony were 11 weeks of age to enhance likelihood of tolerating the procedure. Initially, at 9 weeks, a 5 day course of IP tamoxifen was administered at a dose of 40 mg/kg as outlined previously. After the final dose, mice were observed for a period of 1 week. At this stage, vascular injury was performed in designated operating theatres using anaesthestic induction as described previously. This procedural work was performed by Dr Nadira Yuldasheva.

4.14.1 Surgical arteriotomy

Surgery was aided by use of a OPMI 1-FC dissecting microscope. An aseptic technique was maintained throughout. First, the area of interest was established by removing fur with Veet cream. 0.75% providone-iodine solution was topically administered to sterilise the region. Access was via a small incision in the left mid-thigh with use of fine Iris scissors to perform meticulous and gentle dissection through the tissue layers until the common femoral artery was identified. Crucially, great care was taken to avoid manipulation of the epigastric artery which was vital in maintaining limb perfusion throughout the procedure. After careful isolation, the left femoral artery was differentiated using a loosely tied 8.0 Vicryl suture and a proximal clamp placed at the site of the inguinal ligament. Additionally, there was distal ligation at the saphenopopliteal bifurcation. A single topical drop of Lignol (1% lidocaine and adrenaline) was applied prophylactically in the proximal region to minimise propensity for vasospasm.

Subsequently, an arteriotomy incision was made in the profunda femoris using spring scissors. Once access had been obtained, a 200XT angioplasty guide wire of 0.014 inch diameter was inserted. Once the clamp had been relieved, advancement of the wire for a distance of 1.5-2cm was performed with three repetitions. After removal, the suture was tightened to ligate the vessel proximal to the arteriotomy site. Skin was closed in layers using a continuous 6.0 Vicryl suture. The right limb was used for control purposes and underwent a comparable procedure but without use of a guide wire so that no denudation occurred. After discontinuation of isoflurane and commencement of oxygen, 300µL of Irripod (sterile 0.9% sodium chloride) was

injected IP to optimise hydration. A period of monitored recovery was conducted, with the provision of a soaked diet for 24 hours prior to transfer into their usual cages.

4.14.2 Evans blue staining of residual endothelial injury

Four days after vascular injury, mice were once again anaesthetised using isoflurane as documented. After an incision along the linea alba to expose the inferior vena cava (IVC), 50µL of 5% Evans blue solution was injected. This binds with high affinity to serum albumin, which is unable to penetrate intact endothelium. However, in areas of persisting denudation (i.e. absence of regeneration), albumin can penetrate and embed into the subendothelial ECM to allow visualisation. After a duration of 2 minutes, 4% PFA mixed in PBS was administered directly into the left ventricle using a 27G needle under mechanical pressure. This mediated fixation of tissues, which was confirmed by visualisation of muscle fasciculations. Subsequently, both femoral arteries and surrounding soft tissue could be carefully excised longitudinally up to the aortic bifurcation proximally. Maintenance storage was in 4% PFA until time of analysis.

Images were obtained by Dr Nadira Yuldasheva using an SZ61 Dissecting Stereo microscope with a QiCam digital camera. Careful visualisation enabled dissection of arteries from its surrounding tissue. At 20X magnification, a 5mm measurement from the aortic bifurcation was established as the proximal point of interest. A 5mm segment of artery from this point distally provided the vessel length for analysis. This was performed using ImagePro Plus 6.2 software. Firstly, the control vessel was visualised to confirm absence of denudation. Next, the total area stained blue was

quantified and calculated as a percentage of the total area. This value could then be

subtracted from 100 to identify % endothelial regeneration.
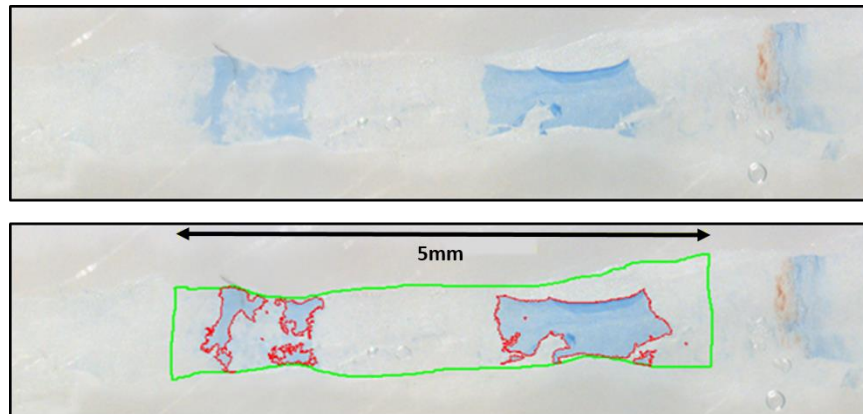
Figure 4-15 – Representative image of femoral artery for assessment of vascular

repair. A 5mm segment was identified (*green*), and the proportion stained with

Evans solution (*blue*) was quantified.

4.15 Statistical analyses

All graphs were produced using GraphPad Prism. This software was also used for

statistical analyses, in addition to Microsoft Excel 2013. Continuous data are

expressed as means with subsequent values in brackets and corresponding error bars

denoting standard error of mean (SEM). Unless otherwise stated, analyses were

performed with the assumption of normal distribution using two-tailed unpaired or

paired Student's t-tests. In the context of unequal variance, unpaired t-testing with

Welch's correction was applied. For GTT and ITT, the area under curve (AUC) was

calculated. For comparison of proportions, chi-square testing was performed. A p-

value of < 0.05 was considered to be of statistical significance and is denoted by a *

symbol on bar charts, whilst non-statistical comparisons are represented as 'n.s'.

Chapter 5 – Results

_____

Exploring in vivo vascular function in mice with endothelium-specific germline SHIP2 haploinsufficiency (ECSHIP2$^{\Delta/+}$)

For the purposes of this subsection, 'WT' denotes control mice whilst 'ECSHIP2$^{\Delta/+}$'

refers to mice with germline endothelium-specific SHIP2 catalytic domain

haploinsufficiency.

5.1 Genotyping

All ECSHIP2$^{\Delta/+}$ (and SHIP2i$^{\Delta/+}$) mice required for breeding and experimental purposes

had their genotype confirmed by DNA PCR. A 1000 base pair ladder was utilised to aid

correct identification of bands observed.

A representative image for Cre PCR with three mice (IDs 130, 131, 132) is shown

below (Figure 5-1). 131 and 132 do not generate any distinct bands and represent the

native gene. 130 generates a transgene (applicable for both *Tie*2-Cre and CAGG-

CreERT2) and is visualised as a single band at 408 base pairs. All gels were

accompanied by negative (-ve) and positive (+ve) controls for verification purposes.
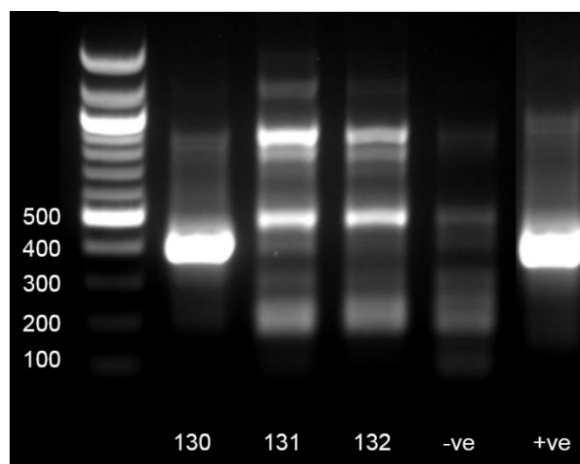
Figure 5-1 – *Tie*2-Cre and CAGG-CreERT2 PCR.

A representative image for SHIP2 PCR with the same three mice is shown in Figure 5-2). 130 and 132 generate a single band at 411 base pairs and reflect the native gene. 131 has *lo*xP sites inserted in one allele of the SHIP2 gene, reflected by a second band at 500 base pairs. Again, all gels were accompanied by negative (-ve) and positive (+ve) controls for verification purposes.
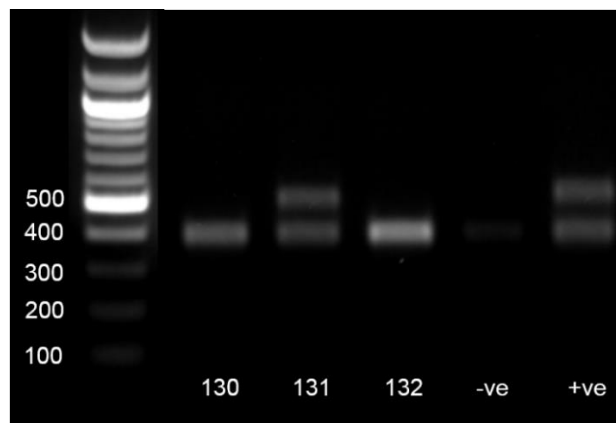
Figure 5-2 – SHIP2 PCR.

5.2 SHIP2KD validation

5.2.1 SHIP2 protein expression in PECs

To confirm adequate SHIP2KD in the vasculature of ECSHIP2$^{\Delta/+}$ mice, PECs were harvested and Western blotting of lysates performed to quantify protein expression using densitometry. These data were generated in conjunction with Dr Nicole Watt. SHIP2 protein abundance was nominally reduced in SHIP2KD mice compared to WT (69 [+/- 9] vs 100 [+/- 13]; p=0.06), although notably, Dubois *et al* have shown that this antibody may still bind truncated SHIP2 (i.e. without its catalytic domain) [377]. Consistent with their observation, however, our representative blot does illustrate a subtle reduction in molecular weight that may be predicted as a consequence of

191

truncating the catalytic region. Our laboratory has previously attempted to quantify

native and truncated SHIP2 protein levels separately, but testing with multiple

antibodies has not unfortunately provided reliable discrimination.
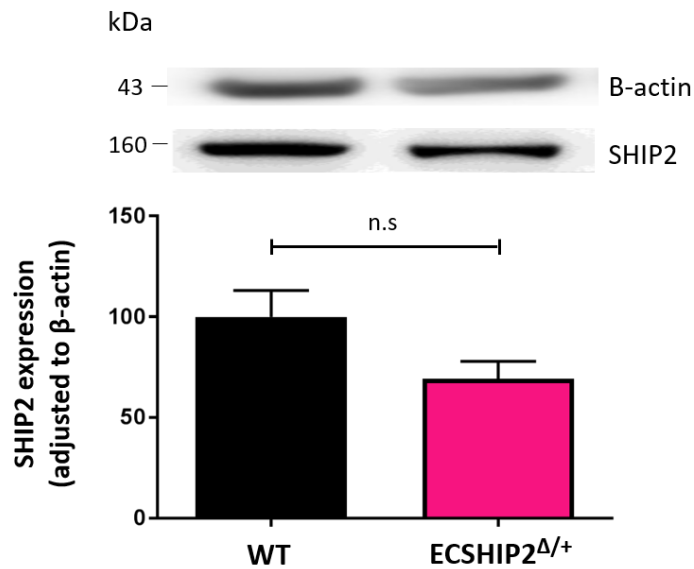
Figure 5-3 – SHIP2 protein expression in ECSHIP2$^{\Delta/+}$ colony (n=5,8).

Our laboratory has also published data on truncated SHIP2 mRNA expression in PECs

using quantitative PCR [449]. This was shown only to be detectable in endothelial cells

derived from ECSHIP2$^{\Delta/+}$ mice, with no expression in WT mice and barely detectable

signal in lung non-endothelial cells or circulating CD11b+ myeloid cells.

5.2.2   SHIP2 activity in PECs

To corroborate findings at protein level and confirm concurrent reduction in catalytic

activity, PEC lysates were used to perform a SHIP2 activity assay. This data was

generated in conjunction with Dr Nicole Watt. Compared with WT, SHIP2KD mice had

reduced enzymatic activity as quantified by PtdIns(3,4)P2 formation/mg protein (516

[+/- 34] vs 888 [+/- 184]; p=0.03).
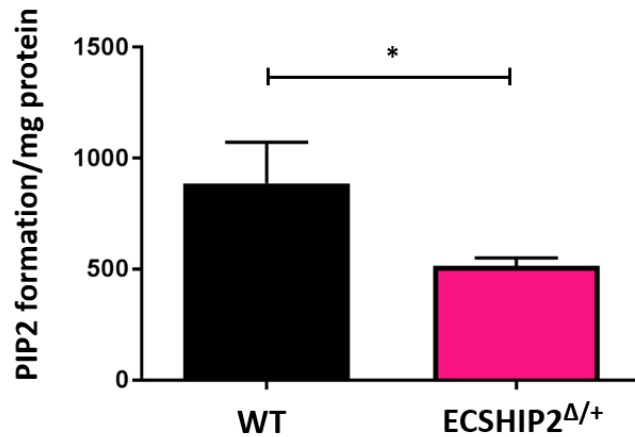
Figure 5-4 – SHIP2 activity assay in ECSHIP2$^{\Delta/+}$ colony (n=9,12).

5.3 Vascular formation in retinas

For initial assessment of vascular structure, 5 day old pups from the ECSHIP2$^{\Delta/+}$ colony

were used to evaluate developmental angiogenesis. Retinas were stained with

isolectin B4 to highlight endothelial cells and flat-mounted for visualisation with

confocal microscopy. Baseline body weights were comparable between WT and

SHIP2KD mice (2.62g [+/- 0.28] vs 2.85g [+/- 0.34]; p=0.19).

Retinas derived from mice with SHIP2KD demonstrated a trend towards impaired

radial outgrowth compared to WT (1242µm [+/- 106] vs 1371µm [+/- 108]; p=0.41). As

the extent of radial outgrowth differs substantially depending on precise timing of

harvest, measurements were normalised to body weight to account for inter-litter

variability. This showed a significant reduction in radial outgrowth in the context of

SHIP2KD (400µm/g [+/- 42] vs 524µm/g [+/- 38]; p=0.048). Frontal regions showed

nominally reduced vascular area in the context of SHIP2KD, although this was not

statistically significant (42% [+/- 2] vs 46% [+/- 2]; p=0.20). No differences were

evident in more mature central retinal regions between SHIP2KD and WT mice (37%

[+/- 1] vs 37% [+/- 1]; p=0.53). Quantification of branch points per 0.04 mm^2 region of

interest showed a statistically significant reduction in frontal regions with SHIP2KD (55

[+/- 2] vs 66 [+/- 1]; p=0.002), with a similar pattern observed in central regions (59

[+/- 2] vs 69 [+/- 2]; p=0.003). Mice with SHIP2KD had nominally fewer tip cells per

mm of vascular front (16 [+/- 1] vs 19 [+/- 1]; p=0.06), and significantly reduced

numbers of filopodia per 100µm of angiogenic front (19 [+/- 1] vs 23 [+/- 1];

p=0.0007). The number of filopodia per individual tip cell was similar between WT and

SHIP2KD mice (23 [+/- 1] vs 23 [+/- 1]; p=0.96).
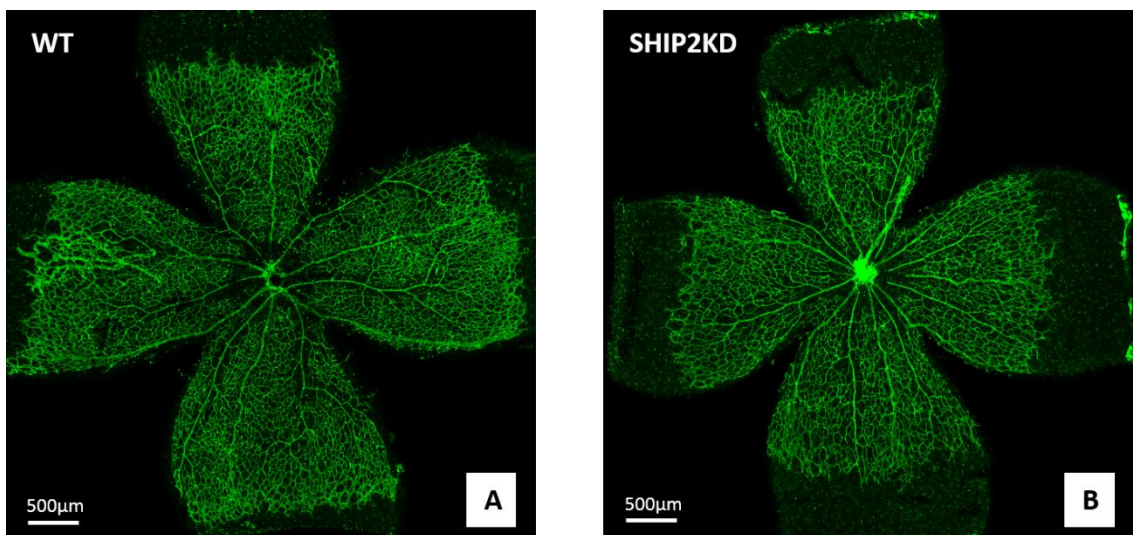
Figure 5-5 – Representative image of mounted retina from WT mice **(Panel A)** and

ECSHIP2$^{\Delta/+}$ mice **(Panel B)** demonstrating disparity in radial outgrowth.
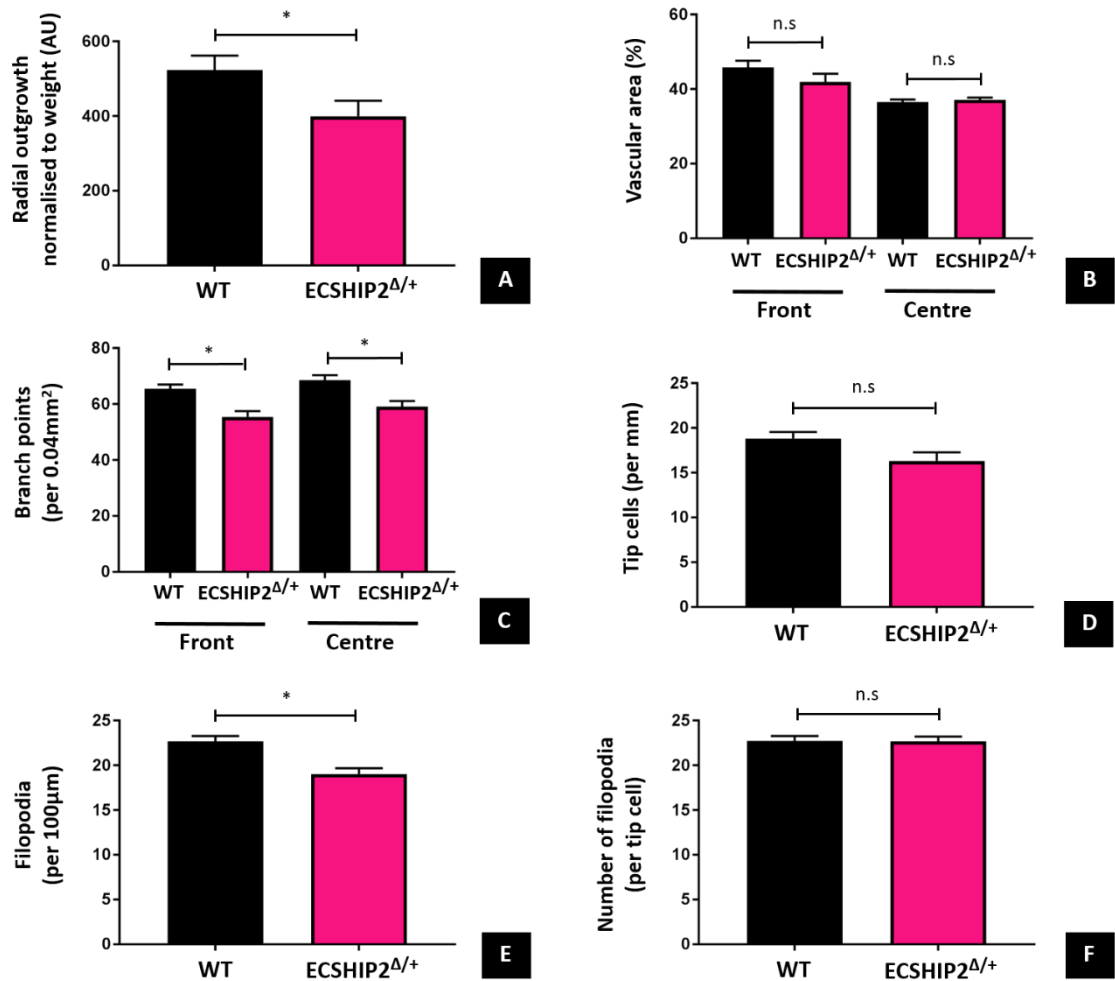
Figure 5-6 – Retinal analysis, with measurements of radial outgrowth **(Panel A)**, total vascular area **(Panel B)**, number of branch points **(Panel C)**, tip cell abundance **(Panel D)**, filopodia abundance **(Panel E)** and filopodia per tip cell **(Panel F)** (n=11,7).

5.4 Oxidative stress in PECs

The data presented above provides evidence of impaired angiogenesis in the context of SHIP2KD. Our other published work has also demonstrated endothelial dysfunction and reduced NO bioavailability in these mice [449]. One potential common explanation for these observations is oxidative stress, and this was therefore assessed. Compared to WT mice, PECs derived from SHIP2KD mice exhibited increased

superoxide production as quantified by DHE fluorescence (22 [+/- 2] vs 10 [+/- 1];

p=0.004).
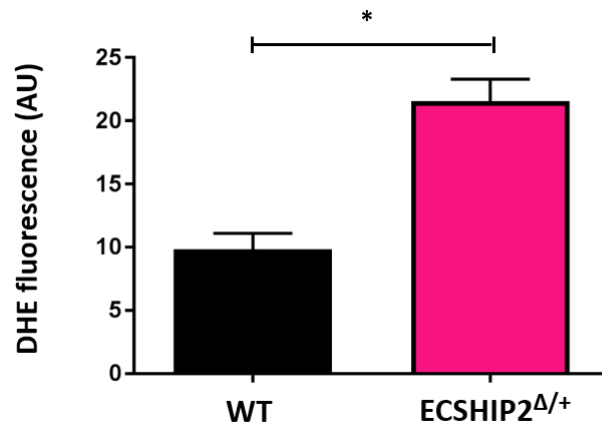
Figure 5-7 – DHE fluorescence, measured in arbitrary units (AU) (n=3,9).

Nox2 is a critical pathophysiological source of superoxide in models of systemic insulin

resistance, and its Rac1 subunit can be activated by PI3K. In view of this, expression of

the Nox2 catalytic gp91 subunit was assessed using Western blotting. This data was

generated in conjunction with Dr Nicole Watt. PECs derived from SHIP2KD mice had

increased Nox2 protein expression compared to WT (116 [+/- 7] vs 96 [+/- 6]; p=0.04).
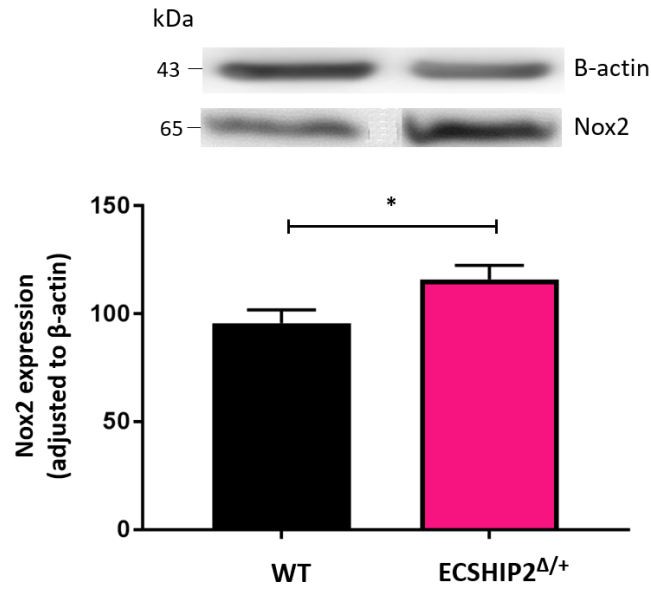
Figure 5-8 – Nox2 protein expression in ECSHIP2$^{\Delta/+}$ colony (n=9,10).

Notably, increased superoxide production in the context of SHIP2KD appeared to be suppressed by concomitant administration of the specific Nox2 antagonist, Gp91ds-tat (0.98 [+/- 0.08] vs 1.25 [+/- 0.09]; p=0.04), suggesting that production was primarily Nox2 enzyme dependent.
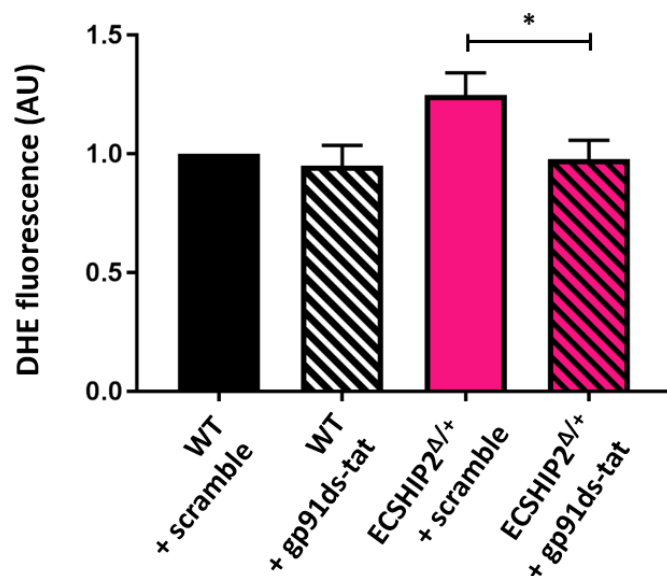
Figure 5-9 – DHE fluorescence assay with or without Nox2 inhibition via gp91ds-tat. All mean fluorescence values are in arbitrary units (AU) and are adjusted for WT without gp91ds-tat (*black bar*) (n=4,7).

Superoxide abundance in the context of SHIP2KD was also normalised by administration of the PI3K inhibitors Wortmannin (0.93 [+/- 0.14] vs 1.43 [+/- 0.15]; p=0.03) and LY294002 (0.96 [+/- 0.12] vs 1.29 [+/- 0.07]; p=0.03). This suggests that increased signalling through the PI3K/AKT axis, which we have demonstrated in SHIP2KD endothelial cells [449], contributes towards this oxidative stress.
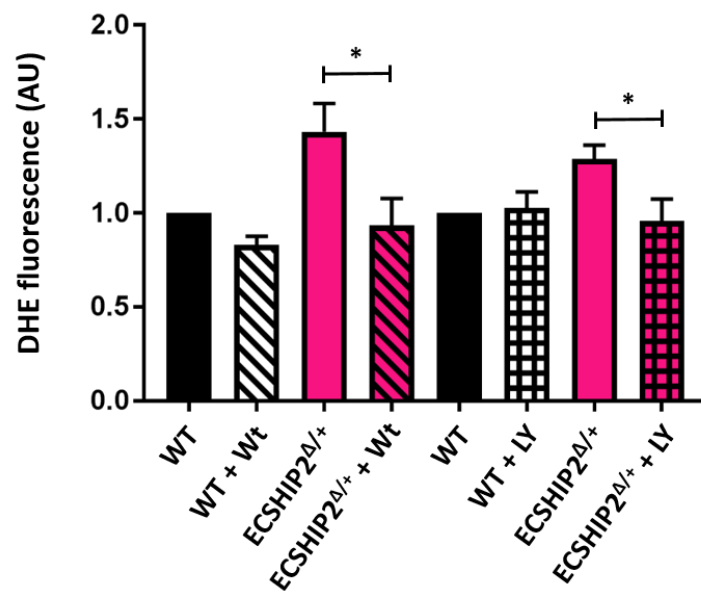
Figure 5-10 – DHE fluorescence assay with or without PI3K inhibition via Wortmannin (*Wt*) or LY294002 (*LY*). All mean fluorescence values are in arbitrary units (AU) and are adjusted for WT without PI3K inhibitor (*black bar*) (n=5,5).

Exploring in vitro vascular function in human umbilical vein endothelial cells (HUVECs)

For the purposes of this subsection, 'control shRNA' refers to HUVECs expressing GFP-targeting shRNA whilst 'SHIP2 shRNA' denotes those expressing SHIP2-targeting shRNA. Similarly, 'vehicle' refers to cells treated with vehicle control, whilst 'SHIP2 SMI' denotes those treated with SHIP2 SMI.

5.5 SHIP2KD validation

5.5.1 Lentiviral dose optimisation

A complementary model using HUVECs was used to validate and extend the mechanistic data derived from ECSHIP2$^{\Delta/+}$ PECs. SHIP2KD was achieved with lentiviral vectors delivering SHIP2-targeting shRNA, with GFP-targeting shRNA serving as a control. Initially, HUVECs were exposed to different SHIP2 shRNA viral vector concentrations (5 MOI, 10 MOI or 20 MOI) or equivalent control shRNA viral vector, with 4 days elapsing prior to collection of cell lysates for Western blotting. Densitometry of bands was performed to quantify total SHIP2 expression.

SHIP2-targeting shRNA reduced total SHIP2 protein expression: 0.28 [+/- 0.04] vs 0.46 [+/- 0.05; p=0.005) at 5 MOI, 0.10 [+/- 0.008] vs 0.38 [+/- 0.05; p=0.008) at 10 MOI, and 0.11 [+/- 0.006] vs 0.44 [+/- 0.10]; p=0.03) at 20 MOI. When normalised to control shRNA, SHIP2 shRNA resulted in 40% SHIP2KD at 5 MOI, 74% SHIP2KD at 10 MOI and 75% knockdown at 20 MOI, respectively. Based on this preliminary data, 10 MOI was used for all subsequent lentiviral transduction experiments as a viral load likely to balance effective gene silencing with minimal toxicity.
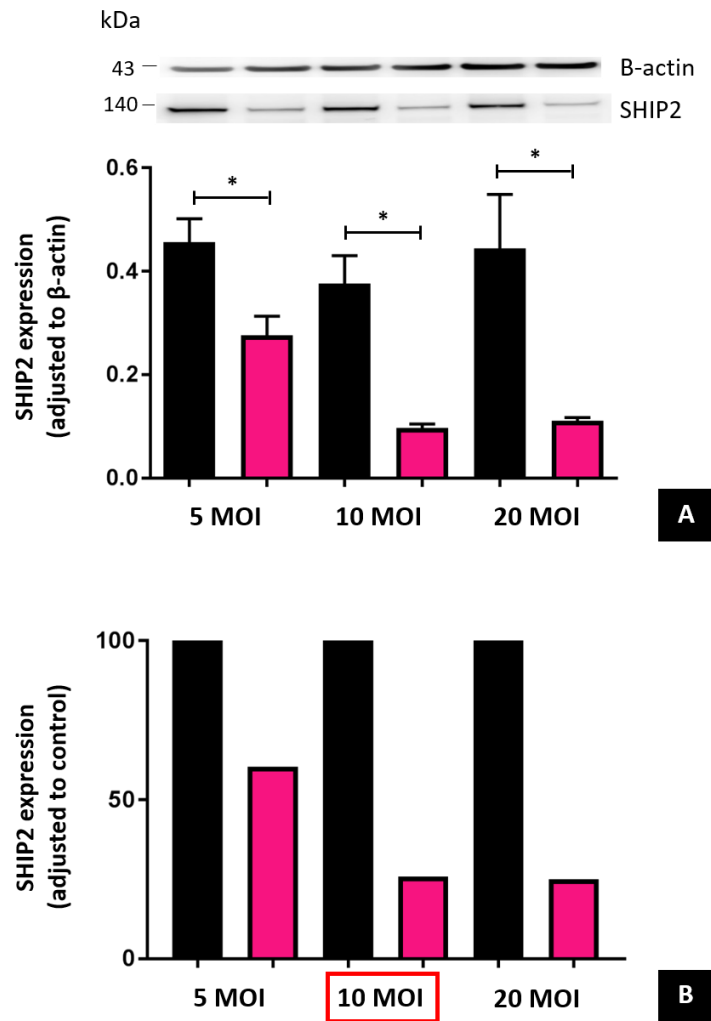
Figure 5-11 – SHIP2 protein expression at different MOI, adjusted to β-actin **(Panel A)** and control **(Panel B)**. Data for control shRNA (*black bar*) and SHIP2-targeting shRNA (*pink bar*) represented. MOI = multiplicity of infection (n=5,5).

5.5.2 SHIP2 activity in HUVECs

To corroborate that protein knockdown was associated with reduced SHIP2 catalytic function in HUVECs, an activity assay was performed. Compared with control, shRNA knockdown of SHIP2 resulted in a 51% reduction in enzymatic activity, as quantified by PtdIns(3,4)P2 formation/mg protein (849 [+/- 117] vs 1747 [+/- 244]; p=0.042).
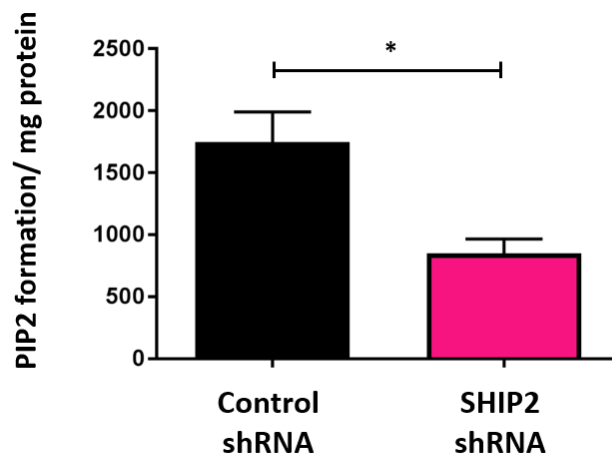
Figure 5-12 – SHIP2 activity assay in HUVECs (n=4,4).

5.6 HUVEC signalling intermediates

5.6.1 PI3K/AKT axis

Given the key role of PI3K/AKT signalling in angiogenesis, and its regulation by SHIP2, HUVEC lysates were used to measure key components of the PI3K/AKT axis. Band densitometry was used to define phosphorylated protein abundance as a proportion of its respective total protein. Cells expressing SHIP2-targeting shRNA had a significant increase in basal pAKT (T308) expression (41 [+/- 6] vs 26 [+/- 9]; p=0.01), peNOS (S1177) expression (134 [+/- 39] vs 99 [+/-9]; p=0.04) and pERK (Y202/204) expression (79 [+/- 12] vs 42 [+/- 5]; p=0.009). Paradoxically, such increases in signalling have previously been implicated in increased cell survival, migration, proliferation and angiogenesis [197] [193].
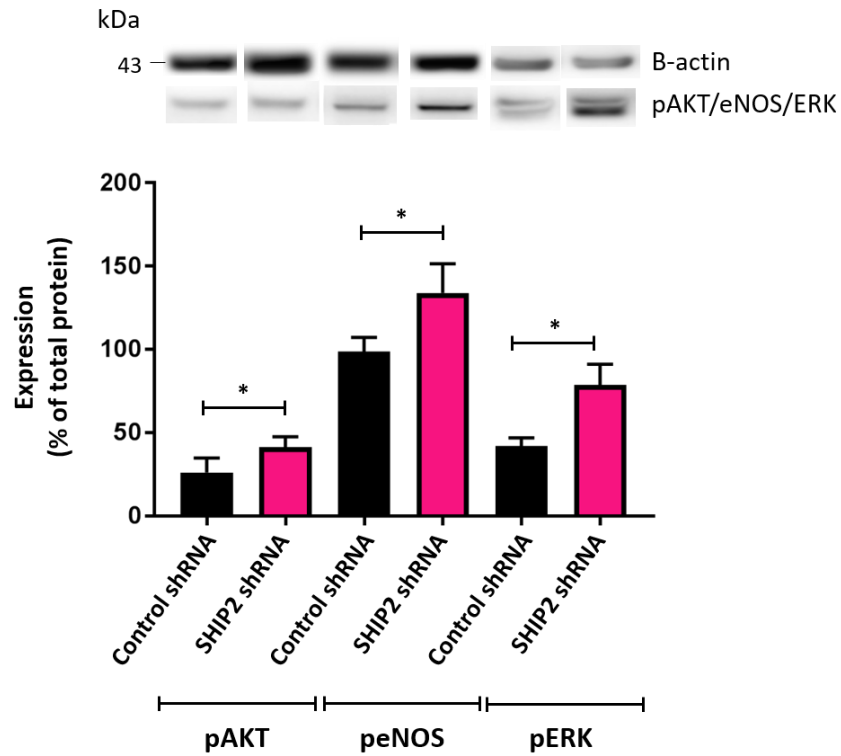
Figure 5-13 – Expression of basal downstream signalling intermediates. All values have been adjusted for β-actin, with phosphorylated protein levels expressed as % of total (n=5,5).

5.6.2 Nox2 protein expression

In order to corroborate observations in PECs that SHIP2KD was associated with increased Nox2-derived superoxide, Nox2 protein (gp91 subunit) expression was quantified. HUVECs expressing SHIP2-targeting shRNA had increased Nox2 protein expression compared to controls (0.19 [+/- 0.02] vs 0.11 [+/- 0.02]; p=0.03).
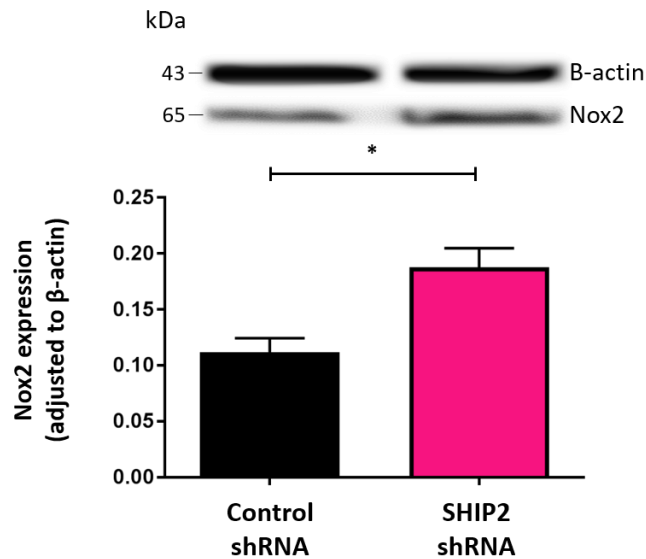
Figure 5-14 – Nox2 protein expression, adjusted for β-actin (n=3,3).

5.6.3 Superoxide production

To ascertain whether increased Nox2 protein was associated with increased superoxide abundance, DHE fluorescence was then quantified. Compared to controls, HUVECs expressing SHIP2-targeting shRNA exhibited increased DHE fluorescence (1.42 vs 1.00; p=0.02). Pertinently, superoxide formation in the context of SHIP2KD appeared to be suppressed by the Nox2-specific inhibitor gp91ds-tat (0.93 vs 1.42; p=0.03) indicating that production was primarily mediated by Nox2 enzyme.
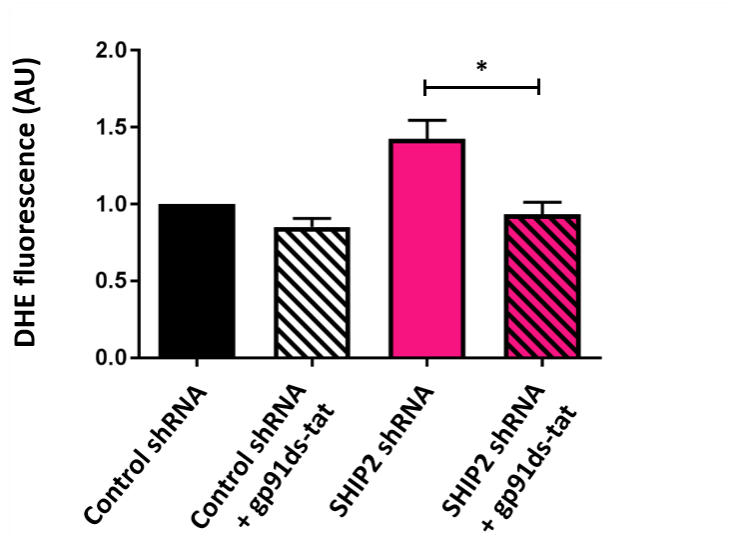
Figure 5-15 – DHE fluorescence assay. All mean values are measured in arbitrary units (AU) and are adjusted for control shRNA (*black bar*) (n=6,6).

Superoxide abundance in the context of SHIP2KD was also suppressed by administration of the PI3K inhibitors Wortmannin (0.87 [+/- 0.15] vs 1.42 [+/- 0.15]; p=0.01) and LY294002 (1.30 [+/- 0.09] vs 1.50 [+/- 0.11]; p=0.049). This suggests that the increased signalling observed through the PI3K/AKT axis contributes towards the oxidative stress associated with SHIP2KD in HUVECs.
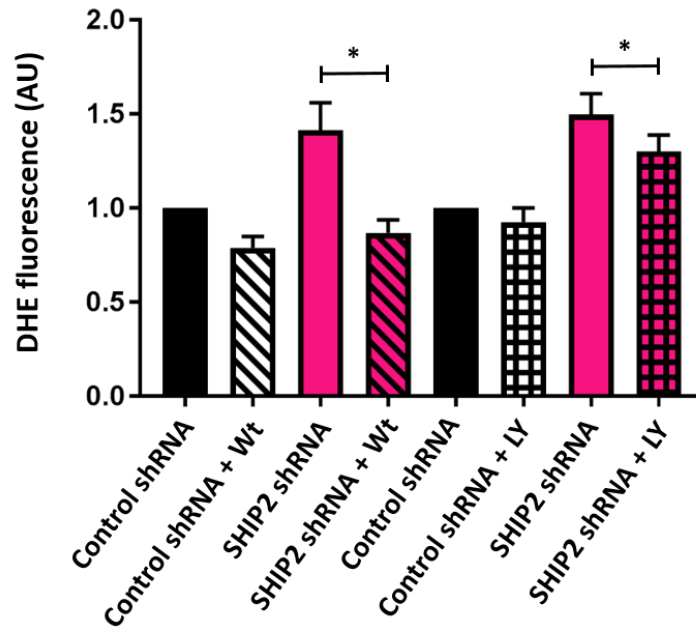
Figure 5-16 – DHE fluorescence assay with or without PI3K inhibition via Wortmannin (*Wt*) or LY294002 (*LY*). All mean fluorescence values are in arbitrary units (AU) and are adjusted for HUVECs expressing control shRNA (*black bar*) (n=5,5).

5.7 Cell migration

5.7.1 Scratch wound assay

In order to assess whether impaired cell migration may underpin the reduced retinal angiogenesis observed with endothelial SHIP2KD, initial screening experiments defined scratch wound closure in our HUVEC model system. SHIP2 shRNA resulted in impaired wound closure at 18 hours compared to controls (33% [+/- 5] vs 54% [+/- 4]; p=0.002).
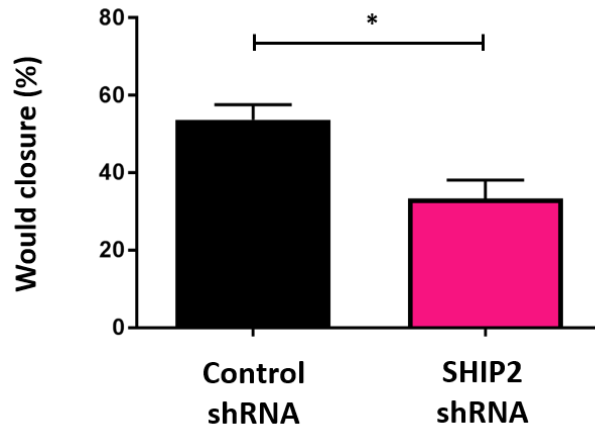
Figure 5-17 – Scratch wound closure in HUVECs exposed to control or SHIP2 shRNA (n=4,4).

Assays were also repeated in the context of pharmacological SHIP2 inhibition using two commercially available SMI, AS1949490 and AS1938909. Consistent with prior experiments, scratch wound closure was assessed over an 18 hour duration. Increased concentrations of SHIP2 SMI broadly resulted in more significant reductions in wound closure versus vehicle control, and this was replicated with both inhibitors. Wound closure in the context of AS1949490 at 10μM was 21% [+/- 1] compared to 43% [+/- 4] for controls; p=0.005. Similarly, AS1938909 at the same concentration resulted in 21% [+/- 1] wound closure compared to 38% [+/- 4] for controls; p=0.02. Given these comparable data, AS1938909 was selected for use in all subsequent assays involving SHIP2 SMI.
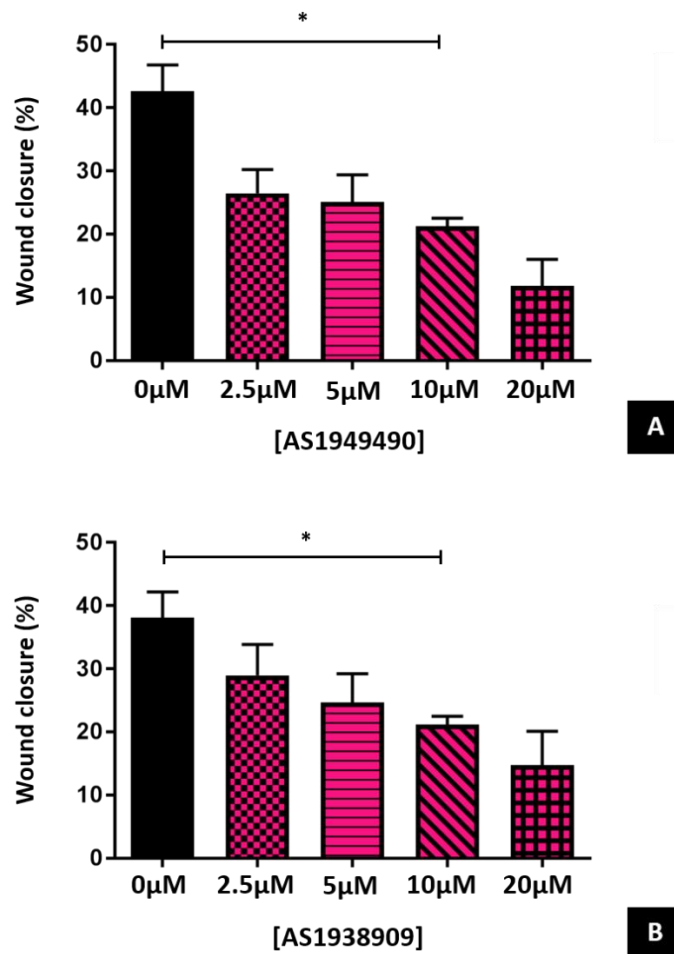
Figure 5-18 – Wound closure at 18 hours after independent exposure of HUVECs to two SHIP2 SMI, AS1949490 **(Panel A)** and AS1938909 **(Panel B)**. An equivalent concentration of DMSO was used for controls (n=4,4).

5.7.2 Boyden chamber assay

Although the scratch assay has clear advantages in being a simple and relatively economical method to study cell migration *in vitro*, it does not incorporate a chemotactic gradient. To circumvent this, we also performed Boyden chamber assays with HUVECs expressing control or SHIP2-targeting shRNA in the context of a 50ng/mL VEGF chemotactic stimulus (or vehicle control). SHIP2KD reduced net number of migrating cells after 6 hours (6.5 [+/- 0.5] vs 8.5 [+/- 0.5]; p=0.04).
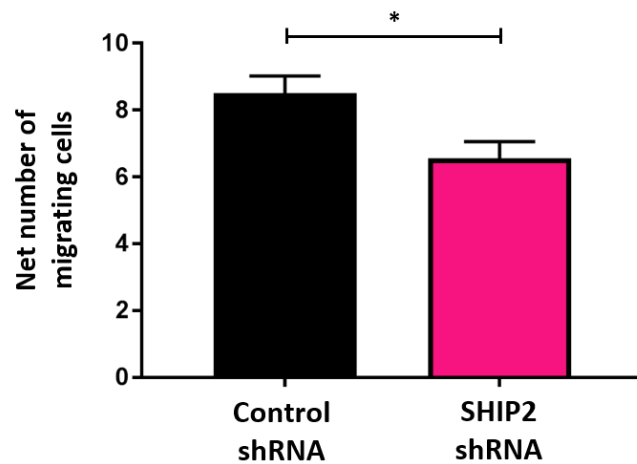
Figure 5-19 – Net number of migrating cells per microscopic field (300μm x 250μm) in Boyden chamber assay, defined as difference in HUVECs with and without exposure to VEGF (n=4,4).

5.8 Cell proliferation

Given that cell proliferation can contribute to angiogenesis and scratch wound closure, this phenomenon was quantified by assessing EdU incorporation. HUVECs expressing SHIP2 shRNA exhibited no differences in the proportion incorporating EdU versus control shRNA (14% [+/- 6] vs 17% [+/- 8]; p=0.43). Similarly, no differences were observed between cells exposed to AS1938909 SMI or vehicle control (25% [+/- 3] vs 26% [+/- 3]; p=0.87). This implies that defects in angiogenesis and scratch wound closure are unlikely to relate to impaired endothelial cell proliferation.
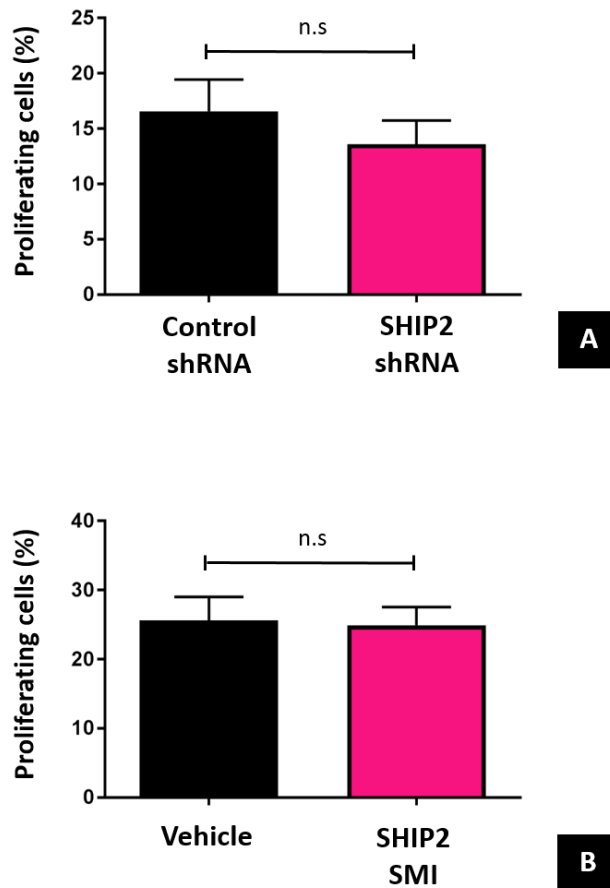
Figure 5-20 – Proliferating cells defined by EdU incorporation, in the context of SHIP2-targeting shRNA **(Panel A)** or SMI **(Panel B)** (n=7,7).

5.9 Cell sprouting

As outlined in the 'introduction' section, angiogenesis is a multi-faceted process. Hence, the 2-dimensional (2D) assays of cell migration and proliferation described only model certain stages of angiogenesis. For this reason, a three-dimensional (3D) fibrin gel bead sprouting assay using HUVECs has been optimised to recapitulate the early stages of angiogenesis, including vessel lumen formation and polarisation of endothelial cells [450]. Some more progressive stages including vessel branching and anastomosis can also be observed.

In beads coated with HUVECs expressing SHIP2-targeting shRNA, there was a reduction in mean number of sprouts per bead after 24 hours incubation (4.7 [+/- 0.7] vs 7.6 [+/- 1.8]; p=0.01). No differences were observed in mean sprout length (76µm [+/- 7] vs 77µm [+/- 7]; p=0.65). Similarly, addition of SHIP2 AS1938909 SMI resulted in a reduction in mean number of sprouts per bead (3.9 [+/- 0.2] vs 5.2 [+/- 0.2]; p=0.03) but no statistically significant difference in mean sprout length (69µm [+/- 4] vs 76µm [+/- 3]; p=0.16).
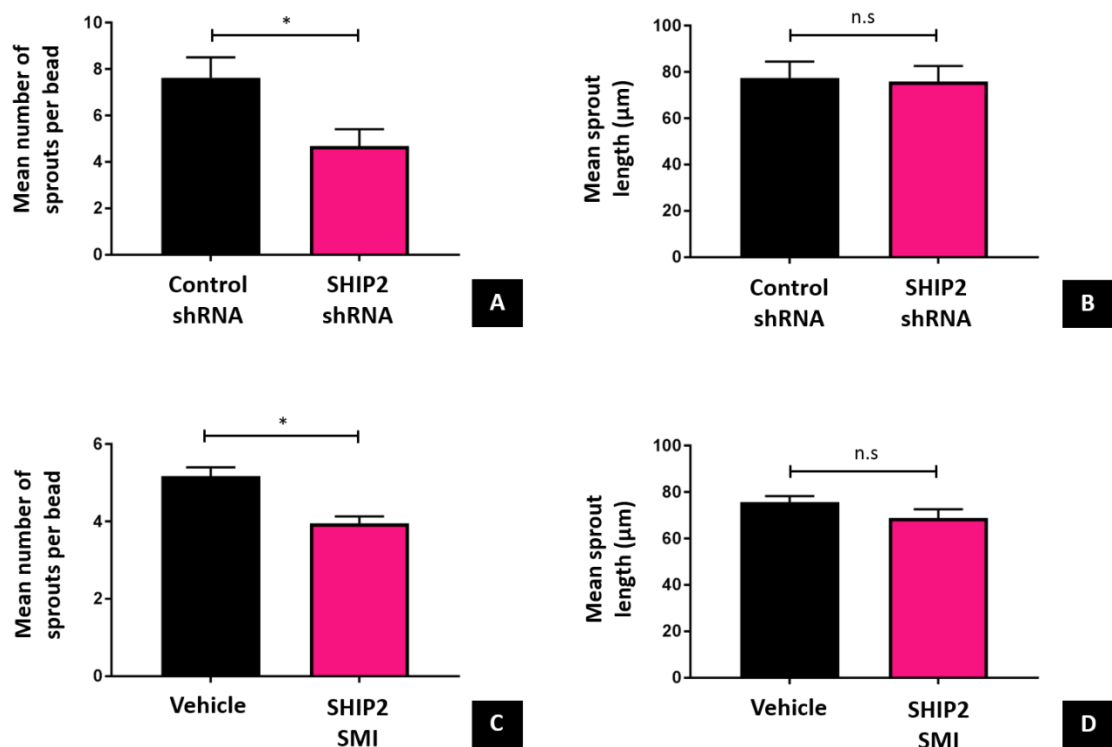
Figure 5-21 – Bead sprouting assay in HUVECs. Quantification of sprout abundance with shRNA **(Panel A)** and SMI **(Panel C)**, and sprout length with shRNA **(Panel B)** and SMI **(Panel D)** (n=4,4).
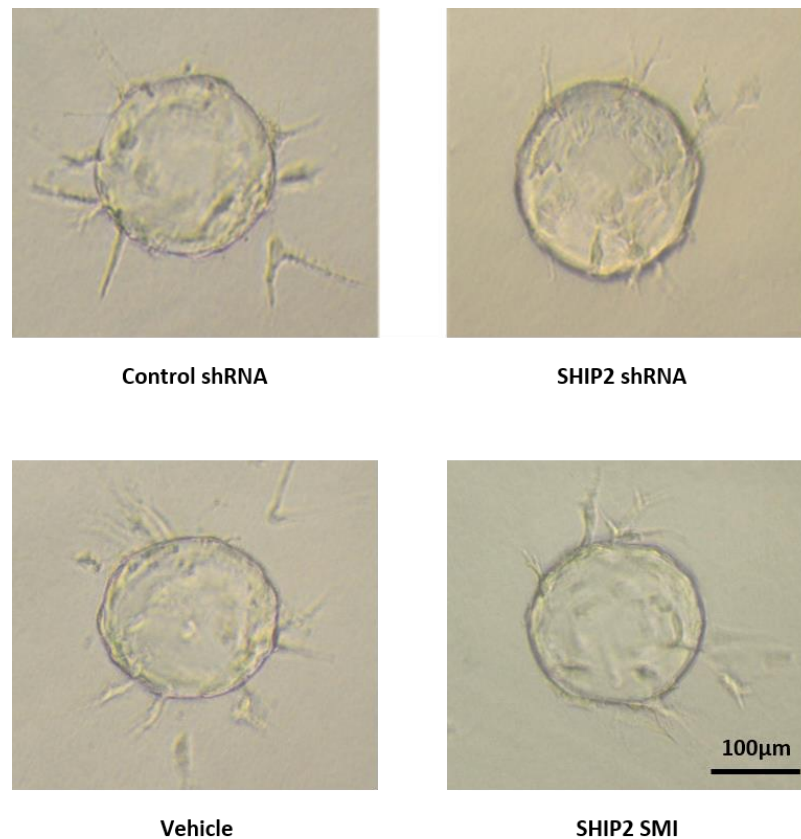
Figure 5-22 – Representative images of control beads (*left*) or those with SHIP2KD via shRNA (*top* right) or SMI (*bottom right*).

5.10 Cell morphology

Since the data presented above indicates that cell migration may contribute to impaired angiogenesis in the setting of SHIP2 knockdown, further experiments were planned to characterise cell motility. As outlined in the introduction, cell migration is a highly orchestrated process involving a well-defined process of cytoskeletal remodelling. The cytoskeleton therefore lends itself as a target to understand the molecular processes occurring during cell migration with greater clarity.

Sparsely seeded HUVECs were exposed to a pro-migratory stimulus of 50ng/ml human VEGF (or vehicle control) for 30 mins, and subsequently stained with phalloidin to

define filamentous actin. Direct visualisation with confocal microscopy enabled identification of individual cells for morphological assessment. In particular, measurements were obtained of total cell and lamellipodial area and perimeter in addition to a semi-quantitative assessment of lamellipodial distribution. Cells with SHIP2KD were nominally larger in area, and this was observed both with VEGF ($3110\mu m^2$ [+/- 445] vs $1900\mu m^2$ [+/- 186]; p=0.04) and without VEGF ($2524\mu m^2$ [+/- 404] vs $1774\mu m^2$ [+/- 195]; p=0.08). Nominally increased total cell perimeter was also noted in the context of SHIP2 shRNA, both with VEGF ($308\mu m$ [+/- 40] vs $270\mu m$ [+/- 17]; p=0.28) and without VEGF ($278\mu m$ [+/- 28] vs $238\mu m$ [+/- 24]; p=0.13). However, this did not approach statistical significance.

Total lamellipodial area was significantly greater in cells with SHIP2KD, both with VEGF ($197\mu m^2$ [+/- 20] vs $76\mu m^2$ [+/- 3]; p=0.03) and without VEGF ($107\mu m^2$ [+/- 10] vs $58\mu m^2$ [+/- 4]; p=0.04). The total perimeter of lamellipodia was also increased in the context of SHIP2KD, and again, this was preserved with VEGF ($123\mu m$ [+/- 17] vs $51\mu m$ [+/- 3]; p=0.04) and without VEGF (82 [+/- 3] vs 33 [+/- 7]; p=0.009). When lamellipodia were quantified as a proportion of cell area, no significant differences were detectable without VEGF (4.1% [+/- 0.4] vs 3.3% [+/- 0.2]; p=0.31). However, in the context of VEGF treatment, there appeared to be higher proportions though this enhancement did not reach statistical significance (5.6% [+/- 0.9] vs 4.0% [+/- 0.4]; p=0.32). When lamellipodia as a proportion of total cell perimeter was calculated, a similar statistically significant pattern was noted, both with VEGF (40.7% [+/- 5.6] vs 18.8% [+/- 1.9]; p=0.03) and without VEGF (30.0% [+/- 2.5] vs 13.6% [+/- 2.3]; p=0.01).
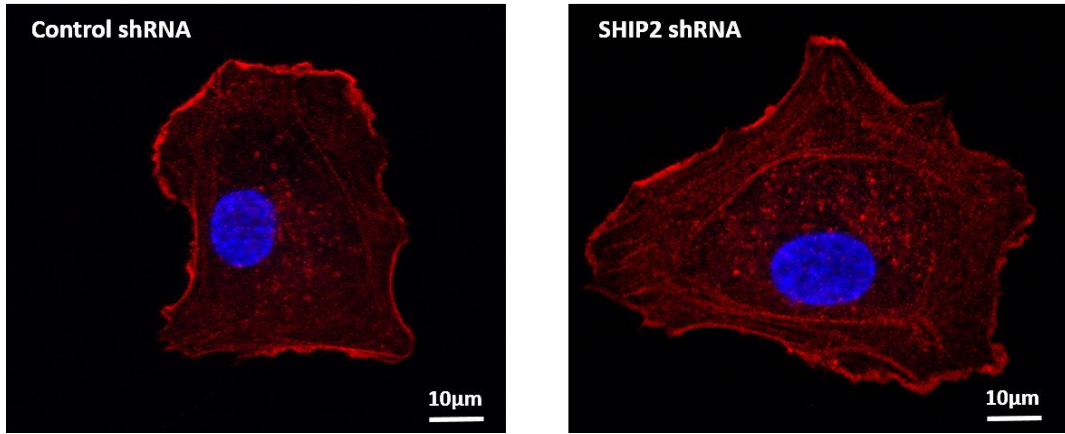
Figure 5-23 – Representative image of single HUVEC (80X magnification) with addition of control shRNA (*left*) or SHIP2-targeting shRNA (*right*).
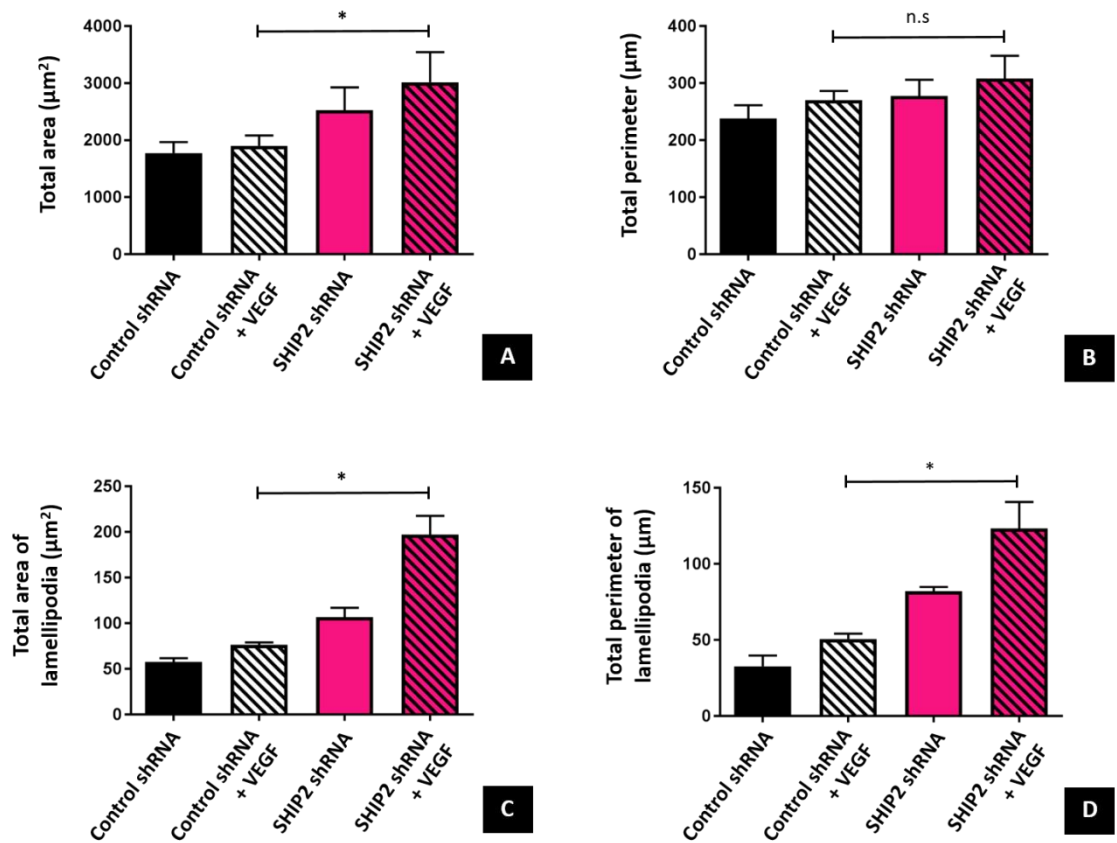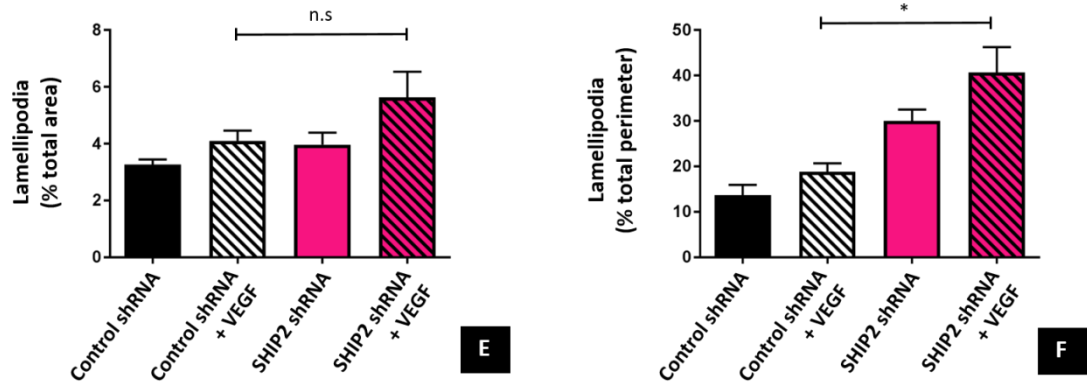
Figure 5-24 – HUVEC morphology of cells treated with control shRNA and SHIP2-targeting shRNA. Assessment made of total area **(Panel A)**, total perimeter **(Panel B)**, lamellipodia area **(Panel C)**, lamellipodia perimeter **(Panel D)**, and lamellipodia as % of total area **(Panel E)** and total perimeter **(Panel F)**. VEGF = vascular endothelial growth factor (n=3,3).

An increase in lamellipodial area is often used to infer increased migratory activity, which is at odds with the hypothesis that SHIPKD impairs cell migration. However, polarisation of lamellipodia is also an essential element of migration, and therefore, an increase in lamellipodial perimeter may suggest a failure of polarised migration. To explore this, a semi-quantitative measure of lamellipodial distribution was made by dividing the image of a single cell into quadrants. This enabled quantification of the area of lamellopodia in each, which could be expressed as a proportion of the total. All measurements were made in cells treated with VEGF. Control cells appeared to have a skewed distribution (Q1 32%, Q2 30%, Q3 18%, Q4 12%; p=0.46). In contrast, cells with SHIP2KD had a more homogenous distribution of lamellipodia (Q1 27%, Q2 23%, Q3 22%, Q4 21%; p=0.36), potentially indicative of a loss of cell polarity.
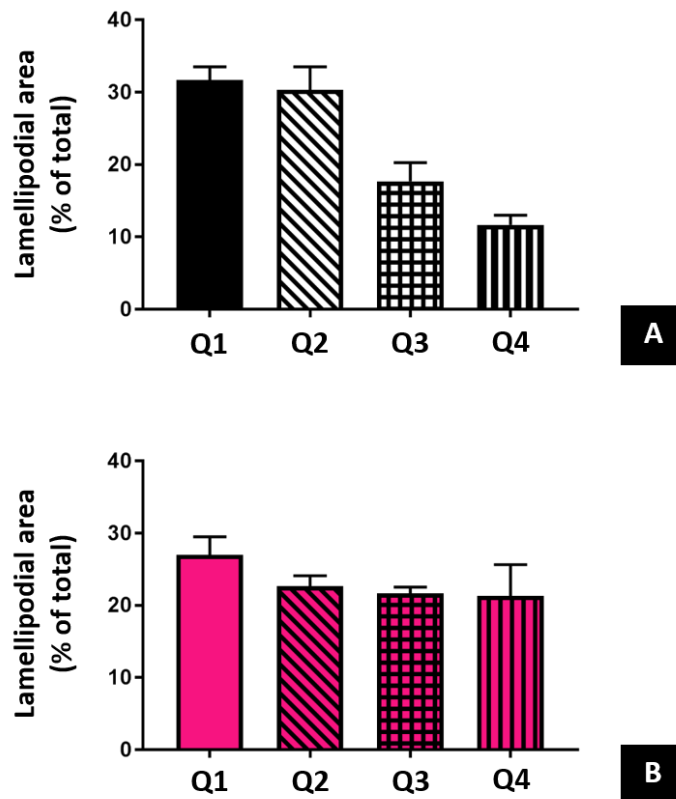
Figure 5-25 – Distribution of lamellipodial area in each quadrant in the context of HUVECs with control **(Panel A)** or SHIP2-targeting shRNA **(Panel B)** (n=3,3).

5.11 Cell polarisation

To define polarity in more detail, the scratch wound assay was used again. In order to close the wound, cells must polarise towards the wound before migrating forwards. The polarity of an individual cell can be easily defined by drawing a line from the nucleus to the Golgi apparatus, and the dynamic correlation between polarisation and directional cell migration has been confirmed in live imaging of transgenic zebrafish embryos [451]. Confluent HUVECs 30 minutes after a mechanical scratch were stained with anti-GM130 antibody (Golgi marker) and Hoescht (nuclear DNA stain) to determine cell polarity. Derived images were used to quantify the proportion of cells

that were forward facing towards the site of scratch (i.e. between -45° and +45° to a line perpendicular to the scratch).

Frequency histograms of raw data for individual cell polarity is shown, both in regions at the site of scratch and in control areas remote from the scratch (see Figure 5-26). Visual analysis of confluent regions of interest distant from the scratch did not reveal any apparent difference in polarity between control and SHIP2KD, both in the context of SHIP2 shRNA and SMI. However, there was apparent disparity at the site of scratch. As depicted in Figure 5-27, HUVECs expressing SHIP2-targeting shRNA had a lower proportion of forward facing cells (25% [+/- 3] vs 39% [+/- 4]; p=0.01). Importantly, no differences in scratch wound polarisation were observed in the context of SHIP2 SMI (34% [+/- 1] vs 35% [+/- 2]; p=0.50). This may imply a non-catalytic role of SHIP2 in cell polarisation.
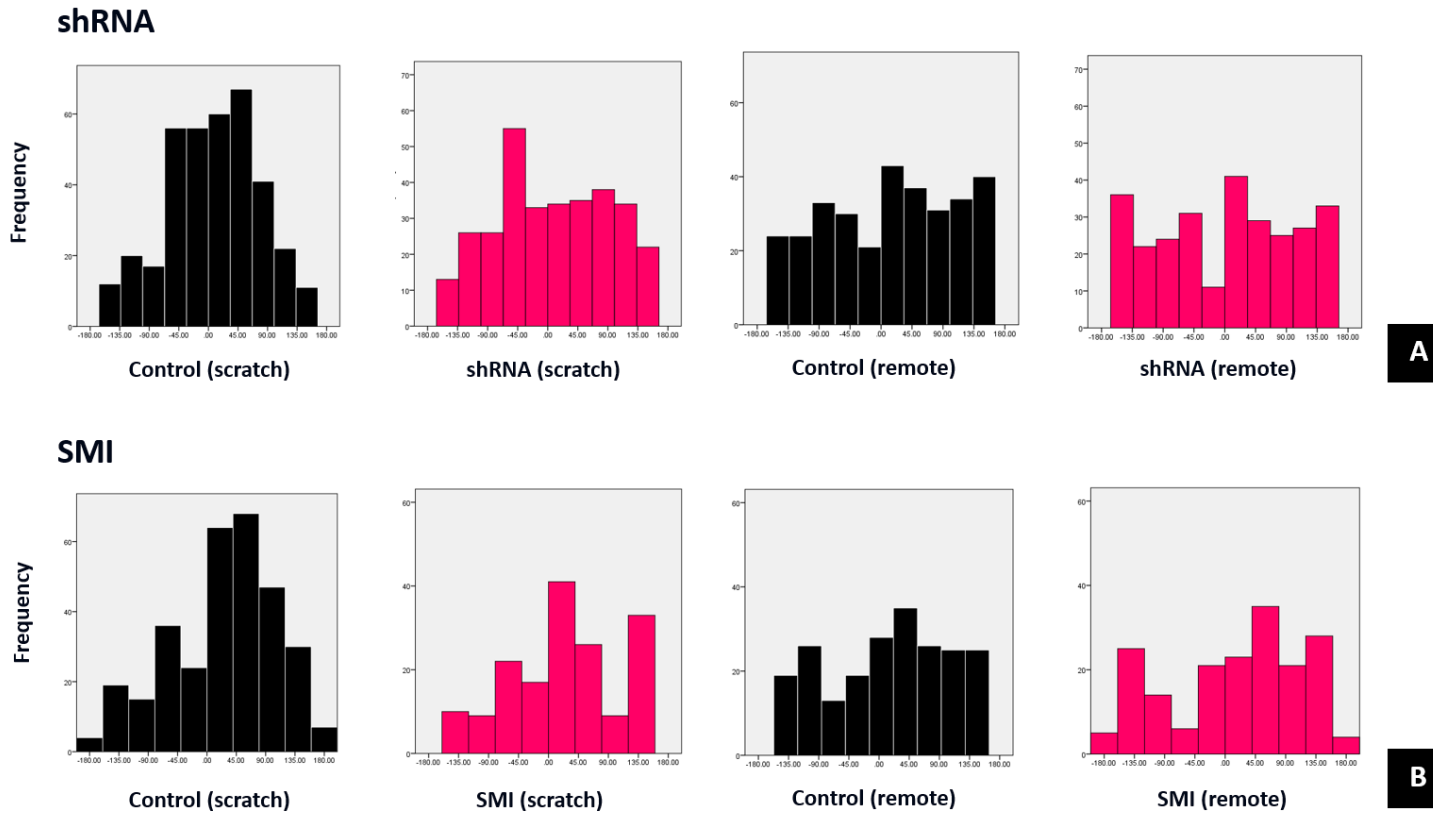
Figure 5-26 – Frequency histograms for individual cell polarity at the site of scratch and in remote areas. Data shown in context of shRNA **(Panel A)** and SMI **(Panel B)**. 'Control' denotes treatment with control shRNA or vehicle (n=4,4).
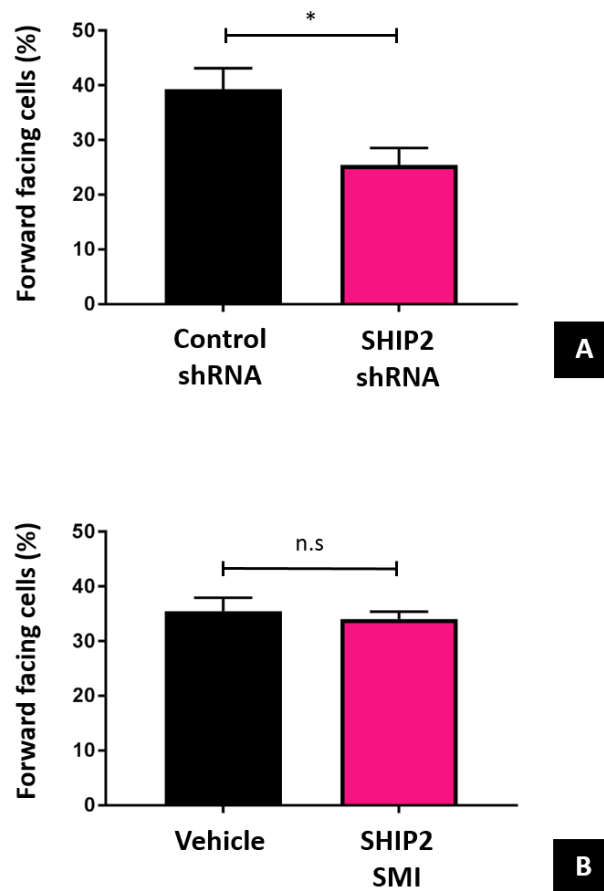
Figure 5-27 – Proportion of forward facing cells at site of scratch in context of SHIP2 shRNA **(Panel A)** or SMI **(Panel B)** (n=4,4).

5.12   SHIP2 localisation

To determine whether SHIP2 localised to the leading edge of cells shortly after scratch wound formation, plated cells were fixed and stained 30 minutes and 1 hour after wounding. Representative images are provided in Figure 5-28, with comparison of confluent cells and those at the site of scratch. In confluent cells, SHIP2 appears to be predominantly peri-nuclear, whilst expression appears increased at the plasma membrane in cells directly adjacent to the wound. It is tempting to speculate that

SHIP2 may be spatially orchestrated to interact with binding partners at the leading of cells and drive the cell to mobilise precisely and dynamically to external cues. However, high resolution immunofluorescence images proved insufficient to quantify this, and alternate methods shall therefore be required to adequately address this hypothesis.
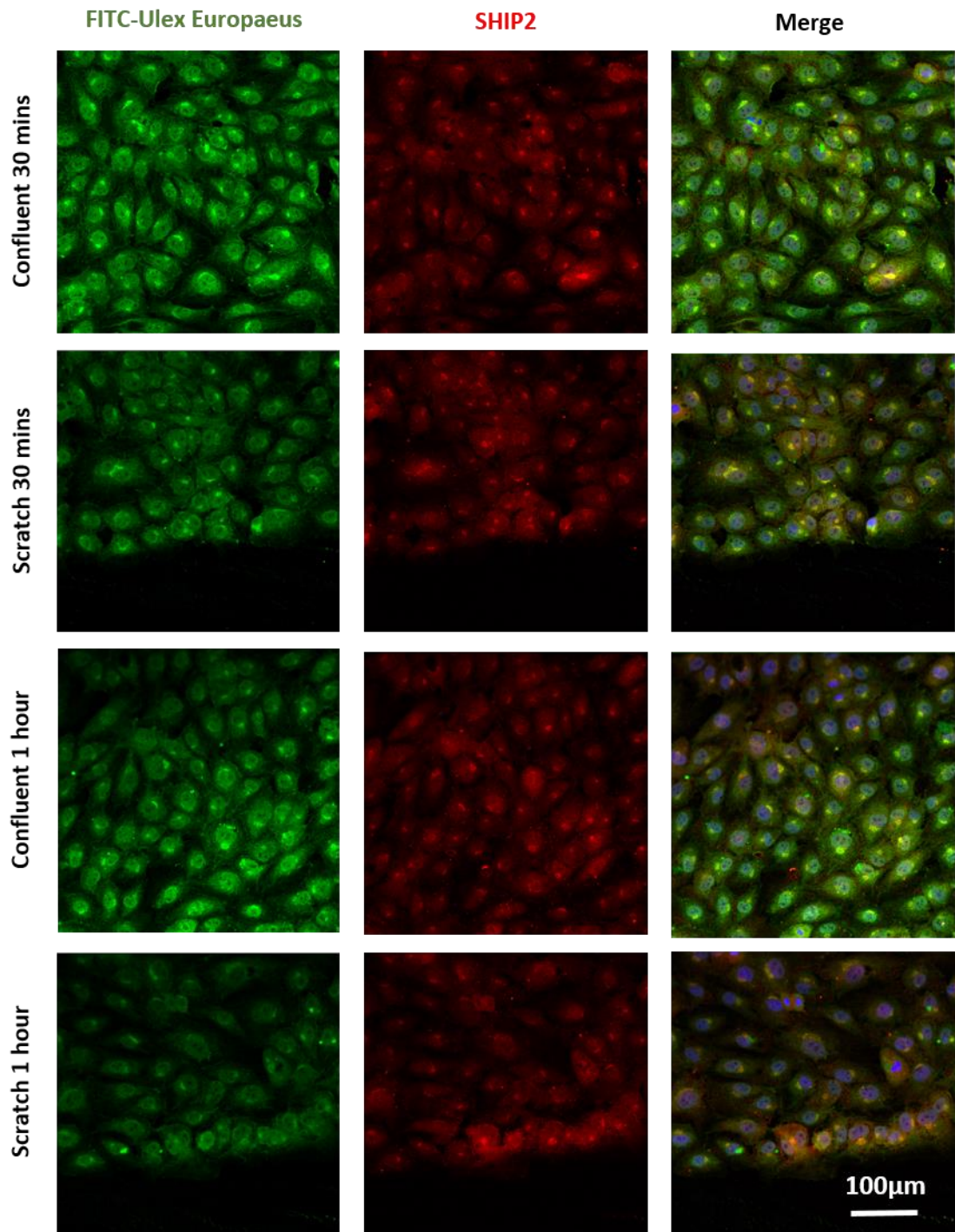
Figure 5-28 – Figure panel (20X magnification) depicting HUVECs stained for endothelium (*green*), SHIP2 (*red*) and nuclei (*blue*). A merged image is provided on the right of each horizontal plane.

FITC-Ulex Europaeus　　　　　**Hoescht**

SHIP2　　　　　**Merge**
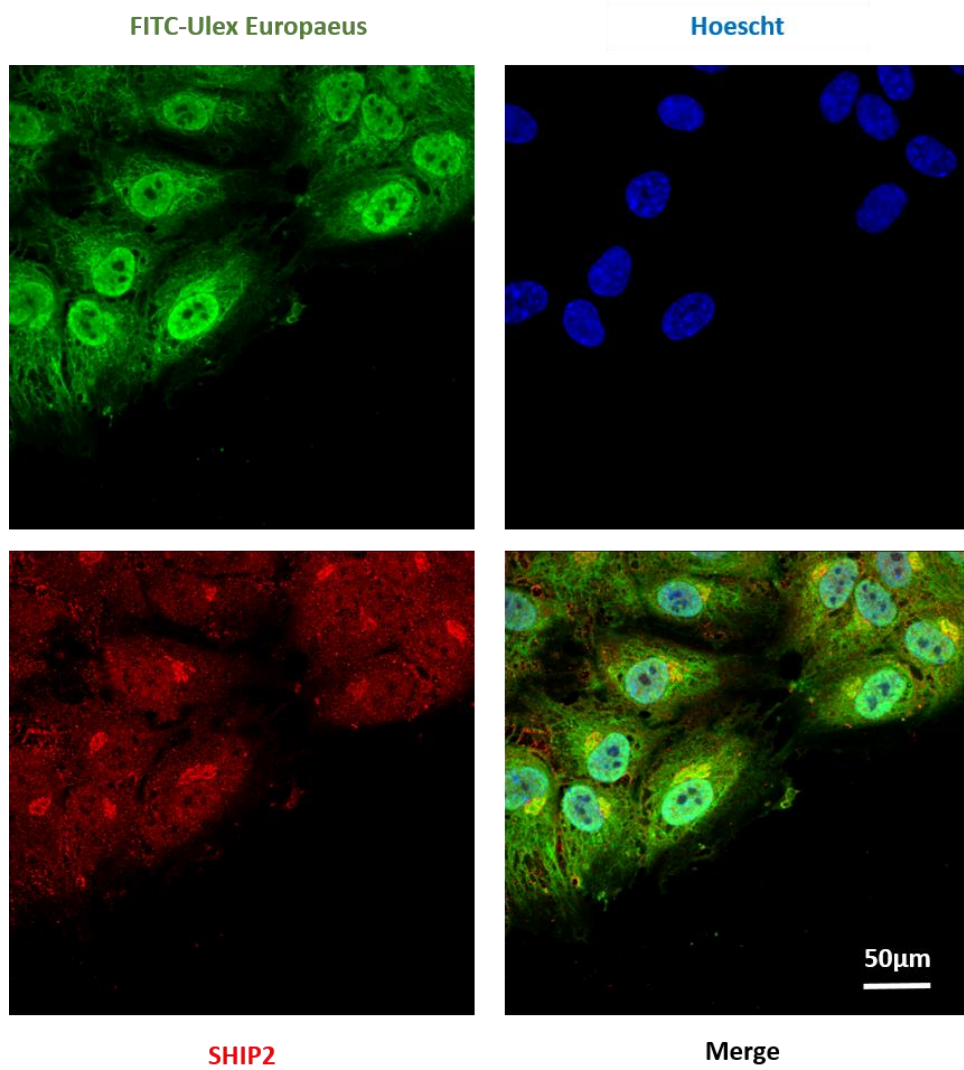
Figure 5-29 – Image of confluent HUVECs at site of scratch (63X magnification), with staining of endothelium (*green*), SHIP2 (*red*) and nuclei (*blue*).

Exploring in vivo metabolic and vascular function in mice with whole body inducible SHIP2 haploinsufficiency (SHIP2i$^{\Delta/+}$)

For the purposes of this subsection, 'WT' denotes control mice whilst 'SHIP2i$^{\Delta/+}$' refers to mice with systemic inducible SHIP2 catalytic domain haploinsufficiency.

5.13   SHIP2KD validation

Published literature suggests that global SHIP2 silencing may enhance insulin sensitivity and glucose tolerance [374], prompting hypotheses that SHIP2 inhibition may be a valuable strategy for patients with metabolic syndrome. However, data presented in the first section of this thesis (and also in a broader publication that includes this data [449]) suggests that endothelium-restricted SHIP2KD may have adverse effects. It is therefore important to consider the impact on metabolic and vascular function of whole body SHIP2KD. We sought to explore this by tamoxifen-inducible whole body deletion of the SHIP2 catalytic domain (SHIP2i$^{\Delta/+}$ mice), effectively mimicking the likely impact of a therapeutic agent.

Firstly, harvesting of liver, aorta, white adipose tissue (WAT) and skeletal muscle (quadriceps) was performed to confirm appropriate reduction in SHIP2 protein in diverse metabolic and vascular tissues. Total SHIP2 protein expression appeared to be reduced in all organs: liver (0.82 [+/- 0.10] vs 1.23 [+/- 0.64], p=0.56), aorta (2.04 [+/- 0.03] vs 3.24 [+/- 0.91]; p=0.24), WAT (6.63 [+/- 0.92] vs 20.73 [+/- 1.68]; p=0.001) and skeletal muscle (0.67 [+/- 0.09] vs 1.12 [+/- 0.04]; p=0.008), although efficiency of knockdown appeared to differ between tissues.
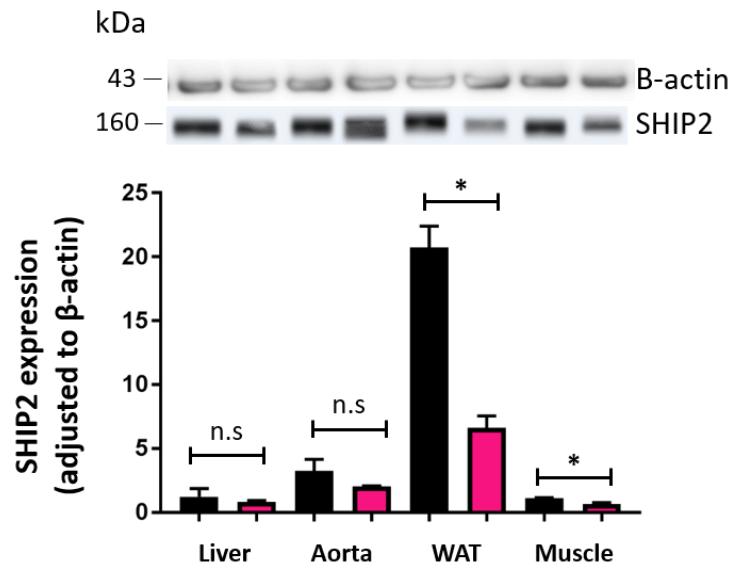
Figure 5-30 – SHIP2 protein expression in harvested organs, with values adjusted to β-actin. WAT = white adipose tissue (n=5,5).

5.14 Metabolic characterisation

5.14.1 Gross body weights

Total body weight was measured on a weekly basis from 1 to 3 months of age (i.e. pre- and post- tamoxifen induction). Growth was comparable throughout this period, with similar mean weight at 3 months of age between WT and SHIP2i$^{\Delta/+}$ mice (28.5 grams [+/- 0.7] vs 27.9 grams [+/- 0.4]; p=0.46).
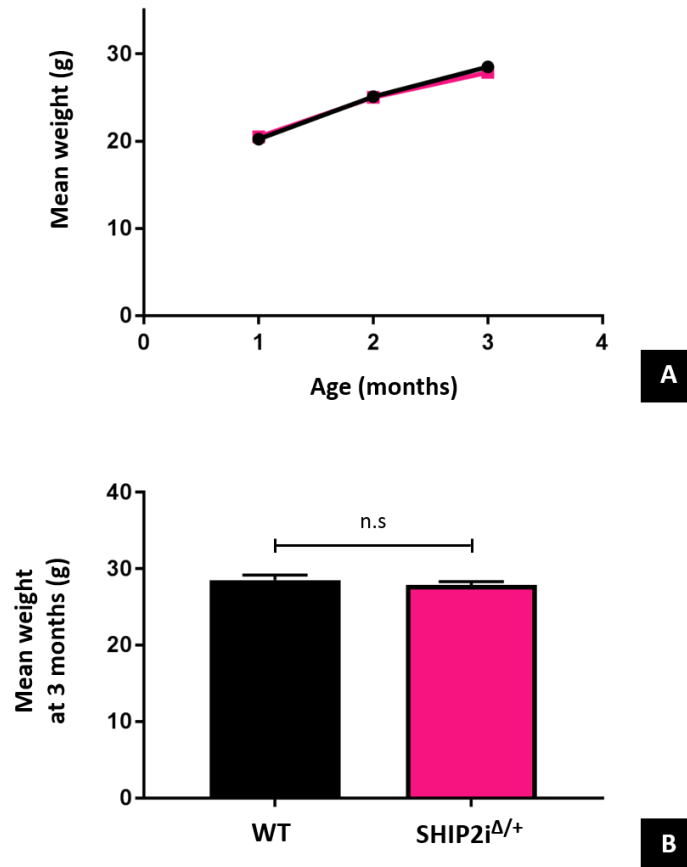
Figure 5-31 – Body weights for WT and SHIP2i$^{\Delta/+}$ mice with growth curves up to 3 months **(Panel A)** and mean body weight at 3 months of age **(Panel B)** (n=8,8).

There were no differences in body weights measured for 3 weeks post-tamoxifen induction. Mean weight at 3 weeks post-induction was comparable between WT and SHIP2i$^{\Delta/+}$ mice (31.3 grams [+/- 0.3] vs 31.7 grams [+/- 0.3]; p=0.36).
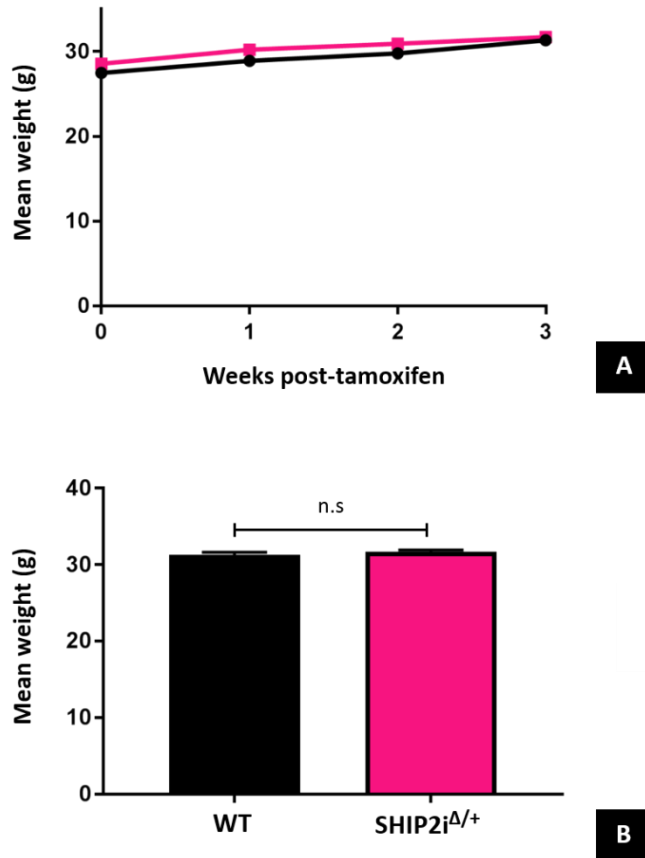
Figure 5-32 – Weekly body weights subsequent to tamoxifen induction **(Panel A)** and mean body weights at 3 weeks post-induction **(Panel B)** (n=8,8).

5.14.2 GTT and ITT

SHIP2 is a known regulator of the PI3K/AKT axis (demonstrated earlier in murine and human endothelial cells), and signalling via this axis mediates the effects of insulin on glucose metabolism. For this reason, formal assessment of whole body glucocompetence was made after tamoxifen-induced SHIP2KD. SHIP2i$^{\Delta/+}$ mice demonstrated significantly enhanced glucose tolerance and insulin sensitivity, as evidenced by GTT (AUC 852 [+/- 22] vs 1104 [+/- 90]; p=0.04) and ITT (AUC 768 [+/- 36] vs 950 [+/- 53]; p=0.02).
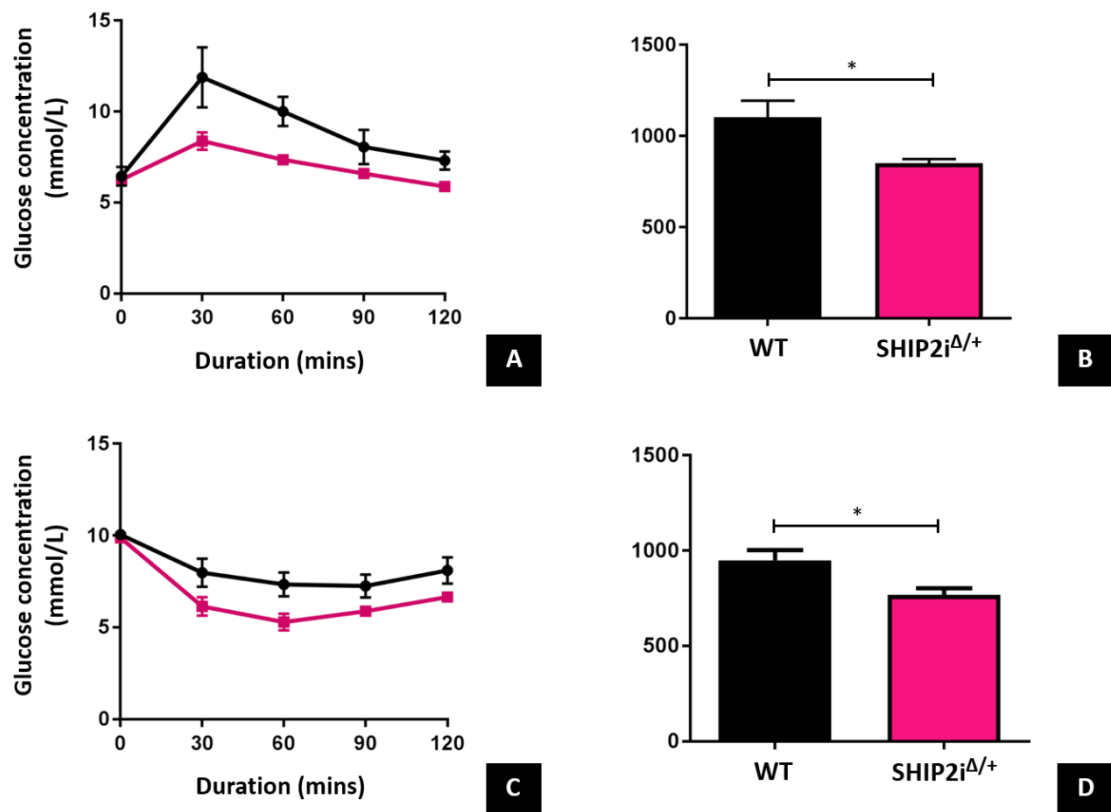
Figure 5-33 – Whole body glucocompetence assessment post-tamoxifen induction, with GTT **(Panel A)** and associated AUC **(Panel B)**, and ITT **(Panel C)** and associated AUC **(Panel D)** (n=5,5).

5.14.3 Fasting glucose and insulin

No differences in fasting plasma glucose concentration were observed between

SHIP2i$^{\Delta/+}$ and WT mice (4.9 mmol/L [+/- 0.4] vs 4.6 mmol/L [+/- 0.4]; p=0.60).

However, mice with SHIP2KD had lower fasting plasma insulin levels (0.36 ng/mL [+/-

0.01] vs 0.49 ng/mL [+/- 0.03]; p=0.003).
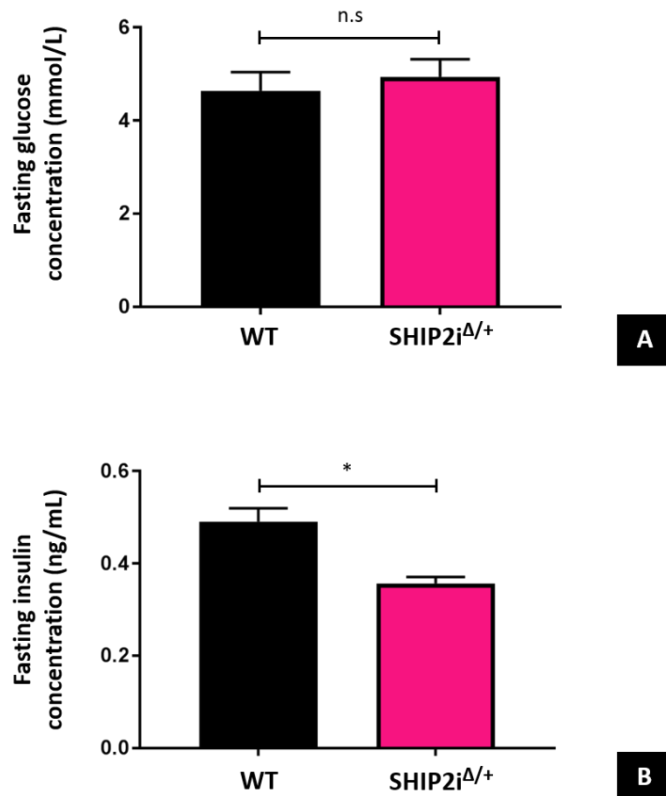
Figure 5-34 – Fasting glucose **(Panel A)** and fasting insulin concentrations **(Panel B)** (n=5,5).

5.14.4 HOMA-IR

Fasting plasma glucose and insulin concentrations were then used in the HOMA model to provide an approximation of systemic insulin resistance. Overall, HOMA-IR score was nominally lower in SHIP2i$^{\Delta/+}$ compared to WT mice (2.25 [+/- 0.15] vs 2.95 [+/- 0.39]; p=0.13). Both mean values were suggestive of preserved insulin sensitivity, being within the 'normal', non-insulin resistant range (< 3). Overall, these data support published work suggesting that SHIP2 loss of function is associated with augmented metabolic insulin sensitivity.
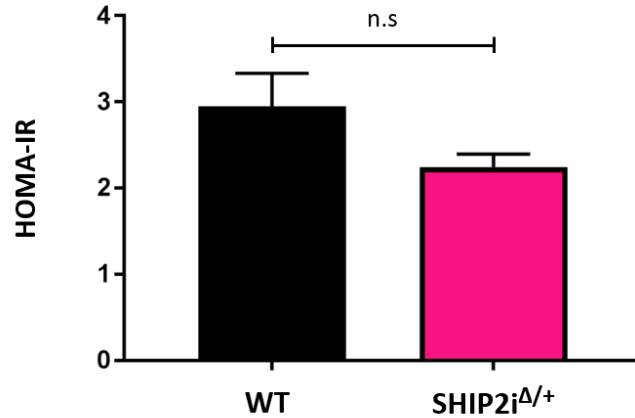
Figure 5-35 – HOMA-IR in WT and SHIP2i$^{\Delta/+}$ mice (n=5,5).

5.15 Angiogenesis after hindlimb ischaemia

As we observed significant defects in retinas from mice with SHIP2KD, we sought to characterise this further in SHIP2i$^{\Delta/+}$ mice using a model of hindlimb ischaemia which may be more translationally relevant. Isolectin B4 staining of skeletal muscle one week after induction of ischaemia was performed to assess the angiogenic phase of vascular regeneration. Vascular area as a percentage of total image area was surprisingly increased in the context of SHIP2KD post-ischaemia (16.9% [+/- 2.0] vs 9.9% [+/- 0.6]; p=0.01). No differences in the number of vessels per image width was observed (15 [+/- 1] vs 15 [+/- 1]; p=0.81).
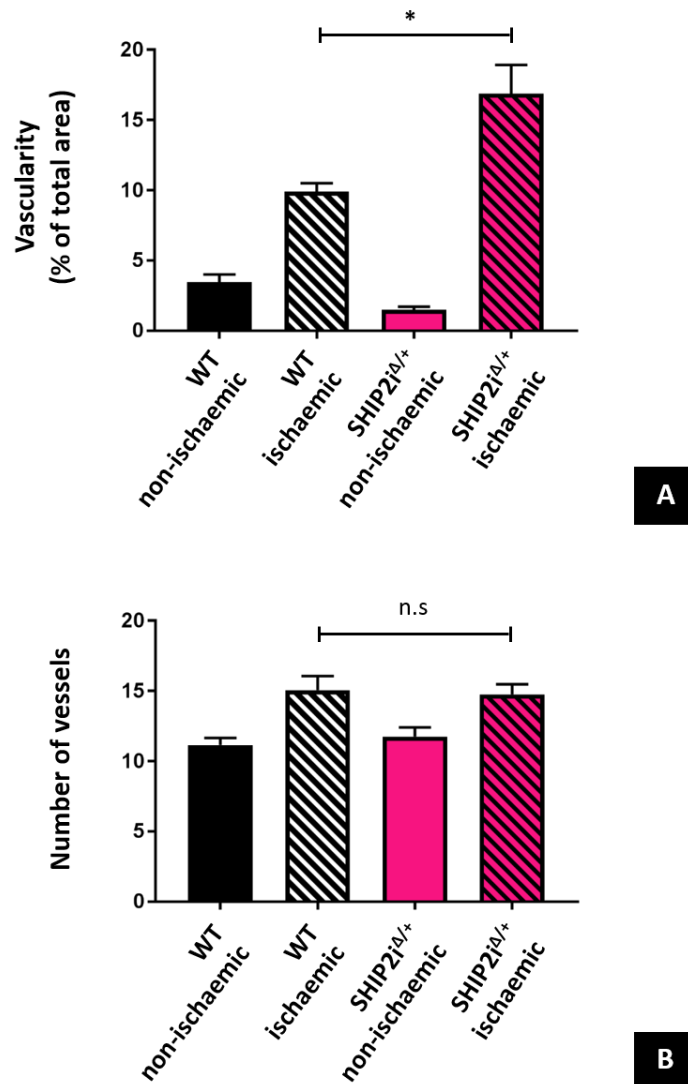
Figure 5-36 – Quantification of vascularity (as % of total area) **(Panel A)** and number of vessels (per image width) **(Panel B)** (n=5,6).

On visualisation, SHIP2KD neovessels post-ischaemia appeared structurally abnormal as depicted by the representative images in Figure 5-37. As increased total vascular area was found in the context of SHIP2KD but without a concurrent increase in vessel number, vessel thickness was determined in ischaemic muscle. In the context of SHIP2KD, thickness was broadly increased with a greater proportion being ≥ 5 pixels

(27.3% vs 20.0%; p<0.001). This is possibly suggestive of abnormal structure in newly

formed capillaries.
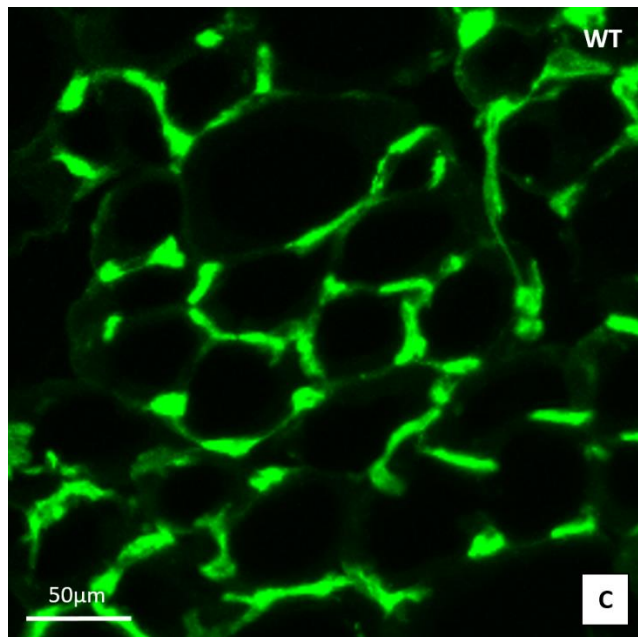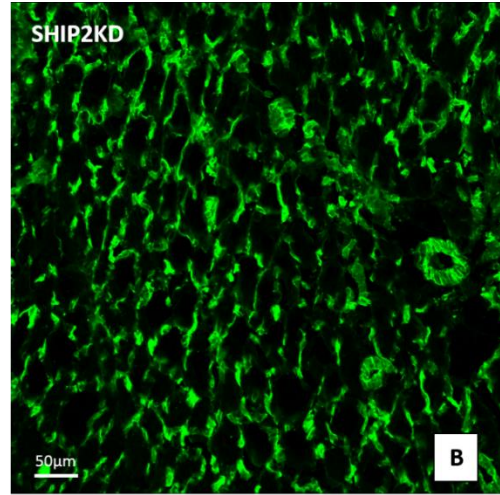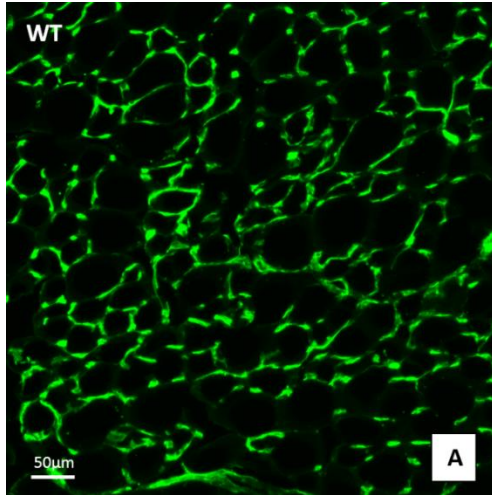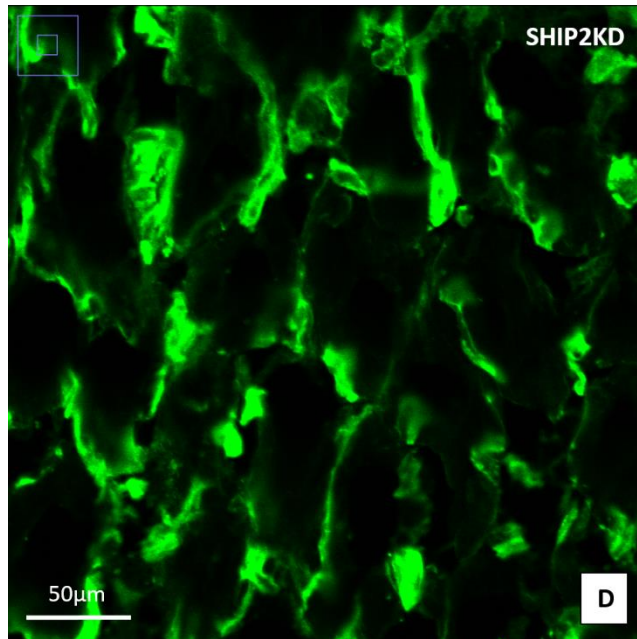
Figure 5-37 – Neovessel formation in ischaemic muscle, stained with isolectin B4 (*green*). Representative images of WT mice with whole **(Panel A)** and magnified segment **(Panel C)**, and SHIP2i$^{\Delta/+}$ mice with whole **(Panel B)** and magnified segment **(Panel D)** (n=5,6).
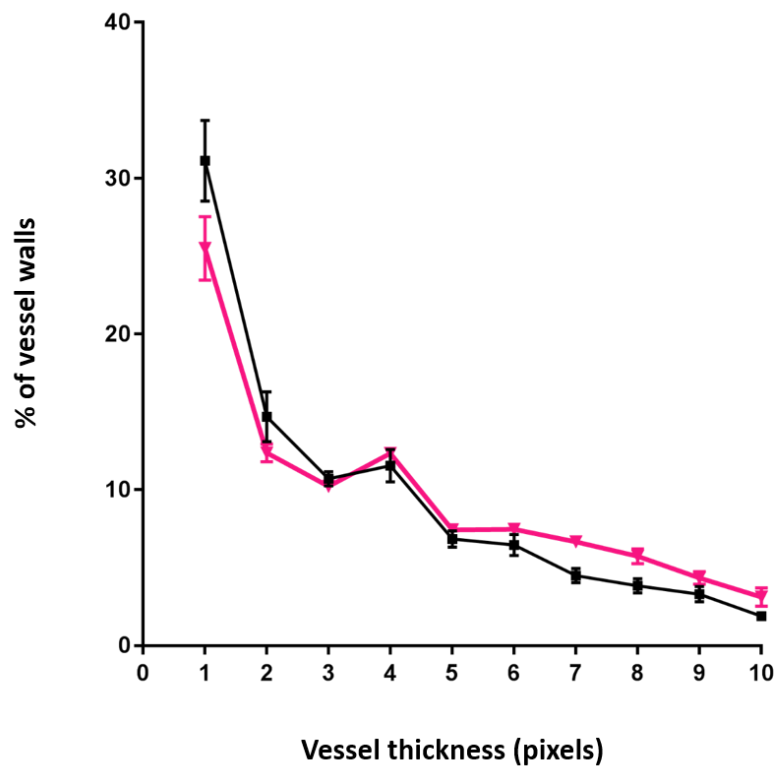
Figure 5-38 – Distribution of vessel thickness determined in ischaemic muscle of WT (*black*) and SHIP2i$^{\Delta/+}$ (*pink*) mice. Measurements were performed in terms of number of pixels (n=5,6).

5.16 Vascular repair after denuding injury

Metabolic insulin sensitivity was enhanced in SHIP2i$^{\Delta/+}$ mice, but endothelium-restricted SHIP2KD impeded vascular function and scratch wound closure. We therefore sought to define the net impact of global SHIP2KD on recovery from endothelial injury. The procedural work was conducted by Dr Nadira Yuldasheva using an established *in vivo* model of vascular injury. SHIP2i$^{\Delta/+}$ mice did not demonstrate any differences in re-endothelialisation compared to WT (56% [+/- 4] vs 56% [+/- 3]; p=0.97).
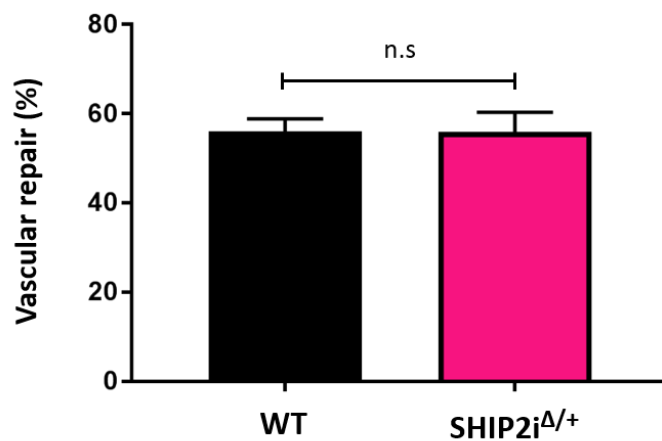
Figure 5-39 – Comparison of endothelial repair after vascular injury in WT and SHIP2i$^{\Delta/+}$ mice (n=9,10).

Chapter 6 – Discussion

_____

6.1 Summary of key findings

The broad aim of this project was to add to existing literature on the role of SHIP2 modulation on metabolic and vascular biology, with a view to informing decisions about the potential for clinical translation.

Studies were initially performed on mice with germline endothelium-specific SHIP2 catalytic domain haploinsufficiency (ECSHIP2$^{\Delta/+}$). These have impaired vascular formation in developing postnatal retinas, associated with increased endothelial PI3K/AKT signalling and Nox2-mediated vascular oxidative stress.

The relevance of these observations to human pathophysiology was explored in a complementary model using HUVECs, which were manipulated using SHIP2-targeting shRNA introduced with lentiviral vectors or a complimentary approach of pharmacological SHIP2 catalytic inhibition. Alterations in signalling intermediates and superoxide generation were recapitulated. This was broadly associated with defects in cell migration and polarisation, though no differences in proliferation were observed. Preliminary studies also suggested that SHIP2 expression may be increased in control cells at the leading edge of a fresh scratch wound.

The impact of whole body SHIP2 deletion was assessed by using mice with inducible knockdown of the SHIP2 catalytic domain (SHIP2i$^{\Delta/+}$), to ascertain the value of pursuing pharmacological SHIP2 antagonists as a therapeutic option. Metabolic characterisation of these mice confirmed enhanced whole body glucose disposal and insulin sensitivity, without differences in body weight. SHIP2i$^{\Delta/+}$ mice exhibited skeletal muscle hypervascularity and increased vessel thickness in the context of hindlimb

ischaemia, although no differences in re-endothelialisation after denuding arterial injury were apparent.

6.2 Effects of endothelium-specific SHIP2KD on angiogenesis

The retina has proved to be a powerful experimental system for vascular phenotypic analysis [436]. It has the inherent advantage of whole plexus visualisation in a uniform plane, and defines the diverse processes implicated in angiogenic blood vessel growth. Additionally, it incorporates intricacies such as blood flow and mural cell interactions that are not recapitulated by *in vitro* models such as those utilised in this project.

Assessment of retinas harvested from 5 day old pups has shown that endothelium-specific SHIP2KD impairs developmental angiogenesis. Of parameters measured, radial outgrowth is deemed to be the most sensitive correlate of post-natal vasculogenesis. Challenges in accurately defining the fifth postnatal day can result in significant relative inter-litter variation in age, which adds to variability in the age-dependent phenomenon of radial outgrowth. To circumvent this limitation, measurements of radial outgrowth were normalised to body weight and this confirmed significant reduction in radial outgrowth in the context of SHIP2KD. Moreover, vascularity and branching complexity was impaired in the less mature frontal regions of the retinas. Notably, there was also nominally reduced abundance of tip cells at the vascular front and significantly fewer filopodia normalised to the angiogenic front.

As highlighted in the introduction section, endothelial cells at the angiogenic front use tip cells and their emerging filopodia to migrate along the chemotactic gradient.

Defects in their abundance would therefore be consistent with impairment in vascular growth during primitive plexus formation. We pursued a harder fixation (2 hours at room temperature) to enable stronger isolectin B4 staining of precise features such as tip cells and filopodia. However, this meant that we were unable to immunostain retinas for proteins of interest, such as Golgi apparatus markers, and so further litters will be required to extend our observations.

To the author's best knowledge, our data is novel in assessing the impact of endothelium-restricted SHIP2 silencing on primitive vascular plexus formation. Interestingly, others have explored the role of PTEN in murine vascular development. As outlined previously, PTEN acts as a separate negative regulator of PI3K signalling by hydrolysing PIP3 at the 3-position to form PtdIns(4,5)P2, and is also a frequently mutated tumour suppressor [360]. Endothelium-specific germline PTEN knockdown in mice results in enhanced tumorigenesis driven by increased angiogenesis, which correlates with augmented migratory and proliferative capacity in vitro. Significantly, early neonatal mortality occurred in germline endothelial PTEN null mice due to cardiac failure and bleeding arising from insufficient morphogenesis of the myocardial wall and blood vessels [452]. Zebrafish embryos lacking functional PTEN also exhibit enhanced angiogenesis. This appeared to be driven by enhanced PI3K/AKT signalling as it could be suppressed by treatment with the PI3K inhibitor LY294002 [453]. Further mechanistic insights from the postnatal retina indicate that endothelial PTEN is a negative regulator of stalk cell proliferation via Notch/Dll4 signalling, with deletion resulting in endothelial hyperplasia, defective sprout lengthening and vascular plexus

patterning [454]. PTEN appears to exhibit dual function in contributing to this observed phenotype, with both phosphatase-dependent and -independent activity.

It is apparent from the conflicting data presented above that angiogenesis is a complex and tightly regulated phenomenon which is likely to exhibit variability depending on factors such as vascular bed, angiogenic programme (e.g. developmental versus pathological) and PI3K manipulating stimuli. Genetic manipulation in the ECSHIP2$^{\Delta/+}$ colony was specifically targeted at the catalytic domain, and so may have preserved non-catalytic activities such as protein-protein interactions. My work solely characterised vascular morphology using endothelial staining, without formal assessment of cell proliferation, cell polarity or vessel regression. Moreover, it remains unclear whether observed defects are a result of aberrant SHIP2 signalling in endothelial cells or also arising from secondary alterations in the pro-angiogenic milieu (e.g. VEGF expression) influenced by broader perturbations in vascular network formation.

6.3 Effects of SHIP2KD on human endothelial cell biology

HUVECs provide a useful experimental analogue of adult human endothelial cells and can therefore provide complimentary support for the relevance of findings *in vivo* to human pathophysiology. Moreover, they are relatively cost-effective, readily available and behave predictably in defined tissue culture conditions. For these reasons, we performed functional *in vitro* assays on HUVECs to extend the observations made in murine models.

6.3.1   Cell migration and proliferation

SHIP2KD with shRNA and pharmacological inhibition of SHIP2 both impaired
endothelial scratch wound closure. This simple assay crudely mimics the migration
and proliferation of cells that are induced during vascular remodelling *in vivo*. In
particular, it incorporates haptotaxis and mechanotaxis via cell-ECM and cell-cell
interactions. However, it does not involve a chemotactic gradient. For this reason,
Boyden chamber assays were also performed to define migration directed towards a
VEGF stimulus, and a similar reduction in net migration was found.

Scratch wound closure and angiogenesis also involve cellular proliferation, and this
was formally explored by quantifying EdU incorporation. No differences were induced
by SHIP2 shRNA or SMI. However, this data must be appraised with a degree of
caution as the 4 hour incubation with EdU was not performed in serum-free media so
may mask a proliferation advantage of diminished SHIP2 activity. Scrutiny of the raw
data also confirmed presence of significant inter-experiment variability, which may
relate to factors such as baseline confluence and cell passage even though efforts
were made to ensure consistency between experiments. A complimentary approach
may therefore be to quantify population doubling time before commencing this assay
to ascertain whether there is agreement.

The aforementioned assays only incorporate specific elements of angiogenesis, which
is a complex, multi-step process. The more sophisticated 3D fibrin gel bead sprouting
assay recapitulates many of the crucial early stages of angiogenesis, including lumen
formation and vessel branching, and hence more closely models the *in vivo* process.
SHIP2KD via shRNA and pharmacological inhibition resulted in a reduced number of

sprouts per bead, but without associated changes in sprout length. The disparity between sprout abundance and length is not entirely surprising as initial sprouting relies primarily upon cell motility in response to directional cues whereas the latter is more proliferation-dependent, supporting data produced by the EdU incorporation assay. Findings could be extended by repeating the assay with use of fibroblasts, layered on top of the gel, to provide additional soluble factors that promote vascular network formation. This is reported in the original protocol [450], but was deemed undesirable in this project as the pro-angiogenic environment is less controlled. Moreover, interpretation of SMI data would be challenging due to effects on fibroblast function.

As outlined in the introduction, most of the published data on the role of SHIP2 in endothelial function *per se* has been reported in the context of *in vitro* lymphangiogenesis. A recent study has presented comparable findings, with SHIP2KD using siRNA and SMI resulting in impaired cell migration as assessed via scratch wound and Boyden chamber assays [394]. In addition, cell proliferation was impaired when evaluated using a tetrazolium salt colorimetric assay (MTS) although this is a more indirect marker of proliferation than EdU incorporation. Matrigel tubulogenesis, cell adhesion and survival were also reduced. Notably, over-expression of wild-type SHIP2 did have some opposing effects but only discernible in the context of cell migration and adhesion. Most recently, SHIP2 expression has been manipulated in colorectal cancer lines. Reduced expression via lentiviral shRNA transduction has been shown to impair cell migration, albeit with preserved cell adhesion and proliferative capacity [455].

6.3.2   Cell morphology and polarity

The process of cell migration is highly orchestrated and involves a well-defined sequence of cytoskeletal remodelling. To characterise this further, morphological assessment of cell dimensions was made. In addition, phalloidin was used as a tool to investigate the abundance and distribution of filamentous actin within individual HUVECs and, more specifically, for assessment of lamellipodia. In contrast with antibodies, phalloidin is much smaller and can therefore more densely label cellular proteins for fluorescent microscopy to enhance image resolution.

Cells expressing SHIP2-targeting shRNA and exposed to VEGF were larger, as determined by total area and perimeter. Abundance of lamellipodia was also greater, but distribution was more homogenous. As a technique, phalloidin staining does have the inherent limitation that its binding inhibits actin dynamics and function meaning that only fixed cells can be assessed. Live cell imaging using compatible probes, such as LifeAct, is therefore better placed for further exploratory studies. Nonetheless, our analysis does generate interesting discussion. An increase in lamellipodial area is often used to infer increased migratory capacity, which may seemingly contradict our results. However, polarisation is also an essential element and the more homogenous distribution in the context of SHIP2KD is possibly suggestive of a loss of cell polarity. Notably, this experiment was performed using sparsely seeded cells exposed to VEGF as a chemotactic stimulus, but it would be interesting to assess whether findings were recapitulated in the context of a scratch wound or angiogenic sprouting, for instance. However, interpretation of actin staining is much more complex in those settings.

As alluded to, it was important to define polarity more directly in view of the defects observed thus far. This was achieved by staining the Golgi apparatus and assessing its position relative to the nucleus. In the context of a mechanical scratch, cells expressing SHIP2-targeting shRNA had a lower proportion of cells polarised towards the wound. This disparity was not observed in confluent areas remote from the site of the wound, where a more uniform distribution of polarisation was observed as expected. Notably, no such trends were observed in the context of SHIP2 SMI. Use of a SMI involves competitive inhibition of the catalytic domain, whilst lentiviral manipulation results in reduced expression of the entire protein. Hence, these findings infer that cell polarity may be primarily mediated by a non-catalytic role of SHIP2, for instance, via intrinsic docking sites mediating protein-protein interactions [351].

6.3.3 SHIP2 localisation

Spatial orchestration of SHIP2 has been shown in multiple cell types, including human astrocytomas, COS-7 cells, HeLa cells and gliomas. We sought to assess this formally in the context of scratch wound formation using antibody-labelled SHIP2. Images were obtained 30 mins and 1 hour post-scratch. Whilst confluent cells in remote regions showed SHIP2 to be predominantly peri-nuclear, localisation appeared more concentrated at the plasma membrane in regions directly adjacent to the wound. The primary limitation of this approach relates to resolution and signal when attempting to quantify membrane localisation, as reflected by representative images in the panel in Figure 5-28.

Nonetheless, the notion of localised accumulation at the leading edge of migrating cells is potentially of relevance. PIP3 has been shown to amass at the leading edge of migrating cells, i.e. at the sites of actin polymerisation, cross-linkage and lamellipodial formation [105]. LL5β also appears to be recruited to this submembranous region by PIP3, enabled by its PH domain [396]. This has been shown to mediate the binding of filamin, which has affinity for SHIP2, and can also facilitate its translocation from the cytosol to the cell membrane [367]. Notably, staining in our experiments was only performed in non-manipulated HUVECs and it would therefore be prudent to explore this further in the context of SHIP2KD to see if there are any disparities. The use of fluorescent phosphoinositide biosensors, linking fluorescent proteins to PH domains specific to PIP3 or PtdIns(3,4)P2, may prove valuable to define this in future live cell imaging experiments. However, this technique is challenged by the requirement for GFP-tagging which would compromise its use in HUVECs treated with control GFP-targeting shRNA. A potential alternative method for consideration is fluorescence recovery after photobleaching (FRAP), a useful technique in biological studies to determine the kinetics of diffusion through tissues and individual cells [456]. However, this also relies on use of GFP fusion proteins.

6.4 Effects of temporal SHIP2KD on whole body biology

6.4.1 Metabolic function

There is the suggestion in published literature that SHIP2 silencing may improve insulin sensitivity and glucose tolerance [374]. This prompts the hypothesis that SHIP2KD may have beneficial effects in those with metabolic syndrome. However,

long-term endothelium-restricted SHIP2KD appears to be broadly detrimental to vascular function and systemic insulin sensitivity [449]. We therefore explored the impact of whole body SHIP2KD on metabolic and vascular biology, using inducible inhibition (SHIP2i$^{\Delta/+}$ mice) to mimic the potential short-term role of a therapeutic pharmacological agent.

In direct contrast with germline SHIP2 catalytic domain haploinsufficiency [377], the inducible transgene allowed us to avoid confounding developmental abnormalities. The tamoxifen induction regime was well tolerated, and no differences in body weight occurred in the following 3 weeks. However, whole body glucocompetence was enhanced in the context of SHIP2KD, as evidenced by GTT and ITT, along with lower fasting plasma insulin levels and HOMA-IR scores. This data is broadly consistent with published work suggesting that SHIP2 is a negative regulator of metabolic insulin sensitivity.

Of note, metabolic profiling was conducted 1 week after completion of the tamoxifen induction regime. It is therefore unclear whether prolonged SHIP2 silencing would have different effects. Our own laboratory has explored the impact of longer-term suppression of endothelial SHIP2 activity by using 10 month old ECSHIP2$^{\Delta/+}$ mice [449]. Compared with control, ECSHIP2$^{\Delta/+}$ mice had impaired glucose normalisation during GTT, higher fasting glucose concentrations and higher HOMA-IR scores. Hyperinsulinaemic-euglycaemic clamp studies suggested insulin resistance, with an approximate 25% reduction in glucose concentrations required to maintain euglycaemia. Moreover, glucose uptake into peripheral organs, namely adipose tissue and skeletal muscle, was reduced. No differences were observed in fasting insulin

concentrations, ITT, levels of serum FFAs and triglycerides and hepatic glucose output. Hence, long-term whole body genetic (or pharmacological) reduction in SHIP2 activity may conceivably have adverse effects on systemic glucose metabolism, in contrast with the short-term effects observed.

6.4.2   Vascular regeneration

6.4.2.1   Angiogenesis after hindlimb ischaemia

As significant defects were observed in developmental retinal angiogenesis in the context of endothelium-specific SHIP2KD, we sought to define the impact of whole-body inducible knockdown. This was achieved by assessment of 'pathological angiogenesis' in skeletal muscle one week after induction of hindlimb ischaemia. These results somewhat contradicted the retinal data, with increased vascular area in SHIP2KD when defined by total area although this was driven by increased vessel diameter rather than number. It is difficult to dissect the relative contribution of SHIP2 manipulation *per se* to the differing phenotypes observed with endothelium-specific and whole body knockdown, as the duration and cell lineage of knockdown differed along with angiogenic stimulus and vascular bed studied. In addition, isolectin B4 is not entirely specific for endothelial cells as it is also weakly positive for macrophages which can themselves modulate angiogenesis. The thresholding approach applied during data analysis allows such weak staining to be ignored, but nonetheless, it would be useful to quantify recruitment of these cells. We did attempt to separately stain for macrophages using anti-CD45 antibody and a more selective anti-F4/80 antibody, but technical problems meant that these data are not yet available.

Interestingly, the diameter of neovessels was also increased in the context of SHIP2KD. There is abundant data to support the notion that neovessel quality, in addition to quantity, is important to achieve adequate perfusion of ischaemic tissues [428]. Indeed, excessive but disordered vasculature is implicated in pathophysiological states including diabetic retinopathy and cancer [76]. It would therefore be relevant to assess vessel coverage with pericytes and VSMCs in future studies. Staining for VE-cadherin could also be performed, which is an endothelium-specific intercellular adhesion molecule and deemed important for regulation of vascular permeability and leukocyte extravasation [457]. FITC-dextran extravasation could be assessed using fluorescent microscopy as a surrogate for vascular permeability. It is also not apparent whether the increased vascularity in the context of SHIP2KD is the consequence of a persistently hypoxic milieu and/or heightened oxidative stress. It may therefore be relevant to explore these processes histologically.

6.4.2.2   Vascular repair after injury

To explore effects of temporal whole body SHIP2 manipulation further, we assessed recovery after endothelial denudation in the femoral artery. No differences in recovery were present between WT and SHIP2KD mice. Although these findings may seem unexpected, it must be borne in mind that the inflammatory response with recruitment of bone marrow-derived cells, particularly leukocytes, is critical in mediating vascular repair via predominantly paracrine mechanisms. This has not been explored in this project, but future experiments could explore leukocyte abundance in bone marrow and peripheral blood in addition to expression of inflammatory

cytokines, such as IL-6 and TNF-α, in the repairing arterial wall. Direct anti-F4/80 staining of denuded endothelium could also be performed to assess recruitment and mobilisation of macrophages to the site of injury.

6.5 Effects of SHIP2KD on cell signalling

6.5.1 PI3K/AKT axis

As PI3K/AKT signalling is regulated by SHIP2 and has a pivotal role in metabolic and vascular biology, we used HUVEC lysates to assess basal activation of these signalling nodes. SHIP2KD resulted in increased activatory phosphorylation of AKT, eNOS and ERK protein. In some ways, these results may appear paradoxical as such increases in signalling have previously been shown to induce a portfolio of cellular processes including migration, proliferation and angiogenesis [458]. However, this data is consistent with published data in our own laboratory from work with ECSHIP2$^{\Delta/+}$ mice [449]. PECs derived from 10 month old mice had increased basal expression of pAKT, peNOS, pPDK1 and pRICTOR. However, insulin- and shear-stimulated induction of peNOS was impaired. This is suggestive of increased basal signalling but a failure to augment this appropriately in response to diverse physiological stimuli. Of note, the effects of SHIP2 inactivation on proximal insulin signalling, such as insulin receptor and IRS1/2 expression and phosphorylation, was not explored in this project. However, no differences were observed in ECSHIP2$^{\Delta/+}$ mice-derived PECs [449].

There is reasonably convincing data to support the suggestion that chronic activation of the PI3K/AKT axis can be detrimental to cellular physiology. In mice with induced cardiac Akt1 activation, there is evidence of adaptive cardiac hypertrophy in the initial

phase but sequentially resulting in impaired angiogenesis and pathological cardiomyopathy [459]. In mice rendered obese with a high-fat diet, chronic AKT activation increased vascular senescence and susceptibility to ischaemic injury [460]. Sustained signalling during vascular development has also been shown to disrupt normal vessel hierarchy and patterning and result in vascular malformations [461].

6.5.2   Oxidative stress

Data derived both from PECs and HUVECs has consistently shown that SHIP2KD is associated with increased superoxide abundance, produced in a Nox2 and PI3K/AKT-dependent manner. Quantification was reliant on the DHE fluorescence assay, which is primarily limited by the fact that DHE oxidation yields at least two products which have differing specificity for superoxide. Nonetheless, our laboratory has also formally assessed superoxide abundance in ECSHIP2$^{\Delta/+}$ PECs via lucigenin-enhanced chemiluminescence and results were complementary [449]. If greater precision was sought, high performance liquid chromatography (HPLC) could be considered to derive the fluorescent product of interest. Nonetheless, the complete normalisation of DHE fluorescence by gp91ds-tat strongly supports the argument that superoxide abundance is genuinely increased.

Others have shown an association between enhanced AKT signalling and oxidative stress [462]. This correlated with increased abundance of the scavenger receptor CD36, which may trigger a detrimental positive feedback loop. Murine research in redox signalling has also highlighted a critical role of oxidant free radicals in the processes of angiogenesis and vascular repair. In the physiological setting, these

appear essential. Re-endothelialisation of injured carotid arteries is enhanced by hypoxia-induced mobilisation of EPCs but this benefit is suppressed in the context of Nox2 inhibition [324]. Vascular regeneration after hindlimb ischaemia is also impaired in mice with Nox2 deletion, and correlates with reduced superoxide abundance [463]. However, effects appear to be more conflicting in the context of pathological states such as DM. In mice with type 1 DM, for instance, inhibition of Nox2-derived ROS overproduction has been shown to improve neovascularisation after hindlimb ischaemia [464]. This has been corroborated by a more recent study where the pathological insult was exposure to cigarette smoke [465].

This intricacy and underlying complexity of oxidative signalling is best considered by the 'redox window' hypothesis, where perturbations have differing effects depending on the setting. It also underscores the effects of unrestrained signalling at multiple nodes in ubiquitous signalling cascades, which are likely to have detrimental effects on vascular function. It would be particularly valuable to assess if Nox2 (and PI3K/AKT) inhibition could rescue the defects in angiogenesis, migration and polarisation observed in SHIP2KD cells.

The potential effects of oxidative stress on actin cytoskeletal remodelling are poorly understood, but oxidative modification is known to be important during normal physiological actin remodelling [466]. However, LDL cholesterol-induced production of ROS results in cytoskeletal disruption and inhibits endothelial cell migration *in vitro* [467]. This appears to be primarily through a superoxide-dependent mechanism, though generation of peroxynitrite has also been reported to directly inhibit actin polymerisation [468]. Accordingly, the observation in our project that SHIP2KD in

HUVECs results in larger cells with more abundant yet homogenous lamellipodia may relate to heightened signalling via the PI3K/AKT axis but with a concurrent increase in oxidative stress. Although the actin cytoskeleton has been traditionally visualised with chemical tools such as fluorescently-labelled phalloidin, they have limited application in living cells. Further exploration using techniques with live cell-compatible probes may therefore be particularly instructive in the temporo-spatial study of actin dynamics [469].

6.6   Project limitations

6.6.1   Use of murine models

In vivo work in this project relied on use of ECSHIP2$^{\Delta/+}$ and SHIP2i$^{\Delta/+}$ mice that had been genetically modified. Although these models aimed to evaluate SHIP2 manipulation in the context of germline endothelium-restricted or inducible global knockdown, respectively, they cannot fully mimic the nuances that exist in human patho(physiology) for which there is no direct corollary. The effects of compensatory mechanisms that may arise secondary to gene knockdown, such as via PTEN or SKIP, cannot be neglected although temporal inhibition and deletion of only one allele should circumvent the risk of genetic redundance traditionally associated with murine knockout models [470]. This project was also subject to inherent limitations associated with murine work, such as unpredictable drifting of the ECSHIP2$^{\Delta/+}$ colony, that caused unavoidable experimental delays.

The models of vascular disease adopted for experimentation purposes are approximations, but cannot fully represent clinical disorders. For instance, the

hindlimb ischaemia model is performed via an acute interruption of blood flow, whilst in humans, peripheral vascular disease has a more indolent and chronic progression which enables collateral vessel formation. Moreover, many strains of mice are far more tolerant of limb ischaemia than humans due to greater collateral vessel abundance [471]. Similarly, femoral artery denudation was used as a mimic of endothelial injury arising from atherogenesis or stent deployment. However, this approach is unlikely to reflect the diverse, non-homogenous distribution of insults that arise in human vasculature and are influenced by shear stress and presence of branch points, for instance. Moreover, no formal assessment of long-term recovery was obtainable.

This project analysed endothelial cells derived from macrovascular, microvascular and venous circulations. One could legitimately argue that these systems are exposed to differing haemodynamic pressures and are therefore likely to express cellular and molecular heterogeneity that may influence observed phenotypes [472]. Nonetheless, a pragmatic approach was adopted based on our laboratory's familiarity with protocols. The agreement between the different approaches in our work suggest that the issues described were not major limitations of the project.

Overall, there is sufficient credence to justify the use of mice for this project. The processes of vascular repair and regeneration after hindlimb ischaemia are highly complex and require orchestration of multiple cell lineages in a 3-dimensional structure. Whole body metabolic function also requires the integrated activity of multiple organ systems. Moreover, we sought to temporally manipulate gene expression via inducible silencing technology to mimic the potential relevance of a

pharmacological agent. All of these requirements infer that alternative experimental techniques are inadequate to address the fundamental aims and hypotheses of this project. Mice were considered the most pragmatic choice of animal, as larger mammals would necessitate additional logistical challenges such as longer breeding durations. Nonetheless, mechanistic data derived from the mice colonies were extended and validated through use of HUVECs, to support the relevance of our observations to human disease.

6.6.2   Statistical methodology

Sufficient numbers of mice from the required genotypes were utilised in key experiments to fulfil pre-defined power calculations, which sought to follow the principle of reducing animal numbers where possible (for example, by selecting a power of 0.9). This pragmatic approach to animal experimentation is consistent with defined ethical paradigms of the 'three R's': reduce, refine and replace. This meant that in these experiments, there remains a chance that statistically non-significant observations represent false negative conclusions. Moreover, the mechanistic studies presented should be viewed as hypotheses generating, and it is impractical for all of these to follow strictly pre-defined power calculations. However, by using complementary approaches, the potential for reaching false positive conclusions was reduced.

A further limitation arose from the risk of experimental bias. It was impractical for all researchers involved in the project to be fully blinded at all stages. Where possible, mouse IDs were used for labelling rather than designated genotypes. The procedural

work and image acquisition was also performed by independent researchers who were blinded to genotype of treatment allocation, and if time permitted, analysis was duplicated by two independent researchers as a means of moderation. By incorporating such a strategy, the data derived in this project are likely to be robust and reproducible.

6.6.3   Temporal manipulation of SHIP2

A portion of the work presented in this thesis relied on temporal deletion of the SHIP2 catalytic domain to ascertain the potential impact of a pharmacological inhibitor in clinically relevant contexts. However, other data are derived from mice with germline loss of the SHIP2 catalytic domain meaning that there was significant variation in the duration of knockdown across mice used throughout this project. For instance, retinal imaging was performed in ECSHIP2$^{\Delta/+}$ pups at 5 days of age (after an approximate 21 day gestation with vascular development beginning around day 7), whilst metabolic and vascular profiling after tamoxifen induction in SHIP2i$^{\Delta/+}$ mice was performed one week after tamoxifen induction of Cre activation. Other data from ECSHIP2$^{\Delta/+}$ PECs reflect SHIP2 inactivation after approximately 10 months. Whilst this disparity was generally intended to define temporal differences in the phenotype of SHIP2 inactivation and remove developmental defects of germline inactivation, logistical reasons necessitated study of angiogenesis and PEC function at different ages of ECSHIP2$^{\Delta/+}$ mice. Nonetheless, the data derived from these models are broadly in agreement and so provide complimentary insights.

Similarly, HUVECs expressing SHIP2-targeting shRNA for 4 days mimicked many of the phenotypic traits observed in mice. However, it will be important for future studies to conduct a more detailed comparison of the impact of short- versus long-term SHIP2 inactivation/inhibition given the literature suggesting that beneficial vascular effects of short-term PI3K/AKT activation may become detrimental over the longer term.

6.6.4 Multiple functions of SHIP2

6.6.4.1 Docking properties

This project varied in the means by which SHIP2 was manipulated. *In vivo* work with murine colonies relied upon targeted genetic deletion of the catalytic domain. HUVECs treated with SMI similarly relied upon competitive inhibition of catalytic activity. In contrast, HUVECs expressing SHIP2-targeting shRNA had diminution of the whole SHIP2 mRNA sequence resulting in reduction of the full protein containing both catalytic and non-catalytic domains. As outlined, both the SH2 and proline-rich domains can interact with a range of effector proteins via intrinsic docking sites, including receptors, adaptors, kinases and cytoskeletal proteins. Certainly, non-catalytic properties have also been reported for other phosphatases implicated in glucose metabolism, including PTEN, SHIP1 and inositol phosphate multikinase (IPMK) [351]. It may therefore be that some of the disparities observed between *in vivo* and *in vitro* data, and between shRNA and SMI manipulation of HUVECs, relate to catalytic versus non-catalytic roles of SHIP2. It will therefore be important to explore this further by genetically manipulating potentially relevant non-catalytic SHIP2 domains both *in vitro* and *in vivo*.

6.6.4.2 Regulation of phosphoinositide metabolism

As highlighted, the catalytic function of SHIP2 is a 5-phosphatase to remove the 5'

phosphate group from PIP3 to generate the reaction product PtdIns(3,4)P2. The

consequence of SHIP2KD should not solely be considered in terms of increased PIP3

accumulation, as PtdIns(3,4)P2 formation will also be reduced. The latter can bind

directly to lamellipodin, a cytoskeletal remodelling effector, and has also been broadly

implicated in insulin signalling and cell membrane dynamics [473]. More specifically, it

has been shown to be required for full activation of AKT, and may be implicated as a

tumour oncogene in colorectal cancer by enhancing chemoresistance, cell migration

and invasion [455]. Accumulating evidence has therefore supported the significance of

PtdIns(3,4)P2 as an important component of the PI3K/AKT signalling network, though

its relative contribution in specific cellular contexts remains uncertain. It should also

be noted that an accumulation of PIP3 upon SHIP2KD may provide more substrate for

PTEN, generating biologically active PtdIns(4,5)P2. This serves as a reminder that the

phosphoinositide milieu is highly complex and inter-dependent, and so inhibition of

SHIP2 catalytic activity will have complex effects related to altered abundance of

many isoforms.

The catalytic efficiency of SHIP2 towards Ins(1,3,4,5)P4 is almost 10-fold greater than

its lipid derivative PIP3. Most significantly, SHIP2 has multiple target substrates aside

from PIP3 [474]. For instance, it can also dephosphorylate PtdIns(4,5)P2 to produce

phosphatidylinositol 4-phoshate (PI(4)P) [355]. This appears to participate in the

control of cell migration in glioblastoma cells [393]. The relative abundance and

function of these different substrates was not formally assessed in this project, though they are likely to have pertinent roles in cell signalling and regulation of multiple distinct pathways. The broad substrate specificity of SHIP2 also has important implications when considering the translation of selective SHIP2 pharmacological inhibitors for any therapeutic purpose.

6.6.4.3 SHIP2 antibody

An anti-SHIP2 antibody was kindly donated by our collaborator (Professor Stephane Schurmans, University of Liege) to quantify total murine SHIP2 protein expression in PECs, whilst a commercially available antibody was used for SHIP2 detection in HUVEC lysates. The challenge with this approach is that there is no antibody available that is specific to mutant truncated SHIP2 protein (i.e. without its catalytic domain), as the antibody utilised recognises an amino acid sequence that is retained in the truncated protein. Representative western blots obtained from PEC lysates do illustrate a subtle reduction in total protein abundance and size. The reduced abundance may relate to impaired transcription and translation of truncated SHIP2 and would be consistent with that reported by other researchers that studied the floxed SHIP2 mice we used [377]. Representative blots derived from transfected HUVEC lysates also demonstrate a significant reduction in total SHIP2 protein abundance when quantified by densitometry, supporting their mechanism of SHIP2 mRNA suppression. The associated impact on SHIP2 catalytic activity in both cases was corroborated by confirmation of reduced SHIP2 activity, as quantified by PtdIns(3,4)P2 formation.

6.7 Future directions

Beyond the topics that have already been highlighted, there are a multitude of areas that could be further explored to build upon the work described in this project. Before these are discussed, there are some general points to consider. Firstly, our work has been based upon SHIP2KD in a haploinsufficient manner. It would be particularly interesting to observe whether SHIP2 overexpression in these contexts has converse effects. As discussed, SHIP2 has multiple effector functions mediated through 5 phosphatase activity in addition to its scaffolding properties and intrinsic docking sites. By characterising these interactions through immunoprecipitation, co-localisation assays (e.g. fluorescence resonance energy transfer [FRET]) and site-directed mutagenesis, a more detailed understanding of the effects of SHIP2 manipulation will be achievable. No spliced isoforms of the SHIP2 protein have yet been reported, but if confirmed, their existence will add further layers of complexity. It also remains unclear if SHIP2, like PTEN, also has a role in nuclear regulation of gene expression. Lastly, enzyme abundance does not always correlate with activity. For this reason, SHIP2 activity assays were conducted to confirm adequate SHIP2 catalytic domain knockdown in transfected HUVECs and PECs. This, however, relies on byproduct quantification, and hence, the alternative malachite green phosphatase assay is a more complimentary strategy to directly measure liberation of phosphate as a consequence of SHIP2 enzymatic activity [475].

6.7.1 Metabolic profiling

We have sought to perform *in vivo* whole body metabolic phenotyping in the context of SHIP2 catalytic domain haploinsufficiency. However, the approaches used to perform profiling are limited by their relatively crude assessment of insulin sensitivity and lack of organ-specific glucose uptake data. It would therefore be instructive to conduct more sophisticated analyses such as hyperinsulinaemic-euglycaemic clamping [476], a method for which our laboratory has some familiarity [477]. However, we have performed HOMA-IR scores which has been shown to correlate well with this approach. Studies could also be extended by assessing hepatic glucose output, glucose uptake into peripheral tissues using tracer studies and measurement of serum FFA and triglycerides to discern lipid profile. A formal assessment of fat distribution, food intake and activity level could also be performed.

A further option for *in vivo* analysis relates to SHIP2 SMI. Indeed, chronic treatment has already been performed in the context of diabetic *db/db* mice with AS1949490, and has been shown to lower plasma glucose concentrations and improve whole body glucose tolerance [370]. The administration regime in this study was as twice daily oral preparations for 7 or 10 days. However, a more sophisticated strategy may be to implant micro-osmotic pumps to enable continuous subcutaneous infusion so that the effects of chronic administration can be assessed [478]. Although this SMI has been shown to be potent and selective for SHIP2 relative to other intracellular phosphatases, the concern of potential off-target effects remains. Hence, further biological characterisation and pharmacokinetic analysis is warranted to understand its potential suitability.

Pertinently, all our *in vivo* studies have only been performed in metabolically unchallenged physiological conditions. It would therefore be useful to repeat the experiments after induction of systemic insulin resistance, and our laboratory has shown that this can be reliably achieved by using a high fat, high calorie diet for 2 months after weaning [479].

6.7.2 Vascular profiling

An extensive exploration of the impact of SHIP2 manipulation on vascular function was achieved through use of PECs and HUVECs. Our initial data was generated from work on retinas with endothelium-restricted germline SHIP2 catalytic domain haploinsufficiency. This was performed in 5 day old pups to assess early vascular network formation, but ought to be extended to older mice to scrutinise vascular remodelling and plexus maturation. Although a clear impairment of vascular formation was elicited in the context of SHIP2KD, it is unclear whether this relates to retarded vessel formation *per se* as opposed to regression of new vasculature. Further explorative imaging could be considered with staining for EdU (proliferation), type IV collagen (regression) and caspase (apoptosis). An assessment of vessel maturation could be achieved by staining pericytes, for instance. In the context of SHIP2KD, we have observed clear defects in cell polarity that may impair cell migration. This could be scrutinised further at the angiogenic front through measurement of capillary diameters, and also combined nuclear and Golgi apparatus staining, though the latter approach may be challenging to interpret in a complex 3D system. The effects of vessel blood flow on dynamic endothelial cell rearrangements such as migration,

stabilisation and regression are also of potential relevance, and could be investigated in the context of mouse retinas and zebrafish as documented in published literature [451].

Vascular function was determined predominantly in HUVECs, so it would be beneficial to explore vasomotor function more formally. This could be performed *ex vivo* using aortic rings, for instance. Indeed, this has been studied in 10 month old ECSHIP2$^{\Delta/+}$ mice and shown to exhibit blunted insulin-mediated vasodilation and less constriction when exposed to the non-selective NOS inhibitor L-NMMA, implying lower NO bioavailability [449]. In addition, the effects of SHIP2KD on macrovascular disease could be delineated by crossing with atherosclerosis-prone ApoE knockout mice.

This project assessed vascular regeneration in the context of hindlimb ischaemia by quantifying vascular density in images of skeletal muscle. It would be helpful to extend this to a functional assessment of reperfusion, such as by performing laser Doppler analysis, and this work is planned for the future. Micro-CT is deemed the gold standard to quantify arteriogenesis in ischaemic limbs, a major driver of reperfusion, and the apparatus has recently been acquired for use in our laboratory. However, this is a technically challenging approach that will require time to establish and optimise [480]. It will also be important to consider hindlimb ischaemia recovery in ECSHIP2$^{\Delta/+}$ mice.

There is evidence from our data to support the notion of broad enhancement of PI3K/AKT signalling and concurrent increase in oxidative stress, factors that have repeatedly been implicated in angiogenesis via diverse mechanisms. Further

mechanistic insights may be derived from quantification of VEGF and other pro-angiogenic ligands in primitive retinas and ischaemic muscle tissues. Given that Notch/Dll4 signalling in response to VEGF (whose receptor signalling is also regulated by SHIP2) is strongly implicated in angiogenesis, an assessment of such signalling components would be equally relevant. The effects of SHIP2 modulation on responses to other stimuli aside from VEGF could be explored, as it is likely to exert a diverse range of responses to chemical and physical stimuli implicated in vascular function and remodelling. Lastly, it would be imperative to explore expression of both total and phosphorylated SHIP2 since they may have differing activity. Although there are highlighted challenges associated with antibody specificity, others report to have reliably discriminated between the two [393].

The functional assays performed with HUVECs were based on established protocols that had been modified and optimised for the purposes of this project. Nonetheless, there are caveats to be borne in mind. For example, the scratch wound assay was performed manually using a pipette tip which was operator-dependent and not consistently reproducible. The IncuCyte imaging system would therefore add further refinement to this approach, and would confer the added benefit of real-time imaging and automated quantification software. Moreover, it is difficult to discriminate the relative contributions of cell migration and proliferation *per se* to observed wound closure. The IncuCyte tool provides an initial correction for the degree of proliferation observed in cells at close proximity to the wound edge to circumvent this limitation. The alternative approach would be to perform a manual scratch wound assay, but with concurrent administration of mitomycin C as an anti-proliferative agent [481].

A concerted attempt was made to explore the effects of SHIP2KD on cell morphology and spatial orchestration. This could be detailed further using time-lapse live cell imaging. This approach has been reported by others, and has shown SHIP2 to recruit Mena (involved in actin filament elongation) to the leading edge of cancer cells to enable invasion and metastatic spread [482]. This could be used as an explorative strategy to assess for the interaction of SHIP2 with other substrates implicated in cytoskeletal remodelling, such as talin and filamin. As alluded to, the use of specific biosensors for PIP3 and PtdIns(3,4)P2 could also be considered to monitor spatial phosphoinositide dynamics during migration and polarisation in response to SHIP2 inhibition or knockdown. This may help to test the hypothesis that dysregulated lamellipodial organisation and cell polarisation observed after SHIP2KD are associated with failure to adequately polarise phosphoinositides.

Potential translational relevance of findings could be extended by studying SHIP2 expression and modulation in vascular tissues derived from human disease specimens. As mentioned earlier, INPPL polymorphisms have been implicated in human clinical disorders including metabolic syndromes such as DM. The potential identification of genetic loci associated with diseases or traits could be performed using genome-wide association studies (GWAS), a well-established and effective strategy that has already identified reproducible loci implicated in cardiovascular disease and DM [483]. Indeed, the strategy of gene searching has already been applied to uncover genotype-phenotype associations that implicate a potential role for SHIP2 in lymphangiogenesis [394].

6.8 Concluding remarks

SHIP2 is a known regulator of insulin signalling that is mediated predominantly via 5' phosphatase activity. The aim of this project was to assess the effects of SHIP2 modulation on metabolic and vascular biology, and this was achieved predominantly in murine models with endothelium-specific and whole body inducible SHIP2 catalytic domain haploinsufficiency. The relevance of observations to human pathophysiology was explored using HUVECs after SHIP2 silencing using lentiviral transduction or pharmacological inhibition. The primary hypothesis was that SHIP2 inhibition has favourable effects on insulin-mediated glucose lowering, vascular repair and regeneration.

Endothelial SHIP2 silencing was shown to impair vascular formation in developing postnatal retinas, associated with increased endothelial PI3K/AKT signalling and vascular oxidative stress. Whole body SHIP2 deletion appeared to improve whole body glucose disposal and insulin sensitivity. Neovessel formation in ischaemic tissues also appeared enhanced, but with potential structural abnormalities. No differences were apparent in re-endothelialisation after denuding arterial injury. Alterations in signalling intermediates and superoxide generation were broadly recapitulated in HUVECs, and were associated with defects in cell migration and polarisation albeit with preserved proliferative capacity.

In summary, SHIP2 activity appears to be critical in systemic metabolic homeostasis. It also has a crucial role in preserving mechanisms implicated in normal vascular biology, potentially by suppressing oxidative stress that arises from unrestrained PI3K-Nox2

signalling. This suggests that caution needs to be exerted when considering SHIP2

inhibition as an interventional strategy in the clinical setting.

Bibliography

1.   Yuan, H.X., Y. Xiong, and K.L. Guan, *Nutrient sensing, metabolism, and cell growth control.* Mol Cell, 2013. **49**(3): p. 379-87.
2.   Reaven, G.M., *Role of insulin resistance in human disease (syndrome X): an expanded definition.* Annu Rev Med, 1993. **44**: p. 121-31.
3.   Wild, S., et al., *Global prevalence of diabetes: estimates for the year 2000 and projections for 2030.* Diabetes Care, 2004. **27**(5): p. 1047-53.
4.   Ovbiagele, B., D. Markovic, and G.C. Fonarow, *Recent US Patterns and Predictors of Prevalent Diabetes among Acute Myocardial Infarction Patients.* Cardiol Res Pract, 2011. **2011**: p. 145615.
5.   Norhammar, A., et al., *Glucose metabolism in patients with acute myocardial infarction and no previous diagnosis of diabetes mellitus: a prospective study.* Lancet, 2002. **359**(9324): p. 2140-4.
6.   Amato, L., et al., *Congestive heart failure predicts the development of non-insulin-dependent diabetes mellitus in the elderly. The Osservatorio Geriatrico Regione Campania Group.* Diabetes Metab, 1997. **23**(3): p. 213-8.
7.   MacDonald, M.R., et al., *Impact of diabetes on outcomes in patients with low and preserved ejection fraction heart failure: an analysis of the Candesartan in Heart failure: Assessment of Reduction in Mortality and morbidity (CHARM) programme.* Eur Heart J, 2008. **29**(11): p. 1377-85.
8.   Kannel, W.B. and D.L. McGee, *Diabetes and cardiovascular disease. The Framingham study.* JAMA, 1979. **241**(19): p. 2035-8.
9.   Harris, M.I., *Epidemiologic studies on the pathogenesis of non-insulin-dependent diabetes mellitus (NIDDM).* Clin Invest Med, 1995. **18**(4): p. 231-9.
10. Booth, G.L., et al., *Relation between age and cardiovascular disease in men and women with diabetes compared with non-diabetic people: a population-based retrospective cohort study.* Lancet, 2006. **368**(9529): p. 29-36.
11. *Is the current definition for diabetes relevant to mortality risk from all causes and cardiovascular and noncardiovascular diseases?* Diabetes Care, 2003. **26**(3): p. 688-96.
12. McGovern, P.G., et al., *Trends in acute coronary heart disease mortality, morbidity, and medical care from 1985 through 1997: the Minnesota heart survey.* Circulation, 2001. **104**(1): p. 19-24.
13. Patel, P.A., et al., *An evaluation of 20 year survival in patients with diabetes mellitus and acute myocardial infarction.* Int J Cardiol, 2016. **203**: p. 141-4.
14. Cubbon, R.M., et al., *Diabetes mellitus is associated with adverse prognosis in chronic heart failure of ischaemic and non-ischaemic aetiology.* Diab Vasc Dis Res, 2013. **10**(4): p. 330-6.
15. Wheatcroft, S.B., et al., *Pathophysiological implications of insulin resistance on vascular endothelial function.* Diabet Med, 2003. **20**(4): p. 255-68.
16. Mercer, B.N., et al., *Diabetes mellitus and the heart.* Int J Clin Pract, 2012. **66**(7): p. 640-7.
17. Mayerl, C., et al., *Atherosclerosis research from past to present--on the track of two pathologists with opposing views, Carl von Rokitansky and Rudolf Virchow.* Virchows Arch, 2006. **449**(1): p. 96-103.

18. Ross, R., *Atherosclerosis--an inflammatory disease.* N Engl J Med, 1999. **340**(2): p. 115-26.

19. Aronson, D. and E.R. Edelman, *Revascularization for coronary artery disease in diabetes mellitus: angioplasty, stents and coronary artery bypass grafting.* Rev Endocr Metab Disord, 2010. **11**(1): p. 75-86.

20. Ross, R., J. Glomset, and L. Harker, *Response to injury and atherogenesis.* Am J Pathol, 1977. **86**(3): p. 675-84.

21. Esper, R.J., et al., *Endothelial dysfunction: a comprehensive appraisal.* Cardiovasc Diabetol, 2006. **5**: p. 4.

22. Napoli, C., et al., *Fatty streak formation occurs in human fetal aortas and is greatly enhanced by maternal hypercholesterolemia. Intimal accumulation of low density lipoprotein and its oxidation precede monocyte recruitment into early atherosclerotic lesions.* J Clin Invest, 1997. **100**(11): p. 2680-90.

23. Sniderman, A.D., T. Scantlebury, and K. Cianflone, *Hypertriglyceridemic hyperapob: the unappreciated atherogenic dyslipoproteinemia in type 2 diabetes mellitus.* Ann Intern Med, 2001. **135**(6): p. 447-59.

24. Flood, C., et al., *Molecular mechanism for changes in proteoglycan binding on compositional changes of the core and the surface of low-density lipoprotein-containing human apolipoprotein B100.* Arterioscler Thromb Vasc Biol, 2004. **24**(3): p. 564-70.

25. Young, S.G. and S. Parthasarathy, *Why are low-density lipoproteins atherogenic?* West J Med, 1994. **160**(2): p. 153-64.

26. Badimon, L., et al., *Cell biology and lipoproteins in atherosclerosis.* Curr Mol Med, 2006. **6**(5): p. 439-56.

27. Han, J., et al., *Native and modified low density lipoproteins increase the functional expression of the macrophage class B scavenger receptor, CD36.* J Biol Chem, 1997. **272**(34): p. 21654-9.

28. Rader, D.J. and E. Pure, *Lipoproteins, macrophage function, and atherosclerosis: beyond the foam cell?* Cell Metab, 2005. **1**(4): p. 223-30.

29. Boisvert, W.A., et al., *A leukocyte homologue of the IL-8 receptor CXCR-2 mediates the accumulation of macrophages in atherosclerotic lesions of LDL receptor-deficient mice.* J Clin Invest, 1998. **101**(2): p. 353-63.

30. Doran, A.C., N. Meller, and C.A. McNamara, *Role of smooth muscle cells in the initiation and early progression of atherosclerosis.* Arterioscler Thromb Vasc Biol, 2008. **28**(5): p. 812-9.

31. Mondy, J.S., et al., *Platelet-derived growth factor ligand and receptor expression in response to altered blood flow in vivo.* Circ Res, 1997. **81**(3): p. 320-7.

32. Lee, R.T. and P. Libby, *The unstable atheroma.* Arterioscler Thromb Vasc Biol, 1997. **17**(10): p. 1859-67.

33. Badimon, J.J., et al., *Local inhibition of tissue factor reduces the thrombogenicity of disrupted human atherosclerotic plaques: effects of tissue factor pathway inhibitor on plaque thrombogenicity under flow conditions.* Circulation, 1999. **99**(14): p. 1780-7.

34. Thim, T., et al., *From vulnerable plaque to atherothrombosis.* J Intern Med, 2008. **263**(5): p. 506-16.

35.   Galis, Z.S., et al., *Increased expression of matrix metalloproteinases and matrix degrading activity in vulnerable regions of human atherosclerotic plaques.* J Clin Invest, 1994. **94**(6): p. 2493-503.

36.   Geng, Y.J. and P. Libby, *Evidence for apoptosis in advanced human atheroma. Colocalization with interleukin-1 beta-converting enzyme.* Am J Pathol, 1995. **147**(2): p. 251-66.

37.   Davies, M.J., *A macro and micro view of coronary vascular insult in ischemic heart disease.* Circulation, 1990. **82**(3 Suppl): p. II38-46.

38.   Lusis, A.J., *Atherosclerosis.* Nature, 2000. **407**(6801): p. 233-41.

39.   Bornfeldt, K.E., *2013 Russell Ross memorial lecture in vascular biology: cellular and molecular mechanisms of diabetes mellitus-accelerated atherosclerosis.* Arterioscler Thromb Vasc Biol, 2014. **34**(4): p. 705-14.

40.   McCarthy, M.J., et al., *Angiogenesis and the atherosclerotic carotid plaque: an association between symptomatology and plaque morphology.* J Vasc Surg, 1999. **30**(2): p. 261-8.

41.   Virmani, R., et al., *Atherosclerotic plaque progression and vulnerability to rupture: angiogenesis as a source of intraplaque hemorrhage.* Arterioscler Thromb Vasc Biol, 2005. **25**(10): p. 2054-61.

42.   Juan-Babot, J.O., et al., *[Neovascularization in human coronary arteries with lesions of different severity].* Rev Esp Cardiol, 2003. **56**(10): p. 978-86.

43.   Uemura, S., et al., *Diabetes mellitus enhances vascular matrix metalloproteinase activity: role of oxidative stress.* Circ Res, 2001. **88**(12): p. 1291-8.

44.   Kohler, H.P. and P.J. Grant, *Plasminogen-activator inhibitor type 1 and coronary artery disease.* N Engl J Med, 2000. **342**(24): p. 1792-801.

45.   Juhan-Vague, I., et al., *Increased plasminogen activator inhibitor activity in non insulin dependent diabetic patients--relationship with plasma insulin.* Thromb Haemost, 1989. **61**(3): p. 370-3.

46.   Svendsen, O.L., et al., *Plasminogen activator inhibitor-1, tissue-type plasminogen activator, and fibrinogen: Effect of dieting with or without exercise in overweight postmenopausal women.* Arterioscler Thromb Vasc Biol, 1996. **16**(3): p. 381-5.

47.   Ajjan, R.A., et al., *Diabetes is associated with posttranslational modifications in plasminogen resulting in reduced plasmin generation and enzyme-specific activity.* Blood, 2013. **122**(1): p. 134-42.

48.   Forstermann, U. and W.C. Sessa, *Nitric oxide synthases: regulation and function.* Eur Heart J, 2012. **33**(7): p. 829-37, 837a-837d.

49.   Wu, K.K. and P. Thiagarajan, *Role of endothelium in thrombosis and hemostasis.* Annu Rev Med, 1996. **47**: p. 315-31.

50.   Yetik-Anacak, G. and J.D. Catravas, *Nitric oxide and the endothelium: history and impact on cardiovascular disease.* Vascul Pharmacol, 2006. **45**(5): p. 268-76.

51.   Furchgott, R.F. and J.V. Zawadzki, *The obligatory role of endothelial cells in the relaxation of arterial smooth muscle by acetylcholine.* Nature, 1980. **288**(5789): p. 373-6.

52. Palmer, R.M., A.G. Ferrige, and S. Moncada, *Nitric oxide release accounts for the biological activity of endothelium-derived relaxing factor.* Nature, 1987. **327**(6122): p. 524-6.

53. Xu, W., et al., *Mapping of the genes encoding human inducible and endothelial nitric oxide synthase (NOS2 and NOS3) to the pericentric region of chromosome 17 and to chromosome 7, respectively.* Genomics, 1994. **21**(2): p. 419-22.

54. Stuehr, D.J., et al., *Purification and characterization of the cytokine-induced macrophage nitric oxide synthase: an FAD- and FMN-containing flavoprotein.* Proc Natl Acad Sci U S A, 1991. **88**(17): p. 7773-7.

55. Dawson, T.M. and S.H. Snyder, *Gases as biological messengers: nitric oxide and carbon monoxide in the brain.* J Neurosci, 1994. **14**(9): p. 5147-59.

56. Moncada, S. and A. Higgs, *The L-arginine-nitric oxide pathway.* N Engl J Med, 1993. **329**(27): p. 2002-12.

57. Kelm, M., et al., *Release of endothelium derived nitric oxide in relation to pressure and flow.* Cardiovasc Res, 1991. **25**(10): p. 831-6.

58. Green, L.C., et al., *Analysis of nitrate, nitrite, and [15N]nitrate in biological fluids.* Anal Biochem, 1982. **126**(1): p. 131-8.

59. Pacher, P., J.S. Beckman, and L. Liaudet, *Nitric Oxide and Peroxynitrite in Health and Disease.* Physiol Rev, 2007. **87**(1): p. 315-424.

60. Ignarro, L.J., *Heme-dependent activation of guanylate cyclase by nitric oxide: a novel signal transduction mechanism.* Blood Vessels, 1991. **28**(1-3): p. 67-73.

61. Erwin, P.A., et al., *Subcellular targeting and differential S-nitrosylation of endothelial nitric-oxide synthase.* J Biol Chem, 2006. **281**(1): p. 151-7.

62. Baylis, C., B. Mitruka, and A. Deng, *Chronic blockade of nitric oxide synthesis in the rat produces systemic hypertension and glomerular damage.* J Clin Invest, 1992. **90**(1): p. 278-81.

63. Noack, E. and M. Feelisch, *Molecular mechanisms of nitrovasodilator bioactivation.* Basic Res Cardiol, 1991. **86 Suppl 2**: p. 37-50.

64. Cachofeiro, V., T. Sakakibara, and A. Nasjletti, *Kinins, nitric oxide, and the hypotensive effect of captopril and ramiprilat in hypertension.* Hypertension, 1992. **19**(2): p. 138-45.

65. Radomski, M.W. and S. Moncada, *The biological and pharmacological role of nitric oxide in platelet function.* Adv Exp Med Biol, 1993. **344**: p. 251-64.

66. Kubes, P., M. Suzuki, and D.N. Granger, *Nitric oxide: an endogenous modulator of leukocyte adhesion.* Proc Natl Acad Sci U S A, 1991. **88**(11): p. 4651-5.

67. Garg, U.C. and A. Hassid, *Nitric oxide-generating vasodilators inhibit mitogenesis and proliferation of BALB/C 3T3 fibroblasts by a cyclic GMP-independent mechanism.* Biochem Biophys Res Commun, 1990. **171**(1): p. 474-9.

68. Paradossi, U., et al., *Endothelial function and carotid intima-media thickness in young healthy subjects among endothelial nitric oxide synthase Glu298-->Asp and T-786-->C polymorphisms.* Stroke, 2004. **35**(6): p. 1305-9.

69. Emdin, C.A., et al., *Phenotypic Consequences of a Genetic Predisposition to Enhanced Nitric Oxide Signaling.* Circulation, 2018. **137**(3): p. 222-232.

70. Cubbon, R.M., et al., *Importance of insulin resistance to vascular repair and regeneration.* Free Radic Biol Med, 2013. **60**: p. 246-63.

71. Van Belle, E., et al., *Endothelial regrowth after arterial injury: from vascular repair to therapeutics.* Cardiovasc Res, 1998. **38**(1): p. 54-68.

72. Hagensen, M.K., et al., *Circulating endothelial progenitor cells do not contribute to plaque endothelium in murine atherosclerosis.* Circulation, 2010. **121**(7): p. 898-905.

73. Hagensen, M.K., et al., *Circulating endothelial progenitor cells do not contribute to regeneration of endothelium after murine arterial injury.* Cardiovasc Res, 2012. **93**(2): p. 223-31.

74. Carmeliet, P., *Angiogenesis in health and disease.* Nat Med, 2003. **9**(6): p. 653-60.

75. Heil, M., et al., *Arteriogenesis versus angiogenesis: similarities and differences.* J Cell Mol Med, 2006. **10**(1): p. 45-55.

76. Potente, M., H. Gerhardt, and P. Carmeliet, *Basic and therapeutic aspects of angiogenesis.* Cell, 2011. **146**(6): p. 873-87.

77. Eltzschig, H.K. and P. Carmeliet, *Hypoxia and inflammation.* N Engl J Med, 2011. **364**(7): p. 656-65.

78. Asahara, T., et al., *Isolation of putative progenitor endothelial cells for angiogenesis.* Science, 1997. **275**(5302): p. 964-7.

79. Aicher, A., A.M. Zeiher, and S. Dimmeler, *Mobilizing endothelial progenitor cells.* Hypertension, 2005. **45**(3): p. 321-5.

80. Laufs, U., et al., *Physical training increases endothelial progenitor cells, inhibits neointima formation, and enhances angiogenesis.* Circulation, 2004. **109**(2): p. 220-6.

81. Aicher, A., et al., *Essential role of endothelial nitric oxide synthase for mobilization of stem and progenitor cells.* Nat Med, 2003. **9**(11): p. 1370-6.

82. Cubbon, R.M., et al., *Human exercise-induced circulating progenitor cell mobilization is nitric oxide-dependent and is blunted in South Asian men.* Arterioscler Thromb Vasc Biol, 2010. **30**(4): p. 878-84.

83. Hirschi, K.K., D.A. Ingram, and M.C. Yoder, *Assessing identity, phenotype, and fate of endothelial progenitor cells.* Arterioscler Thromb Vasc Biol, 2008. **28**(9): p. 1584-95.

84. Prokopi, M., et al., *Proteomic analysis reveals presence of platelet microparticles in endothelial progenitor cell cultures.* Blood, 2009. **114**(3): p. 723-32.

85. Hur, J., et al., *Characterization of two types of endothelial progenitor cells and their different contributions to neovasculogenesis.* Arterioscler Thromb Vasc Biol, 2004. **24**(2): p. 288-93.

86. Petrie, R.J., A.D. Doyle, and K.M. Yamada, *Random versus directionally persistent cell migration.* Nat Rev Mol Cell Biol, 2009. **10**(8): p. 538-49.

87. Baggiolini, M., *Chemokines and leukocyte traffic.* Nature, 1998. **392**(6676): p. 565-8.

88. Zigmond, S.H., *Ability of polymorphonuclear leukocytes to orient in gradients of chemotactic factors.* J Cell Biol, 1977. **75**(2 Pt 1): p. 606-16.

89. Van Haastert, P.J. and P.N. Devreotes, *Chemotaxis: signalling the way forward.* Nat Rev Mol Cell Biol, 2004. **5**(8): p. 626-34.

90.   Krause, M. and A. Gautreau, *Steering cell migration: lamellipodium dynamics and the regulation of directional persistence.* Nat Rev Mol Cell Biol, 2014. **15**(9): p. 577-90.

91.   Lauffenburger, D.A. and A.F. Horwitz, *Cell migration: a physically integrated molecular process.* Cell, 1996. **84**(3): p. 359-69.

92.   Small, J.V., et al., *The lamellipodium: where motility begins.* Trends Cell Biol, 2002. **12**(3): p. 112-20.

93.   Small, J.V., *The actin cytoskeleton.* Electron Microsc Rev, 1988. **1**(1): p. 155-74.

94.   Arjonen, A., R. Kaukonen, and J. Ivaska, *Filopodia and adhesion in cancer cell motility.* Cell Adh Migr, 2011. **5**(5): p. 421-30.

95.   Rottner, K., et al., *VASP dynamics during lamellipodia protrusion.* Nat Cell Biol, 1999. **1**(5): p. 321-2.

96.   Bear, J.E., et al., *Antagonism between Ena/VASP proteins and actin filament capping regulates fibroblast motility.* Cell, 2002. **109**(4): p. 509-21.

97.   Wu, C.F. and D.J. Lew, *Beyond symmetry-breaking: competition and negative feedback in GTPase regulation.* Trends Cell Biol, 2013. **23**(10): p. 476-83.

98.   Regen, C.M. and A.F. Horwitz, *Dynamics of beta 1 integrin-mediated adhesive contacts in motile fibroblasts.* J Cell Biol, 1992. **119**(5): p. 1347-59.

99.   Evans, E., A. Leung, and D. Zhelev, *Synchrony of cell spreading and contraction force as phagocytes engulf large pathogens.* J Cell Biol, 1993. **122**(6): p. 1295-300.

100.   Jay, P.Y., et al., *A mechanical function of myosin II in cell motility.* J Cell Sci, 1995. **108 (Pt 1)**: p. 387-93.

101.   Sheetz, M.P., *Cell migration by graded attachment to substrates and contraction.* Semin Cell Biol, 1994. **5**(3): p. 149-55.

102.   Chen, W.T., *Mechanism of retraction of the trailing edge during fibroblast movement.* J Cell Biol, 1981. **90**(1): p. 187-200.

103.   Levi, S., M.V. Polyakov, and T.T. Egelhoff, *Myosin II dynamics in Dictyostelium: determinants for filament assembly and translocation to the cell cortex during chemoattractant responses.* Cell Motil Cytoskeleton, 2002. **53**(3): p. 177-88.

104.   Lamalice, L., F. Le Boeuf, and J. Huot, *Endothelial cell migration during angiogenesis.* Circ Res, 2007. **100**(6): p. 782-94.

105.   Meili, R., et al., *Chemoattractant-mediated transient activation and membrane localization of Akt/PKB is required for efficient chemotaxis to cAMP in Dictyostelium.* EMBO J, 1999. **18**(8): p. 2092-105.

106.   Rodriguez-Viciana, P., et al., *Role of phosphoinositide 3-OH kinase in cell transformation and control of the actin cytoskeleton by Ras.* Cell, 1997. **89**(3): p. 457-67.

107.   Scita, G., et al., *Signaling from Ras to Rac and beyond: not just a matter of GEFs.* EMBO J, 2000. **19**(11): p. 2393-8.

108.   Nobes, C.D. and A. Hall, *Rho GTPases control polarity, protrusion, and adhesion during cell movement.* J Cell Biol, 1999. **144**(6): p. 1235-44.

109.   Michaelson, D., et al., *Differential localization of Rho GTPases in live cells: regulation by hypervariable regions and RhoGDI binding.* J Cell Biol, 2001. **152**(1): p. 111-26.

110.   Pantaloni, D., C. Le Clainche, and M.F. Carlier, *Mechanism of actin-based motility.* Science, 2001. **292**(5521): p. 1502-6.

111. Svitkina, T.M. and G.G. Borisy, *Arp2/3 complex and actin depolymerizing factor/cofilin in dendritic organization and treadmilling of actin filament array in lamellipodia.* J Cell Biol, 1999. **145**(5): p. 1009-26.

112. Weaver, A.M., et al., *Cortactin promotes and stabilizes Arp2/3-induced actin filament network formation.* Curr Biol, 2001. **11**(5): p. 370-4.

113. Stossel, T.P., et al., *Filamins as integrators of cell mechanics and signalling.* Nat Rev Mol Cell Biol, 2001. **2**(2): p. 138-45.

114. Miki, H., et al., *IRSp53 is an essential intermediate between Rac and WAVE in the regulation of membrane ruffling.* Nature, 2000. **408**(6813): p. 732-5.

115. Krugmann, S., et al., *Cdc42 induces filopodia by promoting the formation of an IRSp53:Mena complex.* Curr Biol, 2001. **11**(21): p. 1645-55.

116. Arias-Romero, L.E. and J. Chernoff, *A tale of two Paks.* Biol Cell, 2008. **100**(2): p. 97-108.

117. Daniels, R.H. and G.M. Bokoch, *p21-activated protein kinase: a crucial component of morphological signaling?* Trends Biochem Sci, 1999. **24**(9): p. 350-5.

118. Bagrodia, S. and R.A. Cerione, *Pak to the future.* Trends Cell Biol, 1999. **9**(9): p. 350-5.

119. Narumiya, S., M. Tanji, and T. Ishizaki, *Rho signaling, ROCK and mDia1, in transformation, metastasis and invasion.* Cancer Metastasis Rev, 2009. **28**(1-2): p. 65-76.

120. Romer, L.H., K.G. Birukov, and J.G. Garcia, *Focal adhesions: paradigm for a signaling nexus.* Circ Res, 2006. **98**(5): p. 606-16.

121. Dippold, H.C., et al., *GOLPH3 bridges phosphatidylinositol-4- phosphate and actomyosin to stretch and shape the Golgi to promote budding.* Cell, 2009. **139**(2): p. 337-51.

122. Zhang, X., et al., *GOLPH3 promotes glioblastoma cell migration and invasion via the mTOR-YB1 pathway in vitro.* Mol Carcinog, 2015. **54**(11): p. 1252-63.

123. Williams, M.R., et al., *The role of 3-phosphoinositide-dependent protein kinase 1 in activating AGC kinases defined in embryonic stem cells.* Curr Biol, 2000. **10**(8): p. 439-48.

124. Morales-Ruiz, M., et al., *Vascular endothelial growth factor-stimulated actin reorganization and migration of endothelial cells is regulated via the serine/threonine kinase Akt.* Circ Res, 2000. **86**(8): p. 892-6.

125. Morales-Ruiz, M., et al., *Sphingosine 1-phosphate activates Akt, nitric oxide production, and chemotaxis through a Gi protein/phosphoinositide 3-kinase pathway in endothelial cells.* J Biol Chem, 2001. **276**(22): p. 19672-7.

126. Swift, M.R. and B.M. Weinstein, *Arterial-venous specification during development.* Circ Res, 2009. **104**(5): p. 576-88.

127. Lawson, N.D., et al., *Notch signaling is required for arterial-venous differentiation during embryonic vascular development.* Development, 2001. **128**(19): p. 3675-83.

128. Lawson, N.D., A.M. Vogel, and B.M. Weinstein, *sonic hedgehog and vascular endothelial growth factor act upstream of the Notch pathway during arterial endothelial differentiation.* Dev Cell, 2002. **3**(1): p. 127-36.

129. Jones, E.A., F. le Noble, and A. Eichmann, *What determines blood vessel structure? Genetic prespecification vs. hemodynamics.* Physiology (Bethesda), 2006. **21**: p. 388-95.

130. Visconti, R.P., C.D. Richardson, and T.N. Sato, *Orchestration of angiogenesis and arteriovenous contribution by angiopoietins and vascular endothelial growth factor (VEGF).* Proc Natl Acad Sci U S A, 2002. **99**(12): p. 8219-24.

131. Eble, J.A. and S. Niland, *The extracellular matrix of blood vessels.* Curr Pharm Des, 2009. **15**(12): p. 1385-400.

132. Luttun, A., et al., *The role of proteinases in angiogenesis, heart development, restenosis, atherosclerosis, myocardial ischemia, and stroke: insights from genetic studies.* Curr Atheroscler Rep, 2000. **2**(5): p. 407-16.

133. Blasi, F. and P. Carmeliet, *uPAR: a versatile signalling orchestrator.* Nat Rev Mol Cell Biol, 2002. **3**(12): p. 932-43.

134. Thurston, G., I. Noguera-Troise, and G.D. Yancopoulos, *The Delta paradox: DLL4 blockade leads to more tumour vessels but less tumour growth.* Nat Rev Cancer, 2007. **7**(5): p. 327-31.

135. Phng, L.K. and H. Gerhardt, *Angiogenesis: a team effort coordinated by notch.* Dev Cell, 2009. **16**(2): p. 196-208.

136. Jakobsson, L., et al., *Endothelial cells dynamically compete for the tip cell position during angiogenic sprouting.* Nat Cell Biol, 2010. **12**(10): p. 943-53.

137. Eilken, H.M. and R.H. Adams, *Dynamics of endothelial cell behavior in sprouting angiogenesis.* Curr Opin Cell Biol, 2010. **22**(5): p. 617-25.

138. Iruela-Arispe, M.L. and G.E. Davis, *Cellular and molecular mechanisms of vascular lumen formation.* Dev Cell, 2009. **16**(2): p. 222-31.

139. Fantin, A., et al., *Tissue macrophages act as cellular chaperones for vascular anastomosis downstream of VEGF-mediated endothelial tip cell induction.* Blood, 2010. **116**(5): p. 829-40.

140. Nicoli, S., et al., *MicroRNA-mediated integration of haemodynamics and Vegf signalling during angiogenesis.* Nature, 2010. **464**(7292): p. 1196-200.

141. He, Z., et al., *Regulation of vascular endothelial growth factor expression and vascularization in the myocardium by insulin receptor and PI3K/Akt pathways in insulin resistance and ischemia.* Arterioscler Thromb Vasc Biol, 2006. **26**(4): p. 787-93.

142. Thangarajah, H., et al., *The molecular basis for impaired hypoxia-induced VEGF expression in diabetic tissues.* Proc Natl Acad Sci U S A, 2009. **106**(32): p. 13505-10.

143. Nagahama, R., et al., *Nanoparticle-mediated delivery of pioglitazone enhances therapeutic neovascularization in a murine model of hindlimb ischemia.* Arterioscler Thromb Vasc Biol, 2012. **32**(10): p. 2427-34.

144. Moens, S., et al., *The multifaceted activity of VEGF in angiogenesis - Implications for therapy responses.* Cytokine Growth Factor Rev, 2014. **25**(4): p. 473-82.

145. Wang, H.U., Z.F. Chen, and D.J. Anderson, *Molecular distinction and angiogenic interaction between embryonic arteries and veins revealed by ephrin-B2 and its receptor Eph-B4.* Cell, 1998. **93**(5): p. 741-53.

146. Gaengel, K., et al., *Endothelial-mural cell signaling in vascular development and angiogenesis.* Arterioscler Thromb Vasc Biol, 2009. **29**(5): p. 630-8.

147.   Pardali, E., M.J. Goumans, and P. ten Dijke, *Signaling by members of the TGF-beta family in vascular morphogenesis and disease.* Trends Cell Biol, 2010. **20**(9): p. 556-67.

148.   Hellstrom, M., et al., *Lack of pericytes leads to endothelial hyperplasia and abnormal vascular morphogenesis.* J Cell Biol, 2001. **153**(3): p. 543-53.

149.   Huang, H., et al., *Targeting the ANGPT-TIE2 pathway in malignancy.* Nat Rev Cancer, 2010. **10**(8): p. 575-85.

150.   Beenken, A. and M. Mohammadi, *The FGF family: biology, pathophysiology and therapy.* Nat Rev Drug Discov, 2009. **8**(3): p. 235-53.

151.   Rutten, J.W., et al., *Interpretation of NOTCH3 mutations in the diagnosis of CADASIL.* Expert Rev Mol Diagn, 2014. **14**(5): p. 593-603.

152.   Warren, C.M. and M.L. Iruela-Arispe, *Signaling circuitry in vascular morphogenesis.* Curr Opin Hematol, 2010. **17**(3): p. 213-8.

153.   Dor, Y., et al., *Conditional switching of VEGF provides new insights into adult neovascularization and pro-angiogenic therapy.* Embo j, 2002. **21**(8): p. 1939-47.

154.   Benjamin, L.E., I. Hemo, and E. Keshet, *A plasticity window for blood vessel remodelling is defined by pericyte coverage of the preformed endothelial network and is regulated by PDGF-B and VEGF.* Development, 1998. **125**(9): p. 1591-8.

155.   Pugh, C.W. and P.J. Ratcliffe, *Regulation of angiogenesis by hypoxia: role of the HIF system.* Nat Med, 2003. **9**(6): p. 677-84.

156.   Hoefer, I.E., et al., *Direct evidence for tumor necrosis factor-alpha signaling in arteriogenesis.* Circulation, 2002. **105**(14): p. 1639-41.

157.   Heil, M., et al., *Blood monocyte concentration is critical for enhancement of collateral artery growth.* Am J Physiol Heart Circ Physiol, 2002. **283**(6): p. H2411-9.

158.   Bliss, M., *The history of insulin.* Diabetes Care, 1993. **16 Suppl 3**: p. 4-7.

159.   Roth, J., et al., *Insulin's discovery: new insights on its ninetieth birthday.* Diabetes Metab Res Rev, 2012. **28**(4): p. 293-304.

160.   Schroder, D. and H. Zuhlke, *Gene technology, characterization of insulin gene and the relationship to diabetes research.* Endokrinologie, 1982. **79**(2): p. 197-209.

161.   Dodson, G. and D. Steiner, *The role of assembly in insulin's biosynthesis.* Curr Opin Struct Biol, 1998. **8**(2): p. 189-94.

162.   Nielsen, J.H., et al., *Regulation of beta-cell mass by hormones and growth factors.* Diabetes, 2001. **50 Suppl 1**: p. S25-9.

163.   Wilcox, G., *Insulin and insulin resistance.* Clin Biochem Rev, 2005. **26**(2): p. 19-39.

164.   Chen, M. and D. Porte, Jr., *The effect of rate and dose of glucose infusion on the acute insulin response in man.* J Clin Endocrinol Metab, 1976. **42**(6): p. 1168-75.

165.   Bratanova-Tochkova, T.K., et al., *Triggering and augmentation mechanisms, granule pools, and biphasic insulin secretion.* Diabetes, 2002. **51 Suppl 1**: p. S83-90.

166.   Burks, D.J. and M.F. White, *IRS proteins and beta-cell function.* Diabetes, 2001. **50 Suppl 1**: p. S140-5.

167. Hunter, S.J. and W.T. Garvey, *Insulin action and insulin resistance: diseases involving defects in insulin receptors, signal transduction, and the glucose transport effector system.* Am J Med, 1998. **105**(4): p. 331-45.

168. Smith, U., *Impaired ('diabetic') insulin signaling and action occur in fat cells long before glucose intolerance--is insulin resistance initiated in the adipose tissue?* Int J Obes Relat Metab Disord, 2002. **26**(7): p. 897-904.

169. Belfiore, A., et al., *Insulin receptor isoforms and insulin receptor/insulin-like growth factor receptor hybrids in physiology and disease.* Endocr Rev, 2009. **30**(6): p. 586-623.

170. Steinberg, H.O., et al., *Insulin-mediated skeletal muscle vasodilation is nitric oxide dependent. A novel action of insulin to increase nitric oxide release.* J Clin Invest, 1994. **94**(3): p. 1172-9.

171. Vincent, M.A., et al., *Skeletal muscle microvascular recruitment by physiological hyperinsulinemia precedes increases in total blood flow.* Diabetes, 2002. **51**(1): p. 42-8.

172. Utriainen, T., et al., *Methodological aspects, dose-response characteristics and causes of interindividual variation in insulin stimulation of limb blood flow in normal subjects.* Diabetologia, 1995. **38**(5): p. 555-64.

173. Cardillo, C., et al., *Vasodilator response to systemic but not to local hyperinsulinemia in the human forearm.* Hypertension, 1998. **32**(4): p. 740-5.

174. Rahmouni, K., et al., *Hypothalamic PI3K and MAPK differentially mediate regional sympathetic activation to insulin.* J Clin Invest, 2004. **114**(5): p. 652-8.

175. Scherrer, U. and C. Sartori, *Insulin as a vascular and sympathoexcitatory hormone: implications for blood pressure regulation, insulin sensitivity, and cardiovascular morbidity.* Circulation, 1997. **96**(11): p. 4104-13.

176. Vicent, D., et al., *The role of endothelial insulin signaling in the regulation of vascular tone and insulin resistance.* J Clin Invest, 2003. **111**(9): p. 1373-80.

177. Cardillo, C., et al., *Insulin stimulates both endothelin and nitric oxide activity in the human forearm.* Circulation, 1999. **100**(8): p. 820-5.

178. O'Callaghan, C.J., et al., *'Physiological' hyperinsulinaemia increases distal artery systolic blood pressure without changing proximal blood pressure.* Clin Sci (Lond), 1997. **93**(6): p. 535-40.

179. DeFronzo, R.A., et al., *The effect of insulin on renal handling of sodium, potassium, calcium, and phosphate in man.* J Clin Invest, 1975. **55**(4): p. 845-55.

180. Rocchini, A.P., et al., *Insulin and renal sodium retention in obese adolescents.* Hypertension, 1989. **14**(4): p. 367-74.

181. ter Maaten, J.C., et al., *Insulin's acute effects on glomerular filtration rate correlate with insulin sensitivity whereas insulin's acute effects on proximal tubular sodium reabsorption correlation with salt sensitivity in normal subjects.* Nephrol Dial Transplant, 1999. **14**(10): p. 2357-63.

182. Mather, K., et al., *Evidence for physiological coupling of insulin-mediated glucose metabolism and limb blood flow.* Am J Physiol Endocrinol Metab, 2000. **279**(6): p. E1264-70.

183. Laakso, M., et al., *Impaired insulin-mediated skeletal muscle blood flow in patients with NIDDM.* Diabetes, 1992. **41**(9): p. 1076-83.

184. Iozzo, P., et al., *Regional myocardial blood flow and glucose utilization during fasting and physiological hyperinsulinemia in humans.* Am J Physiol Endocrinol Metab, 2002. **282**(5): p. E1163-71.

185. Kido, Y., J. Nakae, and D. Accili, *Clinical review 125: The insulin receptor and its cellular targets.* J Clin Endocrinol Metab, 2001. **86**(3): p. 972-9.

186. Becker, A.B. and R.A. Roth, *Insulin receptor structure and function in normal and pathological conditions.* Annu Rev Med, 1990. **41**: p. 99-115.

187. Sesti, G., et al., *Tissue-specific expression of two alternatively spliced isoforms of the human insulin receptor protein.* Acta Diabetol, 1994. **31**(2): p. 59-65.

188. Yamaguchi, Y., et al., *Functional properties of two naturally occurring isoforms of the human insulin receptor in Chinese hamster ovary cells.* Endocrinology, 1991. **129**(4): p. 2058-66.

189. Elchebly, M., et al., *Increased insulin sensitivity and obesity resistance in mice lacking the protein tyrosine phosphatase-1B gene.* Science, 1999. **283**(5407): p. 1544-8.

190. Ueki, K., T. Kondo, and C.R. Kahn, *Suppressor of cytokine signaling 1 (SOCS-1) and SOCS-3 cause insulin resistance through inhibition of tyrosine phosphorylation of insulin receptor substrate proteins by discrete mechanisms.* Mol Cell Biol, 2004. **24**(12): p. 5434-46.

191. Friedman, J.E., et al., *Reduced insulin receptor signaling in the obese spontaneously hypertensive Koletsky rat.* Am J Physiol, 1997. **273**(5 Pt 1): p. E1014-23.

192. Ullrich, A. and J. Schlessinger, *Signal transduction by receptors with tyrosine kinase activity.* Cell, 1990. **61**(2): p. 203-12.

193. Taniguchi, C.M., B. Emanuelli, and C.R. Kahn, *Critical nodes in signalling pathways: insights into insulin action.* Nat Rev Mol Cell Biol, 2006. **7**(2): p. 85-96.

194. Sun, X.J., et al., *Structure of the insulin receptor substrate IRS-1 defines a unique signal transduction protein.* Nature, 1991. **352**(6330): p. 73-7.

195. Sun, X.J., et al., *Role of IRS-2 in insulin and cytokine signalling.* Nature, 1995. **377**(6545): p. 173-7.

196. Vinciguerra, M. and M. Foti, *PTEN and SHIP2 phosphoinositide phosphatases as negative regulators of insulin signalling.* Arch Physiol Biochem, 2006. **112**(2): p. 89-104.

197. Engelman, J.A., J. Luo, and L.C. Cantley, *The evolution of phosphatidylinositol 3-kinases as regulators of growth and metabolism.* Nat Rev Genet, 2006. **7**(8): p. 606-19.

198. Odorizzi, G., M. Babst, and S.D. Emr, *Phosphoinositide signaling and the regulation of membrane trafficking in yeast.* Trends Biochem Sci, 2000. **25**(5): p. 229-35.

199. Songyang, Z., et al., *SH2 domains recognize specific phosphopeptide sequences.* Cell, 1993. **72**(5): p. 767-78.

200. Yu, J., et al., *Regulation of the p85/p110 phosphatidylinositol 3'-kinase: stabilization and inhibition of the p110alpha catalytic subunit by the p85 regulatory subunit.* Mol Cell Biol, 1998. **18**(3): p. 1379-87.

201. DiNitto, J.P., T.C. Cronin, and D.G. Lambright, *Membrane recognition and targeting by lipid-binding domains.* Sci STKE, 2003. **2003**(213): p. re16.

202. Chan, T.O., S.E. Rittenhouse, and P.N. Tsichlis, *AKT/PKB and other D3 phosphoinositide-regulated kinases: kinase activation by phosphoinositide-dependent phosphorylation.* Annu Rev Biochem, 1999. **68**: p. 965-1014.

203. Sarbassov, D.D., et al., *Phosphorylation and regulation of Akt/PKB by the rictor-mTOR complex.* Science, 2005. **307**(5712): p. 1098-101.

204. Gao, T., F. Furnari, and A.C. Newton, *PHLPP: a phosphatase that directly dephosphorylates Akt, promotes apoptosis, and suppresses tumor growth.* Mol Cell, 2005. **18**(1): p. 13-24.

205. Sano, H., et al., *Insulin-stimulated phosphorylation of a Rab GTPase-activating protein regulates GLUT4 translocation.* J Biol Chem, 2003. **278**(17): p. 14599-602.

206. Thong, F.S., C.B. Dugani, and A. Klip, *Turning signals on and off: GLUT4 traffic in the insulin-signaling highway.* Physiology (Bethesda), 2005. **20**: p. 271-84.

207. Marette, A., et al., *Abundance, localization, and insulin-induced translocation of glucose transporters in red and white muscle.* Am J Physiol, 1992. **263**(2 Pt 1): p. C443-52.

208. Cohen, P. and S. Frame, *The renaissance of GSK3.* Nat Rev Mol Cell Biol, 2001. **2**(10): p. 769-76.

209. Berwick, D.C., et al., *The identification of ATP-citrate lyase as a protein kinase B (Akt) substrate in primary adipocytes.* J Biol Chem, 2002. **277**(37): p. 33895-900.

210. Richardson, C.J., S.S. Schalm, and J. Blenis, *PI3-kinase and TOR: PIKTORing cell growth.* Semin Cell Dev Biol, 2004. **15**(2): p. 147-59.

211. Dimmeler, S., et al., *Activation of nitric oxide synthase in endothelial cells by Akt-dependent phosphorylation.* Nature, 1999. **399**(6736): p. 601-5.

212. Montagnani, M., et al., *Insulin-stimulated activation of eNOS is independent of Ca2+ but requires phosphorylation by Akt at Ser(1179).* J Biol Chem, 2001. **276**(32): p. 30392-8.

213. Davis, M.E., et al., *Shear stress regulates endothelial nitric oxide synthase expression through c-Src by divergent signaling pathways.* Circ Res, 2001. **89**(11): p. 1073-80.

214. Burgering, B.M. and R.H. Medema, *Decisions on life and death: FOXO Forkhead transcription factors are in command when PKB/Akt is off duty.* J Leukoc Biol, 2003. **73**(6): p. 689-701.

215. Vivanco, I. and C.L. Sawyers, *The phosphatidylinositol 3-Kinase AKT pathway in human cancer.* Nat Rev Cancer, 2002. **2**(7): p. 489-501.

216. Pouyssegur, J., V. Volmat, and P. Lenormand, *Fidelity and spatio-temporal control in MAP kinase (ERKs) signalling.* Biochem Pharmacol, 2002. **64**(5-6): p. 755-63.

217. Iglarz, M., et al., *Chronic blockade of endothelin receptors improves ischemia-induced angiogenesis in rat hindlimbs through activation of vascular endothelial growth factor-no pathway.* Arterioscler Thromb Vasc Biol, 2001. **21**(10): p. 1598-603.

218. Jiang, Z.Y., et al., *Endothelin-1 modulates insulin signaling through phosphatidylinositol 3-kinase pathway in vascular smooth muscle cells.* Diabetes, 1999. **48**(5): p. 1120-30.

219. Strawbridge, A.B. and J.S. Elmendorf, *Endothelin-1 impairs glucose transporter trafficking via a membrane-based mechanism.* J Cell Biochem, 2006. **97**(4): p. 849-56.

220. Bouzakri, K., et al., *Reduced activation of phosphatidylinositol-3 kinase and increased serine 636 phosphorylation of insulin receptor substrate-1 in primary culture of skeletal muscle cells from patients with type 2 diabetes.* Diabetes, 2003. **52**(6): p. 1319-25.

221. Lemmon, M.A. and J. Schlessinger, *Cell signaling by receptor tyrosine kinases.* Cell, 2010. **141**(7): p. 1117-34.

222. Virkamaki, A., K. Ueki, and C.R. Kahn, *Protein-protein interaction in insulin signaling and the molecular mechanisms of insulin resistance.* J Clin Invest, 1999. **103**(7): p. 931-43.

223. Almind, K., et al., *Aminoacid polymorphisms of insulin receptor substrate-1 in non-insulin-dependent diabetes mellitus.* Lancet, 1993. **342**(8875): p. 828-32.

224. Whitehead, J.P., et al., *Molecular scanning of the insulin receptor substrate 1 gene in subjects with severe insulin resistance: detection and functional analysis of a naturally occurring mutation in a YMXM motif.* Diabetes, 1998. **47**(5): p. 837-9.

225. Araki, E., et al., *Alternative pathway of insulin signalling in mice with targeted disruption of the IRS-1 gene.* Nature, 1994. **372**(6502): p. 186-90.

226. Hansen, T., et al., *Identification of a common amino acid polymorphism in the p85alpha regulatory subunit of phosphatidylinositol 3-kinase: effects on glucose disappearance constant, glucose effectiveness, and the insulin sensitivity index.* Diabetes, 1997. **46**(3): p. 494-501.

227. Willemsen, G., et al., *The Concordance and Heritability of Type 2 Diabetes in 34,166 Twin Pairs From International Twin Registers: The Discordant Twin (DISCOTWIN) Consortium.* Twin Res Hum Genet, 2015. **18**(6): p. 762-71.

228. Grundy, S.M., et al., *Definition of metabolic syndrome: Report of the National Heart, Lung, and Blood Institute/American Heart Association conference on scientific issues related to definition.* Circulation, 2004. **109**(3): p. 433-8.

229. Cubbon, R.M., et al., *Insulin- and growth factor-resistance impairs vascular regeneration in diabetes mellitus.* Curr Vasc Pharmacol, 2012. **10**(3): p. 271-84.

230. Wright, J.J., et al., *Mechanisms for increased myocardial fatty acid utilization following short-term high-fat feeding.* Cardiovasc Res, 2009. **82**(2): p. 351-60.

231. Cook, S.A., et al., *Abnormal myocardial insulin signalling in type 2 diabetes and left-ventricular dysfunction.* Eur Heart J, 2010. **31**(1): p. 100-11.

232. Nishikawa, T., et al., *Normalizing mitochondrial superoxide production blocks three pathways of hyperglycaemic damage.* Nature, 2000. **404**(6779): p. 787-90.

233. Wautier, M.P., et al., *Activation of NADPH oxidase by AGE links oxidant stress to altered gene expression via RAGE.* Am J Physiol Endocrinol Metab, 2001. **280**(5): p. E685-94.

234. Buse, M.G., *Hexosamines, insulin resistance, and the complications of diabetes: current status.* Am J Physiol Endocrinol Metab, 2006. **290**(1): p. E1-E8.

235. Fan, H.C., C. Fernandez-Hernando, and J.H. Lai, *Protein kinase C isoforms in atherosclerosis: pro- or anti-inflammatory?* Biochem Pharmacol, 2014. **88**(2): p. 139-49.

236.　Harja, E., et al., *Mice deficient in PKCbeta and apolipoprotein E display decreased atherosclerosis.* Faseb j, 2009. **23**(4): p. 1081-91.

237.　Kalousova, M., J. Skrha, and T. Zima, *Advanced glycation end-products and advanced oxidation protein products in patients with diabetes mellitus.* Physiol Res, 2002. **51**(6): p. 597-604.

238.　Kilhovd, B.K., et al., *Serum levels of advanced glycation end products are increased in patients with type 2 diabetes and coronary heart disease.* Diabetes Care, 1999. **22**(9): p. 1543-8.

239.　Haffner, S.M., *Epidemiological studies on the effects of hyperglycemia and improvement of glycemic control on macrovascular events in type 2 diabetes.* Diabetes Care, 1999. **22 Suppl 3**: p. C54-6.

240.　Lowell, B.B. and G.I. Shulman, *Mitochondrial dysfunction and type 2 diabetes.* Science, 2005. **307**(5708): p. 384-7.

241.　Murphy, M.P., et al., *Superoxide activates uncoupling proteins by generating carbon-centered radicals and initiating lipid peroxidation: studies using a mitochondria-targeted spin trap derived from alpha-phenyl-N-tert-butylnitrone.* J Biol Chem, 2003. **278**(49): p. 48534-45.

242.　Furukawa, S., et al., *Increased oxidative stress in obesity and its impact on metabolic syndrome.* J Clin Invest, 2004. **114**(12): p. 1752-61.

243.　Adams, J.M., 2nd, et al., *Ceramide content is increased in skeletal muscle from obese insulin-resistant humans.* Diabetes, 2004. **53**(1): p. 25-31.

244.　Chavez, J.A., et al., *A role for ceramide, but not diacylglycerol, in the antagonism of insulin signal transduction by saturated fatty acids.* J Biol Chem, 2003. **278**(12): p. 10297-303.

245.　Song, Y., et al., *TLR4/NF-kappaB/Ceramide signaling contributes to Ox-LDL-induced calcification of human vascular smooth muscle cells.* Eur J Pharmacol, 2017. **794**: p. 45-51.

246.　Ridker, P.M., et al., *Antiinflammatory Therapy with Canakinumab for Atherosclerotic Disease.* N Engl J Med, 2017. **377**(12): p. 1119-1131.

247.　Kamata, H., et al., *Reactive oxygen species promote TNFalpha-induced death and sustained JNK activation by inhibiting MAP kinase phosphatases.* Cell, 2005. **120**(5): p. 649-61.

248.　Nguyen, M.T., et al., *JNK and tumor necrosis factor-alpha mediate free fatty acid-induced insulin resistance in 3T3-L1 adipocytes.* J Biol Chem, 2005. **280**(42): p. 35361-71.

249.　Emanuelli, B., et al., *SOCS-3 inhibits insulin signaling and is up-regulated in response to tumor necrosis factor-alpha in the adipose tissue of obese mice.* J Biol Chem, 2001. **276**(51): p. 47944-9.

250.　Pradhan, A.D., et al., *C-reactive protein, interleukin 6, and risk of developing type 2 diabetes mellitus.* JAMA, 2001. **286**(3): p. 327-34.

251.　Okamoto, Y., et al., *Adiponectin reduces atherosclerosis in apolipoprotein E-deficient mice.* Circulation, 2002. **106**(22): p. 2767-70.

252.　Moroi, M., et al., *Lower ratio of high-molecular-weight adiponectin level to total may be associated with coronary high-risk plaque.* BMC Res Notes, 2013. **6**: p. 83.

253.	Sawada, T., et al., *Low plasma adiponectin levels are associated with presence of thin-cap fibroatheroma in men with stable coronary artery disease.* Int J Cardiol, 2010. **142**(3): p. 250-6.

254.	Bickel, C., et al., *Predictors of leptin concentration and association with cardiovascular risk in patients with coronary artery disease: results from the AtheroGene study.* Biomarkers, 2017. **22**(3-4): p. 210-218.

255.	Lu, L.F., et al., *Interpretation of elevated plasma visfatin concentrations in patients with ST-elevation myocardial infarction.* Cytokine, 2012. **57**(1): p. 74-80.

256.	Betteridge, D.J., *What is oxidative stress?* Metabolism, 2000. **49**(2 Suppl 1): p. 3-8.

257.	Liou, G.Y. and P. Storz, *Reactive oxygen species in cancer.* Free Radic Res, 2010. **44**(5): p. 479-96.

258.	Ali N, K.M., Cubbon RM, *The role of reactive oxygen species in insulin resistance-associated cardiovascular disease.* Diabetes Management, 2015. **5**(3): p. 203-213.

259.	Ushio-Fukai, M. and N. Urao, *Novel role of NADPH oxidase in angiogenesis and stem/progenitor cell function.* Antioxid Redox Signal, 2009. **11**(10): p. 2517-33.

260.	Konior, A., et al., *NADPH oxidases in vascular pathology.* Antioxid Redox Signal, 2014. **20**(17): p. 2794-814.

261.	Zhou, Y., et al., *Reactive oxygen species in vascular formation and development.* Oxid Med Cell Longev, 2013. **2013**: p. 374963.

262.	Dworakowski, R., S.P. Alom-Ruiz, and A.M. Shah, *NADPH oxidase-derived reactive oxygen species in the regulation of endothelial phenotype.* Pharmacol Rep, 2008. **60**(1): p. 21-8.

263.	Lassegue, B., A. San Martin, and K.K. Griendling, *Biochemistry, physiology, and pathophysiology of NADPH oxidases in the cardiovascular system.* Circ Res, 2012. **110**(10): p. 1364-90.

264.	Sumimoto, H., *Structure, regulation and evolution of Nox-family NADPH oxidases that produce reactive oxygen species.* Febs j, 2008. **275**(13): p. 3249-77.

265.	Bartosz, G., *Reactive oxygen species: destroyers or messengers?* Biochem Pharmacol, 2009. **77**(8): p. 1303-15.

266.	Nakashima, I., et al., *Redox-linked signal transduction pathways for protein tyrosine kinase activation.* Antioxid Redox Signal, 2002. **4**(3): p. 517-31.

267.	Corcoran, A. and T.G. Cotter, *Redox regulation of protein kinases.* Febs j, 2013. **280**(9): p. 1944-65.

268.	Ostman, A., et al., *Regulation of protein tyrosine phosphatases by reversible oxidation.* J Biochem, 2011. **150**(4): p. 345-56.

269.	Houstis, N., E.D. Rosen, and E.S. Lander, *Reactive oxygen species have a causal role in multiple forms of insulin resistance.* Nature, 2006. **440**(7086): p. 944-8.

270.	Shoelson, S.E., J. Lee, and A.B. Goldfine, *Inflammation and insulin resistance.* J Clin Invest, 2006. **116**(7): p. 1793-801.

271.	Sukumar, P., et al., *Nox2 NADPH oxidase has a critical role in insulin resistance-related endothelial cell dysfunction.* Diabetes, 2013. **62**(6): p. 2130-4.

272. Voinea, M., et al., *Superoxide dismutase entrapped-liposomes restore the impaired endothelium-dependent relaxation of resistance arteries in experimental diabetes.* Eur J Pharmacol, 2004. **484**(1): p. 111-8.

273. Viswambharan, H., et al., *Selective Enhancement of Insulin Sensitivity in the Endothelium In Vivo Reveals a Novel Proatherosclerotic Signaling Loop.* Circ Res, 2017. **120**(5): p. 784-798.

274. Taniyama, Y. and K.K. Griendling, *Reactive oxygen species in the vasculature: molecular and cellular mechanisms.* Hypertension, 2003. **42**(6): p. 1075-81.

275. Yun, J., et al., *Redox-dependent mechanisms in coronary collateral growth: the "redox window" hypothesis.* Antioxid Redox Signal, 2009. **11**(8): p. 1961-74.

276. Yusuf, S., et al., *Vitamin E supplementation and cardiovascular events in high-risk patients. The Heart Outcomes Prevention Evaluation Study Investigators.* N Engl J Med, 2000. **342**(3): p. 154-60.

277. Vivekananthan, D.P., et al., *Use of antioxidant vitamins for the prevention of cardiovascular disease: meta-analysis of randomised trials.* Lancet, 2003. **361**(9374): p. 2017-23.

278. Gerstein, H.C., et al., *Effects of intensive glucose lowering in type 2 diabetes.* N Engl J Med, 2008. **358**(24): p. 2545-59.

279. Mohan, S., et al., *Diabetic eNOS knockout mice develop distinct macro- and microvascular complications.* Lab Invest, 2008. **88**(5): p. 515-28.

280. Kuhlencordt, P.J., et al., *Accelerated atherosclerosis, aortic aneurysm formation, and ischemic heart disease in apolipoprotein E/endothelial nitric oxide synthase double-knockout mice.* Circulation, 2001. **104**(4): p. 448-54.

281. Kim, J.A., et al., *Reciprocal relationships between insulin resistance and endothelial dysfunction: molecular and pathophysiological mechanisms.* Circulation, 2006. **113**(15): p. 1888-904.

282. Abe, H., et al., *Hypertension, hypertriglyceridemia, and impaired endothelium-dependent vascular relaxation in mice lacking insulin receptor substrate-1.* J Clin Invest, 1998. **101**(8): p. 1784-8.

283. Federici, M., et al., *G972R IRS-1 variant impairs insulin regulation of endothelial nitric oxide synthase in cultured human endothelial cells.* Circulation, 2004. **109**(3): p. 399-405.

284. Salt, I.P., et al., *High glucose inhibits insulin-stimulated nitric oxide production without reducing endothelial nitric-oxide synthase Ser1177 phosphorylation in human aortic endothelial cells.* J Biol Chem, 2003. **278**(21): p. 18791-7.

285. Anderson, H.D., D. Rahmutula, and D.G. Gardner, *Tumor necrosis factor-alpha inhibits endothelial nitric-oxide synthase gene promoter activity in bovine aortic endothelial cells.* J Biol Chem, 2004. **279**(2): p. 963-9.

286. Quagliaro, L., et al., *Intermittent high glucose enhances ICAM-1, VCAM-1 and E-selectin expression in human umbilical vein endothelial cells in culture: the distinct role of protein kinase C and mitochondrial superoxide production.* Atherosclerosis, 2005. **183**(2): p. 259-67.

287. Huijberts, M.S., et al., *Aminoguanidine treatment increases elasticity and decreases fluid filtration of large arteries from diabetic rats.* J Clin Invest, 1993. **92**(3): p. 1407-11.

288. Venugopal, S.K., et al., *Demonstration that C-reactive protein decreases eNOS expression and bioactivity in human aortic endothelial cells.* Circulation, 2002. **106**(12): p. 1439-41.

289. Pasceri, V., J.T. Willerson, and E.T. Yeh, *Direct proinflammatory effect of C-reactive protein on human endothelial cells.* Circulation, 2000. **102**(18): p. 2165-8.

290. Jiang, Z.Y., et al., *Characterization of selective resistance to insulin signaling in the vasculature of obese Zucker (fa/fa) rats.* J Clin Invest, 1999. **104**(4): p. 447-57.

291. Ueno, M., et al., *Regulation of insulin signalling by hyperinsulinaemia: role of IRS-1/2 serine phosphorylation and the mTOR/p70 S6K pathway.* Diabetologia, 2005. **48**(3): p. 506-18.

292. Gogg, S., U. Smith, and P.A. Jansson, *Increased MAPK activation and impaired insulin signaling in subcutaneous microvascular endothelial cells in type 2 diabetes: the role of endothelin-1.* Diabetes, 2009. **58**(10): p. 2238-45.

293. Piatti, P.M., et al., *Hypertriglyceridemia and hyperinsulinemia are potent inducers of endothelin-1 release in humans.* Diabetes, 1996. **45**(3): p. 316-21.

294. Mather, K.J., et al., *Endothelin contributes to basal vascular tone and endothelial dysfunction in human obesity and type 2 diabetes.* Diabetes, 2002. **51**(12): p. 3517-23.

295. Cassaglia, P.A., et al., *Insulin acts in the arcuate nucleus to increase lumbar sympathetic nerve activity and baroreflex function in rats.* J Physiol, 2011. **589**(Pt 7): p. 1643-62.

296. Lambert, G.W., et al., *Sympathetic nervous activation in obesity and the metabolic syndrome--causes, consequences and therapeutic implications.* Pharmacol Ther, 2010. **126**(2): p. 159-72.

297. Imrie, H., et al., *Vascular insulin-like growth factor-I resistance and diet-induced obesity.* Endocrinology, 2009. **150**(10): p. 4575-82.

298. Accili, D., et al., *Early neonatal death in mice homozygous for a null allele of the insulin receptor gene.* Nat Genet, 1996. **12**(1): p. 106-9.

299. Wheatcroft, S.B., et al., *Preserved glucoregulation but attenuation of the vascular actions of insulin in mice heterozygous for knockout of the insulin receptor.* Diabetes, 2004. **53**(10): p. 2645-52.

300. Moller, D.E., et al., *A naturally occurring mutation of insulin receptor alanine 1134 impairs tyrosine kinase function and is associated with dominantly inherited insulin resistance.* J Biol Chem, 1990. **265**(25): p. 14979-85.

301. Duncan, E.R., et al., *Effect of endothelium-specific insulin resistance on endothelial function in vivo.* Diabetes, 2008. **57**(12): p. 3307-14.

302. Gage, M.C., et al., *Endothelium-specific insulin resistance leads to accelerated atherosclerosis in areas with disturbed flow patterns: a role for reactive oxygen species.* Atherosclerosis, 2013. **230**(1): p. 131-9.

303. Rask-Madsen, C., et al., *Loss of insulin signaling in vascular endothelial cells accelerates atherosclerosis in apolipoprotein E null mice.* Cell Metab, 2010. **11**(5): p. 379-89.

304. Liang, C.P., et al., *Increased CD36 protein as a response to defective insulin signaling in macrophages.* J Clin Invest, 2004. **113**(5): p. 764-73.

305. Han, S., et al., *Macrophage insulin receptor deficiency increases ER stress-induced apoptosis and necrotic core formation in advanced atherosclerotic lesions.* Cell Metab, 2006. **3**(4): p. 257-66.

306. Baumgartl, J., et al., *Myeloid lineage cell-restricted insulin resistance protects apolipoproteinE-deficient mice against atherosclerosis.* Cell Metab, 2006. **3**(4): p. 247-56.

307. Van Belle, E., et al., *Restenosis rates in diabetic patients: a comparison of coronary stenting and balloon angioplasty in native coronary vessels.* Circulation, 1997. **96**(5): p. 1454-60.

308. Elezi, S., et al., *Diabetes mellitus and the clinical and angiographic outcome after coronary stent placement.* J Am Coll Cardiol, 1998. **32**(7): p. 1866-73.

309. Abaci, A., et al., *Effect of diabetes mellitus on formation of coronary collateral vessels.* Circulation, 1999. **99**(17): p. 2239-42.

310. Chen, Y.H., et al., *High glucose impairs early and late endothelial progenitor cells by modifying nitric oxide-related but not oxidative stress-mediated mechanisms.* Diabetes, 2007. **56**(6): p. 1559-68.

311. Seeger, F.H., et al., *p38 mitogen-activated protein kinase downregulates endothelial progenitor cells.* Circulation, 2005. **111**(9): p. 1184-91.

312. Larger, E., et al., *Hyperglycemia-induced defects in angiogenesis in the chicken chorioallantoic membrane model.* Diabetes, 2004. **53**(3): p. 752-61.

313. Liu, L., et al., *Remnant-like particles accelerate endothelial progenitor cells senescence and induce cellular dysfunction via an oxidative mechanism.* Atherosclerosis, 2009. **202**(2): p. 405-14.

314. Guo, W.X., et al., *Palmitic and linoleic acids impair endothelial progenitor cells by inhibition of Akt/eNOS pathway.* Arch Med Res, 2008. **39**(4): p. 434-42.

315. Seetharam, D., et al., *High-density lipoprotein promotes endothelial cell migration and reendothelialization via scavenger receptor-B type I.* Circ Res, 2006. **98**(1): p. 63-72.

316. Rossi, F., et al., *HDL cholesterol is a strong determinant of endothelial progenitor cells in hypercholesterolemic subjects.* Microvasc Res, 2010. **80**(2): p. 274-9.

317. Dimmeler, S., et al., *Oxidized low-density lipoprotein induces apoptosis of human endothelial cells by activation of CPP32-like proteases. A mechanistic clue to the 'response to injury' hypothesis.* Circulation, 1997. **95**(7): p. 1760-3.

318. Czepluch, F.S., A. Bergler, and J. Waltenberger, *Hypercholesterolaemia impairs monocyte function in CAD patients.* J Intern Med, 2007. **261**(2): p. 201-4.

319. Verma, S., et al., *C-reactive protein attenuates endothelial progenitor cell survival, differentiation, and function: further evidence of a mechanistic link between C-reactive protein and cardiovascular disease.* Circulation, 2004. **109**(17): p. 2058-67.

320. Schweighofer, B., et al., *The VEGF-induced transcriptional response comprises gene clusters at the crossroad of angiogenesis and inflammation.* Thromb Haemost, 2009. **102**(3): p. 544-54.

321. Chang, J., et al., *Adiponectin prevents diabetic premature senescence of endothelial progenitor cells and promotes endothelial repair by suppressing the p38 MAP kinase/p16INK4A signaling pathway.* Diabetes, 2010. **59**(11): p. 2949-59.

322. Ouchi, N., et al., *Adiponectin stimulates angiogenesis by promoting cross-talk between AMP-activated protein kinase and Akt signaling in endothelial cells.* J Biol Chem, 2004. **279**(2): p. 1304-9.

323. Wolk, R., et al., *Leptin receptor and functional effects of leptin in human endothelial progenitor cells.* Atherosclerosis, 2005. **183**(1): p. 131-9.

324. Schroder, K., et al., *NADPH oxidase Nox2 is required for hypoxia-induced mobilization of endothelial progenitor cells.* Circ Res, 2009. **105**(6): p. 537-44.

325. Ushio-Fukai, M., et al., *Novel role of gp91(phox)-containing NAD(P)H oxidase in vascular endothelial growth factor-induced signaling and angiogenesis.* Circ Res, 2002. **91**(12): p. 1160-7.

326. Ii, M., et al., *Endothelial progenitor thrombospondin-1 mediates diabetes-induced delay in reendothelialization following arterial injury.* Circ Res, 2006. **98**(5): p. 697-704.

327. Kahn, M.B., et al., *Insulin resistance impairs circulating angiogenic progenitor cell function and delays endothelial regeneration.* Diabetes, 2011. **60**(4): p. 1295-303.

328. Cubbon, R.M., et al., *Restoring Akt1 activity in outgrowth endothelial cells from South Asian men rescues vascular reparative potential.* Stem Cells, 2014. **32**(10): p. 2714-23.

329. Murohara, T., et al., *Nitric oxide synthase modulates angiogenesis in response to tissue ischemia.* J Clin Invest, 1998. **101**(11): p. 2567-78.

330. Hayashi, T., et al., *Nitric oxide and endothelial cellular senescence.* Pharmacol Ther, 2008. **120**(3): p. 333-9.

331. Ahanchi, S.S., et al., *Heightened efficacy of nitric oxide-based therapies in type II diabetes mellitus and metabolic syndrome.* Am J Physiol Heart Circ Physiol, 2008. **295**(6): p. H2388-98.

332. Kondo, T., et al., *Knockout of insulin and IGF-1 receptors on vascular endothelial cells protects against retinal neovascularization.* J Clin Invest, 2003. **111**(12): p. 1835-42.

333. Ackah, E., et al., *Akt1/protein kinase Balpha is critical for ischemic and VEGF-mediated angiogenesis.* J Clin Invest, 2005. **115**(8): p. 2119-27.

334. Pedram, A., M. Razandi, and E.R. Levin, *Extracellular signal-regulated protein kinase/Jun kinase cross-talk underlies vascular endothelial cell growth factor-induced endothelial cell proliferation.* J Biol Chem, 1998. **273**(41): p. 26722-8.

335. Astle, M.V., et al., *The inositol polyphosphate 5-phosphatases: traffic controllers, waistline watchers and tumour suppressors?* Biochem Soc Symp, 2007(74): p. 161-81.

336. De Smedt, F., et al., *Cloning and expression of human brain type I inositol 1,4,5-trisphosphate 5-phosphatase. High levels of mRNA in cerebellar Purkinje cells.* FEBS Lett, 1994. **347**(1): p. 69-72.

337. Ijuin, T., et al., *Identification and characterization of a novel inositol polyphosphate 5-phosphatase.* J Biol Chem, 2000. **275**(15): p. 10870-5.

338. Astle, M.V., et al., *Regulation of phosphoinositide signaling by the inositol polyphosphate 5-phosphatases.* IUBMB Life, 2006. **58**(8): p. 451-6.

339. Verstreken, P., et al., *Synaptojanin is recruited by endophilin to promote synaptic vesicle uncoating.* Neuron, 2003. **40**(4): p. 733-48.

340. Ooms, L.M., et al., *The role of the inositol polyphosphate 5-phosphatases in cellular function and human disease.* Biochem J, 2009. **419**(1): p. 29-49.

341. Damen, J.E., et al., *The 145-kDa protein induced to associate with Shc by multiple cytokines is an inositol tetraphosphate and phosphatidylinositol 3,4,5-triphosphate 5-phosphatase.* Proc Natl Acad Sci U S A, 1996. **93**(4): p. 1689-93.

342. Liu, Q., et al., *The SH2-containing inositol polyphosphate 5-phosphatase, ship, is expressed during hematopoiesis and spermatogenesis.* Blood, 1998. **91**(8): p. 2753-9.

343. Schurmans, S., et al., *The mouse SHIP2 (Inppl1) gene: complementary DNA, genomic structure, promoter analysis, and gene expression in the embryo and adult mouse.* Genomics, 1999. **62**(2): p. 260-71.

344. Pesesse, X., et al., *Identification of a second SH2-domain-containing protein closely related to the phosphatidylinositol polyphosphate 5-phosphatase SHIP.* Biochem Biophys Res Commun, 1997. **239**(3): p. 697-700.

345. Hejna, J.A., et al., *Cloning and characterization of a human cDNA (INPPL1) sharing homology with inositol polyphosphate phosphatases.* Genomics, 1995. **29**(1): p. 285-7.

346. Backers, K., et al., *The termination of PI3K signalling by SHIP1 and SHIP2 inositol 5-phosphatases.* Advances in Enzyme Regulation, 2003. **43**(1): p. 15-28.

347. Suwa, A., T. Kurama, and T. Shimokawa, *SHIP2 and its involvement in various diseases.* Expert Opin Ther Targets, 2010. **14**(7): p. 727-37.

348. Olsen, J.V., et al., *Global, in vivo, and site-specific phosphorylation dynamics in signaling networks.* Cell, 2006. **127**(3): p. 635-48.

349. Habib, T., et al., *Growth Factors and Insulin Stimulate Tyrosine Phosphorylation of the 51C/SHIP2 Protein.* Journal of Biological Chemistry, 1998. **273**(29): p. 18605-18609.

350. Sorkin, A. and M. von Zastrow, *Endocytosis and signalling: intertwining molecular networks.* Nat Rev Mol Cell Biol, 2009. **10**(9): p. 609-22.

351. Erneux, C., et al., *SHIP2 multiple functions: a balance between a negative control of PtdIns(3,4,5)P(3) level, a positive control of PtdIns(3,4)P(2) production, and intrinsic docking properties.* J Cell Biochem, 2011. **112**(9): p. 2203-9.

352. Ishihara, H., et al., *Molecular cloning of rat SH2-containing inositol phosphatase 2 (SHIP2) and its role in the regulation of insulin signaling.* Biochem Biophys Res Commun, 1999. **260**(1): p. 265-72.

353. Whisstock, J.C., et al., *The inositol polyphosphate 5-phosphatases and the apurinic/apyrimidinic base excision repair endonucleases share a common mechanism for catalysis.* J Biol Chem, 2000. **275**(47): p. 37055-61.

354. Pesesse, X., et al., *The SH2 domain containing inositol 5-phosphatase SHIP2 displays phosphatidylinositol 3,4,5-trisphosphate and inositol 1,3,4,5-tetrakisphosphate 5-phosphatase activity.* FEBS Lett, 1998. **437**(3): p. 301-3.

355. Nakatsu, F., et al., *The inositol 5-phosphatase SHIP2 regulates endocytic clathrin-coated pit dynamics.* J Cell Biol, 2010. **190**(3): p. 307-15.

356. Dyson, J.M., et al., *SHIP-2 forms a tetrameric complex with filamin, actin, and GPIb-IX-V: localization of SHIP-2 to the activated platelet actin cytoskeleton.* Blood, 2003. **102**(3): p. 940-8.

357. Elong Edimo, W., J.M. Vanderwinden, and C. Erneux, *SHIP2 signalling at the plasma membrane, in the nucleus and at focal contacts.* Adv Biol Regul, 2013. **53**(1): p. 28-37.

358. Deneubourg, L., J.M. Vanderwinden, and C. Erneux, *Regulation of SHIP2 function through plasma membrane interaction.* Adv Enzyme Regul, 2010. **50**(1): p. 262-71.

359. Prasad, N.K., M.E. Werner, and S.J. Decker, *Specific tyrosine phosphorylations mediate signal-dependent stimulation of SHIP2 inositol phosphatase activity, while the SH2 domain confers an inhibitory effect to maintain the basal activity.* Biochemistry, 2009. **48**(27): p. 6285-7.

360. Maehama, T. and J.E. Dixon, *The tumor suppressor, PTEN/MMAC1, dephosphorylates the lipid second messenger, phosphatidylinositol 3,4,5-trisphosphate.* J Biol Chem, 1998. **273**(22): p. 13375-8.

361. Myers, M.P., et al., *The lipid phosphatase activity of PTEN is critical for its tumor supressor function.* Proc Natl Acad Sci U S A, 1998. **95**(23): p. 13513-8.

362. Sasaoka, T., et al., *Inhibition of endogenous SHIP2 ameliorates insulin resistance caused by chronic insulin treatment in 3T3-L1 adipocytes.* Diabetologia, 2005. **48**(2): p. 336-44.

363. Aman, M.J., et al., *The inositol phosphatase SHIP inhibits Akt/PKB activation in B cells.* J Biol Chem, 1998. **273**(51): p. 33922-8.

364. Blero, D., et al., *The SH2 domain containing inositol 5-phosphatase SHIP2 controls phosphatidylinositol 3,4,5-trisphosphate levels in CHO-IR cells stimulated by insulin.* Biochem Biophys Res Commun, 2001. **282**(3): p. 839-43.

365. Tang, X., et al., *PTEN, but not SHIP2, suppresses insulin signaling through the phosphatidylinositol 3-kinase/Akt pathway in 3T3-L1 adipocytes.* J Biol Chem, 2005. **280**(23): p. 22523-9.

366. Vandenbroere, I., et al., *The c-Cbl-associated protein and c-Cbl are two new partners of the SH2-containing inositol polyphosphate 5-phosphatase SHIP2.* Biochem Biophys Res Commun, 2003. **300**(2): p. 494-500.

367. Dyson, J.M., et al., *The SH2-containing inositol polyphosphate 5-phosphatase, SHIP-2, binds filamin and regulates submembraneous actin.* J Cell Biol, 2001. **155**(6): p. 1065-79.

368. Sasaoka, T., et al., *Dual role of SRC homology domain 2-containing inositol phosphatase 2 in the regulation of platelet-derived growth factor and insulin-like growth factor I signaling in rat vascular smooth muscle cells.* Endocrinology, 2003. **144**(9): p. 4204-14.

369. Gorgani-Firuzjaee, S. and R. Meshkani, *SH2 domain-containing inositol 5-phosphatase (SHIP2) inhibition ameliorates high glucose-induced de-novo lipogenesis and VLDL production through regulating AMPK/mTOR/SREBP1 pathway and ROS production in HepG2 cells.* Free Radic Biol Med, 2015. **89**: p. 679-89.

370. Suwa, A., et al., *Discovery and functional characterization of a novel small molecule inhibitor of the intracellular phosphatase, SHIP2.* Br J Pharmacol, 2009. **158**(3): p. 879-87.

371. Annis, D.A., et al., *Inhibitors of the lipid phosphatase SHIP2 discovered by high-throughput affinity selection-mass spectrometry screening of combinatorial libraries.* Comb Chem High Throughput Screen, 2009. **12**(8): p. 760-71.

372. Hori, H., et al., *Association of SH2-containing inositol phosphatase 2 with the insulin resistance of diabetic db/db mice.* Diabetes, 2002. **51**(8): p. 2387-94.

373. Kagawa, S., et al., *Impact of transgenic overexpression of SH2-containing inositol 5'-phosphatase 2 on glucose metabolism and insulin signaling in mice.* Endocrinology, 2008. **149**(2): p. 642-50.

374. Clement, S., et al., *The lipid phosphatase SHIP2 controls insulin sensitivity.* Nature, 2001. **409**(6816): p. 92-7.

375. Brunet, J.F. and A. Pattyn, *Phox2 genes - from patterning to connectivity.* Curr Opin Genet Dev, 2002. **12**(4): p. 435-40.

376. Sleeman, M.W., et al., *Absence of the lipid phosphatase SHIP2 confers resistance to dietary obesity.* Nat Med, 2005. **11**(2): p. 199-205.

377. Dubois, E., et al., *Developmental defects and rescue from glucose intolerance of a catalytically-inactive novel Ship2 mutant mouse.* Cell Signal, 2012. **24**(11): p. 1971-80.

378. Marion, E., et al., *The gene INPPL1, encoding the lipid phosphatase SHIP2, is a candidate for type 2 diabetes in rat and man.* Diabetes, 2002. **51**(7): p. 2012-7.

379. Kaisaki, P.J., et al., *Polymorphisms in type II SH2 domain-containing inositol 5-phosphatase (INPPL1, SHIP2) are associated with physiological abnormalities of the metabolic syndrome.* Diabetes, 2004. **53**(7): p. 1900-4.

380. Kagawa, S., et al., *Impact of SRC homology 2-containing inositol 5'-phosphatase 2 gene polymorphisms detected in a Japanese population on insulin signaling.* J Clin Endocrinol Metab, 2005. **90**(5): p. 2911-9.

381. Ishida, S., et al., *Association of SH-2 containing inositol 5'-phosphatase 2 gene polymorphisms and hyperglycemia.* Pancreas, 2006. **33**(1): p. 63-7.

382. Di Paolo, G. and P. De Camilli, *Phosphoinositides in cell regulation and membrane dynamics.* Nature, 2006. **443**(7112): p. 651-7.

383. Yoshinaga, S., et al., *A phosphatidylinositol lipids system, lamellipodin, and Ena/VASP regulate dynamic morphology of multipolar migrating cells in the developing cerebral cortex.* J Neurosci, 2012. **32**(34): p. 11643-56.

384. Wullschleger, S., et al., *Role of TAPP1 and TAPP2 adaptor binding to PtdIns(3,4)P2 in regulating insulin sensitivity defined by knock-in analysis.* Biochem J, 2011. **434**(2): p. 265-74.

385. Franke, T.F., et al., *Direct regulation of the Akt proto-oncogene product by phosphatidylinositol-3,4-bisphosphate.* Science, 1997. **275**(5300): p. 665-8.

386. El-Lebedy, D., H.M. Raslan, and A.M. Mohammed, *Apolipoprotein E gene polymorphism and risk of type 2 diabetes and cardiovascular disease.* Cardiovasc Diabetol, 2016. **15**: p. 12.

387. DeKroon, R., et al., *APOE4-VLDL inhibits the HDL-activated phosphatidylinositol 3-kinase/Akt Pathway via the phosphoinositol phosphatase SHIP2.* Circ Res, 2006. **99**(8): p. 829-36.

388. Prasad, N.K., et al., *Phosphoinositol phosphatase SHIP2 promotes cancer development and metastasis coupled with alterations in EGF receptor turnover.* Carcinogenesis, 2008. **29**(1): p. 25-34.

389. Mitsushima, M., K. Ueda, and N. Kioka, *Vinexin beta regulates the phosphorylation of epidermal growth factor receptor on the cell surface.* Genes Cells, 2006. **11**(9): p. 971-82.

390. Wendel, H.G., et al., *Survival signalling by Akt and eIF4E in oncogenesis and cancer therapy.* Nature, 2004. **428**(6980): p. 332-7.

391. Yu, J., et al., *MicroRNA-184 antagonizes microRNA-205 to maintain SHIP2 levels in epithelia.* Proc Natl Acad Sci U S A, 2008. **105**(49): p. 19300-5.

392. Choi, Y., et al., *PTEN, but not SHIP and SHIP2, suppresses the PI3K/Akt pathway and induces growth inhibition and apoptosis of myeloma cells.* Oncogene, 2002. **21**(34): p. 5289-300.

393. Elong Edimo, W., et al., *SHIP2 controls plasma membrane PI(4,5)P2 thereby participating in the control of cell migration in 1321 N1 glioblastoma cells.* J Cell Sci, 2016. **129**(6): p. 1101-14.

394. Agollah, G.D., et al., *Evidence for SH2 domain-containing 5'-inositol phosphatase-2 (SHIP2) contributing to a lymphatic dysfunction.* PLoS One, 2014. **9**(11): p. e112548.

395. Cagnol, S. and J.C. Chambard, *ERK and cell death: mechanisms of ERK-induced cell death--apoptosis, autophagy and senescence.* FEBS J, 2010. **277**(1): p. 2-21.

396. Takabayashi, T., et al., *LL5beta directs the translocation of filamin A and SHIP2 to sites of phosphatidylinositol 3,4,5-triphosphate (PtdIns(3,4,5)P3) accumulation, and PtdIns(3,4,5)P3 localization is mutually modified by co-recruited SHIP2.* J Biol Chem, 2010. **285**(21): p. 16155-65.

397. Prasad, N., R.S. Topping, and S.J. Decker, *SH2-containing inositol 5'-phosphatase SHIP2 associates with the p130(Cas) adapter protein and regulates cellular adhesion and spreading.* Mol Cell Biol, 2001. **21**(4): p. 1416-28.

398. Kato, K., et al., *The inositol 5-phosphatase SHIP2 is an effector of RhoA and is involved in cell polarity and migration.* Mol Biol Cell, 2012. **23**(13): p. 2593-604.

399. Larson-Meyer, D.E., et al., *Effect of calorie restriction with or without exercise on insulin sensitivity, beta-cell function, fat cell size, and ectopic lipid in overweight subjects.* Diabetes Care, 2006. **29**(6): p. 1337-44.

400. De Filippis, E., et al., *Exercise-induced improvement in vasodilatory function accompanies increased insulin sensitivity in obesity and type 2 diabetes mellitus.* J Clin Endocrinol Metab, 2006. **91**(12): p. 4903-10.

401. Hamdy, O., et al., *Lifestyle modification improves endothelial function in obese subjects with the insulin resistance syndrome.* Diabetes Care, 2003. **26**(7): p. 2119-25.

402. Sasaki, S., et al., *A low-calorie diet improves endothelium-dependent vasodilation in obese patients with essential hypertension.* Am J Hypertens, 2002. **15**(4 Pt 1): p. 302-9.

403. Hotta, K., et al., *Plasma concentrations of a novel, adipose-specific protein, adiponectin, in type 2 diabetic patients.* Arterioscler Thromb Vasc Biol, 2000. **20**(6): p. 1595-9.

404. Wing, R.R., et al., *Cardiovascular effects of intensive lifestyle intervention in type 2 diabetes.* N Engl J Med, 2013. **369**(2): p. 145-54.

405. Hermann, T.S., et al., *Quinapril treatment increases insulin-stimulated endothelial function and adiponectin gene expression in patients with type 2 diabetes.* J Clin Endocrinol Metab, 2006. **91**(3): p. 1001-8.

406. Koh, K.K., et al., *Vascular and metabolic effects of combined therapy with ramipril and simvastatin in patients with type 2 diabetes.* Hypertension, 2005. **45**(6): p. 1088-93.

407. Istvan, E., *Statin inhibition of HMG-CoA reductase: a 3-dimensional view.* Atheroscler Suppl, 2003. **4**(1): p. 3-8.

408. Economides, P.A., et al., *The effects of atorvastatin on endothelial function in diabetic patients and subjects at risk for type 2 diabetes.* J Clin Endocrinol Metab, 2004. **89**(2): p. 740-7.

409. Collier, C.A., et al., *Metformin counters the insulin-induced suppression of fatty acid oxidation and stimulation of triacylglycerol storage in rodent skeletal muscle.* Am J Physiol Endocrinol Metab, 2006. **291**(1): p. E182-9.

410. Davis, B.J., et al., *Activation of the AMP-activated kinase by antidiabetes drug metformin stimulates nitric oxide synthesis in vivo by promoting the association of heat shock protein 90 and endothelial nitric oxide synthase.* Diabetes, 2006. **55**(2): p. 496-505.

411. Orio, F., Jr., et al., *Improvement in endothelial structure and function after metformin treatment in young normal-weight women with polycystic ovary syndrome: results of a 6-month study.* J Clin Endocrinol Metab, 2005. **90**(11): p. 6072-6.

412. Koh, K.K., et al., *Beneficial effects of fenofibrate to improve endothelial dysfunction and raise adiponectin levels in patients with primary hypertriglyceridemia.* Diabetes Care, 2005. **28**(6): p. 1419-24.

413. Waki, H., T. Yamauchi, and T. Kadowaki, *[Regulation of differentiation and hypertrophy of adipocytes and adipokine network by PPARgamma].* Nihon Rinsho, 2010. **68**(2): p. 210-6.

414. Pistrosch, F., et al., *In type 2 diabetes, rosiglitazone therapy for insulin resistance ameliorates endothelial dysfunction independent of glucose control.* Diabetes Care, 2004. **27**(2): p. 484-90.

415. Hsueh, W.A. and R.E. Law, *PPARgamma and atherosclerosis: effects on cell growth and movement.* Arterioscler Thromb Vasc Biol, 2001. **21**(12): p. 1891-5.

416. Nissen, S.E. and K. Wolski, *Effect of rosiglitazone on the risk of myocardial infarction and death from cardiovascular causes.* N Engl J Med, 2007. **356**(24): p. 2457-71.

417. Home, P.D., et al., *Rosiglitazone evaluated for cardiovascular outcomes in oral agent combination therapy for type 2 diabetes (RECORD): a multicentre, randomised, open-label trial.* Lancet, 2009. **373**(9681): p. 2125-35.

418. Marso, S.P., et al., *Liraglutide and Cardiovascular Outcomes in Type 2 Diabetes.* N Engl J Med, 2016. **375**(4): p. 311-22.

419. Green, J.B., et al., *Effect of Sitagliptin on Cardiovascular Outcomes in Type 2 Diabetes.* N Engl J Med, 2015. **373**(3): p. 232-42.

420. Kim, E.S. and E.D. Deeks, *Empagliflozin/Linagliptin: A Review in Type 2 Diabetes.* Drugs, 2015. **75**(13): p. 1547-57.

421. Zinman, B., et al., *Empagliflozin, Cardiovascular Outcomes, and Mortality in Type 2 Diabetes.* N Engl J Med, 2015. **373**(22): p. 2117-28.

422. Tikkanen, I., et al., *Empagliflozin reduces blood pressure in patients with type 2 diabetes and hypertension.* Diabetes Care, 2015. **38**(3): p. 420-8.

423. Dong, L., et al., *Insulin modulates ischemia-induced endothelial progenitor cell mobilization and neovascularization in diabetic mice.* Microvasc Res, 2011. **82**(3): p. 227-36.

424. Breen, D.M., et al., *Insulin increases reendothelialization and inhibits cell migration and neointimal growth after arterial injury.* Arterioscler Thromb Vasc Biol, 2009. **29**(7): p. 1060-6.

425. Chen, J.X. and A. Stinnett, *Ang-1 gene therapy inhibits hypoxia-inducible factor-1alpha (HIF-1alpha)-prolyl-4-hydroxylase-2, stabilizes HIF-1alpha expression, and normalizes immature vasculature in db/db mice.* Diabetes, 2008. **57**(12): p. 3335-43.

426. Sarkar, K., et al., *Adenoviral transfer of HIF-1alpha enhances vascular responses to critical limb ischemia in diabetic mice.* Proc Natl Acad Sci U S A, 2009. **106**(44): p. 18769-74.

427. Cao, L., et al., *Modulating Notch signaling to enhance neovascularization and reperfusion in diabetic mice.* Biomaterials, 2010. **31**(34): p. 9048-56.

428. Carmeliet, P. and R.K. Jain, *Molecular mechanisms and clinical applications of angiogenesis.* Nature, 2011. **473**(7347): p. 298-307.

429. Di Cristofano, A., et al., *Pten is essential for embryonic development and tumour suppression.* Nat Genet, 1998. **19**(4): p. 348-55.

430. Sauer, B. and N. Henderson, *Site-specific DNA recombination in mammalian cells by the Cre recombinase of bacteriophage P1.* Proc Natl Acad Sci U S A, 1988. **85**(14): p. 5166-70.

431. Schlaeger, T.M., et al., *Uniform vascular-endothelial-cell-specific gene expression in both embryonic and adult transgenic mice.* Proc Natl Acad Sci U S A, 1997. **94**(7): p. 3058-63.

432. Wong, A.L., et al., *Tie2 expression and phosphorylation in angiogenic and quiescent adult tissues.* Circ Res, 1997. **81**(4): p. 567-74.

433. Hayashi, S. and A.P. McMahon, *Efficient recombination in diverse tissues by a tamoxifen-inducible form of Cre: a tool for temporally regulated gene activation/inactivation in the mouse.* Dev Biol, 2002. **244**(2): p. 305-18.

434. Sobczak, M., J. Dargatz, and M. Chrzanowska-Wodnicka, *Isolation and culture of pulmonary endothelial cells from neonatal mice.* J Vis Exp, 2010(46).

435. Bardin, N., et al., *Soluble CD146, a novel endothelial marker, is increased in physiopathological settings linked to endothelial junctional alteration.* Thromb Haemost, 2003. **90**(5): p. 915-20.

436. Pitulescu, M.E., et al., *Inducible gene targeting in the neonatal vasculature and analysis of retinal angiogenesis in mice.* Nat Protoc, 2010. **5**(9): p. 1518-34.

437. Laitinen, L., *Griffonia simplicifolia lectins bind specifically to endothelial cells and some epithelial cells in mouse tissues.* Histochem J, 1987. **19**(4): p. 225-34.

438. Rao, D.D., et al., *siRNA vs. shRNA: similarities and differences.* Adv Drug Deliv Rev, 2009. **61**(9): p. 746-59.

439. Suwa, A., et al., *Glucose metabolism activation by SHIP2 inhibitors via up-regulation of GLUT1 gene in L6 myotubes.* Eur J Pharmacol, 2010. **642**(1-3): p. 177-82.

440. Rey, F.E., et al., *Novel competitive inhibitor of NAD(P)H oxidase assembly attenuates vascular O(2)(-) and systolic blood pressure in mice.* Circ Res, 2001. **89**(5): p. 408-14.

441. Cooper, J.A., *Effects of cytochalasin and phalloidin on actin.* J Cell Biol, 1987. **105**(4): p. 1473-8.

442. De Bock, K., et al., *Role of PFKFB3-driven glycolysis in vessel sprouting.* Cell, 2013. **154**(3): p. 651-63.

443. Clark, M.A., et al., *Differential expression of lectin-binding sites defines mouse intestinal M-cells.* J Histochem Cytochem, 1993. **41**(11): p. 1679-87.

444. Nagy, A., *Cre recombinase: the universal reagent for genome tailoring.* Genesis, 2000. **26**(2): p. 99-109.

445. Matthews, D.R., et al., *Homeostasis model assessment: insulin resistance and beta-cell function from fasting plasma glucose and insulin concentrations in man.* Diabetologia, 1985. **28**(7): p. 412-9.

446. Tekabe, Y., et al., *Imaging VEGF Receptors and alphavbeta3 Integrins in a Mouse Hindlimb Ischemia Model of Peripheral Arterial Disease.* Mol Imaging Biol, 2018.

447. Carmeliet, P., et al., *Vascular wound healing and neointima formation induced by perivascular electric injury in mice.* Am J Pathol, 1997. **150**(2): p. 761-76.

448. Kessler, T., et al., *ADAMTS-7 inhibits re-endothelialization of injured arteries and promotes vascular remodeling through cleavage of thrombospondin-1.* Circulation, 2015. **131**(13): p. 1191-201.

449. Watt, N.T., et al., *Endothelial SHIP2 Suppresses Nox2 NADPH Oxidase-Dependent Vascular Oxidative Stress, Endothelial Dysfunction, and Systemic Insulin Resistance.* Diabetes, 2017. **66**(11): p. 2808-2821.

450. Nakatsu, M.N., J. Davis, and C.C. Hughes, *Optimized fibrin gel bead assay for the study of angiogenesis.* J Vis Exp, 2007(3): p. 186.

451. Franco, C.A., et al., *Dynamic endothelial cell rearrangements drive developmental vessel regression.* PLoS Biol, 2015. **13**(4): p. e1002125.

452. Hamada, K., et al., *The PTEN/PI3K pathway governs normal vascular development and tumor angiogenesis.* Genes & Development, 2005. **19**(17): p. 2054-2065.

453. Choorapoikayil, S., et al., *Loss of Pten promotes angiogenesis and enhanced vegfaa expression in zebrafish.* Dis Model Mech, 2013. **6**(5): p. 1159-66.

454. Serra, H., et al., *PTEN mediates Notch-dependent stalk cell arrest in angiogenesis.* Nat Commun, 2015. **6**: p. 7935.

455. Hoekstra, E., et al., *Lipid phosphatase SHIP2 functions as oncogene in colorectal cancer by regulating PKB activation.* Oncotarget, 2016.

456. Day, C.A., et al., *Analysis of protein and lipid dynamics using confocal fluorescence recovery after photobleaching (FRAP).* Current protocols in cytometry / editorial board, J. Paul Robinson, managing editor ... [et al.], 2012. **CHAPTER**: p. Unit2.19-Unit2.19.

457. Vestweber, D., *VE-cadherin: the major endothelial adhesion molecule controlling cellular junctions and blood vessel formation.* Arterioscler Thromb Vasc Biol, 2008. **28**(2): p. 223-32.

458. Manning, B.D. and L.C. Cantley, *AKT/PKB signaling: navigating downstream.* Cell, 2007. **129**(7): p. 1261-74.

459. Shiojima, I., et al., *Disruption of coordinated cardiac hypertrophy and angiogenesis contributes to the transition to heart failure.* J Clin Invest, 2005. **115**(8): p. 2108-18.

460.   Wang, C.Y., et al., *Obesity increases vascular senescence and susceptibility to ischemic injury through chronic activation of Akt and mTOR.* Sci Signal, 2009. **2**(62): p. ra11.

461.   Sun, J.F., et al., *Microvascular patterning is controlled by fine-tuning the Akt signal.* Proc Natl Acad Sci U S A, 2005. **102**(1): p. 128-33.

462.   Kerr, B.A., et al., *Interference with akt signaling protects against myocardial infarction and death by limiting the consequences of oxidative stress.* Sci Signal, 2013. **6**(287): p. ra67.

463.   Tojo, T., et al., *Role of gp91phox (Nox2)-containing NAD(P)H oxidase in angiogenesis in response to hindlimb ischemia.* Circulation, 2005. **111**(18): p. 2347-55.

464.   Ebrahimian, T.G., et al., *NADPH oxidase-derived overproduction of reactive oxygen species impairs postischemic neovascularization in mice with type 1 diabetes.* Am J Pathol, 2006. **169**(2): p. 719-28.

465.   Haddad, P., et al., *Nox2-containing NADPH oxidase deficiency confers protection from hindlimb ischemia in conditions of increased oxidative stress.* Arterioscler Thromb Vasc Biol, 2009. **29**(10): p. 1522-8.

466.   Moldovan, L., et al., *Reactive oxygen species in vascular endothelial cell motility. Roles of NAD(P)H oxidase and Rac1.* Cardiovasc Res, 2006. **71**(2): p. 236-46.

467.   van Aalst, J.A., et al., *Role of reactive oxygen species in inhibition of endothelial cell migration by oxidized low-density lipoprotein.* J Vasc Surg, 2004. **40**(6): p. 1208-15.

468.   Clements, M.K., et al., *Inhibition of actin polymerization by peroxynitrite modulates neutrophil functional responses.* J Leukoc Biol, 2003. **73**(3): p. 344-55.

469.   McKayed, K.K. and J.C. Simpson, *Actin in action: imaging approaches to study cytoskeleton structure and function.* Cells, 2013. **2**(4): p. 715-31.

470.   Rossi, A., et al., *Genetic compensation induced by deleterious mutations but not gene knockdowns.* Nature, 2015. **524**(7564): p. 230-3.

471.   Lotfi, S., et al., *Towards a more relevant hind limb model of muscle ischaemia.* Atherosclerosis, 2013. **227**(1): p. 1-8.

472.   Aird, W.C., *Phenotypic heterogeneity of the endothelium: I. Structure, function, and mechanisms.* Circ Res, 2007. **100**(2): p. 158-73.

473.   Li, H. and A.J. Marshall, *Phosphatidylinositol (3,4) bisphosphate-specific phosphatases and effector proteins: A distinct branch of PI3K signaling.* Cell Signal, 2015. **27**(9): p. 1789-98.

474.   Chi, Y., et al., *Comparative mechanistic and substrate specificity study of inositol polyphosphate 5-phosphatase Schizosaccharomyces pombe Synaptojanin and SHIP2.* J Biol Chem, 2004. **279**(43): p. 44987-95.

475.   Feng, J., et al., *An improved malachite green assay of phosphate: mechanism and application.* Anal Biochem, 2011. **409**(1): p. 144-9.

476.   Ayala, J.E., et al., *Considerations in the design of hyperinsulinemic-euglycemic clamps in the conscious mouse.* Diabetes, 2006. **55**(2): p. 390-7.

477.   Haywood, N.J., et al., *Insulin-Like Growth Factor Binding Protein 1 Could Improve Glucose Regulation and Insulin Sensitivity Through Its RGD Domain.* Diabetes, 2017. **66**(2): p. 287-299.

478.	Webb, G.C., et al., *Glucagon replacement via micro-osmotic pump corrects hypoglycemia and alpha-cell hyperplasia in prohormone convertase 2 knockout mice.* Diabetes, 2002. **51**(2): p. 398-405.

479.	Rajwani, A., et al., *Increasing circulating IGFBP1 levels improves insulin sensitivity, promotes nitric oxide production, lowers blood pressure, and protects against atherosclerosis.* Diabetes, 2012. **61**(4): p. 915-24.

480.	Simons, M., et al., *State-of-the-Art Methods for Evaluation of Angiogenesis and Tissue Vascularization: A Scientific Statement From the American Heart Association.* Circ Res, 2015. **116**(11): p. e99-132.

481.	Woo, E., et al., *Stability of the antiproliferative effect of mitomycin-C after reconstitution.* J Glaucoma, 1997. **6**(1): p. 33-6.

482.	Rajadurai, C.V., et al., *5'-Inositol phosphatase SHIP2 recruits Mena to stabilize invadopodia for cancer cell invasion.* J Cell Biol, 2016. **214**(6): p. 719-34.

483.	MacArthur, J., et al., *The new NHGRI-EBI Catalog of published genome-wide association studies (GWAS Catalog).* Nucleic Acids Research, 2017. **45**(Database issue): p. D896-D901.